Dissertation zur Erlangung des Doktorgrades
der Fakultät für Chemie und Pharmazie
der Ludwig-Maximilians-Universität München

Cutaneous vaccination - Investigation of different approaches of intradermal vaccine delivery

Laura Engelke-Mücksch (geb. Engelke)
aus
Frankfurt (Oder), Deutschland

2018

Erklärung

Diese Dissertation wurde im Sinne von §7 der Promotionsordnung vom 28. Nov. 2011 von Frau PD Dr. habil. Julia Engert von der Fakultät für Chemie und Pharmazie betreut.

Eidesstattliche Versicherung

Diese Dissertation wurde eigenständig und ohne unerlaubte Hilfe erarbeitet.

Basel, den 28. Mai 2018

Laura Engelke-Mücksch (geb. Engelke)

Dissertation eingereicht am:	13. Juni 2018
1. Gutachter:	PD Dr. habil. Julia Engert
2. Gutachter:	Prof. Dr. Gerhard Winter
Mündliche Prüfung am:	12. Juli 2018

Für meine Familie

ACKNOWLEDGEMENTS

This thesis was prepared at the Department of Pharmacy, Pharmaceutical Technology and Biopharmaceutics at the Ludwig-Maximilians-University Munich (LMU) under the supervision of PD Dr. habil. Julia Engert and Prof. Dr. Gerhard Winter.

Foremost, I would like to express my gratitude towards PD Dr. habil. Julia Engert, my doctoral supervisor, who supported and guided my work on this interesting research topic. I am thankful for her confidence in my work and her constant encouragement and scientific support. I would like to thank her for the guidance granting a productive balance of structure and freedom over the years.
Equally, I would like to thank Prof. Dr. Gerhard Winter for giving me the opportunity to join his research group and being my doctoral supervisor. I highly appreciate his advice and guidance during scientific discussions. This work benefitted from his creativity and his drive to push scientific boundaries. I am grateful for his initiative to provide the framework for scientific and personal development.

Furthermore, I would like to thank Prof. Dr. Wolfgang Frieß for contributing to the great work atmosphere between all research groups at the institute and his encouraging scientific questions during the "Donnerstagsseminar". Also, it was a great pleasure to support the "Biopharmacy" student practical course and seminars under his supervision.

I would also like to thank Cihad Anamur for the collaboration on the BioInkjet project. I very much enjoyed sharing the lab and discussing our joint project with him.

Furthermore, I want to thank our cooperation partners Christian Fellner, Peter Lell (PyroGlobe GmbH, Hettenshausen), Wolfgang Rebel, and Julia Stadler, Susanne Zöls, and Mathias Ritzmann (Clinic for Swine, LMU, Oberschleißheim) who substantially contributed to the *in vivo* needle-free powder immunization study.
Many thanks to Florian Vetter, Christoph Müller, and Prof. Dr. Franz Bracher (Department of Pharmacy, Center for Drug Research, LMU) for performing the GC-MS measurements.
Special thanks go to my Bachelor students Lisa Völk and Denis Hüwel, whose studies contributed to this thesis by providing fundamental knowledge to support my work. Also, I would like to extent my thanks to my intern students Lydia Beresuzkij, Christine

Göttsberger, Regina Happach, and Lena Islinger.
Moreover, I would like to thank our cooperation partners Stefan Henke, Jörg Bender, Heiko Spilgies (IIS Innovative Injektions-Systeme, Andernach) and Tobias Bächle (Pantec Biosolutions, Liechtenstein). Also, I would like to thank Michael K. Schmidt (Center for Neuropathology and Prion Research, ZNP, LMU) for his support with the cryostat sectioning.

I would like to particularly thank my present and former colleagues at the institute. Work life would not have been the same without you. It makes me smile to think about all the festivities, spontaneous gatherings, trips, and adventures we enjoyed together.
It was my greatest pleasure to start into the day with a decent coffee with Matthias Lucke, enjoy an amazing lunch with Alice Hirschmann, Michaela Breitsamer, and Tobias Keil, or add sparkle to the day with Kerstin Hoffman, Marie-Paule Even, and Kay Strüver. Marie-Paule Even and Teresa Kraus, I loved sharing the lab with you. Also, many thanks to Randy Wanner, Elisa Agostini, Stefanie Funke, Roman Mathäs, Corinna Dürr, Madeleine Witting, and Benjamin Werner. Stay as amazing as you all are!

Ebenso danke ich Wiebke Alig, für Ihre Freundschaft und insbesondere Ihr Vertrauen in meine Arbeit und Ihre große Unterstützung.

Vor allem möchte ich meiner Familie danken, die mich stets unterstützt und angespornt hat. Ganz besonders danke ich meinen Eltern Moana und Rainer Engelke, die mit Ihrer Unterstützung in allen Lebensphasen diese Arbeit erst ermöglicht haben. Meinem Ehemann Jonas Mücksch danke ich für sein Verständnis und beeindruckende Fähigkeit mich zu Höchstleistungen zu motivieren. Mit Dir zusammen ist alles möglich! Danke meiner Schwester Maja. Meiner gesamten Familie danke ich von ganzem Herzen, dass Ihr an mich glaubt, für mich da seid und stets die richtigen Worte findet. Ihr seid der Grund für mich immer das Beste zu geben.

Table of contents

List of Abbreviations

ADP	adenosine diphosphate
APC	antigen-presenting cell
BCA	bicinchoninic acid
BCG	bacille Calmette-Guérin
BET	Brunauer-Emmert-Teller
BHA	butylated hydroxyanisole
BSA	bovine serum albumin
CA	cellulose acetate
CD	cluster of differentiation
CMC	carboxmethyl cellulose
CO_2	carbon dioxide
CSSS	cyanoacrylate skin surface stripping
CT	cholera toxin
CTL	cytotoxic T lymphocyte
CV	coefficient of variation
DAPI	4',6-diamidino-2-phenylindole
DC	dendritic cell
dDC	dermal dendritic cell
DLS	dynamic light scattering
DMSO	dimethyl sulfoxide
DNA	deoxyribonucleic acid
DSC	differential scanning calorimetry
DSJI	disposable syringe jet injector
DT	diphtheria toxoid

ELISA	enzyme-linked immunosorbent assay
EP	electroporation
EPI	epidermal powder immunization
Er:YAG	erbium:yttrium aluminum garnet
Er:YSGG	erbium:yttrium scandium gallium garnet
FDA	Food and Drug Administration
FITC	fluorescein isothiocyanate
FITC-PAH	fluorescein isothiocyanate- labeled poly(allylamine) hydrochloride
FNU	formazine nephelometric units
GC-MS	gas chromatography-mass spectrometry
GMP	Good Manufacturing Practice
HIV	human immunodeficiency virus
HMWS	high molecular weight species
HPV	human papillomavirus
hpw	highly purified water
HRP	horseradish peroxidase
i.d.	intradermal
i.m.	intramuscular
IFN-α	interferon alpha
IFN-γ	interferon gamma
Ig	immunoglobulin
IL	interleukin
LAF	laminar air flow
LAL	limulus amebocyte lysate
LbL	layer-by-layer
LC	Langerhans cell

LMWS	low molecular weight species
LSM	laser scanning microscopy
LT	*Escherischia coli* heat-labile toxin
LTR	local transport region
MAZ	microscopic ablation zone
MES	2-(N-morpholino)ethanesulfonic acid
MHC	major histocompatibility complex
MN	microneedle
MTZ	microthermal zone
MUNJI	multiple use nozzle jet injector
MYR	myristylated peptide
N&S	needle and syringe
NKT	natural killer T cell
ODN	oligodeoxynucleotides
OVA	ovalbumin
PAH	poly(allylamine) hydrochloride
PBS	phosphate-buffered saline
PBS-T	phosphate-buffered saline containing Tween® 20
PDMS	polydimethylsiloxane
PEG	polyethylenen glycol
PLGA	poly(lactic-co-glycolic acid)
PMED	particle-mediated epidermal delivery
PMMA	poly(methyl methacrylate)
PS	polystyrene
PSS	polystyrene sulfonate
PVA	polyvinyl alcohol

RD70	rhodamine B-labeled dextrane 70 kDa
RNA	ribonucleic acid
RT	room temperature
RTD	residual thermal damage
s.c.	subcutaneous
SC	stratum corneum
SDS	sodium lauryl sulfate
SDS-PAGE	sodium dodecyl sulfate polyacrylamide gel electrophoresis
SE-HPLC	size exclusion-high performance liquid chromatography
SEM	scanning electron microscopy
SLS	static light scattering
SSA	specific surface area
SUDJI	single-use disposable jet injector
TBS-T	Tris-buffered saline containing Tween® 20
TCA	trichloroacetic acid
TEWL	transepidermal water loss
Tfh	follicular T helper cell
Th	T helper cell
Ti	titanium
TLR	toll-like receptor
TMB	3,3',5,5'-tetramethylbenzidine
TMBE	tert-methylbutylether
TNF	tumor necrosis factor
Treg	regulatory T cell
Tris	tris(hydroxymethyl)aminomethane
UV	ultraviolet
Vis	visible

WHO	World Health Organization
XRPD	X-ray powder diffraction

I

INTRODUCTION

Section 2 of this chapter has been published as L. Engelke, G. Winter, S. Hook, and J. Engert, Recent insights into cutaneous immunization: How to vaccinate via the skin, Vaccine 33(37) (2015) 4663-74. This article was written by myself.

1 Objectives and outline of this thesis

The aim of this thesis is to evaluate selected active intradermal delivery techniques and their potential for cutaneous vaccination. This work focuses in particular on needle-free powder injection and skin microporation using microneedles (MNs) or laser microporation for intradermal antigen delivery. This thesis shall provide an insight into the challenges and opportunities in the development of needle-free vaccination routes via the skin. Furthermore it aims to highlight the great potential of the cutaneous route of vaccination to serve as an alternative to conventional immunization by intramuscular (i.m.) injection.
Different aspects of the development of needle-free vaccination techniques are addressed experimentally and discussed in relation to historical and most recent research. In particular, the intradermal deposition, reproducibility and efficiency of delivery, the induction of an immune reponse, the ease of administration, the simplicity of design and the associated cost-efficiency of development and large scale manufacturing are addressed.
In chapter II a novel design of a hand-held, needle-free powder injector is studied for cutaneous vaccination using a sugar-based microparticle vaccine. In the course of this study, a highly concentrated vaccine using ovalbumin (OVA) as model antigen has been developed using a two-step manufacturing process combining collapse lyophilization and cryogenic milling. The model vaccine properties and long-term storage stability are assessed. Moreover, the loading of the powder injector is characterized by studying the vaccine adhesion onto the device membrane using different oily adhesives. These oily adhesives allow not only for a fixation of the vaccine powder, but can also serve as adjuvant upon intradermal delivery. Therefore, the oily adjuvant is brought in contact with the concentrated vaccine to assess the long-term stability. Finally, the immune response by needle-free powder injection is evaluated *in vivo* using the novel injector device.
Chapter III focuses on the intradermal delivery of micro- and nanoparticles using solid

microneedles (MNs). Compared to the complex engineering required for the development of the powder injector, solid MNs are easy and cost-efficient to manufacture in large scale and commercially available in various configurations. In this chapter the intradermal delivery of micro- and nanoparticles ranging from 0.1 µm to 7.0 µm using two different types of solid MNs is characterized. Thereby, the influence of the particle size as well as the MN tip geometry and application sequence on the intradermal penetration depth and quantitative deposition is studied.
Furthermore, in chapter IV the intradermal delivery of macromolecules and particles from water-soluble films upon fractional laser microporation is evaluated. In comparison to solid MNs, the skin barrier is breached using a fractional erbium:yttrium aluminum garnet (Er:YAG) laser poration device. The intra- and transdermal delivery of fluorescently-labeled dextrane as well as micro- and nanoparticles of 5.0 µm and 0.5 µm from polyvinyl alcohol (PVA)-based film patches is studied over 24 hours upon skin laser microporation.
The different intradermal delivery techniques presented in this thesis allow for a comparison of the utilized approaches with respect to simplicity of design and intradermal delivery efficiency. Research beyond this thesis can be benchmarked against the results and observations presented here. This thesis not only provides a profound overview of needle-free cutaneous vaccination approaches, but also identifies critical aspects and requirements of intradermal vaccine delivery.

2 Recent insights into cutaneous immunization: how to vaccinate via the skin

2.1 Introduction

The skin has been used to induce protective immunity against highly infectious diseases since the very first recorded vaccinations against smallpox in 1796 [1, 2]. Jenners breakthrough eventually lead to the eradication of smallpox by mass vaccination programs, where vaccines were initially administered by subcutaneous (s.c.) inoculation with a lancet and later performed using needle-free jet injectors and bifurcated needles for intradermal (i.d.) vaccine delivery [1, 3, 4]. Furthermore, bacille Calmette-Guérin (BCG) vaccines have been administered intradermally since the early 1920s to prevent tuberculosis [5–7].

Although the skin has been known for centuries to be an attractive site for immunization, recent developments in needle-free systems have renewed the interest in cutaneous vaccination, here defined as the induction of an immune response upon topical, intradermal, or intraepidermal delivery of a vaccine [8]. This route of immunization, sometimes also referred to as skin vaccination or transcutaneous immunization, takes advantage of the unique immunological features of the skin immune system [9–11]. The two uppermost skin layers, the epidermis and the dermis, have a high density of immunocompetent cells such as Langerhans cells (LCs) and dermal dendritic cells (dDCs) (Fig. I.1) [12]. These antigen-presenting cells (APCs) play an important role in developing adaptive immunity through the processing and presenting of antigen [13, 14]. Delivering a vaccine to the skin has been shown to elicit similar or even higher immune responses compared to i.m. injection, even in some cases using lower vaccine doses [15–22]. This could be of special significance for pandemics, when vaccine supply is limited and dose reduction is necessary. By evoking humoral, cellular and, in some cases, mucosal immune responses [23–25], cutaneous vaccination holds the potential to expand the range of applications beyond conventional prophylactic immunization into therapeutic vaccination for cancer and human immunodeficiency virus (HIV) infections [26, 27].

The demand for a safe, pain-free and simple alternative to i.d. and i.m. needle injection has led to the development of alternative techniques to deliver vaccines to the skin. Intradermal vaccination, usually performed with needle and syringe (N&S), can be regarded as the first approach of cutaneous vaccination. However today, the variety of strategies has been expanded, including conventional i.d. injection, but also needle-free vaccine delivery

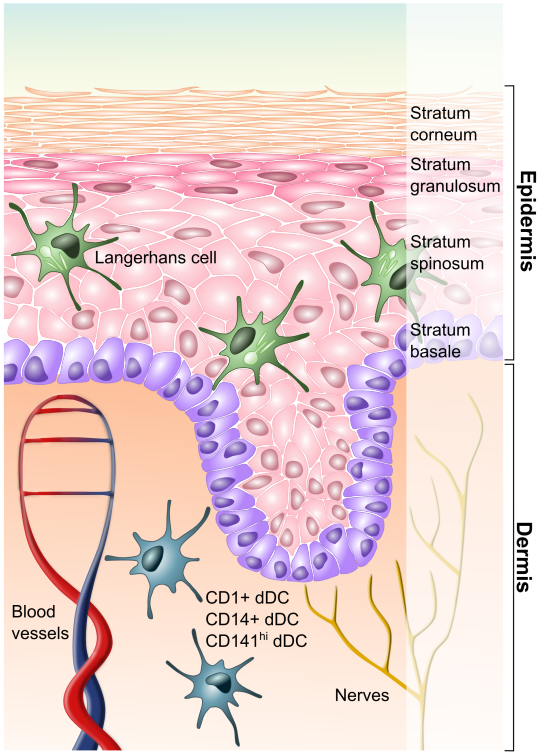

Figure I.1: Professional antigen presenting cells of the superficial skin. Three subsets of professional antigen presenting cells have been identified within the two topmost layers of the skin. Whereas a high density of Langerhans cells (LCs) can be found within the epidermis, $CD1^+$ and $CD14^+$ dermal dendritic cells (dDCs) reside in the underlying dermis.

techniques, stratum corneum (SC)-disruptive approaches, and passive targeting strategies [28]. The simplest techniques involve the passive diffusion of protein or DNA vaccines into intact skin or skin pretreated by tape stripping or abrasion of the SC [29–34]. Active vaccination approaches deliver the antigen directly to immunocompetent cells either by needle-free jet and powder injection or by creating microchannels or transient cavities in the upper skin layers [35–37]. Such active microporation techniques include the use of microneedles, thermal microporation, radiofrequency ablation, and laser poration, as well as electroporation and sonoporation. Here we will review the latest advances in the field of needle-free cutaneous vaccination with special consideration being given to DNA or RNA vaccines and the use of adjuvants for cutaneous vaccination.

2.2 Vaccination via the skin

2.2.1 Antigen presentation

The aim of vaccination is to activate the acquired immune system to induce long-lasting protection against specific pathogens [38]. Upon encountering a pathogen APCs mature and migrate towards draining lymph nodes [13]. By up-regulating antigen-loaded major histocompatibility complexes (MHCs) class I and II as well as co-stimulatory surface molecules, mature APCs initiate the proliferation and differentiation of naïve T cells into effector and memory T cells [13, 39]. Typically, exogenous antigens are presented via (MHC-II complexes to $CD4^+$ T cells, comprising T helper cells (Th cells) and regulatory T cells (Tregs), whereas $CD8^+$ T cells (cytotoxic T cells, CTL) interact with cytosol-derived endogenous antigens loaded onto MHC-I [40, 41]. However this segregation of antigen presentation is not complete as distinct subsets of APCs are able to cross-present exogenous antigens via MHC-I to prime $CD8^+$ T cells [42, 43]. This cross-priming is expected to play an essential role for eliciting immune responses against tumor or virus-infected cells [42].
In addition to the MHC-restricted presentation of proteins and peptides, APCs are able to process and present non-protein antigens, such as lipids, glycolipids and lipopeptides [44]. Surface molecules of the CD1 family are loaded with lipid antigens via endocytotic pathways [45], subsequently priming natural killer T cells (NKTs), which respond by secreting large amounts of Th1 and Th2 cytokines and influencing dendritic cell (DC) maturation [46, 47]. LCs have been found to express large amounts of the group 1 family of CD molecule CD1a and moderate amounts of CD1c [48, 49]. However, all identified molecules of group one and two of the CD1 family have been found on dDCs [49, 50]. CD1d is the only molecule of the CD1 family that has also been detected in mice [51].

2.2.2 Acquired Immune Responses

$CD8^+$ T cells that differentiate and proliferate upon MHC-I interaction into CTLs [41, 52] are able to lyse transformed or infected cells through the production of granzymes and perforin [53]. $CD4^+$ T helper cells play a role in modulating a variety of immune responses. This includes cellular, humoral, regulatory and inflammatory responses [54]. B cells may be activated in either a T cell dependent or independent manner [55]. Upon activation naïve B cells differentiate into antibody secreting plasma cells and memory B cells [56].
Four different subsets of T helper cells are known to reside in the skin Th1, Th2, Th17 and Th22 [51]. Promoted by IL-12, non-polarized $CD4^+$ T cells differentiate into Th1

cells, typically secreting interferon gamma (IFN-γ) and IL-2 [57]. The polarization towards the Th2 subset is enhanced by IL-4 and these cells secrete IL-4, IL-5, IL-10 and IL-13 [57]. While IFN-γ promotes a switch towards IgG2a in mice and stimulates cellular immune responses, IL-4 induces the synthesis of IgG1 and IgE [58]. IL-23 induces the proliferation of Th17 cells that secrete IL-17 and often IL-22 [59, 60]. The Th22 subset, which has been identified recently, can be characterized by the secretion of IL-22 and in the absence of IL-17 or IFN-γ [61, 62]. Healthy skin harbors approximately 8 % mainly Th1-biased effector memory T cells as well as a substantial numbers of central memory and regulatory T cells [63].

2.2.3 Dendritic cell subsets

While the dendritic cell network in the skin differs between mice and human, some similarities exist. The main dendritic cell subsets that have been identified in mice and human skin are the epidermal LCs and dDCs. In both species LCs form a continuous network throughout epidermal keratinocytes and can be characterized by their expression of the lectin receptor langerin (CD207) [51, 64]. In mice, the dDC population constitutes of dermal resident DCs, namely $CD103^+$ DCs and $CD11b^+$ DCs, as well as migratory LCs [65]. Langerin-negative $CD11b^+$ DCs represent the main dermal dendritic cell subset, (approximately 70 % of DC) residing in the dermal skin layer [66]. Langerin-positive $CD103^+$ DCs are found below the epidermal-dermal junction [67]. In addition to these two dermal resident DCs, a third dDC subset has been identified, expressing MHC-II and CD11c, but no CD11b, CD103 or langerin on the cell surface [66, 68]. However, the phenotype of this DC subset has not yet been fully identified [64]. It has been reported that $CD11b^+$ DCs play the main role in initiating $CD4^+$ T cell responses, although all dDCs were able to present viral antigens [69]. Furthermore, $CD11b^+$ DCs were critical promoters of the local proliferation of effector and regulatory T cells [70]. As regards Th1/Th2 differentiation, $CD103^+$ DCs induced IgG2a/c and IgG2b responses, whereas LCs provided an IgG1-based humoral immune response [71]. Interestingly $CD103^+$ DCs are the only DC subset reported to be capable of cross-priming $CD8^+$ T cells [69].

In human skin, three additional langerin-negative subsets of DCs have been identified, referred to as $CD1a^+$, $CD14^+$ and $CD141^{hi}$ DCs [72–74]. Several studies have highlighted the potential of the different DCs subsets in influencing the direction of the immune response with the $CD14^+$ DC subset being shown to preferentially induce a Th1-biased response [14, 75] and to promote the secretion of large amounts of different immunoglob-

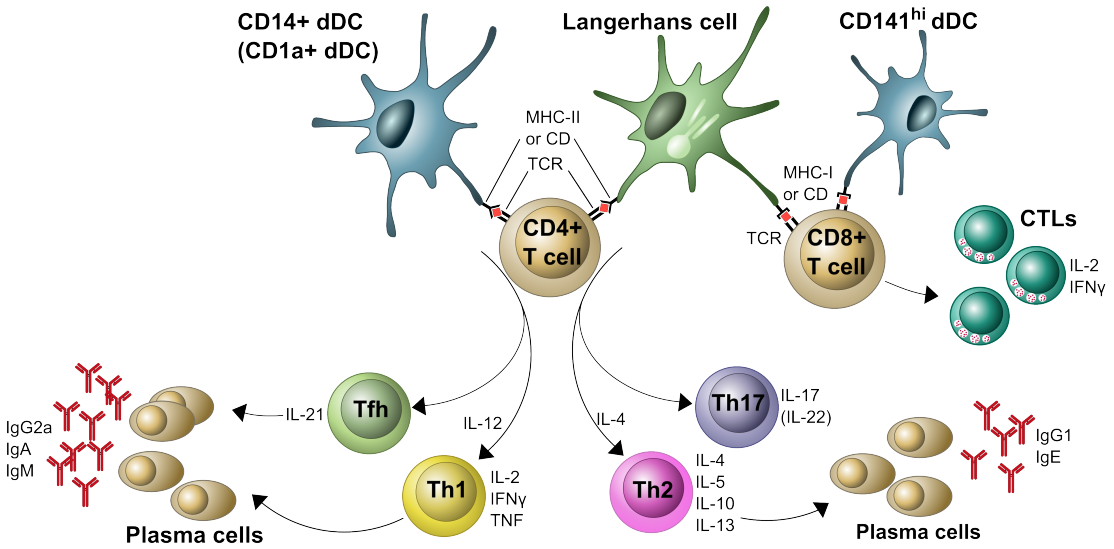

Figure I.2: T cell differentiation upon activation by $CD14^+$ dermal dendritic cells (dDCs) or Langerhans cells (LCs) and cross-presentation of $CD141^{hi}$ dDCs. After antigen processing, dDCs and LCs migrate toward draining lymph nodes, presenting the antigen via the major histocompatibility complexes I and II (MHC-I, MHC-II). By interaction with the T cell receptor (TCR), $CD4^+$ and $CD8^+$ T cells are activated. $CD14^+$ dDCs promote the differentiation of $CD4^+$ T cells into follicular T helper cells (Tfh) and T helper 1 (Th1) cells that secrete large amounts of IL-2, IFN-γ and TNF. Both T cell subsets stimulate the differentiation and proliferation of antibody-secreting plasma cells, which elicit an IgG2a, IgA, and IgM based immune response. On the other hand, LCs induce the differentiation of $CD4^+$ T cells into Th2 cells, indicated by the secretion of IL-4, IL-5, IL-10, and interleukin (IL)-13, and boosting IgG1 and IgE secreting plasma cells. Moreover, $CD8^+$ T cells differentiate and proliferate upon interaction with LCs or $CD141^{hi}$ dDCs into IL-2 and IFN-γ secreting cytotoxic T cells (CTLs) providing a cellular immunity. The differentiation of the Th1 and Th2 subset is furthermore enhanced by IL-12 and IL-4, respectively.

ulins [14, 76]. The recently discovered $CD141^{hi}$ DC subset was shown to efficiently cross-present exogeneous antigens to $CD8^+$ T cells in the periphery [74].

The role of LCs is more complex with these abundant cells being reported to have a role in maintaining tolerance in healthy skin but then being able to induce T cell activation in response to infection [77]. In this case LCs showed a superior ability to initiate antiviral immunity by priming $CD8^+$ T cells and to induce Th17 responses [75, 78, 79].

Figure I.2 gives an overview of the predominant activation routes of the different human DC subsets. Although functional homologues to mouse DCs could be identified, the existing differences in the expression patterns of surface molecules on human and mouse DC affects the transferability of *in vitro* and *in vivo* study results. Another issue impacting on the

transferability of mouse data to humans is the difference in the skin between mice and humans. Mouse skin is thinner and has more hair follicles [80]. Therefore, data from mice must be interpreted with caution.

2.3 Adjuvants for cutaneous vaccination

The best studied adjuvants for cutaneous vaccination are derived from bacterial adenosine diphosphate (ADP)-ribosylating exotoxins [29, 81–84]. Cholera toxin (CT), *Escherischia coli* heat-labile toxin (LT), or subunits of these proteins have commonly been utilized to elicit or enhance the response towards a vaccine given via the cutaneous route [29, 33, 81]. It was shown that CT and LT applied onto intact mouse skin induce the production of toxin-specific antibodies [81]. Moreover, CT-adjuvanted formulations induced superior immune responses against diphtheria and tetanus toxoid [81, 82, 85]. It has not yet been clarified how bacterial ADP-ribosylating toxins influence the type of immune reaction. However, several studies report the induction of Th2-biased immunity [81, 86]. Additionally, CTL proliferation has been observed, indicating activation of epidermal LCs [87].
The second group of adjuvants that were utilized cutaneously are specific ligands of toll-like receptors (TLRs) [88]. These receptors play a major role in the detection of pathogens and are therefore an ideal target for enhancing the immune reaction [89]. One of the most important adjuvants of TLR ligands to date are the CpG oligodeoxynucleotides (ODN) [90]. Prokaryotic CpG motifs are less methylated and are therefore recognized by TLR9, a receptor subtype of the TLR family [91–93]. CpG ODN induce the production of pro-inflammatory cytokines such as IL-12 and IFN-α [89], promoting a Th1 biased immune response upon vaccination [88, 94]. Furthermore, TLR9 agonists have been shown to be able to convert an established Th2-based immune response upon DNA vaccination into a Th1-directed response [95].
Other TLR ligands, such as imiquimod (TLR7 ligand) or polyinosinic:polycytidylic acid (poly I:C) (TLR3 ligand) have also been investigated for cutaneous vaccination [96, 97]. Both adjuvants elicit the proliferation of $CD8^+$ T cells, thereby indicating a cellular immune response [96–98]. Moreover, poly I:C additionally provides a Th1/Th2-balanced humoral immunity [97]. Imiquimod has until now mainly been studied with the focus on tumor immunity [96, 99]. As a commercial product it is already in use as an immunomodulator for the treatment of human papillomavirus (HPV) infections [100]. Although imiquimod can be administered cutaneously alone it showed a superior activation of the immune system when combined with anti-CD40 ligands or UV light [96, 99].

As shown in table I.1, there is a wide variety of adjuvants that have been utilized in cutaneous vaccination studies, also including alum [88, 101], Quillaja saponins [15], and other chemical substances [102]. Additional investigations are necessary to further clarify how the type of adjuvant used and the route of administration influence the type of immune response generated.
In addition, the extent of skin irritation upon delivery to the skin using different adjuvants needs to be evaluated, and a suitable experimental model to investigate immediate and long-term skin reactions remains to be developed. One example highlighting this aspect is alum as cutaneous vaccination adjuvant, which has been used for i.d. immunization against hepatitis A before [103, 104]. Adverse reactions after i.d. injection have been reported, such as long lasting skin papules and dermatitis [104]. Furthermore, it was shown that aluminum hydroxide can lead to the development of persistent intradermal granulomas when used for i.d. hyposensitization [105]. This implies that alum adjuvants might not be suitable for vaccination strategies that involve an i.d. vaccine delivery.

2.4 Needle-free injection techniques for cutaneous vaccination

2.4.1 Jet injection

The very first approach of needle-free vaccination used jet injectors. In the 1950s multiple use nozzle jet injectors (MUNJIs) were extensively used in mass immunization programs and played a major role in the smallpox eradication [3]. However, increasing numbers of hepatitis B infections as well as epidemiologic and animal-model studies provided growing evidence that cross infections were linked to the utilization of MUNJIs, causing the termination of jet vaccination campaigns [28, 106]. The discovered safety issues finally led to the development of disposable syringe jet injectors (DSJIs) and single-use disposable jet injector (SUDJI) [28, 107].
Conventional jet injector systems actuate a piston using a spring or compressed gas [3]. By pressing the fluid through a nozzle with a diameter of $80 - 360$ µm [3], a liquid jet is generated that encounters the skin with a velocity between $100 - 200$ m/s [108]. The high impaction force of the jet initiates a piercing of the skin surface including the underlying tissue [109]. After reaching a critical depth, the liquid does not penetrate further into the tissue but instead forms a liquid depot in the skin [110]. Under these conditions it is possible to achieve either a mainly subcutaneous (s.c.), or intramuscular (i.m.) deposition of the liquid [28]. However, due to inter-individual variations, jet injector systems might

Table I.1: Overview of adjuvants, sorted by the extent of utilization, and their effects on the immune response upon cutaneous vaccination compared to non-adjuvanted (w/o) studies.

Adjuvant	Cutaneous vaccination technique	Antigen	Type of immunity	Investigated parameter	Reference
w/o	Intact skin	OVA, TT, DT	Th2[a]	IgG1 ↑	[31,171,203]
	Tape stripping	OVA	Th2[a]	IgG1 ↑, IgE	[32]
	Microneedles	DT	Th2[a]	IgG1/IgG2a ↑	[132]
	Laser poration	DT, bGal	Th2[a]	IgG1 ↑, IgE	[149]
ADP-ribosylating toxins					
Whole protein, subunits, or recombinant subunits of Cholera toxin (CT), *E. coli* heat-labile toxin (LT)	Intact skin	TT, LT, DT	Th2[a]	IgG1 ↑, IL-5 ↑	[81,86]
	Warm waxing	pDNA	Th2[a], Cellular	IgG1 ↑, IL-4 ↑, CTL	[23,168]
	Nanoparticles	pDNA, OVA	Th1[b]	INF-γ ↑	[83,84]
	Microneedles	DT, Influenza	Th1[b]	IgG1/IgG2a ↓	[85,132]
	Powder injection	Influenza	Th1[b], Mucosal	IgG2a ↑, IFN-γ ↑, IgA	[18,25]
TLR agonists					
CpG (TLR9)	Laser poration	Phl p 5, bGal	Th1[b]	IgG2a ↑, IL-4 ↓	[149,153]
	Electroporation	SIINFEKL	Cellular	CTL	[159]
	Powder injection	Influenza	Th1[b], Mucosal, Cellular	IgG2a ↑, IFN-γ ↑, IgA, CTL	[25,88]
Imiquimod (TLR7)	Intact skin	SIINFEKL + anti-CD40 mAb (i.v.)/UVB	Cellular	CTL	[96,99]
Poly (I:C) (TLR3)	Microneedles	OVA	Th1[c], Cellular	IgG2c ↑, CTL	[97,98]
Quillaja saponins					
Quil-A	Nanopatch	Influenza	n.d.	IgG	[15]
QS-21	Powder injection	Influenza	Mucosal	IgA	[18]
Alum	Tape stripping	bGal	n.d.	IgG	[101]
	Powder injection	DT	Th2[b]	IgG1 ↑, IL-4 ↑	[88]
Other adjuvants					
c-di-AMP	Nanoparticles	OVA	n.d.	OT-II cell proliferation ↑	[173]
Mannan-coated liposomes	Hair plucking	pDNA	Th1[b]	IFN-γ ↑	[34]
Deformable liposomes	Hair plucking	pDNA	Mucosal	IgA	[175-177,188]
Poly[di(carboxylate-phenoxy)phosphazene]	Microneedles	HBsAg	n.d.	IgG	[102]

[a] Evaluated by IgG1/IgG2a ratio.

[b] Investigated parameter compared to non-adjuvanted (w/o) cutaneous vaccination.

[c] Investigated parameter compared to vaccination by injection.

w/o - Without adjuvant.

n.d. - No differentiation between humoral Th1/Th2, cellular, or mucosal immunity.

fail to reach the target tissue and often induce local reactions (related to the penetration depth) such as pain, bruising, and redness of the vaccination site [28, 110].
Novel approaches using a pulsed jet are expected to minimize these effects [111]. The recently developed pulsed jet injector system employs a voltage-regulated piezoelectric transducer [112]. The activation leads to a fast expansion of the piezoelectric elements, simultaneously accelerating a piston which pushes the liquid through a nozzle of $50-100$ µm [112]. In comparison to conventional jet injectors, the pulsed piezoelectrical technology can create narrow liquid jets of very small volumes between $2-15$ µL [112]. By controlling the velocity and jet volume, it is possible to achieve penetration depths around 200 µm or to target layers of the skin specifically [112, 113]. The pulsed microjet technology represents a promising strategy to perform cutaneous vaccination, targeting the upper layers of the skin and diminishing the risk of pain and bruising. However, high production and disposable costs might remain major issues for the establishment of pulsed jet injectors as single-use devices.

2.4.2 Powder injection

The principle of ballistic powder injection, often referred to as biolistics, was exploited for vaccination for the first time in 1996 [114]. The immune response after cutaneous powder injection of a DNA vaccine was investigated using the gene gun technology [114]. As summarized by Kis *et al.*, different kinds of particles and technologies have been utilized to deliver dry particles into the epidermal layer of the skin [35]. The basic mechanism of injection involves the fast expansion of helium gas to accelerate the particles towards the skin [115, 116]. When the particles encounter the surface, high impaction forces result in the penetration of the particles into the epidermal and dermal layer [117, 118]. A bench-top device that uses a pressure-regulated helium gas supply has been developed [119]. With this system, it was reported that a higher pressure resulted in deeper jet penetration, whereas the particle distribution increased with the nozzle diameter [119].
Two types of particles have been commonly used for powder injection. With the gene gun, or the closely related particle-mediated epidermal delivery (PMED) technology, $1-3$ µm DNA- or protein-coated gold particles are delivered into the skin. Sugar-based particles with a lower density but larger size (between $20-70$ µm) are used for epidermal powder immunization (EPI) [114, 120]. Powder injection facilitates the administration of both DNA or RNA vaccines and conventional protein vaccines in a dry, solid state [18, 121]. By targeting the epidermal and dermal layers of the skin, powder injection efficiently

exploits the unique immunology of the skin. It induces comparable or higher antibody titers compared to conventional vaccination and holds the potential to elicit cellular and mucosal immune responses [25, 121–123]. Moreover, powder injection might represent a convenient strategy for genetic immunization and holds great potential for a range of applications, such as the treatment of type 1 diabetes [124]. Powder injection also allows for the combination of different vaccine formulations. Deng *et al.* developed a delivery system that comprises protein-loaded nanoparticles in microparticles (nano-in-micro) for ballistic powder injection, a system that could also be exploited for genetic skin vaccination [125]. The increased stability of dry vaccine formulations delivered by pain-free powder injection circumvents the storage issue of liquid vaccines. However, the analytical effort for vaccine characterization remains high. Moreover, helium gas as accelerator medium increases the device production costs. Because of changing skin properties, the total amount of intracutaneous powder deposition can vary, representing a major challenge for EPI.

2.5 Microporation technologies

2.5.1 Microneedles

Microporation technologies for the delivery of macromolecular drugs, biopharmaceuticals and vaccines are developing rapidly [36, 126]. These technologies promote the formation of micron-sized pores into the skin, transiently breaching the main protective barrier [36]. Four main types of microneedles have been developed: solid, coated, hollow, and dissolving microneedles [reviewed in [127–129]]. The most common technique for cutaneous vaccination involves the direct coating of antigen onto solid microneedles [15–17]. However, dissolving microneedles have also been extensively investigated [130, 131]. The aim of this technology as regards vaccination is to pierce the SC bringing the vaccine in contact with cutaneous APCs [132]. By avoiding penetration into deeper dermal regions, safe, minimally-invasive and pain-free immunization can be achieved [132]. The utilization of mechanical applicators, such as the Macroflux® technology (Zosano, USA) or the MicronJet® device (Nanopass technologies, Israel) minimizes confounding factors and allows for a uniform administration [128]. Different microneedle technologies for vaccination are widely investigated in research and clinical trials [16, 97, 133–135]. One system, currently attracting attention, is the Nanopatch™ Technology (Vaxxas, Australia), which is under investigation with an undisclosed vaccine candidate and was given WHO funding for a polio vaccination research project [136–138]. Comparative studies using microneedle

arrays have demonstrated superiority over intradermal or intramuscular vaccination in a number of applications [16, 17, 97]. Comparable or higher antibody titers and Th1/Th2 balanced immune responses were observed [16, 97, 139].
Microporation technologies, most notably microneedles, have become a popular tool for cutaneous vaccination. Over the last decade, production costs of microneedles have been minimized and the reproducibility of insertion has been improved by utilizing mechanical applicators. However, achieving an even coating thickness on solid microneedles, defined breaking points of dissolving microneedles, and, in general, the release of the antigen from the microneedle system are critical parameters [140, 141]. Dissolving or decomposing microneedles are particularly promising technologies if mechanical and physicochemical stability of the biocompatible materials can be ensured.

2.5.2 Thermal microporation technologies

The application of short heat pulses is the basic principle that is shared by all thermal microporation technologies [36]. The heat pulses are applied to locally restricted areas of the superficial skin creating microchannels due to decomposition and vaporization of the treated tissue [142]. The short duration ensures a negligible heat transfer that would otherwise damage the surrounding tissue [36].
At present, three different strategies that utilize this technology have been developed. One method developed by the now defunct Altea Technologies (USA) employed electrically resistive filaments that were heated by a controlled voltage pulse [143, 144]. Another approach, termed radio frequency ablation (RF), is the basis of the ViaDerm™ technology (Transpharma Medical, Israel) [145, 146]. This technique uses an array of microelectrodes to induce ionic vibrations within the surrounding skin cells [147]. Laser-based systems represent the third strategy of thermal microporation. Originally developed for medical surgery [148], these devices use infrared light at $\lambda = 2.94$ µm generated by an Erbium doped yttrium aluminum garnet (Er:YAG) laser [149]. The absorption of the infrared light induces vibrations within the water molecules leading to vaporization [148, 150]. Currently, several laser poration systems are available, such as the P.L.E.A.S.E.® laser device (Precise Laser Epidermal System, Pantec Biosolutions, Liechtenstein) or the Epiture Easytouch™ system (Norwood Abbey, Australia) [36, 151].
Depending on the microporation systems being used and the conditions under which it is used, micron-sized pores of $30 - 200$ µm in diameter and $30 - 200$ µm in depth are created, facilitating vaccine delivery to cutaneous APCs [144, 151, 152]. Several reports

have shown that cutaneous vaccination using laser poration elicits Th2-typed immune responses [149, 153]. Interestingly, it was also observed that T cell polarization can be changed by targeting different skin layers [149]. Moreover, nano- and microparticles can be delivered into the dermis upon laser microporation, indicating the potential for combined cutaneous delivery approaches [154].

Similarly to microneedles, ablative microporation technologies allow the selective targeting of specific skin layers. However, the epidermal and dermal layer thicknesses differ with and between individuals, representing a major challenge for the reproducibility of ablative microporation. In addition, these systems are costly and less convenient due to the requirement for an additional step applying antigen after microporation. These disadvantages are shared by the time-consuming vaccination strategies that use electroporation or sonoporation. The simultaneous application of vaccine is feasible for both systems but it remains unclear how the antigen is affected by the electric current or the ultrasound used to create the micropores.

2.6 Transdermal electroporation

The first investigations using transdermal electroporation (EP) for cutaneous vaccination were conducted in 1999 by Misra et al. [155]. Derived from in vitro transfection experiments of DNA into living cells [156, 157], this technique is used to temporarily disrupt the organized structure of the skin. It was shown that electrical pulses create transient and reversible pores, allowing for the permeation of a drug into the tissue [37, 158]. These local transport regions (LTRs) are generated in the SC by exceeding a predetermined voltage threshold between $50 - 100$ V [158].

Different outcomes of the vaccination efficacy of transdermal EP have been reported. Humoral immune responses to diphtheria toxoid (DT) were lower as compared to intradermal injection, whereas higher antibody titres to myristylated peptide (MYR) were reported [155]. Moreover, equivalent cellular responses were observed for EP and conventional i.d. vaccination [159]. Most notably, Zhao *et al.* reported that electroporation alone promoted the migration of LCs to regional lymph nodes [159]. This indicates the ability of electroporation to serve as a physical adjuvant, an advantage that could be exploited for combined cutaneous vaccination approaches.

2.7 Sonoporation

During the last decade the application of ultrasound, referred to as sonoporation or sonophoresis, was identified as a promising technology for vaccination via the skin [160]. Similarly to transdermal EP, ultrasound at a frequency of 20 kHz creates localized transient regions changing the barrier properties of the skin [161]. Remarkably, the structural changes remain for several hours without inducing severe skin damage [162]. The prolonged permeability allows for the stepwise application of ultrasound and drugs or vaccines. Additionally, a simultaneous application of the vaccine and sonoporation is feasible [163].

The potential of low-frequency ultrasound to induce an immune response in mice has been investigated using tetanus toxoid as a model vaccine [160, 164]. It was shown that the concentration of the chemical enhancer sodium lauryl sulfate (SDS), which is commonly utilized for sonoporation, affects the vaccination outcome [164]. Whereas higher antibody titers were detected using a 0.5 % (w/w) SDS solution during sonication, lower titres were elicited when SDS was not used or when higher concentrations were used [164]. Furthermore, the application of low-frequency ultrasound alone triggered the activation of LCs [160]. Interestingly, even non-disruptive sonication conditions enhance the cytokine production, which could also affect the immune response [165]. As with transdermal EP, sonoporation can be used as a potential adjuvant for cutaneous vaccination.

2.8 Stratum corneum-disruptive approaches

The complete removal of the SC to circumvent its barrier capacity is one of the oldest techniques to enhance transdermal drug delivery and can be achieved by tape stripping or skin abrasion [166]. By directly applying a protein vaccine to the viable epidermis, a Th2-type immune response is elicited [32]. Furthermore, skin abrasion was recently trialed in humans and resulted in the development of a humoral and cellular immunity [167].

Transfollicular delivery of vaccines after hair plucking has been investigated as an alternative strategy of minimally-invasive vaccination. Several pretreatments, such hot or cold waxing, and cyanoacrylate skin surface stripping (CSSS) can be used to create channels in the skin or to induce the hair follicles into growth stage before the application of the vaccine [23, 168]. This approach evokes both humoral and cellular immunity [23].

2.9 Passive targeting strategies

The easiest way to perform cutaneous vaccination is to apply antigen to intact skin. Efficient immunization has been achieved using protein vaccines, although molecules larger than five hundred daltons usually cannot pass the intact SC [169], which would be necessary to directly deliver antigen to dermal APCs. However, Naito et al. reported that ovalbumin applied without adjuvant for more than 16 hours elicited a humoral immune response in mice [170]. Further exploiting this strategy of contact prolongation, hydrogel patch formulations were recently investigated [171]. It was proposed that hydrogel-based approaches facilitate the delivery of antigenic proteins between $45 - 150$ kDa [31]. The cutaneous delivery of vaccines through intact skin has been suggested to occur by three main mechanisms: The generation of a concentration gradient, a widening of intracellular gaps due to hydration, and transfollicular diffusion [31]. Several studies in mice and humans confirmed the successful activation of LCs and the induction of antigen-specific Th2-biased immune responses using hydrogel patches [31, 171, 172]. Moreover, it was demonstrated that antigen-loaded nanoparticles were efficiently delivered via hair follicles in intact skin and provide the ability to stimulate antigen-specific $CD4^+$ and $CD8^+$ T cells [173].

Although these approaches represent the least invasive method of cutaneous vaccination, the induction of a protective immunity comparable to other techniques remains to be proven. It could be expected that even minimally invasive approaches elicit stronger immune responses compared to the passive diffusion strategies. However, there is also the potential to combine passive and minimally invasive technologies.

Vesicular systems act as both chemical adjuvants and physical delivery systems for cutaneous vaccination. They form vehicles for the cutaneous delivery of protein and DNA or RNA vaccines, facilitating passive diffusion into the intact or physically-pretreated skin [174]. Various vesicular systems, reported to elicit immune responses to different extents, have been investigated including charged liposomes [174], niosomes [175], transfersomes [176], ethosomes [177], cubosomes [178] and fusogenic vesosomes, which contain bilayer destabilizing agents [179].These vehicle systems represent a further alternative for DNA- or RNA-based vaccination and can be easily combined with several other active vaccine delivery technologies [174, 179].

Table I.2: Overview of routes that have been investigated for genetic skin vaccination using nucleic acid (NA) vaccines.

Cutaneous vaccination technique	pNA encoded antigen	Adjuvant	Reference
SC-disruptive and passive vaccine delivery techniques			
SC removed	Influenza	+	[34]
	HBsAg	−	[189]
Warm waxing	bGal, OVA	+	[23]
	Bacillus anthracis antigen PA63, HIV-1 gp160	+	[168]
Liposomes	JEV E protein	−	[174]
	HBsAg	−	[188]
Nanoparticles	bGal	+	[83]
Microporation techniques			
Microneedles	Hepatitis C virus protein	−	[187]
Thermal poration	rdAd vector expressing bGal	−	[24]
Powder injection	Influenza	+/−	[122,184,185]
	HBsAg	−	[121]
	GAD65	−	[124]
	Rabies virus	−	[186]
Jet injection	Influenza	−	[180]
	bGal	+/−	[181]
	Plasmodium falciparum circumsporozoite protein	−	[182]
	HIV-1 gp160, p17, p24, p37B, rev, reverse transcriptase	+/−	[183,191,222,223]

2.10 Potential of genetic skin vaccination

Genetic vaccination using DNA or RNA is a novel approach of evoking protective immune responses against infectious diseases. Cutaneous vaccination offers several strategies for introducing antigen-encoding nucleic acid vaccines to cells. Jet injection [180–183], powder injection delivering gold particles with the gene-gun, PMED™ or EPI technique[122, 184–186], microneedles [187], sonoporation [162], cationic liposomes (termed lipoplexes) [174, 188], SC-disruptive approaches [189], and transfollicular delivery routes [23] have been shown to facilitate cutaneous vaccination. Additionally, transdermal electroporation is expected to efficiently enhance skin vaccination with nucleic acid vaccines [190, 191] as electroporation also enhanced the immune response upon intramuscular DNA vaccination [192].

Considering techniques using needles, DNA tattooing is an intensively studied approach for genetic skin vaccination [193]. It has been shown to facilitate the antigen expression

in the dermal tissue and to evoke a humoral and cellular immunity [194–196]. By DNA tattooing, non-professional immune cells provided a superior antigen expression compared to skin APCs [197, 198]. This indicates that keratinocytes might play a major role for the induction of an immune response upon cutaneous vaccination using nucleic acids. Moreover, cross-presentation supported by keratinocytes was found be an important route to prime naïve $CD8^+$ T cells [199, 200]. Regarding the tattooing technique, it remains to be evaluated whether and to which extent the findings can be transferred to needle-free genetic vaccination approaches.

Most of these approaches were originally developed for in vitro transfection of living cells and have now been transferred to antigen delivery [156, 157]. For successful transfection of skin cells it is essential to introduce the DNA or RNA to skin cell nuclei. This is a major challenge as penetration through two barriers, the outer cell membrane and the nuclear membrane, must be achieved. Active delivery approaches, transiently affecting the integrity of living skin cells, could be expected to elicit a superior immunity compared to passive delivery approaches. Further investigation is needed to determine the efficacy of antigen-encoding nucleic acid vaccines compared to conventional immunization using protein antigens, especially focusing on cutaneous delivery approaches. Table I.2 provides an overview of different strategies of skin vaccination that have been exploited for DNA or RNA vaccination.

2.11 Latest trends in cutaneous vaccination

Considering recent developments, microneedles have been particularly in the focus of studies for cutaneous vaccination. It appears that dissolving or biodegradable microneedles are suitable for the delivery of conventional protein antigens as well as for the delivery of amyloid-β in a therapeutic mouse model of Alzheimer's disease [97, 131, 201]. Other advanced approaches use biodegradable solid or microparticle-containing tips whereby antigen or antigen loaded nanoparticles are released upon dissolution and degradation of the microneedle matrix [97, 98]. Vaccine-coated nanopatches and cubosome formulations applied after microneedle pretreatment have also been studied for cutaneous vaccination in mice [15, 178]. In addition, laser microporation and micro- and nanoparticle delivery technologies have been successfully utilized to elicit humoral responses to protein antigens [149, 154, 202]. Other cutaneous delivery strategies, which are particularly attractive for their ease of use, are hydrogel patches and the delivery via hair follicles [168, 203]. Hydrogels based on hyaluronic acid have been shown to elicit an immune response against

protein antigens after application for 24 h [171, 172]. Moreover, liquid DNA vaccine formulations and also nanoparticles have been delivered via hair follicles indicating the importance of this route of cutaneous vaccination [23, 173].
In addition to the previously discussed needle-free vaccination techniques, which are still mainly restricted to research, a variety of conventional and needle-free i.d. vaccination devices are currently under investigation, in clinical trials or are already available on the market [134, 204, 205]. One example having reached market authorization is the BD Soluvia™ device (Becton-Dickinson, USA) [206], which is utilized for seasonal influenza vaccination with the i.d. vaccines Intanza™, IDflu™, and Fluzone™ (Sanofi Pasteur, France) [206, 207]. Also, the microneedle-based MicronJet® system (Nanopass technologies, Israel) has been cleared by the Food and Drug Administration (FDA) and was shown to provide an improved immune response compared to i.d. Mantoux or i.m. injection [133, 134, 208]. Moreover, West Pharmaceutical Services (USA) have developed the syringe West intradermal (ID) adapter, which improves the reproducibility of i.d. vaccine delivery by the Mantoux technique [28]. Intradermal vaccines are developed in order to improve safety and efficacy and for possible dose sparing effects [209]. While many studies report positive results as regards immune responses, in some cases i.d. vaccination has been shown to result in lower antibody titers compared to conventional i.m. vaccination [210].
Although several needle-free jet injector technologies have already been successfully used for i.m., s.c., and also i.d. vaccination, latest-generation DSJIs are currently undergoing clinical trials [211–213]. Only recently, the needle-free i.m. administration of the Afluria® influenza vaccine using the PharmaJet Stratis® (PharmaJet, USA) has been approved by the FDA, although the device itself is licensed since 2011 [214, 215]. However, other jet injector devices have also received FDA clearance before and after, such as the Biojector® 2000, Lectrajet®, Avant Guardian™ 101, Mini-Ject, or the Injex™ system [216–220]. To best of our knowledge, i.d. vaccines administered by needle-free jet injectors are investigated in humans but remain to be licensed for combined use [212, 221–223].

2.12 Conclusion

Vaccination is the most important tool in public health care for combating infectious diseases. However, storage issues for liquid vaccines, the use of syringes and the need for professional assistance limits its convenience and acceptance. Nevertheless, vaccination by conventional needle injection represents the state-of-the-art, is highly reliable and provides good cost-benefit ratio.

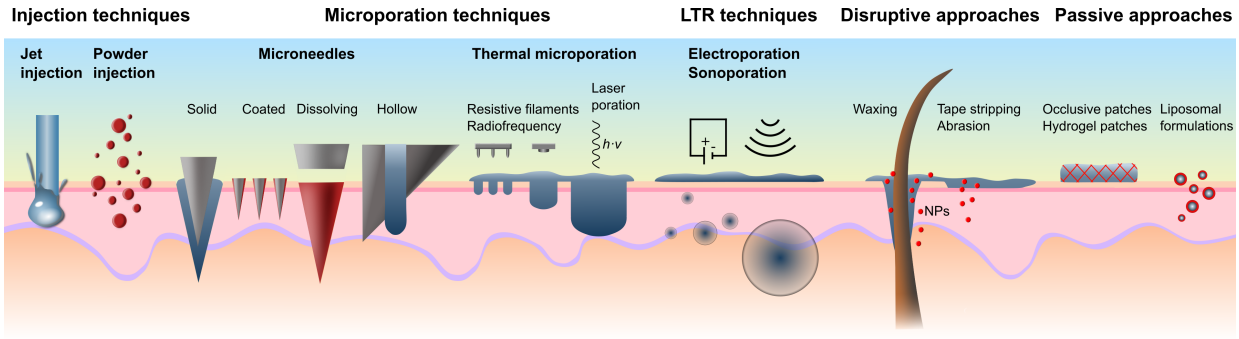

Figure I.3: Active vaccine delivery techniques and passive approaches for cutaneous vaccination. The injection, microporation and LTR techniques are displayed in representative dimensions relative to the epidermal layer of the skin. The dimensions of the devices were exemplarily chosen using typical sizes of the presented systems. LTR - local transport region; NPs - nanoparticles. Adapted from [107]

Cutaneous vaccination is an attractive alternative for conventional vaccination. Many different technologies for cutaneous vaccine delivery are under development each with its own strengths and weaknesses. While the technologies impact on the skin to different extents, the systems are in general non- or minimally invasive. Figure I.3 gives an overview of active and passive techniques for cutaneous vaccination. Needle-free jet and powder injection and microporation technologies overcome the SC using mechanical approaches, whereas electroporation, sonoporation and passive vaccine delivery techniques employ physicochemical strategies. The passive diffusion of antigen upon topical application is the easiest but also most time-intensive route of vaccination, limiting its convenience. Finally, it may be that not all vaccines are suitable for cutaneous vaccination and that it is necessary to evaluate the safety and effectiveness on a case-by-case basis.
The innovative approaches to a vaccination via the skin discussed here are highly promising and safe alternatives to conventional needle injection. The potential that new or different types of immune responses can be stimulated by cutaneous vaccination as opposed to conventional i.m. immunization is also intriguing. Although the production costs of these new vaccines still exceed those of conventional vaccination, the cutaneous vaccine delivery technologies have the potential to minimize vaccine doses and to bypass common vaccination-related limitations.

Bibliography

[1] A. M. Stern, H. Markel, The history of vaccines and immunization: familiar patterns, new challenges, Health Affairs 24 (2005) 611–621.

[2] E. Jenner, An inquiry into the causes and effects of the variolae vaccinae: a disease discovered in some of the western counties of England, particularly Gloucestershire, and known by the name of the Cow Pox, Printed for the Author by Sampson Low, London, 1798.

[3] D. Gothier, Nadelfreie Injektionssysteme, TechnoPharm 2 (2012) 68–76.

[4] S. Pattanayak, D. D. Arora, C. L. Sehgal, N. G. Raghavan, P. K. Topa, Y. K. Subrahmanyam, Comparative studies of smallpox vaccination by the bifurcated needle and rotary lancet techniques, Bull World Health Organ 42 (1970) 305–310.

[5] P. Andersen, T. M. Doherty, The success and failure of BCG - implications for a novel tuberculosis vaccine, Nat Rev Microbiol 3 (2005) 656–662.

[6] BCG vaccine. WHO position paper, Wkly Epidemiol Rec 79 (2004) 25–40.

[7] B. B. Trunz, P. E. M. Fine, C. Dye, Effect of BCG vaccination on childhood tuberculous meningitis and miliary tuberculosis worldwide: a meta-analysis and assessment of cost-effectiveness, Lancet 367 (2006) 1173–1180.

[8] J. F. Nicolas, B. Guy, Intradermal, epidermal and transcutaneous vaccination: from immunology to clinical practice, Expert Rev Vaccines 7 (2008) 1201–1214.

[9] P. Karande, S. Mitragotri, S. M. Pankaj Karande, Transcutaneous immunization: an overview of advantages, disease targets, vaccines, and delivery technologies, Annu Rev Chem Biomol Eng 1 (2010) 175–201.

[10] S. M. Bal, Z. Ding, E. van Riet, W. Jiskoot, J. A. Bouwstra, Advances in transcutaneous vaccine delivery: do all ways lead to Rome?, J Control Release 148 (2010) 266–282.

[11] T. W. Prow, X. Chen, N. A. Prow, G. J. P. Fernando, C. S. E. Tan, A. P. Raphael, D. Chang, M. P. Ruutu, D. W. K. Jenkins, A. Pyke, M. L. Crichton, K. Raphaelli, L. Y. H. Goh, I. H. Frazer, M. S. Roberts, J. Gardner, A. A. Khromykh, A. Suhrbier, R. A. Hall, M. A. F. Kendall, Nanopatch-targeted skin vaccination against West Nile Virus and Chikungunya virus in mice, Small 6 (2010) 1776–1784.

[12] C. Bangert, P. M. Brunner, G. Stingl, Immune functions of the skin, Clin Dermatol 29 (2011) 360–376.

[13] J. Banchereau, R. M. Steinman, Dendritic cells and the control of immunity, Nature

392 (1998) 245–252.

[14] E. Klechevsky, R. Morita, M. Liu, Y. Cao, S. Coquery, L. Thompson-Snipes, F. Briere, D. Chaussabel, G. Zurawski, A. K. Palucka, Y. Reiter, J. Banchereau, H. Ueno, Functional Specializations of Human Epidermal Langerhans Cells and $CD14^+$ Dermal Dendritic Cells, Immunity 29 (2008) 497–510.

[15] G. J. P. Fernando, X. Chen, C. A. Primiero, S. R. Yukiko, E. J. Fairmaid, H. J. Corbett, I. H. Frazer, L. E. Brown, M. A. F. Kendall, Nanopatch targeted delivery of both antigen and adjuvant to skin synergistically drives enhanced antibody responses, J Control Release 159 (2012) 215–221.

[16] Y.-C. Kim, F.-S. Quan, D.-G. Yoo, R. W. Compans, S.-M. Kang, M. R. Prausnitz, Improved influenza vaccination in the skin using vaccine coated microneedles, Vaccine 27 (2009) 6932–6938.

[17] Y. Kim, F. Quan, D. Yoo, R. W. Compans, S. Kang, M. R. Prausnitz, Enhanced Memory Responses to Seasonal H1N1 Influenza Vaccination of the Skin with the Use of Vaccine-Coated Microneedles, J Infect Dis 201 (2010) 190–198.

[18] D. Chen, R. Endres, Y.-F. F. Maa, C. R. Kensil, P. Whitaker-Dowling, A. Trichel, J. S. Youngner, L. G. Payne, Epidermal powder immunization of mice and monkeys with an influenza vaccine, Vaccine 21 (2003) 2830–2836.

[19] R. T. Kenney, S. A. Frech, L. R. Muenz, C. P. Villar, G. M. Glenn, Dose sparing with intradermal injection of influenza vaccine, N Engl J Med 351 (2004) 2295–2301.

[20] I. Leroux-Roels, E. Vets, R. Freese, M. Seiberling, F. Weber, C. Salamand, G. Leroux-Roels, Seasonal influenza vaccine delivered by intradermal microinjection: A randomised controlled safety and immunogenicity trial in adults, Vaccine 26 (2008) 6614–6619.

[21] K. W. Bernard, J. Mallonee, J. C. Wright, F. L. Reid, S. Makintubee, R. A. Parker, D. M. Dwyer, W. G. Winkler, Preexposure immunization with intradermal human diploid cell rabies vaccine. Risks and benefits of primary and booster vaccination, JAMA 257 (1987) 1059–1063.

[22] H. S. Das, P. Sawant, R. G. Shirhatti, K. Vyas, S. Vispute, S. Dhadphale, V. Patrawalla, N. Desai, Efficacy of low dose intradermal hepatitis B vaccine: results of a randomized trial among health care workers, Trop Gastroenterol 23 (2002) 120–121.

[23] G. Xiao, X. Li, A. Kumar, Z. Cui, Transcutaneous DNA immunization following waxing-based hair depilation elicits both humoral and cellular immune responses, Eur J Pharm Biopharm 82 (2012) 212–217.

[24] J. Bramson, K. Dayball, C. Evelegh, Y. H. Wan, D. Page, A. Smith, Enabling topical immunization via microporation: a novel method for pain-free and needle-free delivery of adenovirus-based vaccines, Gene Ther 10 (2003) 251–260.

[25] D. Chen, S. B. Periwal, K. Larrivee, C. Zuleger, C. A. Erickson, R. L. Endres, L. G. Payne, Serum and mucosal immune responses to an inactivated influenza virus vaccine induced by epidermal powder immunization, J Virol 75 (2001) 7956–7965.

[26] H. Yagi, H. Hashizume, T. Horibe, Y. Yoshinari, M. Hata, A. Ohshima, T. Ito, M. Takigawa, A. Shibaki, H. Shimizu, N. Seo, Induction of therapeutically relevant cytotoxic T lymphocytes in humans by percutaneous peptide immunization, Cancer Res 66 (2006) 10136–10144.

[27] I. M. Belyakov, S. A. Hammond, J. D. Ahlers, G. M. Glenn, J. A. Berzofsky, Transcutaneous immunization induces mucosal CTLs and protective immunity by migration of primed skin dendritic cells, J Clin Invest 113 (2004) 998–1007.

[28] B. G. Weniger, M. J. Papania, Alternative vaccine delivery methods, in: S. A. Plotkin, W. A. Orenstein, P. A. Offit (Eds.), Vaccines, 6th ed., Elsevier/Saunders, Philadelphia, 2013, pp. 1200–1231. URL: http://bit.ly/Vaccines6thChap61a. doi:10.1016/B978-1-4557-0090-5.00063-X.

[29] G. M. Glenn, T. Scharton-kersten, R. Vassell, G. R. Matyas, C. R. Alving, Transcutaneous immunization with bacterial ADP-ribosylating exotoxins as antigens and adjuvants, Infect Immun 67 (1999) 1100–1106.

[30] G. M. Glenn, D. N. Taylor, X. Li, S. Frankel, A. Montemarano, C. R. Alving, Transcutaneous immunization: a human vaccine delivery strategy using a patch, Nat Med 6 (2000) 1403–1406.

[31] Y. Ishii, T. Nakae, F. Sakamoto, K. Matsuo, K. Matsuo, Y.-S. Quan, F. Kamiyama, T. Fujita, A. Yamamoto, S. Nakagawa, N. Okada, A transcutaneous vaccination system using a hydrogel patch for viral and bacterial infection, J Control Release 131 (2008) 113–120.

[32] J. Strid, J. Hourihane, I. Kimber, R. Callard, S. Strobel, Disruption of the stratum corneum allows potent epicutaneous immunization with protein antigens resulting in a dominant systemic Th2 response, Eur J Immunol 34 (2004) 2100–2109.

[33] R. McKenzie, A. L. Bourgeois, S. A. Frech, D. C. Flyer, A. Bloom, K. Kazempour, G. M. Glenn, Transcutaneous immunization with the heat-labile toxin (LT) of enterotoxigenic Escherichia coli (ETEC): protective efficacy in a double-blind, placebo-controlled challenge study, Vaccine 25 (2007) 3684–3691.

[34] S. Watabe, K.-Q. Xin, A. Ihata, L.-J. Liu, A. Honsho, I. Aoki, K. Hamajima, B. Wahren, K. Okuda, Protection against influenza virus challenge by topical application of influenza DNA vaccine, Vaccine 19 (2001) 4434–4444.

[35] E. Kis, G. Winter, J. Myschik, Devices for intradermal vaccination, Vaccine 30 (2012) 523–538.

[36] A. K. Banga, Microporation applications for enhancing drug delivery, Expert Opin Drug Deliv 6 (2009) 343–354.

[37] A.-R. Denet, R. Vanbever, V. Préat, Skin electroporation for transdermal and topical delivery, Adv Drug Deliv Rev 56 (2004) 659–674.

[38] S. M. Kaech, E. J. Wherry, R. Ahmed, Effector and memory T-cell differentiation: implications for vaccine development, Nat Rev Immunol 2 (2002) 251–262.

[39] F. Sallusto, J. Geginat, A. Lanzavecchia, Central memory and effector memory T cell subsets: function, generation, and maintenance, Annu Rev Immunol 22 (2004) 745–763.

[40] E. S. Trombetta, I. Mellman, Cell biology of antigen processing in vitro and in vivo, Annu Rev Immunol 23 (2005) 975–1028.

[41] C. Watts, Capture and processing of exogenous antigens for presentation on MHC molecules, Annu Rev Immunol 15 (1997) 821–850.

[42] M.-L. Lin, Y. Zhan, J. A. Villadangos, A. M. Lew, The cell biology of cross-presentation and the role of dendritic cell subsets, Immunol Cell Biol 86 (2008) 353–362.

[43] S. L. Jongbloed, A. J. Kassianos, K. J. McDonald, G. J. Clark, X. Ju, C. E. Angel, C.-J. J. Chen, P. R. Dunbar, R. B. Wadley, V. Jeet, A. J. E. Vulink, D. N. J. Hart, K. J. Radford, Human $CD141^+$ $(BDCA\text{-}3)^+$ dendritic cells (DCs) represent a unique myeloid DC subset that cross-presents necrotic cell antigens, J Exp Med 207 (2010) 1247–1260.

[44] M. Brigl, M. B. Brenner, CD1: antigen presentation and T cell function, Annu Rev Immunol 22 (2004) 817–890.

[45] D. B. Moody, S. A. Porcelli, Intracellular pathways of CD1 antigen presentation, Nat Rev Immunol 3 (2003) 11–22.

[46] D. I. Godfrey, M. Kronenberg, Going both ways: Immune regulation via CD1d-dependent NKT cells, J Clin Invest 114 (2004) 1379–1388.

[47] S. Gillessen, Y. N. Naumov, E. E. S. Nieuwenhuis, M. A. Exley, F. S. Lee, N. Mach, A. D. Luster, R. S. Blumberg, M. Taniguchi, S. P. Balk, J. L. Strominger, G. Dranoff,

S. B. Wilson, CD1d-restricted T cells regulate dendritic cell function and antitumor immunity in a granulocyte-macrophage colony-stimulating factor-dependent fashion, Proc Natl Acad Sci USA 100 (2003) 8874–8879.

[48] M. Peiser, A. Grützkau, R. Wanner, G. Kolde, A. Grutzkau, R. Wanner, G. Kolde, CD1a and CD1c cell sorting yields a homogeneous population of immature human Langerhans cells, J Immunol Methods 279 (2003) 41–53.

[49] M. T. Ochoa, A. Loncaric, S. R. Krutzik, T. C. Becker, R. L. Modlin, "Dermal dendritic cells" comprise two distinct populations: $CD1^+$ dendritic cells and $CD209^+$ macrophages, J Invest Dermatol 128 (2008) 2225–2231.

[50] G. Gerlini, H. P. Hefti, M. Kleinhans, B. J. Nickoloff, G. Burg, F. O. Nestle, Cd1d is expressed on dermal dendritic cells and monocyte-derived dendritic cells, J Invest Dermatol 117 (2001) 576–582.

[51] M. B. Teunissen, M. Haniffa, M. P. Collin, Insight into the immunobiology of human skin and functional specialization of skin dendritic cell subsets to innovate intradermal vaccination design, Curr Top Microbiol Immunol 351 (2012) 25–76.

[52] S. M. Kaech, R. Ahmed, Memory $CD8^+$ T cell differentiation: initial antigen encounter triggers a developmental program in naive cells, Nature Immunol 2 (2001) 415–422.

[53] J. A. Trapani, M. J. Smyth, Functional significance of the perforin/granzyme cell death pathway, Nat Rev Immunol 2 (2002) 735–747.

[54] R. V. Luckheeram, R. Zhou, A. D. Verma, B. Xia, $CD4^+$T cells: differentiation and functions, Clin Dev Immunol 2012 (2012) 925135.

[55] M.-I. Yuseff, P. Pierobon, A. Reversat, A.-M. Lennon-Duménil, How B cells capture, process and present antigens: a crucial role for cell polarity, Nat Rev Immunol 13 (2013) 475–486.

[56] M. G. McHeyzer-Williams, R. Ahmed, B cell memory and the long-lived plasma cell, Curr Opin Immunol 11 (1999) 172–179.

[57] F. Y. Liew, TH1 and TH2 cells: a historical perspective, Nat Rev Immunol 2 (2002) 55–60.

[58] T. L. Stevens, A. Bossie, V. M. Sanders, R. Fernandez-Botran, R. L. Coffman, T. R. Mosmann, E. S. Vitetta, Regulation of antibody isotype secretion by subsets of antigen-specific helper T cells, Nature 334 (1988) 255–258.

[59] L. E. Harrington, R. D. Hatton, P. R. Mangan, H. Turner, T. L. Murphy, K. M. Murphy, C. T. Weaver, Interleukin 17-producing $CD4^+$ effector T cells develop via

a lineage distinct from the T helper type 1 and 2 lineages, Nature Immunol 6 (2005) 1123–1132.

[60] S. Romagnani, E. Maggi, F. Liotta, L. Cosmi, F. Annunziato, Properties and origin of human Th17 cells, Mol Immunol 47 (2009) 3–7.

[61] T. Duhen, R. Geiger, D. Jarrossay, A. Lanzavecchia, F. Sallusto, Production of interleukin 22 but not interleukin 17 by a subset of human skin-homing memory T cells, Nature Immunol 10 (2009) 857–863.

[62] S. Trifari, C. D. Kaplan, E. H. Tran, N. K. Crellin, H. Spits, Identification of a human helper T cell population that has abundant production of interleukin 22 and is distinct from T_H-17, T_H1 and T_H2 cells, Nature Immunol 10 (2009) 864–871.

[63] R. a. Clark, B. Chong, N. Mirchandani, N. K. Brinster, K.-i. Yamanaka, R. K. Dowgiert, T. S. Kupper, The vast majority of CLA^+ T Cells are resident in normal skin, J Immunol 176 (2006) 4431–4439.

[64] F. Ginhoux, L. G. Ng, M. Merad, Understanding the murine cutaneous dendritic cell network to improve intradermal vaccination strategies, in: M. Teunissen (Ed.), Intradermal Immunization. Curr Top Microbiol Immunol, volume 351, 2010/11/09 ed., Springer, Berlin, Heidelberg, 2010, pp. 1–24. URL: http://link.springer.com/10.1007/82_2010_115. doi:10.1007/82_2010_115.

[65] M. Merad, F. Ginhoux, M. Collin, Origin, homeostasis and function of Langerhans cells and other langerin-expressing dendritic cells, Nat Rev Immunol 8 (2008) 935–947.

[66] F. Ginhoux, K. Liu, J. Helft, M. Bogunovic, M. Greter, D. Hashimoto, J. Price, N. Yin, J. Bromberg, S. A. Lira, E. R. Stanley, M. Nussenzweig, M. Merad, The origin and development of nonlymphoid tissue $CD103^+$ DCs, J Exp Med 206 (2009) 3115–3130.

[67] L. S. Bursch, L. Wang, B. Igyarto, A. Kissenpfennig, B. Malissen, D. H. Kaplan, K. A. Hogquist, Identification of a novel population of $Langerin^+$ dendritic cells, J Exp Med 204 (2007) 3147–3156.

[68] S. Henri, L. F. Poulin, S. Tamoutounour, L. Ardouin, M. Guilliams, B. de Bovis, E. Devilard, C. Viret, H. Azukizawa, A. Kissenpfennig, B. Malissen, $CD207^+$ $CD103^+$ dermal dendritic cells cross-present keratinocyte-derived antigens irrespective of the presence of Langerhans cells, J Exp Med 207 (2010) 189–206.

[69] S. Bedoui, P. G. Whitney, J. Waithman, L. Eidsmo, L. Wakim, I. Caminschi, R. S. Allan, M. Wojtasiak, K. Shortman, F. R. Carbone, A. G. Brooks, W. R. Heath,

Cross-presentation of viral and self antigens by skin-derived CD103$^+$ dendritic cells, Nature Immunol 10 (2009) 488–495.

[70] J. B. McLachlan, D. M. Catron, J. J. Moon, M. K. Jenkins, Dendritic cell antigen presentation drives simultaneous cytokine production by effector and regulatory T cells in inflamed skin, Immunity 30 (2009) 277–288.

[71] K. Nagao, F. Ginhoux, W. W. Leitner, S.-I. Motegi, C. L. Bennett, B. E. Clausen, M. Merad, M. C. Udey, Murine epidermal Langerhans cells and langerin-expressing dermal dendritic cells are unrelated and exhibit distinct functions, Proc Natl Acad Sci USA 106 (2009) 3312–3317.

[72] F. O. Nestle, X. G. Zheng, C. B. Thompson, L. A. Turka, B. J. Nickoloff, Characterization of dermal dendritic cells obtained from normal human skin reveals phenotypic and functionally distinctive subsets, J Immunol 151 (1993) 6535–6545.

[73] M. Haniffa, F. Ginhoux, X. N. Wang, V. Bigley, M. Abel, I. Dimmick, S. Bullock, M. Grisotto, T. Booth, P. Taub, C. Hilkens, M. Merad, M. Collin, Differential rates of replacement of human dermal dendritic cells and macrophages during hematopoietic stem cell transplantation, J Exp Med 206 (2009) 371–385.

[74] M. Haniffa, A. Shin, V. Bigley, N. McGovern, P. Teo, P. See, P. S. Wasan, X. N. Wang, F. Malinarich, B. Malleret, A. Larbi, P. Tan, H. Zhao, M. Poidinger, S. Pagan, S. Cookson, R. Dickinson, I. Dimmick, R. F. Jarrett, L. Renia, J. Tam, C. Song, J. Connolly, J. K. Y. Chan, A. Gehring, A. Bertoletti, M. Collin, F. Ginhoux, Human tissues contain CD141^{hi} cross-presenting dendritic cells with functional homology to mouse CD103$^+$ nonlymphoid dendritic cells, Immunity 37 (2012) 60–73.

[75] E. Klechevsky, M. Liu, R. Morita, R. Banchereau, L. Thompson-Snipes, A. K. Palucka, H. Ueno, J. Banchereau, Understanding human myeloid dendritic cell subsets for the rational design of novel vaccines, Hum Immunol 70 (2009) 281–288.

[76] C. Caux, C. Massacrier, B. Vanbervliet, B. Dubois, I. Durand, M. Cella, A. Lanzavecchia, J. Banchereau, CD34$^+$ hematopoietic progenitors from human cord blood differentiate along two independent dendritic cell pathways in response to granulocyte-macrophage colony-stimulating factor plus tumor necrosis factor alpha: II. Functional analysis, Blood 90 (1997) 1458–1470.

[77] J. Seneschal, R. A. Clark, A. Gehad, C. M. Baecher-Allan, T. S. Kupper, Human epidermal Langerhans cells maintain immune homeostasis in skin by activating skin resident regulatory T cells, Immunity 36 (2012) 873–884.

[78] A. M. G. van der Aar, R. de Groot, M. Sanchez-Hernandez, E. W. M. Taanman,

R. A. W. van Lier, M. B. M. Teunissen, E. C. de Jong, M. L. Kapsenberg, Cutting edge: virus selectively primes human langerhans cells for CD70 expression promoting $CD8^+$ T cell responses, J Immunol 187 (2011) 3488–3492.

[79] A. R. Mathers, B. M. Janelsins, J. P. Rubin, O. A. Tkacheva, W. J. Shufesky, S. C. Watkins, A. E. Morelli, A. T. Larregina, Differential capability of human cutaneous dendritic cell subsets to initiate Th17 responses, J Immunol 182 (2009) 921–933.

[80] R. L. Bronaugh, R. F. Stewart, E. R. Congdon, Methods for in vitro percutaneous absorption studies. II. Animal models for human skin, Toxicol Appl Pharmacol 62 (1982) 481–488.

[81] T. Scharton-Kersten, J.-m. Yu, R. Vassell, D. O'Hagan, C. R. Alving, G. M. Glenn, Transcutaneous immunization with bacterial ADP-ribosylating exotoxins, subunits, and unrelated adjuvants, Infect Immun 68 (2000) 5306–5313.

[82] G. M. Glenn, M. Rao, G. R. Matyas, C. R. Alving, Skin immunization made possible by cholera toxin, Nature 391 (1998) 851–852.

[83] Z. Cui, R. J. Mumper, The effect of co-administration of adjuvants with a nanoparticle-based genetic vaccine delivery system on the resulting immune responses, Eur J Pharm Biopharm 55 (2003) 11–18.

[84] G. Mattheolabakis, G. Lagoumintzis, Z. Panagi, E. Papadimitriou, C. D. Partidos, K. Avgoustakis, Transcutaneous delivery of a nanoencapsulated antigen: Induction of immune responses, Int J Pharm 385 (2010) 187–193.

[85] Z. Ding, S. M. Bal, S. Romeijn, G. F. A. Kersten, W. Jiskoot, J. A. Bouwstra, Transcutaneous immunization studies in mice using diphtheria toxoid-loaded vesicle formulations and a microneedle array, Pharm Res 28 (2011) 145–158.

[86] S. A. Hammond, D. Walwender, C. R. Alving, G. M. Glenn, Transcutaneous immunization: T cell responses and boosting of existing immunity, Vaccine 19 (2001) 2701–2707.

[87] R. Kahlon, Y. Hu, C. H. Orteu, A. Kifayet, J. D. Trudeau, R. Tan, J. P. Dutz, Optimization of epicutaneous immunization for the induction of CTL, Vaccine 21 (2003) 2890–2899.

[88] D. Chen, C. A. Erickson, R. L. Endres, S. B. Periwal, Q. Chu, C. Shu, Y.-F. Maa, L. G. Payne, Adjuvantation of epidermal powder immunization, Vaccine 19 (2001) 2908–2917.

[89] R. D. Weeratna, S. R. Makinen, M. J. McCluskie, H. L. Davis, TLR agonists as vaccine adjuvants: comparison of CpG ODN and Resiquimod (R-848), Vaccine 23

(2005) 5263–5270.

[90] C. R. Alving, K. K. Peachman, M. Rao, S. G. Reed, Adjuvants for human vaccines, Curr Opin Immunol 24 (2012) 310–315.

[91] S. Bauer, C. J. Kirschning, H. Häcker, V. Redecke, S. Hausmann, S. Akira, H. Wagner, G. B. Lipford, Human TLR9 confers responsiveness to bacterial DNA via species-specific CpG motif recognition, Proc Natl Acad Sci USA 98 (2001) 9237–42.

[92] F. Takeshita, C. A. Leifer, I. Gursel, K. J. Ishii, S. Takeshita, M. Gursel, D. M. Klinman, Cutting edge: role of Toll-like receptor 9 in CpG DNA-induced activation of human cells, J Immunol 167 (2001) 3555–3558.

[93] S. Akira, K. Takeda, T. Kaisho, Toll-like receptors: critical proteins linking innate and acquired immunity, Nature Immunol 2 (2001) 675–680.

[94] M. Diwan, M. Tafaghodi, J. Samuel, Enhancement of immune responses by co-delivery of a CpG oligodeoxynucleotide and tetanus toxoid in biodegradable nanospheres, J Control Release 85 (2002) 247–262.

[95] R. Schirmbeck, J. Reimann, Modulation of gene-gun-mediated Th2 immunity to hepatitis B surface antigen by bacterial CpG motifs or IL-12, Intervirology 44 (2001) 115–123.

[96] T. Warger, G. Rechtsteiner, B. Schmid, P. Osterloh, H. Schild, M. P. Radsak, Transcutaneous immunization with imiquimod is amplified by CD40 ligation and results in sustained cytotoxic T-lymphocyte activation and tumor protection, Clin Rev Allergy Immunol 32 (2007) 57–65.

[97] P. C. DeMuth, Y. Min, D. J. Irvine, P. T. Hammond, Implantable silk composite microneedles for programmable vaccine release kinetics and enhanced immunogenicity in transcutaneous immunization, Adv Healthc Mater 3 (2014) 47–58.

[98] P. C. Demuth, W. F. Garcia-Beltran, M. L. Ai-Ling, P. T. Hammond, D. J. Irvine, Composite dissolving microneedles for coordinated control of antigen and adjuvant delivery kinetics in transcutaneous vaccination, Adv Funct Mater 23 (2013) 161–172.

[99] P. Stein, G. Rechtsteiner, T. Warger, T. Bopp, T. Fuhr, S. Prufer, H.-C. Probst, M. Stassen, P. Langguth, H. Schild, M. P. Radsak, UV exposure boosts transcutaneous immunization and improves tumor immunity: cytotoxic T-cell priming through the skin, J Invest Dermatol 131 (2011) 211–219.

[100] H. Slade, M. Owens, M. Tomai, R. Miller, Imiquimod 5% cream (Aldara™), Exp Opin Invest Drugs 7 (1998) 437–449.

[101] M. J. Choi, H. I. Maibach, Topical vaccination of DNA antigens: topical delivery of

DNA antigens, Skin Pharmacol Appl Skin Physiol 16 (2003) 271–282.

[102] A. K. Andrianov, D. P. DeCollibus, H. A. Gillis, H. H. Kha, A. Marin, M. R. Prausnitz, L. A. Babiuk, H. Townsend, G. Mutwiri, Poly[di(carboxylatophenoxy)phosphazene] is a potent adjuvant for intradermal immunization, Proc Natl Acad Sci USA 106 (2009) 18936–18941.

[103] R. J. Brindle, C. A. Morris, R. Berger, J. B. Kurtz, Inadequate response to intradermal hepatitis A vaccine, Vaccine 12 (1994) 483–484.

[104] U. Carlsson, L. Brudin, I. Eliasson, B. G. Hansson, Hepatitis A vaccination by intracutaneous low dose administration: a less expensive alternative, Scand J Infect Dis 28 (1996) 435–438.

[105] M. Vogelbruch, B. Nuss, M. Korner, A. Kapp, P. Kiehl, W. Bohm, Aluminium-induced granulomas after inaccurate intradermal hyposensitization injections of aluminium-adsorbed depot preparations, Allergy 55 (2000) 883–887.

[106] J. Canter, An outbreak of hepatitis b associated with jet injections in a weight reduction clinic, Arch Intern Med 150 (1990) 1923.

[107] S. Mitragotri, Immunization without needles, Nat Rev Immunol 5 (2005) 905–916.

[108] A. Arora, M. R. Prausnitz, S. Mitragotri, Micro-scale devices for transdermal drug delivery, Int J Pharm 364 (2008) 227–236.

[109] J. Baxter, S. Mitragotri, Jet-induced skin puncture and its impact on needle-free jet injections: experimental studies and a predictive model, J Control Release 106 (2005) 361–373.

[110] S. Mitragotri, Current status and future prospects of needle-free liquid jet injectors, Nature Reviews Drug Discovery 5 (2006) 543–548.

[111] J. C. Stachowiak, T. H. Li, A. Arora, S. Mitragotri, D. A. Fletcher, Dynamic control of needle-free jet injection, J Control Release 135 (2009) 104–112.

[112] A. Arora, I. Hakim, J. Baxter, R. Rathnasingham, R. Srinivasan, D. A. Fletcher, S. Mitragotri, Needle-free delivery of macromolecules across the skin by nanoliter-volume pulsed microjets, Proc Natl Acad Sci USA 104 (2007) 4255–4260.

[113] J. C. Stachowiak, M. G. von Muhlen, T. H. Li, L. Jalilian, S. H. Parekh, D. A. Fletcher, Piezoelectric control of needle-free transdermal drug delivery, J Control Release 124 (2007) 88–97.

[114] C. Condon, S. C. Watkins, C. M. Celluzzi, K. Thompson, L. D. Falo Jr., DNA-based immunization by in vivo transfection of dendritic cells, Nat Med 2 (1996) 1122–1128.

[115] M. Kendall, T. Mitchell, P. Wrighton-Smith, Intradermal ballistic delivery of micro-

particles into excised human skin for pharmaceutical applications, J Biomech 37 (2004) 1733–1741.

[116] D. Chen, R. L. Endres, C. A. Erickson, K. F. Weis, M. W. McGregor, Y. Kawaoka, L. G. Payne, Epidermal immunization by a needle-free powder delivery technology: immunogenicity of influenza vaccine and protection in mice, Nat Med 6 (2000) 1187–1190.

[117] W. J. Mulholland, M. A. F. Kendall, N. White, B. J. Bellhouse, Characterization of powdered epidermal vaccine delivery with multiphoton microscopy, Phys Med Biol 49 (2004) 5043–5058.

[118] M. A. F. Kendall, The delivery of particulate vaccines and drugs to human skin with a practical, hand-held shock tube-based system, Shock Waves 12 (2002) 23–30.

[119] J. Liu, N. C. Hogan, I. W. Hunter, Intradermal needle-free powdered drug injection by a helium-powered device, Conf Proc IEEE Eng Med Biol Soc 2012 (2012) 2068–2071.

[120] D. Chen, Y.-F. Maa, J. R. Haynes, Needle-free epidermal powder immunization, Exp Rev Vaccines 1 (2002) 265–276.

[121] M. J. Roy, M. S. Wu, L. J. Barr, J. T. Fuller, L. G. Tussey, S. Speller, J. Culp, J. K. Burkholder, W. F. Swain, R. M. Dixon, G. Widera, R. Vessey, A. King, G. Ogg, A. Gallimore, J. R. Haynes, D. H. Fuller, Induction of antigen-specific $CD8^+$ T cells, T helper cells, and protective levels of antibody in humans by particle-mediated administration of a hepatitis B virus DNA vaccine, Vaccine 19 (2000) 764–778.

[122] P. T. Loudon, E. J. Yager, D. T. Lynch, A. Narendran, C. Stagnar, A. M. Franchini, J. T. Fuller, P. A. White, J. Nyuandi, C. A. Wiley, M. Murphey-Corb, D. H. Fuller, GM-CSF increases mucosal and systemic immunogenicity of an H1N1 influenza DNA vaccine administered into the epidermis of non-human primates, PLoS ONE 5 (2010) e11021.

[123] D. Chen, C. Zuleger, Q. Chu, Y.-F. Maa, J. Osorio, L. G. Payne, Epidermal powder immunization with a recombinant HIV gp120 targets Langerhans cells and induces enhanced immune responses, AIDS Res Hum Retroviruses 18 (2002) 715–722.

[124] K. S. Goudy, B. Wang, R. Tisch, Gene gun-mediated DNA vaccination enhances antigen-specific immunotherapy at a late preclinical stage of type 1 diabetes in nonobese diabetic mice, Clin Immunol 129 (2008) 49–57.

[125] Y. Deng, R. Mathaes, G. Winter, J. Engert, Encapsulation of antigen-loaded silica nanoparticles into microparticles for intradermal powder injection, Eur J Pharm Sci

63 (2014) 154–166.

[126] M. R. Prausnitz, R. Langer, Transdermal drug delivery, Nat Biotech 26 (2008) 1261–1268.

[127] Y.-C. Kim, J.-H. Park, M. R. Prausnitz, Microneedles for drug and vaccine delivery, Adv Drug Deliv Rev 64 (2012) 1547–1568.

[128] R. F. Donnelly, T. R. Raj Singh, A. D. Woolfson, Microneedle-based drug delivery systems: microfabrication, drug delivery, and safety, Drug Deliv 17 (2010) 187–207.

[129] M. R. Prausnitz, Microneedles for transdermal drug delivery, Adv Drug Deliv Rev 56 (2004) 581–587.

[130] Y. Hiraishi, T. Nakagawa, Y.-S. Quan, F. Kamiyama, S. Hirobe, N. Okada, S. Nakagawa, Performance and characteristics evaluation of a sodium hyaluronate-based microneedle patch for a transcutaneous drug delivery system, Int J Pharm 441 (2012) 570–579.

[131] S. Hirobe, H. Azukizawa, K. Matsuo, Y. Zhai, Y.-S. Quan, F. Kamiyama, H. Suzuki, I. Katayama, N. Okada, S. Nakagawa, Development and clinical study of a self-dissolving microneedle patch for transcutaneous immunization device, Pharm Res 30 (2013) 2664–2674.

[132] Z. Ding, F. J. Verbaan, M. Bivas-Benita, L. Bungener, A. Huckriede, D. J. van den Berg, G. Kersten, J. A. Bouwstra, Microneedle arrays for the transcutaneous immunization of diphtheria and influenza in BALB/c mice, J Control Release 136 (2009) 71–78.

[133] Y. Levin, E. Kochba, R. Kenney, Clinical evaluation of a novel microneedle device for intradermal delivery of an influenza vaccine: are all delivery methods the same?, Vaccine 32 (2014) 4249–4252.

[134] The University of Hong Kong, Dose Sparing Intradermal S-OIV H1N1 Influenza Vaccination Device. Bethesda, MD: National Library of Medicine (US), 2010. URL: `https://clinicaltrials.gov/ct2/show/NCT01049490`, [accessed 2015-01-08].

[135] The University of Hong Kong, VZV Vaccine for Hematopoietic Stem Cell Transplantation (VZIDST). Bethesda, MD: National Library of Medicine (US), 2014. URL: `https://clinicaltrials.gov/ct2/show/NCT02329457`, [accessed 2015-01-08].

[136] S. Elvidge, Merck tests needle-free vaccines, Nat Biotech 30 (2012) 1155.

[137] Vaxxas Inc., Vaxxas initiates program with Merck to optimize delivery of next generation vaccines utilizing novel mechanism for immune system activation. Cambridge, MA, USA/Brisbane, QLD, Australia, 2012. URL:

http://www.vaxxas.com/news/vaxxas-initiates-program-with-merck-to-optimize-delivery-of-next-generation-vaccines, [accessed 2013-03-05].

[138] Vaxxas Inc., Vaxxas initiates research project on advancing next generation technology for polio vaccine delivery. Cambridge, MA, USA/Brisbane, QLD, Australia, 2014. URL: http://www.vaxxas.com/news/vaxxas-initiates-research-project-on-advancing-next-generation-technology-for-polio-vaccine-delivery/, [accessed 2014-10-04].

[139] Q. Zhu, V. G. Zarnitsyn, L. Ye, Z. Wen, Y. Gao, L. Pan, I. Skountzou, H. S. Gill, M. R. Prausnitz, C. Yang, R. W. Compans, Immunization by vaccine-coated microneedle arrays protects against lethal influenza virus challenge, Proc Natl Acad Sci USA 106 (2009) 7968–7973.

[140] H. S. Gill, M. R. Prausnitz, Coated microneedles for transdermal delivery, J Control Release 117 (2007) 227–237.

[141] J. W. Lee, J.-H. Park, M. R. Prausnitz, Dissolving microneedles for transdermal drug delivery, Biomaterials 29 (2008) 2113–2124.

[142] J.-H. Park, J.-W. Lee, Y.-C. Kim, M. R. Prausnitz, The effect of heat on skin permeability, Int J Pharm 359 (2008) 94–103.

[143] J. A. Eppstein, Microporation of tissue for delivery of bioactive agents. United States: Altea Technologies, Inc., assignee. Pat. US6527716, 2003.

[144] A. V. Badkar, A. M. Smith, J. A. Eppstein, A. K. Banga, Transdermal delivery of interferon alpha-2B using microporation and iontophoresis in hairless rats, Pharm Res 24 (2007) 1389–1395.

[145] A. C. Sintov, I. Krymberk, D. Daniel, T. Hannan, Z. Sohn, G. Levin, Radiofrequency-driven skin microchanneling as a new way for electrically assisted transdermal delivery of hydrophilic drugs, J Control Release 89 (2003) 311–320.

[146] G. Levin, A. Gershonowitz, H. Sacks, M. Stern, A. Sherman, S. Rudaev, I. Zivin, M. Phillip, Transdermal delivery of human growth hormone through RF-microchannels, Pharm Res 22 (2005) 550–555.

[147] Z. Avrahami, Transdermal drug delivery and analyte extraction. United States: Elecsys Ltd., assignee. Pat. US6148232, 2000.

[148] J. T. Walsh, T. F. Deutsch, Er:YAG laser ablation of tissue: measurement of ablation rates, Lasers Surg Med 9 (1989) 327–337.

[149] R. Weiss, M. Hessenberger, S. Kitzmueller, D. Bach, E. E. Weinberger, W. D. Krautgartner, C. Hauser-Kronberger, B. Malissen, C. Boehler, Y. N. Kalia, J. Thalhamer,

S. Scheiblhofer, Transcutaneous vaccination via laser microporation, J Control Release 162 (2012) 391–399.

[150] K. L. Vodop'yanov, Bleaching of water by intense light at the maximum of the λ= 3 μm absorption band, JETP 70 (1990) 114–121.

[151] J. Yu, D. R. Kalaria, Y. N. Kalia, Erbium:YAG fractional laser ablation for the percutaneous delivery of intact functional therapeutic antibodies, J Control Release 156 (2011) 53–59.

[152] M. Stern, G. Levin, Transdermal delivery system for dried particulate or lyophilized medications. United States: TransPharma Medical Ltd., assignee. Pat. US7363075, 2008.

[153] M. Hessenberger, R. Weiss, E. E. Weinberger, C. Boehler, J. Thalhamer, S. Scheiblhofer, Transcutaneous delivery of CpG-adjuvanted allergen via laser-generated micropores, Vaccine 31 (2013) 3427–3434.

[154] E. A. Genina, A. N. Bashkatov, L. E. Dolotov, G. N. Maslyakova, V. I. Kochubey, I. V. Yaroslavsky, G. B. Altshuler, V. V. Tuchin, Transcutaneous delivery of micro- and nanoparticles with laser microporation, J Biomed Opt 18 (2013) 111406.

[155] A. Misra, S. Ganga, P. Upadhyay, Needle-free, non-adjuvanted skin immunization by electroporation-enhanced transdermal delivery of diphtheria toxoid and a candidate peptide vaccine against hepatitis B virus, Vaccine 18 (1999) 517–523.

[156] E. Neumann, M. Schaefer-Ridder, Y. Wang, P. H. Hofschneider, Gene transfer into mouse lyoma cells by electroporation in high electric fields, EMBO J 1 (1982) 841–845.

[157] G. Chu, H. Hayakawa, P. Berg, Electroporation for the efficient transfection of mammalian cells with DNA, Nucleic Acids Res 15 (1987) 1311–1326.

[158] U. F. Pliquett, R. Vanbever, V. Preat, J. C. Weaver, Local transport regions (LTRs) in human stratum corneum due to long and short 'high voltage' pulses, Bioeletrochem Bioenerg 47 (1998) 151–161.

[159] Y. L. Zhao, S. N. Murthy, M. H. Manjili, L. J. Guan, A. Sen, S. W. Hui, Induction of cytotoxic T-lymphocytes by electroporation-enhanced needle-free skin immunization, Vaccine 24 (2006) 1282–1290.

[160] A. Tezel, S. Paliwal, Z. Shen, S. Mitragotri, Low-frequency ultrasound as a transcutaneous immunization adjuvant, Vaccine 23 (2005) 3800–3807.

[161] J. I. V. Kushner, D. Kim, P. T. C. So, D. Blankschtein, R. S. Langer, Dual-channel two-photon microscopy study of transdermal transport in skin treated with low-

frequency ultrasound and a chemical enhancer, J Invest Dermatol 127 (2007) 2832–2846.

[162] A. Tezel, S. Dokka, S. Kelly, G. E. Hardee, S. Mitragotri, Topical delivery of antisense oligonucleotides using low-frequency sonophoresis, Pharm Res 21 (2004) 2219–2225.

[163] S. Mitragotri, D. Blankschtein, R. Langer, Transdermal drug delivery using low-frequency sonophoresis, Pharm Res 13 (1996) 411–420.

[164] A. Dahlan, H. O. Alpar, P. Stickings, D. Sesardic, S. Murdan, Transcutaneous immunisation assisted by low-frequency ultrasound, Int J Pharm 368 (2009) 123–128.

[165] E. H. Choi, M. J. Kim, B.-I. Yeh, S. K. Ahn, S. H. Lee, Iontophoresis and sonophoresis stimulate epidermal cytokine expression at energies that do not provoke a barrier abnormality: lamellar body secretion and cytokine expression are linked to altered epidermal calcium levels, J Invest Dermatol 121 (2003) 1138–1144.

[166] B. W. Barry, Novel mechanisms and devices to enable successful transdermal drug delivery, Eur J Pharm Sci 14 (2001) 101–114.

[167] E. H. Eypper, P. V. Johnson, E. I. Purro, E. L. Hohmann, Transcutaneous immunization of healthy volunteers with an attenuated Listeria monocytogenes vaccine strain and cholera toxin adjuvant, Vaccine 31 (2013) 3257–3261.

[168] B. R. Sloat, K. Kiguchi, G. Xiao, J. DiGiovanni, W. Maury, Z. Cui, Transcutaneous DNA immunization following waxing-based hair depilation, J Control Release 157 (2012) 94–102.

[169] J. D. Bos, M. M. H. M. Meinardi, The 500 Dalton rule for the skin penetration of chemical compounds and drugs, Exp Dermatol 9 (2000) 165–169.

[170] S. Naito, J.-i. Maeyama, T. Mizukami, M. Takahashi, I. Hamaguchi, K. Yamaguchi, Transcutaneous immunization by merely prolonging the duration of antigen presence on the skin of mice induces a potent antigen-specific antibody response even in the absence of an adjuvant, Vaccine 25 (2007) 8762–8770.

[171] K. Matsuo, Y. Ishii, Y. Kawai, Y. Saiba, Y. S. Quan, F. Kamiyama, S. Hirobe, N. Okada, S. Nakagawa, Analysis of transcutaneous antigenic protein delivery by a hydrogel patch formulation, J Pharm Sci 102 (2013) 1936–1947.

[172] S. Hirobe, K. Matsuo, Y.-S. Quan, F. Kamiyama, H. Morito, H. Asada, Y. Takaya, Y. Mukai, N. Okada, S. Nakagawa, Clinical study of transcutaneous vaccination using a hydrogel patch for tetanus and diphtheria, Vaccine 30 (2012) 1847–1854.

[173] A. Mittal, A. S. Raber, U. F. Schaefer, S. Weissmann, T. Ebensen, K. Schulze, C. A. Guzmán, C.-M. Lehr, S. Hansen, Non-invasive delivery of nanoparticles to hair follicles: A perspective for transcutaneous immunization, Vaccine 31 (2013) 3442–3451.

[174] J.-Y. Cheng, H.-N. Huang, W.-C. Tseng, T.-L. Li, Y.-L. Chan, K.-C. Cheng, C.-J. Wu, Transcutaneous immunization by lipoplex-patch based DNA vaccines is effective vaccination against Japanese encephalitis virus infection, J Control Release 135 (2009) 242–249.

[175] P. N. Gupta, V. Mishra, A. Rawat, P. Dubey, S. Mahor, S. Jain, D. P. Chatterji, S. P. Vyas, Non-invasive vaccine delivery in transfersomes, niosomes and liposomes: a comparative study, Int J Pharm 293 (2005) 73–82.

[176] D. Mishra, V. Dubey, A. Asthana, D. K. Saraf, N. K. Jain, Elastic liposomes mediated transcutaneous immunization against Hepatitis B, Vaccine 24 (2006) 4847–4855.

[177] D. Mishra, P. K. Mishra, V. Dubey, M. Nahar, S. Dabadghao, N. K. Jain, Systemic and mucosal immune response induced by transcutaneous immunization using Hepatitis B surface antigen-loaded modified liposomes, Eur J Pharm Sci 33 (2008) 424–433.

[178] T. Rattanapak, J. Birchall, K. Young, M. Ishii, I. Meglinski, T. Rades, S. Hook, Transcutaneous immunization using microneedles and cubosomes: mechanistic investigations using optical coherence tomography and two-photon microscopy, J Control Release 172 (2013) 894–903.

[179] V. Mishra, S. Mahor, A. Rawat, P. Dubey, P. N. Gupta, P. Singh, S. P. Vyas, Development of novel fusogenic vesosomes for transcutaneous immunization, Vaccine 24 (2006) 5559–5570.

[180] J. Haensler, C. Verdelet, V. Sanchez, Y. Girerd-Chambaz, A. Bonnin, E. Trannoy, S. Krishnan, P. Meulien, Intradermal DNA immunization by using jet-injectors in mice and monkeys, Vaccine 17 (1999) 628–638.

[181] Z. Cui, L. Baizer, R. J. Mumper, Intradermal immunization with novel plasmid DNA-coated nanoparticles via a needle-free injection device, J Biotechnol 102 (2003) 105–115.

[182] J. E. Epstein, E. J. Gorak, Y. Charoenvit, R. Wang, N. Freydberg, O. Osinowo, T. L. Richie, E. L. Stoltz, F. Trespalacios, J. Nerges, J. Ng, V. Fallarme-Majam, E. Abot, L. Goh, S. Parker, S. Kumar, R. C. Hedstrom, J. Norman, R. Stout, S. L. Hoffman, Safety, tolerability, and lack of antibody responses after administration of a

PfCSP DNA malaria vaccine via needle or needle-free jet injection, and comparison of intramuscular and combination intramuscular/intradermal routes, Hum Gene Ther 13 (2002) 1551–1560.

[183] A. Bråve, K. Ljungberg, A. Boberg, E. Rollman, M. Isaguliants, B. Lundgren, P. Blomberg, J. Hinkula, B. Wahren, Multigene/multisubtype HIV-1 vaccine induces potent cellular and humoral immune responses by needle-free intradermal delivery, Mol Ther 12 (2005) 1197–1205.

[184] M. D. Macklin, D. McCabe, M. W. McGregor, V. Neumann, T. Meyer, R. Callan, V. S. Hinshaw, W. F. Swain, Immunization of pigs with a particle-mediated DNA vaccine to influenza A virus protects against challenge with homologous virus, J Virol 72 (1998) 1491–1496.

[185] P. Dégano, D. F. Sarphie, C. R. M. Bangham, Intradermal DNA immunization of mice against influenza A virus using the novel PowderJect system, Vaccine 16 (1998) 394–8.

[186] D. L. Lodmell, M. J. Parnell, J. R. Bailey, L. C. Ewalt, C. A. Hanlon, One-time gene gun or intramuscular rabies DNA vaccination of non-human primates: comparison of neutralizing antibody responses and protection against rabies virus 1 year after vaccination, Vaccine 20 (2001) 838–844.

[187] H. S. Gill, J. Soderholm, M. R. Prausnitz, M. Sallberg, J. Söderholm, M. R. Prausnitz, M. Sällberg, J. Soderholm, M. R. Prausnitz, M. Sallberg, Cutaneous vaccination using microneedles coated with hepatitis C DNA vaccine, Gen Ther 17 (2010) 811–814.

[188] J. Wang, J.-h. Hu, F.-q. Li, G.-z. Liu, Q.-g. Zhu, J.-y. Liu, H.-j. Ma, C. Peng, F.-g. Si, Strong cellular and humoral immune responses induced by transcutaneous immunization with HBsAg DNA-cationic deformable liposome complex, Exp Dermatol 16 (2007) 724–729.

[189] J. A. Mikszta, J. B. Alarcon, J. M. Brittingham, D. E. Sutter, R. J. Pettis, N. G. Harvey, Improved genetic immunization via micromechanical disruption of skin-barrier function and targeted epidermal delivery, Nat Med 8 (2002) 415–419.

[190] N. Y. Sardesai, D. B. Weiner, Electroporation delivery of DNA vaccines: prospects for success, Curr Opin Immunol 23 (2011) 421–429.

[191] D. Hallengärd, A. Bråve, M. Isaguliants, P. Blomberg, J. Enger, R. Stout, A. King, B. Wahren, A combination of intradermal jet-injection and electroporation overcomes in vivo dose restriction of DNA vaccines, Genet Vaccines Ther 10 (2012) 5.

[192] M. Selby, C. Goldbeck, T. Pertile, R. Walsh, J. Ulmer, Enhancement of DNA vaccine potency by electroporation in vivo, J Biotechnol 83 (2000) 147–152.

[193] K. Oosterhuis, P. Ohlschläger, J. H. van den Berg, M. Toebes, R. Gomez, T. N. Schumacher, J. B. Haanen, Preclinical development of highly effective and safe DNA vaccines directed against HPV 16 E6 and E7, Int J Cancer 129 (2011) 397–406.

[194] A. D. Bins, A. Jorritsma, M. C. Wolkers, C.-F. Hung, T.-C. Wu, T. N. M. Schumacher, J. B. A. G. Haanen, A rapid and potent DNA vaccination strategy defined by in vivo monitoring of antigen expression, Nat Med 11 (2005) 899–904.

[195] D. Pokorna, I. Rubio, M. Müller, DNA-vaccination via tattooing induces stronger humoral and cellular immune responses than intramuscular delivery supported by molecular adjuvants, Genet Vaccines Ther 6 (2008) 4.

[196] B. E. Verstrepen, A. D. Bins, C. S. Rollier, P. Mooij, G. Koopman, N. C. Sheppard, Q. Sattentau, R. Wagner, H. Wolf, T. N. M. Schumacher, J. L. Heeney, J. B. A. G. Haanen, Improved HIV-1 specific T-cell responses by short-interval DNA tattooing as compared to intramuscular immunization in non-human primates, Vaccine 26 (2008) 3346–3351.

[197] A. Porgador, K. R. Irvine, A. Iwasaki, B. H. Barber, N. P. Restifo, R. N. Germain, Predominant role for directly transfected dendritic cells in antigen presentation to $CD8^+$ T cells after gene gun immunization, J Exp Med 188 (1998) 1075–1082.

[198] J. H. van den Berg, B. Nuijen, J. H. Beijnen, A. Vincent, H. van Tinteren, J. Kluge, L. A. E. Woerdeman, W. E. Hennink, G. Storm, T. N. Schumacher, J. B. A. G. Haanen, Optimization of intradermal vaccination by DNA tattooing in human skin, Hum Gene Ther 20 (2009) 181–189.

[199] J. H. Cho, J. W. Youn, Y. C. Sung, Cross-priming as a predominant mechanism for inducing $CD8^+$ T cell responses in gene gun DNA immunization, J Immunol 167 (2001) 5549–5557.

[200] A. D. Bins, M. C. Wolkers, M. D. van den Boom, J. B. A. G. Haanen, T. N. M. Schumacher, In vivo antigen stability affects DNA vaccine immunogenicity, J Immunol 179 (2007) 2126–2133.

[201] K. Matsuo, H. Okamoto, Y. Kawai, Y.-S. Quan, F. Kamiyama, S. Hirobe, N. Okada, S. Nakagawa, Vaccine efficacy of transcutaneous immunization with amyloid β using a dissolving microneedle array in a mouse model of Alzheimer's disease, J Neuroimmunol 266 (2014) 1–11.

[202] Y. G. Bachhav, A. Heinrich, Y. N. Kalia, Controlled intra- and transdermal protein

delivery using a minimally invasive Erbium:YAG fractional laser ablation technology, Eur J Pharm Biopharm 84 (2013) 355–364.

[203] K. Matsuo, Y. Ishii, Y.-S. S. Quan, F. Kamiyama, Y. Mukai, Y. Yoshioka, N. Okada, S. Nakagawa, Transcutaneous vaccination using a hydrogel patch induces effective immune responses to tetanus and diphtheria toxoid in hairless rat, J Control Release 149 (2011) 15–20.

[204] P. van Damme, A study to assess the acceptability and usability of a new device for intradermal vaccination. Bethesda, MD: National Library of Medicine (US), 2013. URL: https://clinicaltrials.gov/ct2/show/NCT01963338, [accessed 2015-03-05].

[205] Immunomic Therapeutics Inc., A safety and immunogenicity phase Ic study of CryJ2 -DNA-LAMP plasmid vaccine for assessment of intradermal (ID) route of administration using the Biojector 2000 device. Bethesda, MD: National Library of Medicine (US), 2014. URL: https://clinicaltrials.gov/ct2/show/NCT02146781, [accessed 2015-03-05].

[206] G. Icardi, A. Orsi, A. Ceravolo, F. Ansaldi, Current evidence on intradermal influenza vaccines administered by Soluvia licensed micro injection system, Hum Vaccin Immunother 8 (2012) 67–75.

[207] Medgadget LLC., Sanofi Pasteur's Fluzone intradermal flu vaccine approved in U.S., 2011. URL: https://www.medgadget.com/2011/05/sanofi_pasteurs_fluzone_intradermal_flu_vaccine_approved_in_us.html, [accessed 2014-10-17].

[208] P. van Damme, F. Oosterhuis-Kafeja, M. van der Wielen, Y. Almagor, O. Sharon, Y. Levin, Safety and efficacy of a novel microneedle device for dose sparing intradermal influenza vaccination in healthy adults, Vaccine 27 (2009) 454–459.

[209] D. Zehrung, C. Jarrahian, A. Wales, Intradermal delivery for vaccine dose sparing: overview of current issues, Vaccine 31 (2013) 3392–3395.

[210] A. J. Mohammed, S. AlAwaidy, S. Bawikar, P. J. Kurup, E. Elamir, M. M. A. Shaban, S. M. Sharif, H. G. A. M. van der Avoort, M. A. Pallansch, P. Malankar, A. Burton, M. Sreevatsava, R. W. Sutter, Fractional doses of inactivated poliovirus vaccine in Oman, N Engl J Med 362 (2010) 2351–2359.

[211] PharmaJet Inc., Inactivated influenza via jet injection (IIJI). Bethesda, MD: National Library of Medicine (US), 2014. URL: https://clinicaltrials.gov/show/NCT02290691, [accessed 2015-01-08].

[212] Muhimbili University of Health and Allied Sciences, A phase II trial to assess the safety and immunogenicity of DNA priming administered by the ID Zetajet® with or without ID Derma Vax™ electroporation followed by IM MVA boosting in healthy volunteers in Tanzania and Mozambique (TaMoVac II), 2012. URL: https://clinicaltrials.gov/ct2/show/NCT01697007, [accessed 2015-01-08].

[213] Serum Institute of India Limited, Safety & immunogenicity of MMR vaccine by DSJI to that by needle-syringe in 15-18 months old children. Bethesda, MD: National Library of Medicine (US), 2014. URL: https://clinicaltrials.gov/ct2/show/NCT02253407, [accessed 2015-03-05].

[214] PharmaJet Inc., FDA approves use of AFLURIA®, influenza vaccine with PharmaJet's needle-free injector. King of Prussia, PA/Golden, CO, USA, 2014. URL: http://pharmajet.com/fda-approves-afluria-influenza-vaccine-pharmajets-needle-free-injector/, [accessed 2014-10-05].

[215] PharmaJet Inc., 510(k) premarket notification: PharmaJet® Stratis 0.5 mL needle-free injection system. Silver Spring, MD: U.S. Food and Drug Administration, 2011. URL: https://www.accessdata.fda.gov/cdrh_docs/pdf11/K111517.pdf, [accessed 2015-03-26].

[216] Bioject Inc., 510(k) Premarket Notification - Biojector® 2000 Needle-Free Injection Management System. Silver Spring, MD: U.S. Food and Drug Administration, 2012. URL: http://www.accessdata.fda.gov/cdrh_docs/pdf12/k121270.pdf, [accessed 2015-03-06].

[217] D'Antonio Consultants International, D'Antonio Consultants International Inc., 510(k) Premarket Notification: LectraJet Needle-free Injection System. Silver Spring, MD: U.S. Food and Drug Administration, 2009. URL: https://www.accessdata.fda.gov/cdrh_docs/pdf9/K090959.pdf, [accessed 2015-03-06].

[218] Avant Medical Corporation, 510(k) Premarket Notification - Avant Guardian 101. Silver Sping, MD: U.S. Food and Drug Administration, 2003. URL: http://www.accessdata.fda.gov/cdrh_docs/pdf2/k024018.pdf, [accessed 2015-03-06].

[219] BioValve Technologies, BioValve Technologies Inc., 510(k) Premarket Notification - Mini-Ject Needlefree Injection System. Silver Spring, MD: U.S. Food and Drug Administration, 2004. URL: http://www.accessdata.fda.gov/cdrh_docs/pdf3/k032976.pdf, [accessed 2015-03-06].

[220] Rösch AG Medizintechnik, 510(k) Premarket Notification: Injex Rojex. Silver Sping, MD: U.S. Food and Drug Administration, 2002. URL: http://

www.accessdata.fda.gov/cdrh_docs/pdf2/K020786.pdf, [accessed 2015-03-06].

[221] S. Resik, A. Tejeda, P. M. Lago, M. Diaz, A. Carmenates, L. Sarmiento, N. Alemañi, B. Galindo, A. Burton, M. Friede, M. Landaverde, R. W. Sutter, Randomized controlled clinical trial of fractional doses of inactivated poliovirus vaccine administered intradermally by needle-free device in Cuba, J Infect Dis 201 (2010) 1344–1352.

[222] M. Bakari, S. Aboud, C. Nilsson, J. Francis, D. Buma, C. Moshiro, E. A. Aris, E. F. Lyamuya, M. Janabi, K. Godoy-Ramirez, A. Joachim, V. R. Polonis, A. Bråve, P. Earl, M. Robb, M. Marovich, B. Wahren, K. Pallangyo, G. Biberfeld, F. Mhalu, E. Sandström, Broad and potent immune responses to a low dose intradermal HIV-1 DNA boosted with HIV-1 recombinant MVA among healthy adults in Tanzania, Vaccine 29 (2011) 8417–8428.

[223] A. Joachim, C. Nilsson, S. Aboud, E. F. Lyamuya, M. L. Robb, M. A. Marovich, C. Ochsenbauer, B. Wahren, E. Sandström, G. Biberfeld, G. Ferrari, V. R. Polonis, Antibody-mediated inhibition of HIV-1 elicited by HIV-I DNA priming and boosting with heterologous HIV-1 recombinant MVA in healthy Tanzanian adults, Retrovirology 9 (2012) O53.

II

NEEDLE-FREE POWDER INJECTION FOR CUTANEOUS VACCINATION WITH A HIGHLY CONCENTRATED OVALBUMIN MODEL VACCINE

A detailed list of contributions is listed in section 5.

Further results associated to this project have been published as Engert, J. et al., A pilot study using a novel pyrotechnically driven prototype applicator for epidermal powder immunization in piglets. Int J Pharm 545(1-2) (2018) 215-228.

1 Introduction

Since decades, the idea of needle-free injections appears as a highly attractive approach for parenteral drug and vaccine delivery, promising low invasiveness, reduced pain, improved ease of administration, and avoiding the use of sharps. The first jet injector devices were used for multiple injections during mass immunization programs, leading to high numbers of cross-infections [1–3]. Later, disposable jet injectors (DSJIs or SUDJIs) were introduced and, until today, various types of jet injectors were developed and licenced for i.m., s.c., or i.d. injection [1, 4]. Despite the high number of DSJI systems developed, only a limited number of devices is commercially used for drug or vaccine administration. Examples are Sumavel™DosePro™ [5] and the tri- and quadrivalent Afluria® vaccines approved for the use with PharmaJet® Stratis® [6]. More recently, Takeda Pharmaceuticals announced a collaboration to bring their antibody candidate Entyvio® to the market for s.c. administration using the needle-free injecton system PRIME [7]. Although in principle appealing, jet injectors mostly remained high-cost developments without major advantage over conventional injections using N&S.

In comparison to jet injectors, ballistic powder injection introduces an additional aspect which underlines a potentially stronger benefit over conventional injections. The administration of dry formulations by powder injection not only exploits the aforementioned advantages of needle-free injections, but also exhibits the potential to enhance the storage

stability of the drug candidate. Developments of needle-free powder injectors facilitate a deposition of various kinds of powders and loadings into the skin, such as $1 - 3$ µm DNA-coated gold microparticles [8–10], $1 - 5$ µm polymer microspheres [11], or 20-53 µm sugar-based microparticles loaded with protein antigens [12, 13]. Due to a superficial delivery limited to the skin tissue, needle-free powder injection provides the strongest potential as tool for cutaneous vaccination. The reproducible breaching of the skin barrier to deliver a vaccine into viable skin layers is the major challenge of powder injection and is highly dependent on the skin condition [14]. The successfull i.d. delivery into the viable skin with a high density of APCs allows for an effective induction of immune responses, dependent on the main skin layer targeted. Whereas humoral and also cellular responses can be elicited by epidermal LCs, dDCs in the underlying dermal layer mainly provide humoral responses. However, the underlying immunological processes are complex and dependent on multiple factors including the type of antigen, adjuvant, as well as the skin layer as discussed in section 2.

In this study a novel type of powder injector, which differed from predecessor devices by its type of particle acceleration, was used. The powder injector in this study contained a pyrotechnically driven particle accelerator [15], whereas the classical gene gun and handheld PowderJect® device rely on a helium gas-triggered acceleration of particles [11, 16, 17]. The relatively large dimensions, complex preparation processes, and the use of expensive helium gas have limited the success of these devices for cutaneous vaccination in the past. The overall aim of this study was to evaluate the performance of the novel needle-free powder injector to generate an immune response upon intradermal delivery of a powdered vaccine.

In this work, three main objectives were addressed. First, based on low-dose vaccine developments for powder injection [18], a highly concentrated vaccine formulation was developed using OVA as model antigen (Section 3.1). The trehalose and mannitol-based vaccine was manufactured by a two-step process combining collapse lyophilization and cryogenic grinding, generating particles in a size range of 20-80 µm [19]. The properties of the highly concentrated vaccine was compared to placebo and low-dose formulations, which were tested for powder injection before [15, 18]. Furthermore, the stability of the highly concentrated vaccine was evaluated in a long-term stability study over 12 months (Section 3.2).

To facilitate the intradermal powder administration, the vaccine powder needs to be attached to a titanium (Ti) membrane within the needle-free injection device. To ensure

particle adhesion, the vaccine powder is homogeneously coated using an oily liquid for fixation. This liquid may be composed of a mixture of oils with adjuvant properties [20]. Upon device actuation, the oily adjuvant is delivered simultaneously with the vaccine powder into the skin [20]. For this study, a mixture of the oily components in relative ratios of the Adjuvant System 03 (AS03®) was used. AS03 is an emulsion based on squalene, DL-α-tocopherol, and polysorbate 80 and was licenced in 2008 for the use with the pandemic influenza vaccine Pandemrix® [21].

The second objective of this study was focused on the characterization of the adhesion/adjuvant oil properties. The strength of vaccine powder adhesion was evaluated for different oily liquids and mixtures based on the oily components of AS03 (Section 3.3). The oil-device membrane interaction was characterized by surface angle measurements and a correlation between vaccine powder adhesion and adhesion oil properties was evaluated. Additionally, the effect of the highly concentrated vaccine powder on the oil stability was evaluated under UV/Vis exposure and thermal stress (Section 3.4).

The last section of this chapter focuses on the main objective of this study, the evaluation of needle-free powder injection for cutaneous vaccination using a highly concentrated OVA model vaccine (Section 3.5). The *in vivo* immunization study compared cutaneous immunization using powder injection to conventional i.m. injection. Furthermore, the approach of simultaneous adjuvant oil delivery using the AS03 oily mixture was studied in comparison to paraffin as oily adhesive without expected adjuvant activity despite its known effect as oily depot in Freund's adjuvant system [22].

This study reveals a high potential of needle-free powder injection for cutaneous vaccination but also highlights issues and hurdles for the development of highly sophisticated technologies for intradermal delivery.

2 Materials and Methods

2.1 Materials

Bovine serum albumin (BSA), 5α-cholestane, free and horseradish peroxidase (HRP)-linked goat anti-porcine IgG antibody, Hydranal® dry methanol, OVA grade V and VII, mouse anti-OVA antibody, polysorbate 80, porcine albumin, porcine IgG, squalane, squalene, sterile Dulbecco's phosphate-buffered saline (PBS), 3,3',5,5'-tetramethylbenzidine (TMB) substrate, TMB stop reagent, tert-methylbutylether (TMBE), D/L-α-tocopherol,

Tween® 20 were obtained from Sigma Aldrich (Taufkirchen, Germany). Mannitol, highly liquid paraffin, polyethylene glycol 400 and 600 (PEG 400, PEG 600), butylated hydroxyanisole (BHA), disodium carbonate, potassium chloride, sodium hydrogen carbonate, and potassium dihydrogen phosphate were from Merck (Darmstadt, Germany). Trehalose dihydrate was from VWR Prolabo (Darmstadt, Germany). Adjuvant System 03 (AS03®) adjuvant emulsion was derived from Pandemrix® vaccine (GlaxoSmithKline, Rixensart, Belgium) and was kindly provided by the Bavarian State Ministry of Environment and Public Health. Sodium dihydrogen phosphate dihydrate and disodium hydrogenphosphate were purchased from AppliChem (Darmstadt, Germany) and sodium chloride was obtained from Bernd Kraft (Duisburg, Germany). Anti-mouse detection antibody (λ_{ex} 778 nm and λ_{em} 795 nm) was purchased from LI-COR (Bad Homburg, Germany). NuPAGE® 10 % Bis-Tris protein gels (1.0 mm, 12 wells) and 2-(N-morpholino)ethanesulfonic acid (MES) SDS running buffer were obtained from Life technologies (Carlsbad, USA). Sylgard 184 silicone elastomer kit was purchased from Dow Corning (Seneffe, Belgium).

2.2 Preparation of model vaccines and oily adjuvant

2.2.1 Vaccine preparation by collapse lyophilization and cryogenic milling

The model vaccine at 200 µg/mg was prepared by dissolving 2 parts OVA and 8 parts trehalose dihydrate/mannitol in 1:1 (w/w) ratio in 10 mM PBS (pH 7.0, 50 mM ionic strength), resulting in 15 % (w/w) solid content. Placebo solutions and compositions with 25 µg/mg OVA content were prepared similarly. After filtration using a 0.22 µm cellulose acetate (CA) membrane filter (VWR International, Darmstadt, Germany), 2 g of the compounded solution was pipetted into type I transparent 10R glass vials (Mglas, Münnerstadt, Germany), semi-stoppered with 20 mm Westar® RS lyophilization stoppers (Westpharma, Exton, USA) and collapse lyophilized using an Epsilon 2-6D freeze dryer (Christ, Osterode am Harz, Germany) using a cycle described before [19]. Subsequently, lyophilisates were cryomilled in aliquots of 1.5 g using a MM301 CryoMill (Retsch Technology, Haan, Germany). Upon pre-cooling using liquid nitrogen, the milling was performed at 25 Hz for 15 s. The powder was partitioned by sieving into powder particles ranging in size from $20 - 80$ µm and aliquoted into 10R vials under a glovebox flushed with nitrogen with a relative humidity below 10 %. The final model vaccine contained a dose of 0 µg, 25 µg, or 200 µg OVA per mg vaccine powder. For long-term storage stability analysis, lyophilisates and cryomilled powder aliquots containing 200 µg/mg OVA were stored at

$2 - 8$ °C, 25 °C and 40 °C for up to 12 months. The stability of the highly concentrated lyophilizates and cryomilled powder was analyzed after 1, 3, 6, 9, and 12 months storage. For vaccination studies, the OVA-loaded vaccine powder was manufactured under aseptic conditions. The formulation compounding was performed under laminar air flow (LAF) and compounded solution was lyophilized under clean room conditions using an Epsilon 2-12D freeze dryer (Christ, Osterode am Harz, Germany). Equipment with direct product contact was autoclaved for 121 °C at 2 bar for 15 min or depyrogenized using dry heat at 250 °C for at least 30 min.

2.2.2 Preparation of liquid vaccine for injection

Approximately 10 mg OVA grade VII was dissolved in 10 mL sterile Dulbeccos PBS and filtered through a 0.22 µm CA filter (VWR International, Darmstadt, Germany). The OVA concentration was determined by UV/Vis spectroscopy ($\lambda = 280$ nm). Subsequently, the solution was diluted to a concentration of 0.8 mg/mL OVA and mixed with an equal volume of AS03 adjuvant emulsion in transparent 10R vials, resulting in a final OVA concentration of 0.4 mg/mL. The liquid model vaccine emulsion was stored $2 - 8$ °C overnight before application in the *in vivo* immunization study described in section 2.6.1.

2.2.3 Preparation of oily adjuvant mixtures

The oily adjuvant for *in vivo* immunization study was prepared based on the mass ratios of AS03, which delivers 10.69 mg squalene, 11.86 mg DL-α-tocopherol and 4.86 mg polysorbate 80 per dose. Furthermore, the adjuvant composition was altered to investigate the oily adjuvant stability using mass ratios as shown in table II.1. Mixtures were prepared by weighing the components into a transparent 10R glass vial and mixing under aseptic conditions using a magnetic stirrer at ~ 50 rpm. Oily mixture F1 was used for needle-free powder injection in the *in vivo* immunization study described in section 2.6.1.

2.3 Analytical characterization of the model vaccine

2.3.1 Turbidity

The turbidity was analyzed upon reconstitution of lyophilisates and cryomilled powder as described before using a Nephla turbidimeter (Hach Lange, Düsseldorf, Germany). Samples were reconstituted with highly purified water (hpw) to match the liquid composition prior lyophilisation. Reconstituted samples were diluted 1:1, transferred into flat-bottom

Table II.1: Compositions of oily adjuvant mixtures.

Formulation	Squalene [%]	D/L-α-Tocopherol [%]	Polysorbate 80 [%]
F1	39.0	43.3	17.7
F1*	39.0	43.3	17.7
F2	69.5	21.6	8.9
F3	99.9	0.1	-

* stabilized with 0.02 % butylated hydroxyanisole (BHA)

glass cuvettes (Hach Lange, Düsseldorf, Germany) and allowed to stand for 6 h at room temperature (RT) prior to analysis. The turbidity was determined by analyzing the scattering signal of light at $\lambda = 860$ nm at an angle of 90 °and was presented in formazine nephelometric units (FNU). The turbidity of each condition was determined as average of three samples.

2.3.2 Subvisible particles by light obscuration

Subvisible particles were analyzed by light obscuration using a PAMAS SVSS-C40 (PAMAS, Rutesheim, Germany) upon reconstitution and dilution as described in section 2.3.1. A volume of 0.4 mL was used to flush the system. Cumulative particle counts ≥ 1 µm, ≥ 5 µm, ≥ 10 µm, and ≥ 25 µm were calculated as the average of three consecutive measurements of 0.3 mL sample using the PMA software (PAMAS, Rutesheim, Germany). Each sample condition was analyzed in triplicates.

2.3.3 Size exclusion chromatography

Size exclusion-high performance liquid chromatography (SE-HPLC) was carried out using a Dionex HPLC system equipped with a Dionex UVD170u UV/VIS-detector (Dionex, Idstein, Germany). A TSKgel G3000SWxl (Tosoh Bioscience, Stuttgart, Germany) was used for separation with 50 mM PBS (pH 7.0, 150 mM sodium chloride) as mobile phase. The samples were reconstituted as described in section 2.3.1. Three samples of each preparation step and condition were analyzed. The separation was accomplished at a flow rate of 0.5 mL/min and peak areas were evaluated using Chromeleon 6.60 (Dionex, Idstein, Germany). An OVA standard curve using five dilutions was generated to evaluate the total

protein recovery relative to the liquid formulation prior processing.

2.3.4 Western Blot analysis

For Western Blot analysis, lyophilizate and cryomilled powder samples were reconstituted as described in section 2.3.1 and diluted to 0.2 mg/mL OVA. Subsequently, the samples were mixed 1:1 with sample loading buffer (4 % SDS, 20 % glycerol, 0.001 % bromophenol blue in 250 mM tris(hydroxymethyl)aminomethane (Tris) hydrochloride at pH 6.8) and heated for 20 min at 90 °C. Separation by sodium dodecyl sulfate polyacrylamide gel electrophoresis (SDS-PAGE) was performed loading 10 µL sample into a 10 % Bis-Tris protein gel using MES SDS as running buffer. 5 µL MagicMark™ XP Western protein standard was used as molecular weight standard in the range of $20 - 200$ kDa.

After separation, blotting onto a nitrocellulose membrane (Hybond-ECL™, Amersham Bioscience, Freiburg, Germany) was performed at 100 mV for 1.5 h under cooling. Upon blotting, OVA detection was performed stepwise under constant shaking at 100 rpm in a horizontal shaker (VWR Ismaning, Germany). In detail, membranes were blocked with 5 % BSA in 50 mM Tris-buffered saline containing 0.1 % Tween® 20 (TBS-T, 150 mM NaCl, pH 7.4) for 2 h at RT. After washing with TBS-T, membranes were incubated overnight at $2 - 8$ °C with mouse anti-OVA primary antibody diluted in TBS-T containing 1 % BSA. Subsequently, membranes were washed and anti-mouse detection antibody (λ_{ex} 778 nm and λ_{em} 795 nm) in TBS-T containing 1 % BSA was added and incubated for 2 h at RT. After washing, membranes were analyzed using a LI-COR Odyssey scanner (LI-COR, Lincoln, USA).

2.3.5 Residual moisture analysis

The residual moisture content was determined by Karl-Fisher direct injection using a 737 KF coulometer (Metrohm, Filderstadt, Germany). Samples were prepared by weighing $20 - 30$ mg lyophilizate or cryomilled powder into 2R vials under a glovebox flushed with pressurized air at a relative humidity below 10 %. Vials were crimped and approximately 2 mL dry methanol was injected to the dry sample. The samples were placed into an ultrasonic water bath (Sonorex TK52, Bandelin electronics, Berlin, Germany) for 10 min extraction. The water content in mg per g methanol was determined by injecting 1 mL sample into the coulometric titrator. Each sample was analyzed at least four times.

2.3.6 Differential scanning calorimetry

The thermodynamic behavior of the vaccine lyophilizates and the cryomilled powder was analyzed by differential scanning calorimetry (DSC) using a Mettler Toledo 821e system (Gießen, Germany). Approximately 5−15 mg of dry sample was weighed into an aluminum pan and subsequently cold-sealed under a glovebox flushed with nitrogen and a relative humidity below 10 %. Sample analysis was performed in two cycles heating from -10 °C to 180 °C with a rate of 10 °C/min. Thermal events were evaluated using the StarE software (Mettler Toledo, Gießen, Germany). The instrument was calibrated by heating indium from 0 °C up to 150 °C at rate of 10°C/min. Data were evaluated using OriginPro 9.1.0G (OriginLab, Northampton, Massachusetts, USA).

2.3.7 X-ray powder diffraction

Mannitol polymorphs in dry samples were analyzed using a XRD 3000 TT diffractometer (Seifert, Ahrenberg, Germany) equipped with a copper anode (λ= 0.154 nm, 40 kV, 30 mA). Measurements were taken between $5 - 45$ ° 2-Theta in intervals of 0.1 °2-Theta with a duration of 4 s. Excipient modifications were qualitatively evaluated by comparison of the obtained diffraction curves with literature [23, 24].

2.3.8 Scanning electron analysis

Scanning electron microscopy of model vaccine lyophilizates and cryomilled powder was performed using a Joel JSM-6500F electron microscope (Ebersberg, Germany). Dry samples were attached to self-adhesive carbon tape (Bal-tec GmbH, Witten, Germany) and carbon-sputtered using a MED 020 coating system (Bal-tec GmbH, Witten, Germany). Images were taken at 5.0 kV operation voltage and a magnification of 500x.

2.3.9 Specific surface area analysis

The specific surface area (SSA) of the lyophilizates was determined by nitrogen-cooled krypton gas adsorption using an Autosorb-1MP analyzer (Quantachrome, Odelzhausen, Germany). After degassing of $100 - 150$ mg sample under vacuum at RT, the krypton adsorption was determined. Each sample was analyzed twice, measuring eleven points over a p/p_0 range of $0.05 - 0.3$. SSAs were evaluated according to the multipoint Brunauer-Emmert-Teller (BET) fitting method using the Autosorb-1 software.

2.3.10 Helium pycnometry

The true density of model vaccine lyophilisates was determined by helium pycnometry (AccuPyc 1330, Micrometrics, Aachen, Germany). Approximately 300 mg lyophilizate sample was analyzed after ten preliminary cleaning cycles with analytical grade helium. The true density was calculated as average of six consecutive measurements.

2.3.11 Endotoxin measurements

The endotoxin content of the liquid and reconstituted model vaccines was evaluated based on kinetic chromogenic limulus amebocyte lysate (LAL) assay. Samples were analyzed using an EndoSafe®-PTS™ portable test system using cartridges with a sensitivity of 0.005 EU/mL (Charles River Laboratories, LArbresle, France) according to the manufacturers instructions.

2.4 Vaccine powder adhesion study

2.4.1 Vaccine powder adhesion testing

The adhesion of model vaccine powder to Ti membranes using different liquid mixtures was tested using a customized drop apparatus as described before [25]. The adhesion of placebo and OVA-loaded vaccine powder at concentrations of 25 µm/mg and 200 µg/mg were investigated using the oily mixtures shown in table II.1, squalane, squalene, highly liquid paraffin, D/L-α-tocopherol, polysorbate 80, PEG400, and PEG600. An area of 20x10 cm^2 on Ti membranes were covered with a thin film of liquid mixture using a cotton swab. Approximately 3 mg model vaccine powder was sprinkled homogenously over the surface and gently pressed onto the membrane. Excess powder was removed by gentle tapping and the loaded membrane was fixed to the drop apparatus. The membrane carrier was accelerated by free fall over 1 m distance using a weight of 382 g. The carrier was dropped five times and the remaining model vaccine powder was measured by weighing. Each condition was analyzed in triplicates.

2.4.2 Surface tension and contact angle measurements

The surface tension and contact angles of the oily mixtures as shown in table II.1, squalane, squalene, highly liquid paraffin, D/L-α-tocopherol, and polysorbate 80 were analyzed using a drop shape analyzer DSA25S (Küss, Hamburg, Germany). The surface tension was

determined using the pendant drop configuration and the surface angle of a 2 µL sessile drop was determined on Ti, hydrophilic glass, and hydrophobic polydimethylsiloxane (PDMS) surfaces. The contact angle was determined 30 s after first contact with the solid surface. The work of adhesion as well as polar and disperse interactions were calculated using water and diiodomethane as hydrophilic and hydrophobic reference liquids. The PDMS surface was prepared following the instructions of the Sylgard 184 silicon elastomer kit.

2.5 Adjuvant oil stability study

2.5.1 Long-term storage and stress test oil-vaccine

Dry vaccine powder containing 200 µg OVA/mg was prepared as described in section 2.2.1. Squalene, D/L-α-tocopherol and polysorbate 80 were weighed into a type I clear 10R glass vial and mixed, matching the compositions definde in table II.1. The inner surface of type I clear 2R glass vials were covered with $\sim$ 10 mg of the oily mixture using a cotton swab. Subsequently, $\sim$ 50 mg vaccine powder was distributed inside the vial in one half of the sample set. The inner walls of the transparent 2R vials were completely covered with oily adhesive alone or with oil+vaccine powder, respectively. All samples were prepared under a glovebox flushed with nitrogen with a relative humidity below 10 %. Six samples were prepared for every time point of a specific storage condition, with and without vaccine powder. For the long-term stability investigations, the samples were stored for six months at $2 - 8$ °C, 25 °C and 40 °C. The stress test involved the exposure to and shielding from UV light using aluminum foil for 7 d using a Suntest CPS (Heraeus, Original Hanau, Germany). The UV/Vis stress conditions employed an irradiance of 550 W/m^2 for 48.2 h using light at 200-800 nm, resulting in an illuminance of 6 mio. lux h. During UV/Vis exposure, a temperature of 35 °C was measured in the Suntest CPS system.

2.5.2 GC-MS analysis

Gas chromatography-mass spectrometry (GC-MS) analysis was performed in full-scan mode using a Varian Saturn Ion Trap 2000 system equipped with a CP-3800 GC (Varian, Darmstadt, Germany). The separation was achieved using a Varian VF-5ms column (30 m x 0.25 mm x 0.25 mm) and helium as carrier gas at a flow rate of 1.4 ml/min. Aliquots of 1 µL sample were injected at 250 °C and electron ionization was performed at 270 °C ion source temperature and 70 eV ionization energy.
For organic extraction of the sample oils, a solution containing 10 µg/mL 5α-cholestane as

internal reference standard in TMBE was prepared. TMBE with 5α-cholestane was added to the sample vials to dissolve the oily components. Upon mixing, the suspension was transferred quantitatively into a tube containing water-free sodium sulfate and centrifuged for 2 min at 14,000 rpm. The supernatant was diluted 1:2500 using TMBE containing 5α-cholestane and samples were analyzed by GC-MS analysis. Calibration curves of squalene, squalan, and D/L-α-tocopherol were prepared in TMBE containing 5α-cholestane as internal reference standard. The conditions tested included a five point calibration in the range of ± 20 % of the highest and lowest expected concentration. The obtained calibration curves provided good precision and accuracy. Statistical analysis was performed using OriginPro 9.1.0G (OriginLab, Northampton, Massachusetts, USA).

2.6 In vivo vaccination study in piglets

2.6.1 Immunization

Domestic cross-breed piglets between six and seven weeks old were assigned to four different vaccination groups by weight II.2. Immunization was performed by needle-free powder injection or i.m. injection (control). For powder injection, piglets were anesthetized for $10 - 15$ min using 5 % isoflurane (Isoba® MAC 1.5 vol % Essex Tierarznei, Munich, Germany) as inhalational anesthetic. During anesthesia, the vital functions of the pigs were continuously monitored. The ventrolateral region between mammary ridge and the lateral side of the body was cleaned with water and bristles were removed using a trimmer. The application site was marked by tattooing and labeled using a black marker. Two verum groups received a dose of $1 - 2$ mg vaccine powder loaded with 200 µg OVA/mg vaccine using highly liquid paraffin (B) or oily AS03 adjuvant (C) as adhesive. A dose of $1 - 2$ mg vaccine powder without OVA model antigen, attached to the injection device using paraffin, was applied by powder injection in the placebo group (A). The vaccine was administered by powder injection on day 0 and 14 to opposite sites of the body. The positive control group (D) received an i.m. injection of 0.5 mL liquid vaccine, described in section 2.2.2, into opposite sites of the neck (trapezius muscle) on day 0 and 14. Serum samples for all groups were collected before and 1 d, 14 d, 21 d, and 28 days after immunization. The health status of the piglets was checked on a daily basis using a score system. The experimental protocol was approved by the Government Office of Upper Bavaria, Munich, Germany (authorization reference number $55.2.1.54 - 2532 - 87 - 12$; 30. Aug. 2012).

Table II.2: Overview of treatment groups in the *in vivo* immunization study.

Group	Route of administration	OVA dose	Oil adhesive	Adjuvant	Immunization time points
A	Powder injection	-	Paraffin	-	days 0, 14
B	Powder injection	200 µg	Paraffin	-	days 0, 14
C	Powder injection	200 µg	AS03	+	days 0, 14
D	i.m.	200 µg	AS03	+	days 0, 14

2.6.2 Quantification of OVA-specific porcine IgG

The OVA-specific antibody titer in serum samples was determined using an direct enzyme-linked immunosorbent assay (ELISA). In brief, 96-well, clear, flat-bottom microtiter plates (Nunc Maxisorp™, VWR, Germany) were coated overnight at $2 - 8$ °C using 50 µL of 10 µg/mL OVA in 50 mM carbonate-bicarbonate coating buffer (pH 9.6). Microtiter plates were washed between each subsequent step with 10 mM PBS containing 0.05 % (w/w) Tween® 20 (PBS-T, pH 7.4, 150 mM NaCl) using a Hydroflex plate washer (Tecan, Männedorf, Switzerland). Blocking was performed using 100 µL 5 % (m/v) BSA in PBS-T and incubation for 1 h at RT. Serum samples were diluted 1:25 using 1 % (m/v) BSA in PBS-T and a two-fold serial dilution was pipetted into every row of the microtiter plate, resulting in 50 µL per well. Each sample was measured twice. A pooled sample of 28 d sera of the i.m. control group (D) (1:200) served as positive control in two rows per microtiter plate. Samples were incubated for 1 h at RT and 50 µL HRP-linked anti-porcine IgG secondary antibody (1:40,000) was added for 1 h at RT. Detection was performed by enzymatic reaction using 50 µL TMB substrate solution at RT. Reaction was stopped after 10 min by directly adding 50 µL TMB stop solution and absorbance was measured at $\lambda = 450$ nm using a Fluostar plate reader (BMG labtech, Offenburg, Germany). The OVA-specific antibody titer was determined as inflection point upon four parameter logistic regression of each sample curve using Origin 8G (OriginLab, Northampton, Massachusetts, USA). Statistical analysis of the antibody titer was performed using ANOVA on ranks (Kruskal-Wallis, $\alpha = 0.05$) using SigmaPlot 12.5 (Systat Software, San Jose, California, USA).

2.6.3 Quantification of total porcine IgG

Total serum immunoglobulin (Ig)G was determined by sandwich ELISA, which was developed for the *in vivo* study. Briefly, coating was performed by incubating 50 µL goat anti-porcine IgG capture antibody (1:20,000) in 50 mM carbonate-bicarbonate coating buffer (pH 9.6) overnight at $2 - 8$ °C in 96-well, clear, flat-bottom microtiter plates. Between each following step, microtiter plates were washed with PBS-T (pH 7.4, 150 mM NaCl) using a Hydroflex plate washer (Tecan, Männedorf, Switzerland). Blocking was performed using 100 µL of 5 % (m/v) BSA in PBS-T, incubating for 1 h at RT. Serum samples were diluted in 1 % (m/v) BSA in PBS-T. Each sample was analyzed in duplicates using 50 µL sample per well, incubating for 1 h at RT. Detection was performed as described in section 2.6.2 using HRP-linked anti-porcine IgG (1:20,000) as secondary antibody and TMB substrate. The porcine IgG concentration of each sample was calculated by means of a standard curve that was measured separately for each microtiter plate. Dilutions of porcine IgG and porcine albumin at 1:3.3 ratio in 10 mM PBS (pH 7.4), matching the IgG content relative to total serum proteins [26], was used to generate the standard curve. The total porcine IgG ELISA was developed by two-step chessboard titration (CBT) providing a detection range of $1 - 100$ nm/mL porcine IgG ($R^2 > 0.999$). The developed ELISA provided low intra- and interassay variability with relative coefficient of variation (CV) < 5 % except for the high concentration standard, which showed an interassay CV of 14 %. A standard curve was included to each microtiter plate. Statistical analysis was performed using SigmaPlot 12.5 applying a one-way ANOVA on ranks (Kruskal-Wallis, $\alpha = 0.05$).

3 Results and Discussion

3.1 Development and characterization of a highly concentrated model vaccine for needle-free intradermal powder injection

3.1.1 Preparation of low and highly concentrated OVA model vaccine

Previous studies have shown that the preparation of a low dose vaccine powder using OVA as model antigen at a concentration of 25 µg/mg was feasible, resulting in a vaccine powder with good stability and suitable properties for needle-free powder injection [18, 19]. Considering a maximum dose of $1 - 2$ mg vaccine powder delivered by needle-free intradermal injection, only $25 - 50$ µg OVA would be delivered into the skin. Comparable

doses have been used for cutaneous vaccination in mice [27, 28]. However, the relatively low potency of OVA as model antigen likely requires a higher dosing in larger animals. To facilitate a high dosing in the *in vivo* immunization study in piglets, a highly concentrated vaccine powder at 200 µg/mg was developed and characterized in relation to low-dose vaccine formulations.

The simultanous preparation of vaccine at 0 µg/mg, 25 µg/mg, and 200 µg/mg OVA in one lyophilization cycle was possible and resulted in comparable cake appearance for all formulations. Temperature probe monitoring revealed a completion of primary drying after $10 - 12$ h for 25 µg/mg and 200 µg/mg OVA formulations, applying aggressive primary drying conditions at +45 °C and 2 mbar as described before [18]. The initiation of secondary drying after around 31 h at +45 °C and 0.03 mbar highlights the possibility to further reduce the primary drying time and thereby improve cost and time efficiency for vaccine manufacturing.

The second step of vaccine preparation for powder injection by cryogenic milling resulted in a white vaccine powder with comparable appearance for all OVA concentrations. The vaccine powder as placebo formulation or 25 µg/mg and 200 µg/mg OVA-loaded formulation exhibited similar macroscopic properties upon manufacturing.

3.1.2 Ovalbumin antigen stability

The OVA protein stability of model vaccines with concentrations of 25 µg/mg and 200 µg/mg was evaluated by SE-HPLC. The relative amount of OVA monomer, dimer, and high molecular weight (HMWS) and low molecular weight species (LMWS) during the processing was evaluated for the low and highly concentrated vaccine formulations (Tab. II.3). The OVA monomer recovery remained constant at approximately 91 % for the liquid formulations and after lyophilization and cryogenic milling of 25 µg/mg and 200 µg/mg OVA formulations. Furthermore, around 8.3 % dimer and 1 % HMWS were detected for model vaccine lyophilizates and the cryomilled powder. Upon cryogenic milling the relative amount of HMWS increased to 1.6 % and 1.1 % for the 25 µg/mg and 200 µg/mg OVA powder, respectively. Compared to the liquid formulations with 0.9 % and vaccine lyophilizates with 1.4 % and 1.1 % HMWS, the increase was minimal and not considered to affect the vaccine quality negatively. Also, no fragmentation, indicated by increased LMWS, was detected by SE-HPLC analysis.

The results suggest that the protein remained stable during collapse lyophilization and cryogenic milling. Neither increased processing-related aggregation, nor fragmentation

Table II.3: Protein composition by SE-HPLC of OVA model vaccine at 25 µg/mg and 200 µg/mg prior and after processing by lyophilization and cryogenic milling.

Formulation		Monomer [%]	Dimer [%]	HMWS [%]	LMWS [%]
25 µg/mg OVA					
Liquid	(Liq)	90.8 ± 0.2	8.3 ± 0.1	0.9 ± 0.1	n.d.
Lyophilizate	(Lyo)	90.2 ± 0.1	8.4 ± 0.1	1.4 ± 0.1	n.d.
Cryomilled powder	(Cryo)	90.4 ± 0.2	8.0 ± 0.1	1.6 ± 0.1	n.d.
200 µg/mg OVA					
Liquid	(Liq)	90.7 ± 0.0	8.4 ± 0.0	0.9 ± 0.1	n.d.
Lyophilizate	(Lyo)	90.6 ± 0.0	8.5 ± 0.0	1.0 ± 0.0	n.d.
Cryomilled powder	(Cryo)	90.6 ± 0.0	8.3 ± 0.0	1.1 ± 0.0	n.d.

was detected. The processing of highly concentrated OVA formulation at 200 µg/mg did not affect the monomer content negatively.

3.1.3 Subvisible particles and turbidity analysis

The visual appearance and the subvisible particle content of the placebo and OVA-loaded vaccine was characterized by turbidity and light obscuration analysis upon reconstitution of lyophilizate and cryomilled powder samples (Fig. II.1). Generally low particle counts of $1,000 - 2,000$ particles ≥ 1 µm /mL were detected for all liquid formulations prior to lyophilization independent of the OVA target content. The particle counts of the placebo formulation remained low after collapse lyophilization but increased to 4,000 particles/mL ≥ 1 µm upon cryogenic milling. Moreover, OVA-loaded formulations showed largely concentration- and also processing-dependent particle counts upon collapse lyophilization and cryogenic milling. Comparable particle counts of 6,410 particles ≥ 1 µm/mL and 7,069 particles ≥ 1 µm/mL were detected for vaccine lyophilizates at 25 µg/mg and 200 µg/mg, respectively. However, major differences in the particle counts of low and high dose vaccine formulations were observed after subsequent cryogenic milling. While the 25 µg/mg cryomilled powder showed 13,602 particles≥ 1 µm/mL, particle counts increased significantly for the 200 µg/mg vaccine powder with values around 160,000-170,000 particles/mL in separate batches.

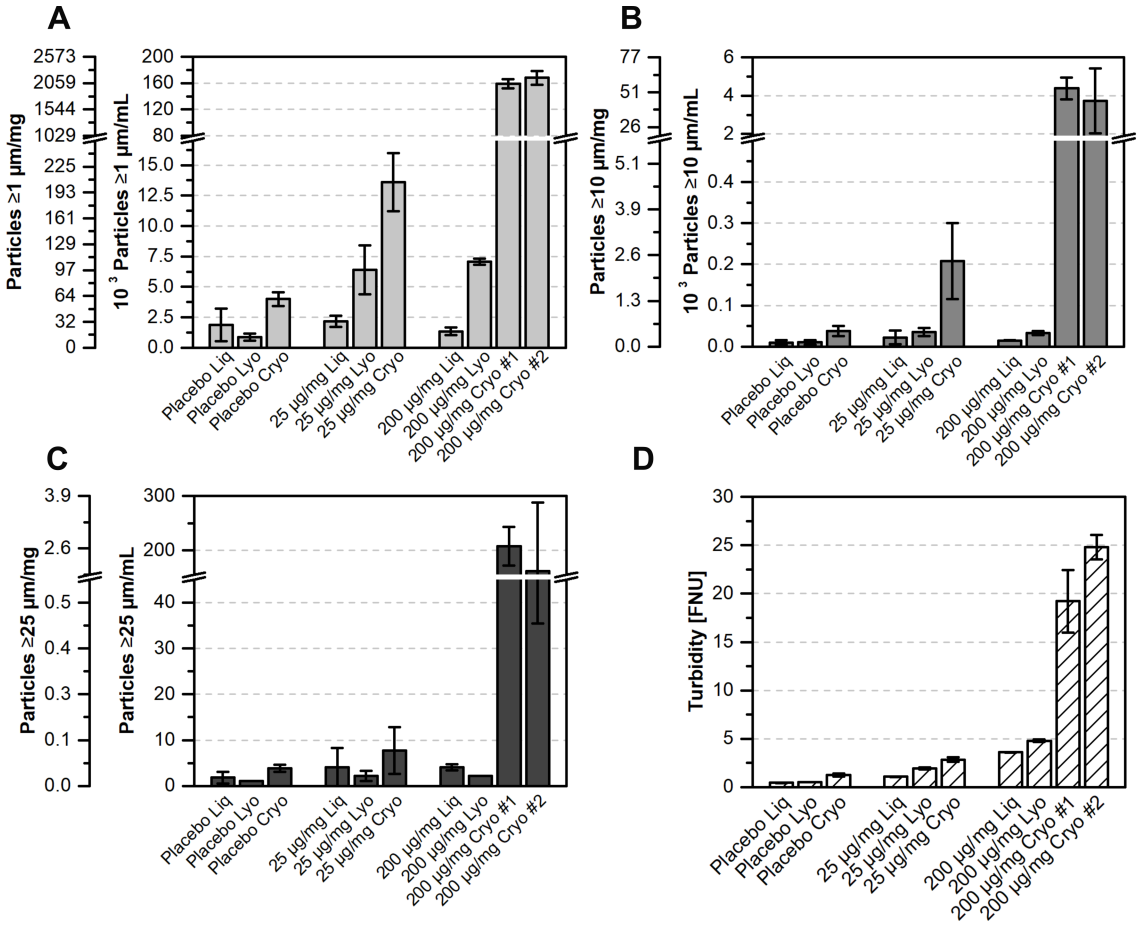

Figure II.1: Subvisible particle counts of placebo and model vaccine with an OVA content of 25 µg/mg and 200 µg/mg prior (Liq) and after processing by collapse lyophilization (Lyo) and cryogenic milling (Cryo). The subvisible particle counts $\geq$ 1 µm (A), $\geq$ 10 µm (B), and $\geq$ 25 µm (C) per mg dry vaccine and per mL reconstituted formulation are shown. Furthermore, the turbidity of the reconstituted samples is provided (D).

The observations found for particles $\geq$ 1 µm were also confirmed by cumulative counts of larger particles $\geq$ 10 µm and $\geq$ 25 µm. While a low number of particles was detected for all liquid formulations and lyophilizates with values below 40 particles $\geq$ 10 µm/mL and less than 5 particles $\geq$ 25 µm/mL, cryogenic milling led to increased particle counts in the presence of OVA model antigen. Formulations with high dose OVA of 200 µg/mg exhibited notably higher particle count of around 4,000 particles $\geq$ 10 µm/mL and 200 particles $\geq$ 25 µm/mL where as the low dose OVA vaccine remained relatively low with counts of around 200 particles/mL and 8 particles/mL $\geq$ 10 µm and $\geq$ 25 µm, respectively.

The turbidity of placebo and OVA loaded formulations showed values depending on the

OVA concentration and the processing step. In general, the turbidity in increased with increasing OVA content. Lowest values around $0.5 - 1$ FNU were detected for the placebo formulation prior and after two-step processing. The OVA vaccine at 25 µg/mg showed turbidity values between $1-3$ FNU, which increased with each processing step. As observed by subvisible particle analysis, most pronounced differences in turbidity were detected for the highly concentrated OVA vaccine after cryogenic milling. The liquid formulation and vaccine lyophilizates at 200 µg/mg OVA provided values between of 3.6 FNU and 4.8 FNU, whereas the turbidity was increased by cryomilling to up to 25 FNU.

The results suggest that the OVA model antigen concentration represents the major parameter that influences the subvisible particle quality attribute of the model vaccine for needle-free intradermal powder injection. The most pronounced increase in subvisible particle counts and also turbidity was detected for the highly concentrated OVA cryomilled vaccine powder at 200 µg/mg. In some cases, even visible particles were observed after reconstitution. Despite the relatively high subvisible particle counts of the 200 µg/mg vaccine powder, regulatory requirements for subvisible particulates would be met, allowing a maximum of 6,000 particles $\geq$ 10 µm and 600 particles $\geq$ 25 µm per container for parenteral formulations [29, 30]. Moreover, with respect to vaccination, particles in the submicron range could further enhance immune responses and serve as adjuvant for vaccination [31].

The vaccine preparation as a liquid formulation and collapse-dried lyophilizates showed comparable results for the subvisible particle content independent of the antigen concentration in a range of $0 - 200$ µg/mg OVA. The cryomilling process increased the particle content in all formulations. Empty milling tests (graphs not shown) revealed that about 48,000 particles $\geq$ 1 µm were generated per milling beaker, which represents the worst case scenario of foreign matter that could be introduced into the 1.5 g vaccine powder prepared by cryomilling. This means the cryomilling process itself could increase the particle counts $\geq$ 1 µm by $\sim 3,500$ particles per milliliter of reconstituted formulation. Similarly, around 20 additional particles $\geq$ 10 µm and less than 1 particle $\geq$ 25 µm would be found after cryogenic milling of vaccine lyophilizates. Considering the particle counts detected for particles $\geq$ 1 µm, this value is well comparable to the difference in particle counts found for the placebo formulation after cryogenic milling. At an OVA content of 25 µg/mg particle counts were higher, indicating that the increase in counts was caused not only by foreign but also protein particles. This observation was even more pronounced for the highly concentrated vaccine at 200 µg/mg OVA where the largest part of increase in subvisible particle counts was most likely generated by proteinaceous matter. Although this

indicates changes in the physicochemical properties of the OVA model antigen at higher concentrations, it remains to be assessed if this affects the immunological potency of the molecule for vaccination.

3.1.4 Lyophilizate and cryomilled powder characteristics

The properties of model vaccine after processing by collapse lyophilization and cryogenic milling were evaluated by residual moisture, specific surface area and true density analysis. The residual moisture content of the model vaccine lyophilizates and cryomilled powder with varying OVA content was determined by Karl-Fischer titration. In general, low moisture contents between $0.4 - 0.6$ % were found for lyophilizates loaded with $0 - 200$ µg/mg OVA (Fig. II.2). Processing by cryogenic milling increased the residual moisture content to $0.6 - 1.1$ %. Comparing the different OVA concentrations revealed a concentration-dependent non-linear decrease of the residual moisture content most pronounced for the cryomilled vaccine powder. In general, higher OVA concentrations lowered the residual moisture content of the vaccine.

The results show that the highly-concentrated OVA vaccine at 200 µg/mg provided a slightly lower moisture content compared to the 25 µg/mg OVA model vaccine. However, the differences observed were small and good comparability of the OVA-loaded vaccine at 25 µg/mg and 200 µg/mg can be assumed. Although the residual moisture content increased after cryomilling, it remained below 1 % for the antigen-loaded vaccine formulations and provided suitable properties for following studies.

The SSA of the vaccine lyophilizates and the cryomilled powder was determined by multipoint BET analysis. Figure II.2 shows that an increasing antigen concentration lowers the SSA of the lyophilizates and cryomilled powder. Within a range from $0 - 200$ µg/mg OVA, the SSA decreased non-linear with increasing OVA concentration from 0.45 m^2/g to 0.25 m^2/g for the vaccine lyophilizates. Cryogenic milling upon lyophilization increased the SSA of all formulations to $1.7 - 2$ m^2/g. The OVA antigen concentration showed a less pronounced effect on the SSA of the cryomilled powder compared to the vaccine lyophilizates.

In general, lower SSAs, which are generally associated with larger pores, reduces the speed of secondary drying leading higher residual moisture contents [32]. However, in this study, the highly concentrated OVA vaccine at 200 µg/mg exhibited the lowest SSA value but also the lowest residual moisture content. This observation was likely driven by two effects. First, as aforementioned, the aggressive lyophilization cycle applied in this study provided

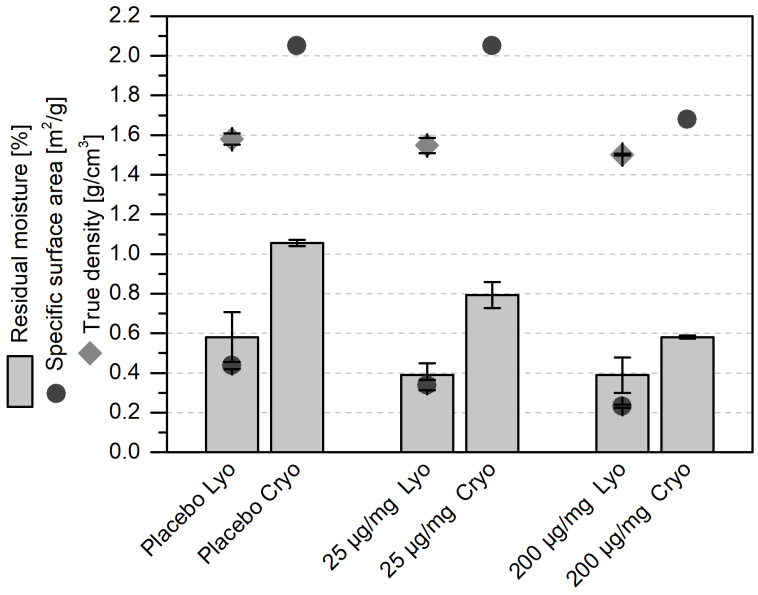

Figure II.2: Residual moisture content (bars), specific surface area (circles), and true density (diamond) of model vaccine lyophilizates (Lyo) and cryomilled powder (Cryo) without antigen (placebo) and with 25 µg/mg and 200 µg/mg OVA.

long primary and secondary drying times at a high temperature of +45 °C, leading to complete drying for all formulations. Secondly, it has been reported that a higher protein content leads to faster drying due to lowering of the cake resistance and results in reduced residual moisture contents. It can be therefore assumed that the increase OVA antigen concentration had a superior influence on the final moisture content compared to the lyophizate pore structure.

The true density of the OVA vaccine was assessed by helium pycnometry. The results show that the true density of the lyophilizates decreases slightly with increasing OVA concentration (Fig. II.2). Placebo vaccine lyophilizates provided a density of 1.58 g/cm^3 whereas OVA-loaded lyophilizates exhibited values of 1.55 g/cm^3 and 1.50 g/cm^3 at concentrations of 25 µg/mg and 200 µg/mg, respectively. The results show that the OVA concentration provided a notable impact on the residual moisture content and SSA of the lyophilizates and cryomilled powder. However, lower SSA values were not obtained due to densification of the lyophilizate formulation at higher OVA concentrations but these were most likely derived from differences in freezing and drying behavior during lyophilization. On the other hand, an inferior effect of the OVA content on the true density was observed.

Previous studies at 25 µg/mg OVA using a ternary mixture of trehalose, mannitol, and dextrane with 15 % solid content have found comparable results of with values of $\sim$ 1.5 %

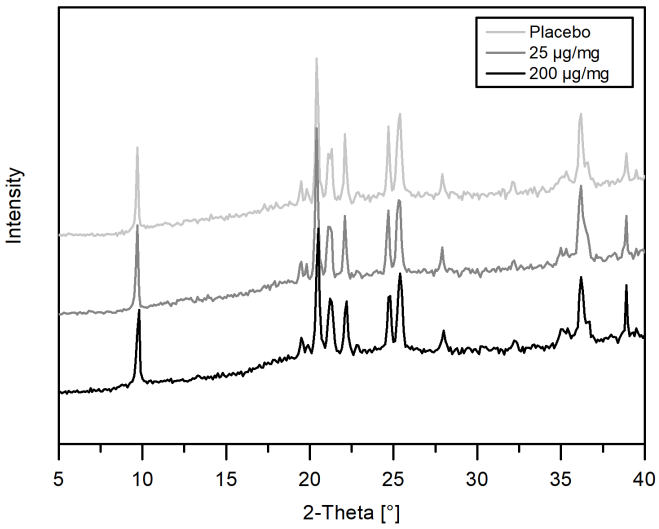

Figure II.3: XRPD patterns of placebo and model vaccine lyophilizates with 25 µg/mg and 200 µg/mg OVA.

moisture content of the cryomilled powder, 0.3 m^2/g and 1.5 m^2/g SSA of lyophilizates and cryomilled powder, and a true density of the cryomilled powder around 1.5 g/cm^3 [18]. Comparing the true density measurements of the lyophilizates in this study and the cryomilled powder in the previous study indicates that cryogenic milling did not notably affect the true density of the vaccine. More likely, the formulation composition and, to a lower extent, the lyophilization process impact the final SSA and density of the product [18]. The results obtained in this study at a high concentration of 200 µg/mg OVA were well comparable to the placebo and low dose formulations used in this setup but also compared to the previous study referenced above.

3.1.5 Characterization of excipient modification

The crystallinity of mannitol was investigated by X-ray powder diffraction (XRPD) and DSC. The qualitative investigation of mannitol polymorphs by XRPD revealed that δ-mannitol was formed by collapse lyophilization independent of the OVA content in the range of 0 µg/mg to 200 µg/mg (Fig. II.3). The δ-modification of mannitol was confirmed by a peak at 9.7 °2-Theta in all formulations. The absence of a peak at 17.9 °2-Theta indicates that no mannitol hydrate was formed during lyophilization. The profiles suggest that trehalose remained in the amorphous state during drying. Furthermore, the XRPD profile did not change upon cryogenic milling for all formulations.
DSC analysis of the OVA vaccine at different concentrations revealed a comparable melting

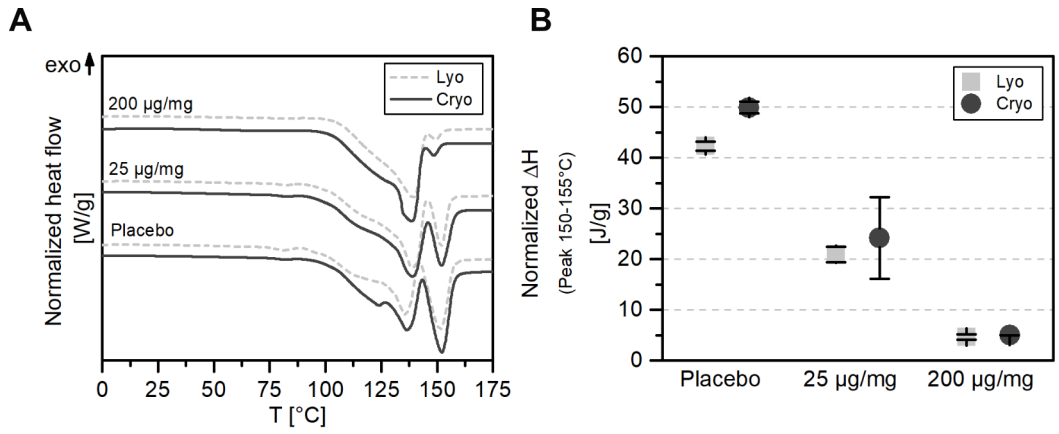

Figure II.4: DSC thermograms (A) of placebo and 25 µg/mg and 200 µg/mg OVA-loaded vaccine lyophilizates (Lyo) and cryomilled powder (Cryo) and peak enthalpies (B) of the second mannitol melting endotherm around 150-155 °C in dependence of the OVA vaccine concentration.

profile for all formulations. The detected endothermic events occured in comparable temperature ranges between $100 - 160$ °C (Fig. II.4). Within this range, vaccine lyophilizates showed overlapping thermal events between 90-145 °C and a distinct melting endotherm around $150 - 155$ °C. The peak enthalpy at $150 - 155$ °C thereby decreased non-linear with increasing OVA antigen concentration. No differences in the DSC profiles were observed between vaccine lyophilizates and the cryomilled powder of the respective OVA concentration.

Previous studies have reported an endothermic peak around 166 °C that is associated with the melting of different modifications of mannitol, including the δ-modification [24, 33]. The δ-mannitol polymorph is a thermodynamically instable modification at ambient conditions, with a relatively high kinetic stability [24]. This modification remains stable upon mechanical stress and long-term storage [24]. In fact, cryogenic milling of the vaccine lyophilizates did not change the mannitol modification of the vaccine formulations. Besides that, heating at rates below 10 K/min induces the transition of δ-mannitol into the β-modification, which consequently contributes to the endothermic melting of this mannitol polymorph [24, 33].

The literature value of mannitol melting was confirmed by analysis of the pure crystalline excipient used in this study, which showed a melting endotherm around 166 °C (data not shown). The combined analysis of crystalline mannitol in combination with crystalline trehalose revealed a shifting of the mannitol melting endotherm towards lower temperatures by up to 5 °C (data not shown). These findings suggest that the melting peak of crystalline

mannitol within the multi-component formulations used in this study ocurred at a temperature below 166 °C. It can be assumed that the endothermic peak around $150 - 155$ °C was derived from the melting of crystalline δ-mannitol within the sample. The drop of peak enthalpy with increasing OVA concentration would indicate a decrease of crystalline content in the vaccine lyophilizates and cryomilled powder with increasing antigen content. However, the analysis of additional OVA concentrations would be required to confirm this hypothesis.

In the formulation composition used in this study, mannitol acted as a bulking agent, leading to a stable lyophilizate cake and cryomilled powder. It can be expected that the presence of a crystalline mannitol modification increases the density of the final product. With the generation of kinetically stable δ-mannitol by freeze-drying it was possible to take advantage of a good storage stability and increased density compared to amorphous mannitol. It has to be noted that a higher OVA antigen content most likely reduced the relative amount of crystalline mannitol in the sample, consequently reducing the density (Section 3.1.4). However, the high comparability of measured density values at all OVA concentrations from $0 - 200$ µg/mg reveal that despite a lower degree of crystallinity, the highly concentrated OVA vaccine provided suitable properties for needle-free intradermal powder injection.

3.2 Long-term stability of the highly concentrated vaccine

3.2.1 Ovalbumin antigen stability

The long-term stability of the highly concentrated vaccine at 200 µg/mg OVA was evaluated over a period of 12 months, storing model vaccine lyophilizates and cryomilled powder at $2 - 8$ °C, 25 °C, and 40 °C. The antigen stability during the long-term stability study was evaluated by SE-HPLC and Western blot analysis. SE-HPLC results showed constantly high monomer contents around 90 % for the lyophilizate and cryomilled powder over 12 months storage at up to 40 °C (Fig. II.5). Similarly, the dimer and high molecular weight species (HMWS) content remained constant around $8 - 9$ % and 1 %, respectively. Also, no formation of LMWS was detected by SE-HPLC over time. The total protein recovery decreased slightly over a storage period of 12 months but stayed above ~ 90 % for all storage conditions.

The antigenicity of the protein after vaccine processing and storage at different conditions was assessed by Western blot analysis. The Western blots of the vaccine formulation at

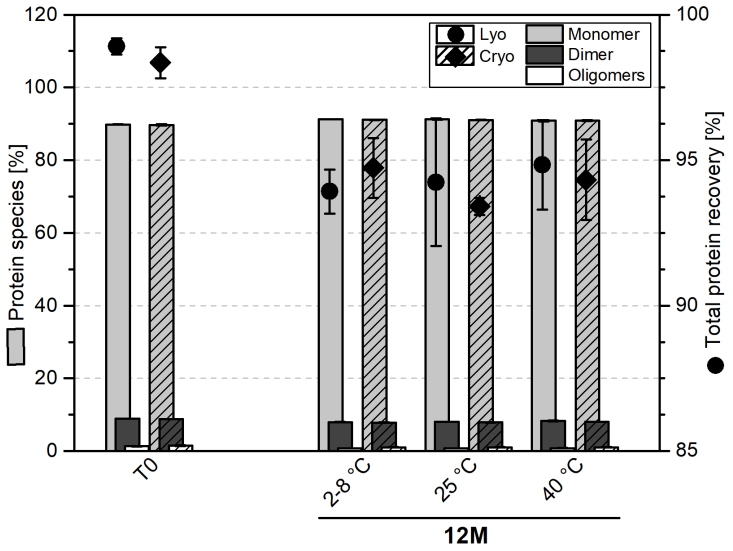

Figure II.5: Relative OVA monomer, dimer, and oligomer composition (bars, left Y-axis) and total protein recovery (symbols, right Y-axis) of the highly concentrated 200 µg/mg OVA vaccine lyophilizates and cryomilled powder at stability study initiation (T0) and after 12 months storage at $2-8$ °C, 25 °C, 40 °C.

200 µg/mg OVA prior and after processing by lyophilization and cryogenic milling showed up to five bands associated with the OVA antigen (Fig. II.6). The most pronounced band was detected around 40 kDa associated to OVA monomer. Moreover, a distinct dimer band of approximately 80 kDa as well as a trimer band of around 120 kDa were observed above the OVA monomer. In some cases, further bands at higher molecular weights were seen, however these were no longer clearly distinguishable. Besides higher molecular weight species, an additional band was detected directly below the OVA monomer band. This lower band exhibited a slightly lower molecular weight and showed higher mobility during electrophoretic separation by SDS-PAGE. The low band provided a molecular weight below 40 kDa and was considered a fragment of the OVA monomer with maintained antigenicity.

Over a storage period of 12 months, comparable patterns of relative OVA composition were detected for stored lyophilizates and the cryomilled powder. The antigenicity of the protein during processing and storage was maintained. A slight increase in band intensity of the OVA low molecular weight fragment was observed, however relative to the monomer band intensity, the observed change was negligible. Furthermore, no differences were detected between cold, ambient, and accelerated storage conditions.

The results obtained by SE-HPLC and Western blot analysis show that the OVA antigen remained stable during 12 months storage at up to 40 °C. Unlike previous studies, which

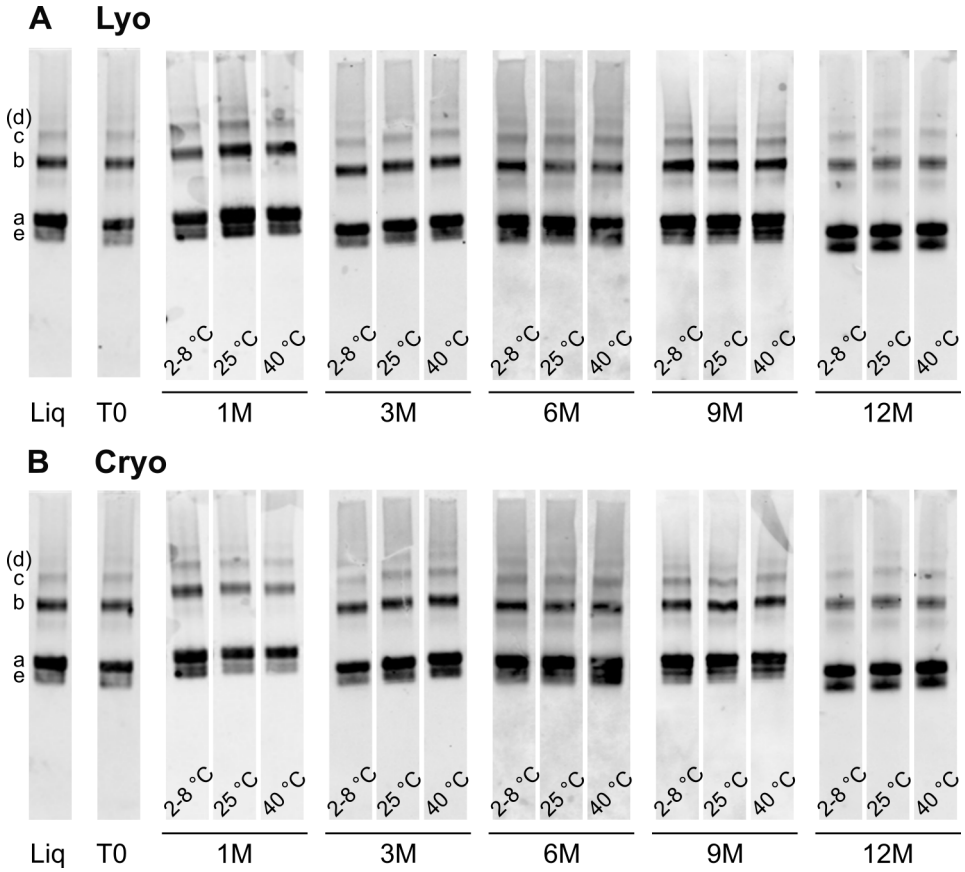

Figure II.6: Western blots of model vaccine lyophilizates (A) and cryomilled powder (B) at 200 µg/mg OVA during 12 months storage at $2-8$ °C, 25 °C, 40 °C. The bands detected by Western blot analysis correspond to the OVA monomer (a), dimer (b), oligomers (c, d), and lower molecular weight species (e). The latter were not detected by SE-HPLC.

observed a loss of antigenicity of influenza vaccine-loaded cryomilled vaccine powder after 6 months storage at 40 °C [15], the model antigen OVA used in this study maintained the antigenicity over storage time and exhibited a comparable monomer, dimer, and oligomer composition at all times.

3.2.2 Subvisible particles and turbidity analysis

The physicochemical stability of the vaccine lyophilizates and cryomilled powder with 200 µg/mg OVA was studied by light obscuration and turbidity analysis. As discussed in section 3.1.3, the subvisible particle counts of the model vaccine at initial testing remained constant prior and after collapse lyophilization with counts below 50 particles ≥ 1 µm per mg dry vaccine (Fig. II.7). Cryogenic milling of the vaccine lyophilizates increased the

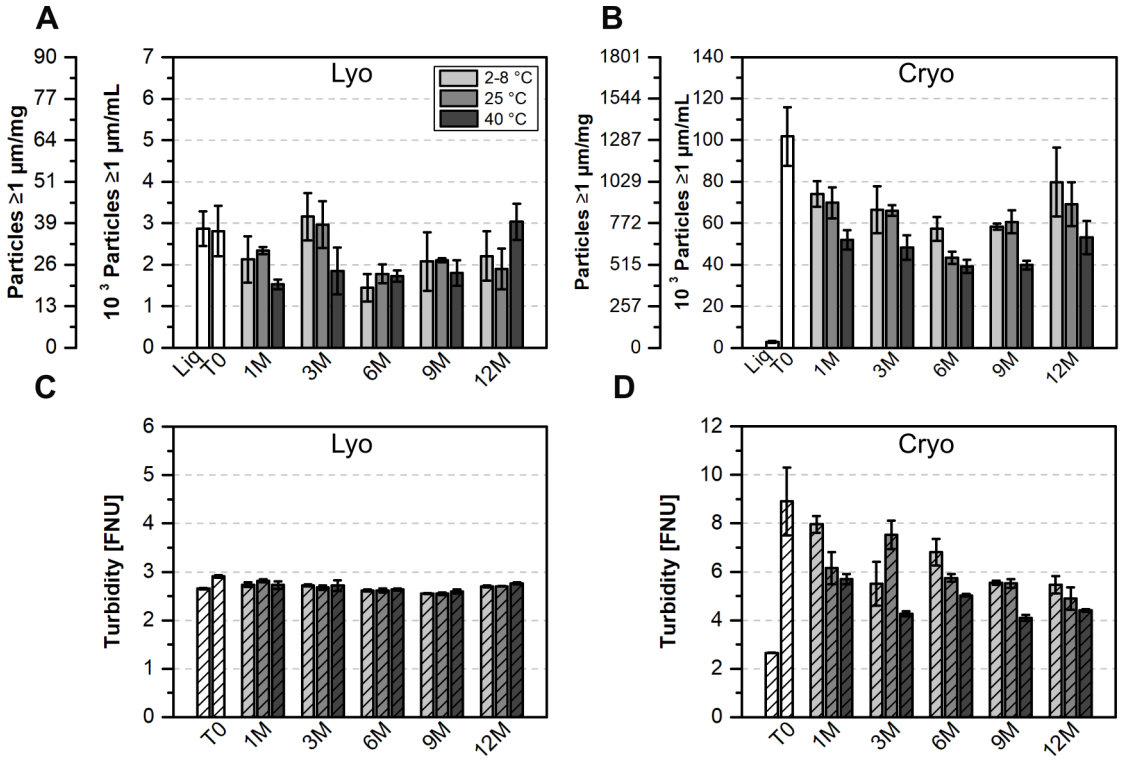

Figure II.7: Cumulative subvisible particle counts $\geq$ 1 µm and turbidity of reconstituted highly concentrated 200 µg/mg OVA vaccine lyophilizates (A, C) and cryomilled powder (B,D) over 12 months storage at $2-8$ °C, 25 °C, 40 °C.

subvisible particle content significantly to about 1,300 particles $\geq$ 1 µm/mg.

The storage of the vaccine lyophilizates and cryomilled powder at $2-8$ °C, 25 °C, and 40 °C over 12 months revealed constant particle counts for lyophilizates and a decrease in subvisible particles $\geq$ 1 µm for the cryomilled powder (Fig. II.7). Over a period of 12 months, the cumulative counts of particles $\geq$ 1 µm did not change in stored model vaccine lyophilizates independent of the stoarge condition. For the cryomilled powder, on the other hand, a slight decrease of particle counts $\geq$ 1 µm to approximately 500-1,000 particles/mg was detected. Thereby, higher counts were found for cold storage whereas the storage at an accelerated temperature of 40 °C led to lower particle counts. The difference in particle counts observed after 12 months, was derived from a software update of the analytical instrument and was not considered to reflect a real change in particle counts for the model vaccine.

The cumulative counts of particles $\geq$ 10 µm and $\geq$ 25 µm showed values below 2 particles/mg vaccine for all samples (data not shown). No clear trends could be detected for

larger particles over a storage period of 12 months at different conditions. Considering the distribution of subvisible particles, it can be concluded that the main fraction of particles found in the model vaccine were smaller than 10 µm and only a minor amount of larger particles would delivered into the skin upon needle-free powder injection. Per vaccine dose of $1 - 2$ mg cryomilled vaccine powder a maximum of 4,000 particles in the micron size range would be delivered into the skin.

The analysis of the sample turbidity showed a comparable trend over time as observed for the subvisible particle counts. Higher turbidity values were generally associated with a higher count of particles ≥ 1 µm and a decrease of turbidity over 12 months storage was observed.

The decrease of subvisible particle counts and turbidity could be explained by intermolecular changes, e.g. particle or aggregate ripening, within the dry formulation. It can be assumed that over time, larger protein aggregates were formed which could not be detected by light obscuration due to fast sedimentation, or by protein stability analysis, e.g. SE-HPLC. Stress testing at elevated temperatures accelerated structural changes within the dry vaccine, leading to higher amounts of insoluble OVA aggregates and lower particle counts and turbidity values. Although this hypothesis was supported by decreasing particle counts, no increase in soluble aggregates could be detected by SE-HPLC or Western blot analysis (Section 3.2.1). However, a slight decrease in total protein recovery was observed, indicating a loss of protein by formation of insoluble OVA antigen aggregates in the cryomilled powder. However it has to be noted that due to the generally high protein concentration after reconstitution around 30 mg/mL, the loss in protein by insoluble particle formation might not be clearly detectable.

Considering the low number of particles that would be delivered by needle-free intradermal powder injection and the generally low loss of soluble OVA antigen over 12 months, it can be assumed that the model vaccine powder provided good storage stability at up to 40 °C. In general, slighlty superior stability was found for the model lyophilizates, indicated by negligible changes in physicochemical quality attributes compared to the cryomilled powder. Nevertheless, the results show that the vaccine powder provided suitable long-term stability and was suitable to be stored up to 3 months at $2 - 8$ °C in preparation of the *in vivo* immunization study.

3.2.3 Residual moisture analysis

The residual moisture of the 200 µg/mg OVA vaccine lyophilizates and the cryomilled powder was analyzed by Karl-Fischer titration. At initial testing, the highly concentrated lyophilizates and cryomilled powder exhibited a moisture content of 0.5 % and 0.7 %, respectively. At cold storage conditions at $2-8$ °C, the residual moisture content remained stable over 12 months storage for the lyophilizates and increased minimally to $0.8-0.9$ % for the cryomilled powder. With increasing storage temperature, the moisture content increased over storage time to up to 0.8 % for the vaccine lyophilizates and up to 1.6 % for the cryomilled powder, both stored at 40 °C.
The results show that the storage at higher temperature led to increased residual moisture levels. Thereby, the cryomilled powder showed higher differences to the initial testing as compared to the vaccine lyophilizates. In general, the residual moisture remained below 1 % for up to 6 months and below 2 % for up to 12 months storage at all conditions. The generally low moisture content indicate good long-term stability of the model vaccine in its primary packaging over a storage period of 12 months at up to 40 °C.

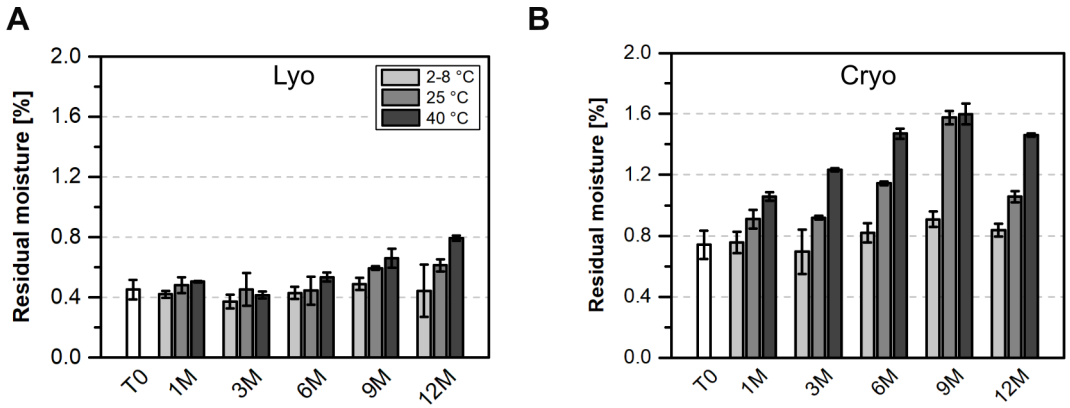

Figure II.8: Residual moisture contents of highly concentrated 200 µg/mg OVA vaccine lyophilizates (A) and cryomilled powder (B) during 12 months storage at $2-8$ °C, 25 °C, 40 °C.

3.2.4 Characterization of excipient modification

The stability of the mannitol excipient modification in the highly concentrated OVA vaccine lyophilizates and cryomilled powder was evaluated by XRPD and DSC analysis. The XRPD patterns of the dry samples prior and after storage for 12 months at $2-8$ °C, 25 °C, and 40 °C reveal a stable δ-mannitol modification over the entire storage time (Fig. II.9).

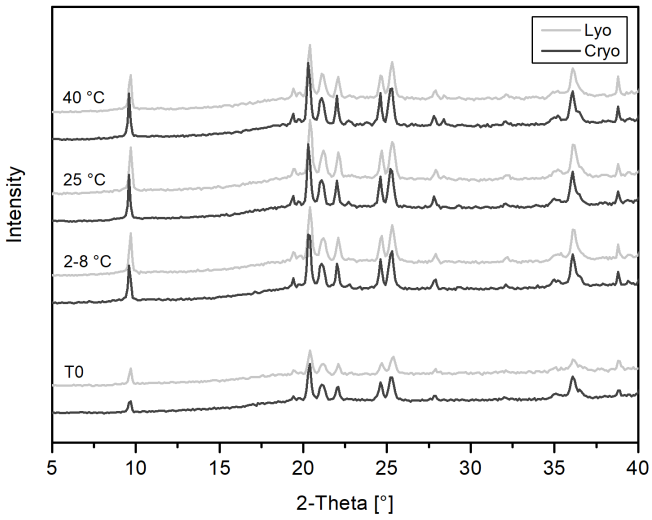

Figure II.9: XRPD patterns of the highly concentrated 200 µg/mg OVA vaccine lyophilizates and cryomilled powder at stability study initiation (T0) and after 12 months storage at $2-8$ °C, 25 °C, 40 °C.

The profiles of the lyophilizates and the cryomilled powder did not change over time and exhibited a peak at 9.7 °2-Theta in all samples. This peak indicates the presence of δ-mannitol, while the absence of a peak at 17.2 °2-Theta shows that no mannitol hydrate was present in any sample. A slight increase in peak height could indicate the increase of crystalline mannitol in the sample, assuming similar sample masses for XRPD analysis.

The amount of crystalline mannitol was studied by DSC. All lyophilizate and cryomilled powder samples exhibited a similar DSC profile as discussed in section 3.1.5. Overlaid endothermic events were detected in a temperature range between 90 °C and approximately 150 °C (Fig. II.10A). Dependent on the sample type and storage condition the endothermic melting shifted towards lower temperatures. The highest melting temperatures were detected at the initial testing time point with minimally lower temperatures for the cryomilled powder. Over storage time and with increasing storage temperatures, the melting onset shifted towards lower temperatures as indicated in figure II.10).

It can be assumed that the shifting of the melting temperatures was associated with the increase in residual moisture content. As discussed in section 3.2.3, vaccine lyophilizates showed inferior changes compared to cryomilled vaccine powders, particularly when stored at elevated temperatures.

The DSC profiles also reveal minimal changes in the peak enthalpy of the second, single melting endotherm between around $140-150$ °C. Compared to initial values, the melting

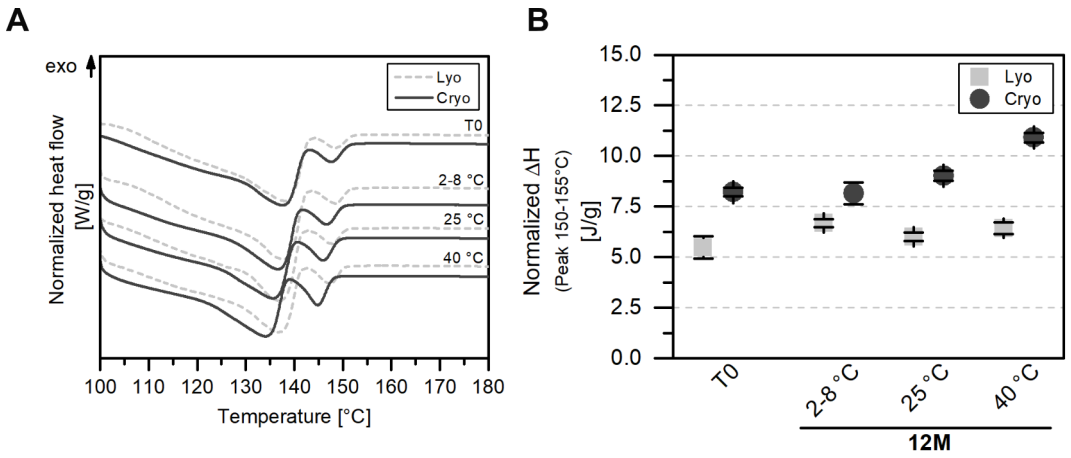

Figure II.10: DSC thermograms (A) of the highly concentrated 200 µg/mg OVA vaccine lyophilizates and cryomilled powder at stability study initiation (T0) and after 12 months storage at $2-8$ °C, 25 °C, 40 °C and respective peak enthalpies (B) of the second mannitol melting endotherm.

enthalpy increased slightly after 12 months storage of the lyophilizates and the cryomilled powder. This could indicate a formation of crystalline mannitol over time. Although recrystallization can affect the OVA antigen stability, no pronounced changes in protein stability were detected by SE-HPLC and Western blot analysis (Section 3.2.1). The results show that the storage of highly concentrated vaccine lyophilizates and cryomilled powder was possible for 12 months at up to 40 °C.

3.3 Characterization of the vaccine-oil-adhesion on hydrophilic and hydrophobic surfaces

3.3.1 Vaccine-oil adhesion on the device membrane

The needle-free powder injection device used in this study was composed of two main parts, a pharmaceutical and pyrotechnical part, which were assembled directly before application [15]. While the pyrotechnical part provided the trigger to actuate the device, the pharmaceutical part was in direct product contact. Within the pharmaceutical part, a defined area of a Ti membrane was coated with oily adjuvant followed by vaccine powder. Upon actuation of the device, a high energy pulse was transferred from the Ti membrane to the vaccine power, accelerating the powder particles to up to 500 m/s [15]. The vaccine powder, which was coated homogeneously onto the membrane, was accelerated as particle cloud through an orifice of approximately $1-2$ cm towards the skin surface.

For the loading of the device with vaccine powder, two main requirements had to be balanced to optimize the device performance. First, appropriate fixation of the vaccine powder was required to ensure reproducible loading, adherence of powder in alignment with the orifice and to provide sufficient transportation stability. On the other hand, the mixture used for vaccine fixation also needed to exhibit suitable properties to release the particles upon device actuation. Besides that, the fixation mixture had to be biocompatible and possibly serve as adjuvant for the simultaneous delivery of vaccine powder together with the fixation mixture [20].

The adhesion of the vaccine powder on the Ti membrane of the powder injection device was studied with different OVA loadings and oily mixtures and pure components for fixation. Approximately $0.1 - 0.5$ mg oil was coated onto an area of 20 mm x 10 mm on the Ti membrane followed by loading of the vaccine powder. Using this technique, approximately $0.8 - 2.5$ mg vaccine powder could be attached to the Ti membrane. The relative powder adhesion was determined as the measured powder loading after drop testing relative to the initial vaccine powder loading Q_{m/m_0} (%).

After completion of the drop test, the amount of vaccine powder that remained on the Ti surface was notably reduced (Fig. II.11). Depending on the oily mixture or component used for fixation, the adhesion of the vaccine powder lowered to varying extents. The oily mixture F1, based on the relative composition of the oily components of the adjuvant AS03 (Tab. II.1), showed a relatively low reduction of attached powder with $45 - 65$ % remaining vaccine. Comparably high values around $60 - 70$ % were found for the oily mixture F1*, stabilized with BHA, as well as the pure components α-tocopherol and polysorbate 80. Interestingly, although insufficient spreading of α-tocopherol on the Ti membrane was observed, the oil provided suitable properties to retain the vaccine powder on the membrane during drop tests. Oily mixture F2, with half-concentration α-tocopherol and polysorbate 80 relative to F1, showed reduced powder adhesion compared to oily mixture F1 with about $25 - 50$ % remaining vaccine after the drop test. Similarly, intermediate adhesion was found using highly liquid paraffin for vaccine powder fixation. The lowest particle retention on the Ti membrane was provided using the oily mixture F3 and the pure components squalene, and squalane with a particle adhesion below or equal to ~ 20 %. The oily mixture F3 was composed of a low content of 0.1 % α-tocopherol and pure squalene, in absence of additional polysorbate 80.

The OVA concentration of the model vaccine powder did not exhibit a clear effect on the adhesion properties on the Ti membrane. The powder adhesion differed only slightly

between the placebo and 25 µg/mg and 200 µg/mg OVA-loaded vaccine powder and no clear trend could be detected. However, it has to be noted that the amount of vaccine powder coated onto the membrane largely affected the percentage of remaining vaccine powder. Generally, higher initial coating increased the relative loss upon drop testing. It can be assumed that the embedding of particles in the oily liquid was superior with a lower number of particles. For this reason large standard deviations could be observed in some samples. Furthermore, it is worth noting that a partial dissolution of vaccine powder in the components, e.g. polysorbate 80, could have affected the adhesion measurements due to retention of dissolved vaccine. However, despite the mentioned limitations, clear differences between the oily liquids could be detected.

The results show that the oily mixture F1 provided suitable properties for the fixation of the highly concentrated model vaccine powder for the *in vivo* immunization study. Compared to other mixtures and components, the drop tests revealed good reproducibility and a relatively high attachment of the vaccine powder on the Ti device membrane. Using this oily mixture, the pharmaceutical device part can be loaded and transported safely without the loss or dislocation of the vaccine powder within the device. Using highly liquid paraffin as non-adjuvant oil, lower vaccine powder adhesion was detected compared to the oily mixture F1. This indicates lower stability within the device during transportation and highlights the need of gentle handling for the *in vivo* study.

3.3.2 Contact angle and work of adhesion of different oily mixtures

To evaluate the differences between the oily formulations and their ability to ensure particle adhesion on the Ti membrane, the surface tension and contact angle of the oily liquids was studied by pendant and sessile drop analysis. Comparable surface tensions were found for the oily mixtures F1 − F3 with values around 31 − 35 mN/m (Tab. II.4). The main component of the oily mixtures, squalene, showed a surface tension of 34.1 mN/m, whereas the saturated equivalent, squalane, provided a slightly lower value of 28.4 mN/m. On the other hand, α-tocopherol and polysorbate 80 provided slightly higher surface tensions of 36.6 mN/m and 35.2 mN/m, respectively.

Besides the surface tension, the contact angles of the oily mixtures on the Ti device membrane were studied in comparison to hydrophilic glass and hydrophobic PDMS reference surfaces. Figure II.11 shows that the contact angles of the oily mixtures were relatively small on the Ti membrane and close to the values detected for the glass surface. Larger contact angles were detected on the PDMS surface. This indicates that the Ti membrane

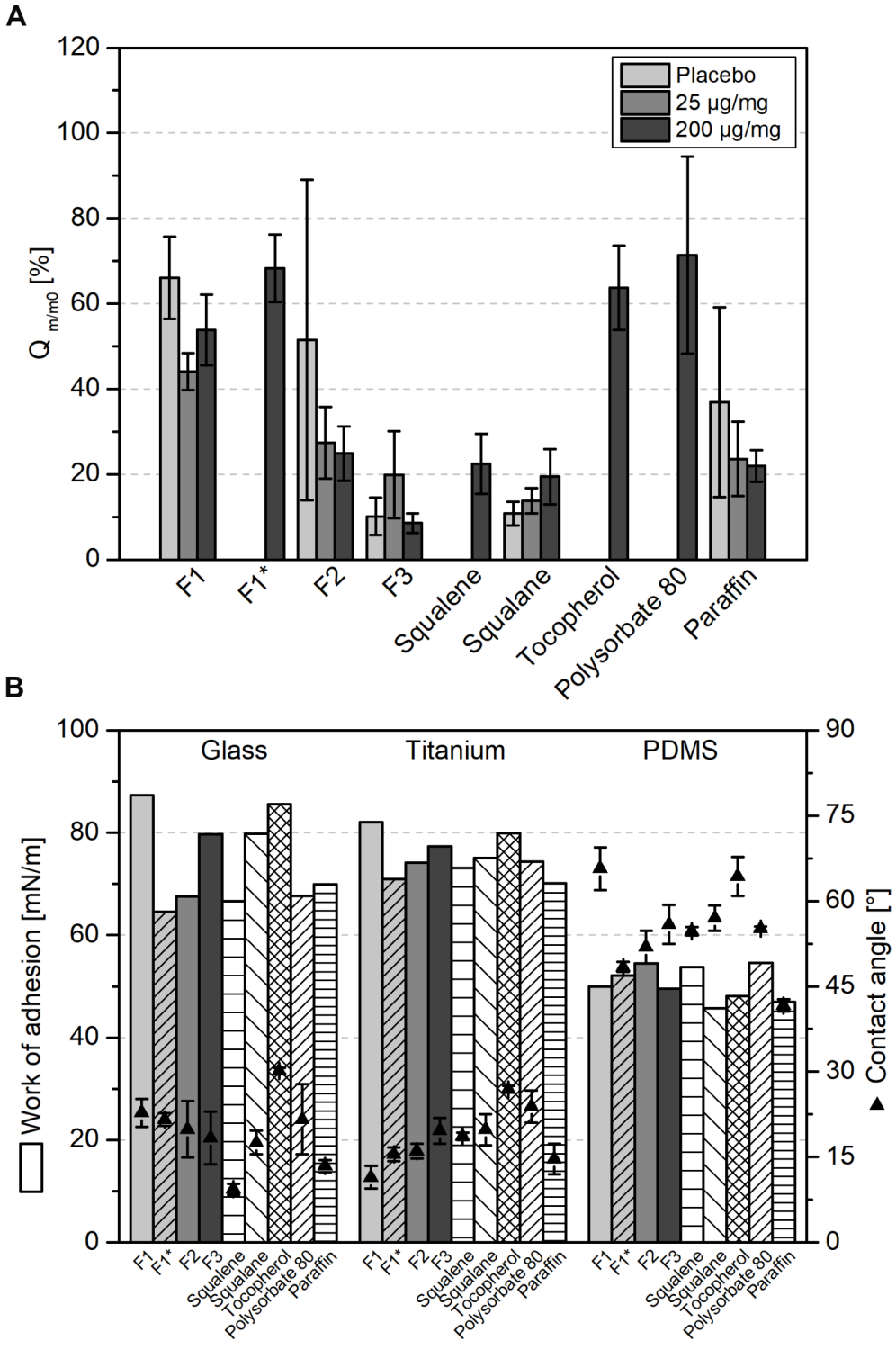

Figure II.11: Relative powder adhesion at different OVA concentrations on the Ti membrane using different adhesion oils and mixtures (A) and the calculated work of adhesion and measured contact angle of the oily liquids on a hydrophilic glass surface, the Ti membrane, and hydrophobic PDMS (B).

provided hydrophilic surface properties rather than hydrophobic interactions. Small contact angles indicate high interaction of the oily liquids with the Ti membrane, which could lead to superior spreading of the liquid and would thus be beneficial for vaccine powder adhesion.

Whereas relatively low contact angles of the oily liquids on the Ti membrane of 11.5° and 14.7° were detected for mixture F1 and highly liquid paraffin, slightly higher values in the range of 15°−20° were found for the oily mixtures F1*, F2, F3, squalene, and squalane (Fig. II.11). α-Tocopherol and polysorbate 80, which already provided the highest surface tension, also revealed the largest contact angles on the Ti surface.

Based on the surface tension and contact angle of the oily liquids, the work of adhesion W_{ls} was calculated using the Young-Dupré equation (Eq. II.1), where σ_l is the surface tension of the liquid and Θ is the contact angle of a sessile drop on the solid surface [34].

$$W_{ls} = \sigma_l(1 + cos\Theta) \tag{II.1}$$

The work of adhesion W_{ls} represents the work required to separate a drop from a clean, solid surface and was evaluated based on the surface tension and contact angle of the oily liquids (Eq. II.1) [35]. Considering this equation, the work of adhesion W_{ls} reaches the maximum interaction value at a contact angle of 0° and its lowest value at 180°. The work of adhesion thereby constitutes of polar and disperse interactions of the liquid with the solid surface.

For the oily liquids tested in this study, the work of adhesion was generally well comparable for all mixtures and pure components. No clear differences could be detected. The oily mixture F1 showed the highest work of adhesion with a value of 82 mN/m. The mixture provided a relatively strong interaction exhibiting an intermediate surface tension and low contact angle on the Ti membrane. On the other hand, paraffin showed a slightly lower work of adhesion around 70 mN/m. Calculations of disperse and polar interactions using the Owen-Wendt-Rabel-Kaelble equation (Eq. II.2) revealed a predominant disperse type of interaction for all oily liquids tested (data not shown) [36–38].

$$\frac{\sigma_l(1 + cos\Theta)}{2} = \sqrt{\sigma_l^p * \sigma_s^p} + \sqrt{\sigma_l^d * \sigma_s^d} \tag{II.2}$$

The comparison of the presented results with the vaccine powder adhesion revealed no clear trend in relation to the surface tension, contact angle, or work of adhesion of the oily

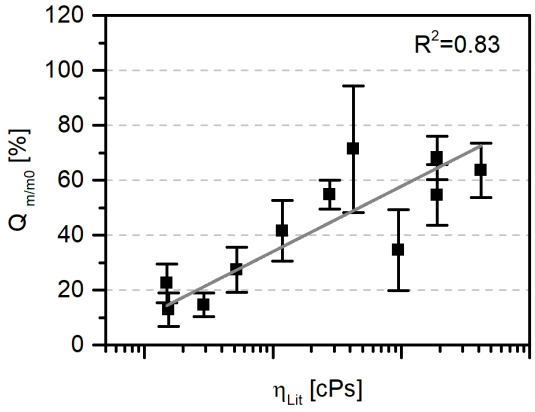

Figure II.12: Relative powder adhesion upon drop testing plotted against the viscosity of different adhesion liquids and mixtures in logarithmic scale.

liquids. For the pure components, minimally superior vaccine adhesion was detected for the oily liquids with higher surface tension, e.g. α-tocopherol and polysorbate 80. However, paraffin with the lowest surface tension provided superior particle adhesion compared to squalene or oily mixture F3.

It has to be noted that the powder adhesion as well as the contact angle measurements depend on multiple parameters. The investigation of the oily liquids mainly focused on the interaction with the Ti membrane. However, for powder adhesion, the interaction of the oily mixtures and the vaccine needs to be considered similarly. Besides that, the contact angle measurements were strongly influenced by measurement time, lower limit of detection, surface tension, and the viscosity of the liquid sample. The Pelofsky equation reveals a correlation of surface tension with molecular mass and viscosity of a liquid (Eq. II.3), where A' is equal to σ_l at infinite viscosity, C is a non-dimensional constant, M the molecular weight (g/mol), κ the thermal conductivity (cal/s cm^2), R the gas constant (1.986 cal/mol K), and η the dynamic viscosity of the liquid (cPs) [39].

$$\sigma_l = A' \exp\left(\frac{C}{R}\frac{M\kappa}{\eta}\right) \tag{II.3}$$

The equation underlines the interconnection of multiple parameters in surface tension and surface interaction measurements. As byproduct of this study, a correlation between the powder adhesion and the oily liquid viscosity was found (Fig. II.12). Literature-based viscosity values were plotted relative to the powder adhesion, revealing the following rela-

Table II.4: Overview of the relative powder adhesion as average of all measurements performed for each oily liquid and the respective liquid surface tension (σ_l) measured by pendant drop analysis and viscosity values as provided by the supplier. The theoretical viscosity of the oily mixtures F1 – F3 was calculated relative to the composition provided in Table II.1.

Formulation	Adhesion average $Q_{m/m0}$ [%]	Surface tension σ_l [mN/m]	Viscosity η_{Lit} [cPs]
F1	54.7	33.9	1900
F1*	68.3	32.1	1900
F2	34.6	35.1	955
F3	12.9	30.6	15
Squalene	22.5	34.1	15
Squalane	14.7	28.4	29
D/L-α-Tocopherol	63.7	36.6	4200
Polysorbate 80	71.3	35.2	425
Paraffin	27.5	26.0	52.5
PEG 400	41.6	36.6	118
PEG 600	54.8	n.d.	277.5

tionship (R^2=0.83):

$$Q_{m/m_0} \sim ln\left(\frac{\eta}{\eta_0}\right) \tag{II.4}$$

The viscosity of the oily mixtures was calculated based on the relative composition of the pure components (Tab. II.4). Besides viscosity, further factors are likely affecting the vaccine powder adhesion. Within this study, all oily liquids showed comparable surface tension and contact angles on the Ti surface. However, it can assumed that these parameters would also influence the adhesion strength. Further studies are needed to support the presented finding.

Considering the *in vivo* immunization study, the contact angle measurements and the work of adhesion reveal suitable properties for the loading of the needle-free powder injector using mixture F1 as oily adhesive. Based on the oily components of the AS03 adjuvant, the simultaneous delivery of the oily mixture together with the vaccine powder should

potentiate the immune response upon i.d. delivery. Notably, the low amount of oil below 0.5 mg, which can be coated onto the Ti device membrane, will likely limit the adjuvantation. The effect of the adjuvant oil therefore requires close evaluation during the *in vivo* immunization study.

3.4 Stability of the oily adjuvants in contact with model vaccine

3.4.1 Calibration curve and recovery test

The main objective of this part of the study was to evaluate the oil stability when stored in direct contact with the highly concentrated vaccine and to ensure suitable stability for the *in vivo* immunization study. For this purpose, the relative composition of the oily adjuvant components of AS03 was varied according to table II.1 to evaluate the influence on the oil stability relative to the target composition F1. Higher doses of tocopherol have been reported to lower the stability of unsaturated triglycerides [40], an effect which could also be expected with squalene, one unsaturated component of AS03. For this reason, oily mixtures with lower α-tocopherol contents compared to the target composition F1 were included in this study (F2, F3).
It has to be mentioned that α-tocopherol in AS03 emulsions is considered as essential adjuvant for vaccination, with lower α-tocopherol contents being linked to reduced adjuvant potency [41]. Consequently, composition F1 and to unknown extent F2 could be expected to act as synergistic adhesion and adjuvant mixture of squalene and α-tocopherol.
The addition of polysorbate 80 was required to ensure a spreading of the oily liquid on the Ti membrane. Preliminary tests have shown that the addition of α-tocopherol to squalene, in absence of polysorbate 80, notably reduced the spreading of the liquid on the Ti device membrane. To ensure a homogeneous loading of the vaccine powder onto the Ti membrane, the addition of polysorbate 80 was required despite the known oxidation-related destabilizing effect of polysorbate. No polysorbate 80 was required for the spreading of the oily mixture F3 with only 0.1 % α-tocopherol as antioxidant additive in the oily mixture. To assess the effect of antioxidants on the oil stability, one mixture containing 0.02 % BHA as stabilizing antioxidant (F1*) has been included in this setup. In case high amounts of tocopherol would accelerate the oil degradation, additional stabilization using alternative antioxidants such as BHA could improve the overall mixture stability. Furthermore, squalane was included in this study to represent the saturated alternative to its' unsaturated chemical equivalent squalene.

The stability of the oily liquids as provided in table II.1 as well as squalane was studied by GC-MS analysis. Either the oily liquid alone or coated with vaccine powder was exposed to UV/Vis light or thermal stress. The recovery of the oily main components squalene, squalane, and α-tocopherol was determined upon ether extraction by GC-MS relative to 5α-cholestane as internal standard.
Calibration curves of all components tested were prepared within a concentration range 20 % below the lowest and above the highest expected concentration. For all components calibration curves with good accuracy and precision were obtained ($R^2 > 0.99$).
Furthermore, a recovery study was performed to evaluate the suitability of the method to assess the oil stability. For this purpose, samples at the target oil content and ±20 % were prepared, with and without vaccine powder. Ether extraction was performed and the samples were analyzed by GC-MS. Squalene showed good recovery between $86 - 100$ % for all oily mixtures. Squalane provided second highest recovery values between $78 - 101$ %. In general, recovery rates between $80 - 120$ % were considered acceptable for the analytical approach. The recovery evaluation shows that the vaccine powder did not notably affect the extraction and quantification of squalene or squalane within the utilized sample preparation conditions.
Beside these oils, the recovery of α-tocopherol was highly dependent on the oil composition and sample preparation. For the oily mixtures F1, F1*, and F2, the α-tocopherol recovery was between $63 - 121$ %. Compared to the squalene and squalane recovery the analysis of α-tocopherol provided lower precision. Moreover, exceptionally poor recovery was obtained for the oily mixture F3 with only 0.1 % tocopherol content. Whereas $63 - 92$ % recovery was found for oil samples alone, an average of only 0.3 % was achieved for the sample preparation with vaccine powder. It can be assumed that the low amount of α-tocopherol adsorbed to the vaccine powder and could not be fully extracted for quantification. The evaluation of the oil stability was therefore limited to squalene and squalane analysis and the quantification of α-tocopherol for F1, F1*, and F2 only.

3.4.2 UV/Vis stress test of the oily adjuvant

The UV/Vis stress test was performed to evaluate the stability of different oil compositions and oil components and to assess the impact of the highly concentrated protein-loaded vaccine powder on the oil stability. UV/Vis light exposure significantly reduced the squalene recovery in F1-F3 compared to the samples shielded from light, which only underwent minimal thermal stress (Fig. II.13). Notably, no significant differences between light expo-

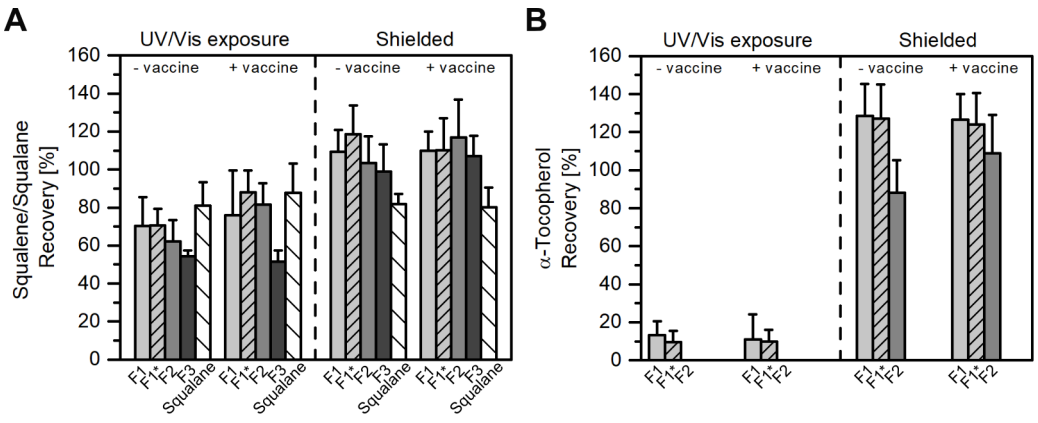

Figure II.13: Recovery of squalene/squalane (A) and α-tocopherol (B) from different oily liquids without or in direct contact with protein-loaded vaccine powder after UV/Vis light exposure or shielded from light (Two sample t-test, $\alpha = 0.05$, n=6, * $p < 0.05$, ** $p < 0.01$, *** $p < 0.001$).

sure and shielding was detected for squalane-containing samples. This indicates a superior stability of squalene over its' unsaturated chemical equivalent, squalene, even in presence of an antioxidant.

On the other hand, a trend of decreasing squalene recoveries upon UV/Vis exposure were associated with lower contents of α-tocopherol. A significantly lower recovery of $\sim$ 50 % was detected for the mixture F3 containing only 0.1 % tocopherol. The results suggest that higher tocopherol contents improved the stability and recovery of squalene under UV/Vis light. Light exposure led to the degradation of α-tocopherol, as confirmed by very low recoveries around 10 % remaining tocopherol in the mixtures F1* and F1*. For oily mixture F2, the α-tocopherol content was below the limit of quantification after UV/Vis exposure. It can be therefore expected that squalene is stabilized by α-tocopherol under UV/Vis light and the oil stability improves with increasing α-tocopherol content.

Besides the influence of the oil composition on the oil stability, the results show that the vaccine powder contact did not influence the oil stability negatively (Fig. II.13). In fact, upon UV/Vis exposure, the squalene recovery was significantly higher for the formulations F1* and F3 when in direct contact with the protein-loaded vaccine powder. An explanation for these findings could be a shielding effect that the vaccine powder provided, consequently influencing the oily liquid stability. The white color of the powder absorbs distinct wavelengths of the visible light, could thus affecting the light inferference with the oily components. For the samples shielded from UV/Vis light, no effect of the vaccine powder on the squalene, squalane, or tocopherol recovery was detected. Therefore it

can be concluded that the increased squalene recovery in samples after UV/Vis light was not attributed to an enhanced extraction efficiency but due to the stabilizing effect of the protein-loaded vaccine powder itself.

3.4.3 Long-term and thermal stability of the oily adjuvant

The long-term oil stability was evaluated after 3 and 6 months storage at $2-8$ °C, 25 °C, and 40 °C. Figure II.14 shows the squalene, squalane, and α-tocopherol recoveries of the different oily mixtures stored without or in direct contact with the highly concentrated vaccine. The recovery of squalene and α-tocopherol in all oil mixtures remained relatively stable for up to six months storage at $2-8$ °C. With increasing storage temperature, the squalene recovery decreased notably for all oily mixtures as well as pure squalane. Similar observations could be made for the recovery values of α-tocopherol under accelerated storage condition.

Following 3 months storage at 40 °C, about $80-90$ % squalene/squalane was recovered from the sample. On the other hand, the tocopherol recovery was dependent on the oil composition, showing lower recovery values around 55 % after 3 months for mixture F2. Interestingly, the oily mixture F1* stabilized with 0.02 % BHA showed higher squalene recoveries after 3 months compared to the original composition F1 for all storage conditions. After 6 months storage, differences in the squalene and α-tocopherol recovery of the mixtures F1-F3 could be noticed. A slight trend of decreasing stability associated with lower concentrations of α-tocopherol was observed. Generally, a reduction in squalene recovery was also associated with a loss in α-tocopherol. The most pronounced difference was detected for the oily mixture F3 that provided a notably lower squalene recovery around 40 % after 6 months storage at 40 °C without vaccine powder. On the other hand, the recovery was significantly increased when the same oil mixture was stored in direct contact with the protein-loaded vaccine powder.

Generally, it was noticed that the storage stability of the oily mixtures and components increased in contact with vaccine powder. Higher squalene, squalane, and α-tocopherol recoveries were detected for a striking majority of the samples. For several conditions, statistically significant higher recoveries were found. This indicates that the vaccine powder most likely exhibits a stabilizing effect on the oily mixtures under UV/Vis exposure as well as thermal stress.

It can be summarized that higher contents of α-tocopherol and the presence of protein-loaded vaccine powder improved the stability of the oily adjuvant mixture. The results

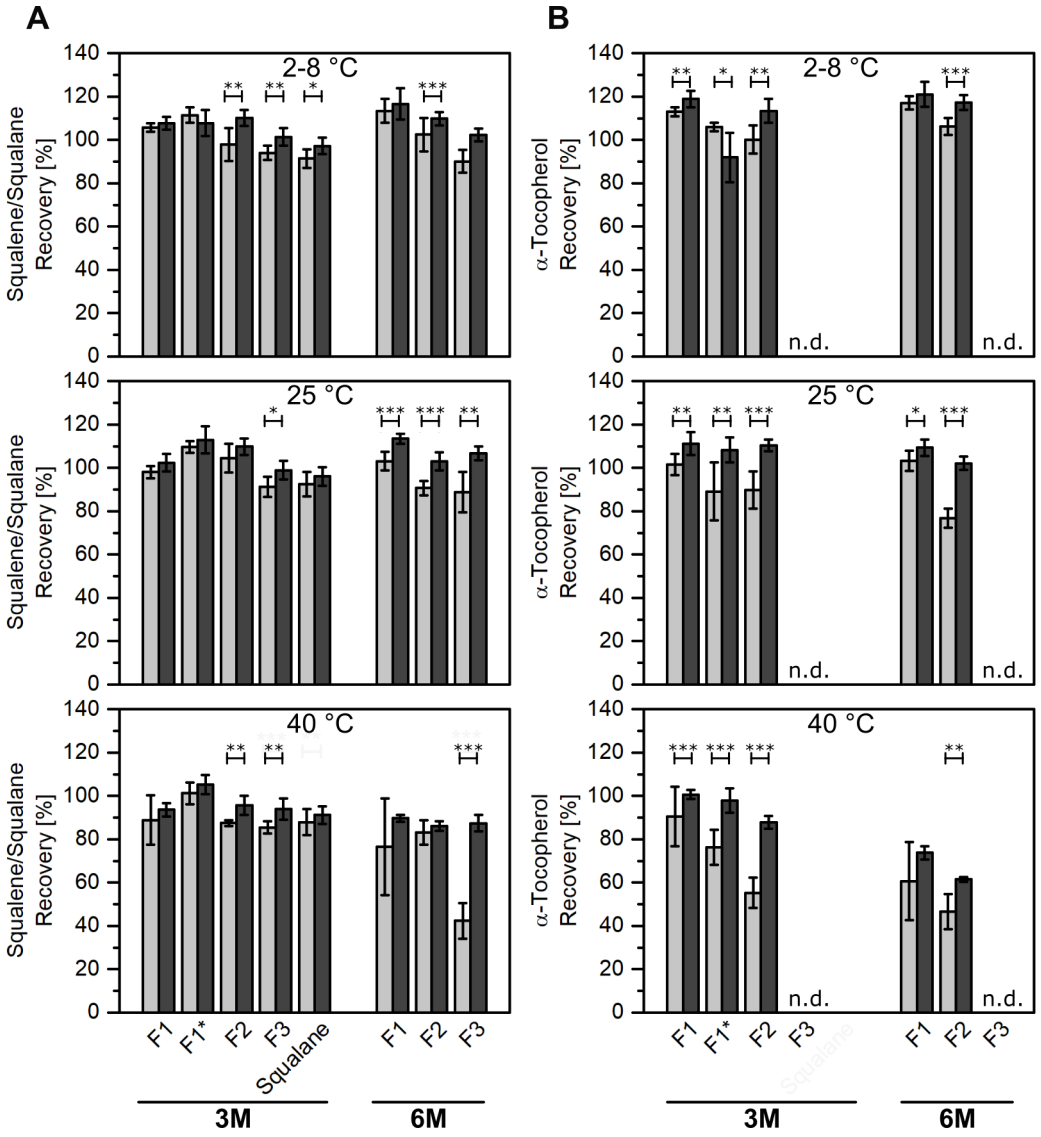

Figure II.14: Recovery of squalene/squalane (A) and α-tocopherol (B) from different oily liquids stored without (light grey) or in direct contact with highly concentrated protein-loaded vaccine powder (dark grey) for 3 and 6 months at $2-8$ °C, 25 °C, and 40 °C (Two sample t-test, $\alpha = 0.05$, n=6, * $p < 0.05$, ** $p < 0.01$, *** $p < 0.001$).

also indicate a beneficial effect of BHA as additional antioxidant, however further studies to fully evaluate a possible effect including other antioxidants remain to be conducted. Besides that, the loading and storage of the oily adjuvant mixture F1 and the vaccine powder is feasible. A storage for up to 3 months at $2 - 8$ °C can be readily supported from the oil stability perspective. However, further investigations are needed to assess the vaccine powder and antigen stability during storage in contact with the oily mixture.
For the *in vivo* immunization study the oily mixture F1, based on the oily components of squalene-based AS03, was used as oily adhesive with adjuvant properties. Notably, other oily components with suitable adhesion properties could be used for the vaccine powder loading onto the device. Squalane could represent a suitable alternative to its' unsaturated equivalent, squalene, providing adjuvant potency and enhanced chemical stability due to the fully saturated structure.

3.5 *In vivo* immunization study with a highly concentrated vaccine administered by powder injection

3.5.1 Evaluation of vaccine properties for needle-free powder injection

Highly concentrated OVA vaccine was prepared under aseptic conditions using endotoxin-low excipients. All preparation processes that required open product handling were performed under LAF. One exception was vaccine powder sieving and aliquotation, which was performed under dry nitrogen atmosphere to avoid moisture uptake by the vaccine powder. The cryomilled vaccine for *in vivo* immunization with a concentration of 200 µg/mg OVA as well as the OVA-AS03 emulsion were prepared using OVA grade VII as model vaccine with high purity and low endotoxin content.
The highly concentrated OVA model vaccine used for immunizaton was characterized using selected methods (Tab. II.5). No changes in lyophilizate characteristics were detected considering the residual moisture, SSA, XRPD profile or DSC curves (data not shown). A higher monomer content and reduced oligomer contents were detected for the OVA grade VII vaccine compared to the lower grade OVA (Tab. II.5). Similar to the observations in section 3.1.2, cryomilling induced the formation of a small amount of HMWS. Furthermore, slightly increased subvisible particle counts, but comparable turbidities compared to the results discussed in section 3.1.3 were detected.
The endotoxin content of the highly concentrated OVA vaccine powder was analyzed using a chromogenic LAL assay. Low values of 31.6 EU/mg vaccine, 35.9 EU/mg, and

Table II.5: Results of SE-HPLC, subvisible particles, residual moisture, and SSA analysis of the placebo and highly concentrated model vaccine used in the *in vivo* study, prepared with of target content of 200 µg/mg OVA grade VII. Subvisible particle and turbidity analysis was restricted to lyophilizates only due to material restrictions. (n.a.= not analyzed, n.d.= not detected)

Analysis		**Placebo**	**200 µg/mg OVA**	
		(Lyo)	(Lyo)	(Cryo)
SE-HPLC				
Monomer	[%]	-	96.5 ± 0.0	96.3 ± 0.1
Dimer	[%]	-	3.4 ± 0.0	3.5 ± 0.0
HMWS	[%]	-	n.d.	0.2 ± 0.0
LMWS	[%]	-	n.d.	n.d.
Subvisible particles				
Particles $\geq$ 1 µm/mL		1,448	9,997	n.a.
Particles $\geq$ 10 µm/mL		6	10	n.a.
Particles $\geq$ 25 µm/mL		1	2	n.a.
Turbidity	[FNU]	2.9	1.7	n.a.
Residual moisture	[%]	0.6 ± 0.0	0.4 ± 0.0	n.a.
SSA	[m^2/g]	0.41	0.19	n.a.

63.1 EU/mg were found for the liquid 200 µg/mg OVA formulation prior processing and after lyophilization and cryomilling, respectively. The results suggest a cryomilling-related increase of endotoxins in the vaccine. However, it remains unclear whether this increase was induced by sample preparation variability or processing-dependent introduction of endotoxins. Considering an applied dose of 1 mg vaccine powder per needle-free injection, the endotoxin levels of the highly concentrated vaccine were within Pharmacopoeial requirements for influenza vaccine (split virion) allowing a maximum of 100 EU per dose [42, 43]. In comparison, 732 EU endotoxins per mg OVA were detected for the model antigen grade V. No detectable amounts of endotoxins have been found in the liquid placebo formulation prior lyophilization and cryogenic milling. It can be therefore assumed that the final endotoxin content of the placebo vaccine powder was within Pharmacopoeial limits.

To sum up, the placebo and the highly concentrated vaccine with a concentration of 200 µg/mg OVA provided suitable properties and quality for intradermal administration

using the needle-free powder injection device.

3.5.2 Compatibility of the liquid ovalbumin-AS03 emulsion vaccine

Besides the model vaccine for needle-free powder injection, the compatibility of the OVA liquid vaccine with the AS03 emulsion was tested. The adjuvant AS03 is a liquid emulsion with a milky-white appearance and was used for i.m. vaccination in 1:1 dilution with the Pandemrix® influenza vaccine. For the vaccination of an adult, usually 2.5 mL of subunit vaccine is mixed with 2.5 mL adjuvant emulsion, providing an absolute adjuvant dose of 10.69 mg squalene, 11.86 mg α-tocopherol, and 4.86 mg polysorbate 80 [21]. This procedure was adapted to study the compatibility with OVA.
The visual and microscopic inspection of the antigen-adjuvant mixtures gave no signs of reduced quality of the vaccine emulsion (data not shown). Furthermore, the hydrodynamic diameter measured by dynamic light scattering (DLS) was comparable for AS03 emulsion diluted with PBS and 0.8 mg/mL OVA with values of around 164 nm (PDI= 0.09) and 165 nm (PDI=0.09), respectively. Although the analysis of the OVA-AS03 emulsion was not feasible by SDS-PAGE and Coomassie blue staining due to emulsion-related blurring of bands, Western blot analysis revealed a profile comparable to OVA standard as discussed in section 3.2 (data not shown).
The liquid OVA vaccine for i.m. injection with a concentration of 0.8 mg/mL provided and endotoxin content of 107 EU/mL and 79.1 EU/mL for the immunization on day 0 and 14, respectively. Considering the subsequent 1:1 dilution with presumably endotoxin-free AS03 adjuvant emulsion and the administration of 0.5 mL, the endotoxin levels were below the Pharmacopoeial limits [42, 43].
The liquid vaccine for i.m. injection in the positive control group C exhibited suitable properties and quality for the use in the *in vivo* study.

3.5.3 Characterization of the powder injection site

The *in vivo* immunization study evaluating vaccination by needle-free powder injection was performed in piglets. Due to the device dimensions and the employed approach of particle administration, this study would not have been feasible with smaller animal species, e.g. mice. Furthermore, it has been reported that pig skin represents a well suitable model for human skin [44–46]. Since pig skin reportedly exhibits a thicker SC [44] compared to humans, piglets with a maximum age of seven weeks at the time of study initiation were included to maximize similarity to human skin.

Table II.6: Theoretical penetration depths of model polystyrene (PS) particles and (FITC)-loaded vaccine powder, calculated by equations II.5-II.7 based on a model used by Kendall *et al.* [14]. The particle velocities and *in vivo* penetration depths, as well as the PS particle density and diameter were taken from [15]. Experimental penetration depths were obtained using PS particles and FITC-loaded vaccine powder with particle radii of 21 µm and 10-40 µm, respectively.

Particle type	ρ_p [g/cm^3]	r_p [µm]	v_i [m/s]	$v_{i,\mathrm{ve}}$ [m/s]	$d_{\mathrm{p,calc}}$ [µm]	$d_{\mathrm{p},in\ vivo}$ [µm]
PS particles	1.1	10	516	294	$23-38$	n.d.
		21	518	395	$47-81$	$50-120$
		30	521	433	$70-121$	n.d.
FITC-loaded	1.55	10	526	354	$33-55$	n.d.
powder		25	526	449	$82-142$	$20-120$
		40	526	476	$131-229$	n.d.

In a preliminary study, which was actively supported by myself, the particle penetration into pig skin was assessed *in vivo* [15]. Histological images of skin sections upon needle-free powder injection of 40 µm polystyrene (PS) model particles or model vaccine loaded with fluorescein isothiocyanate (FITC) revealed an intradermal deposition below the SC in the epidermal and upper dermal layer.

A theoretical evaluation of the penetration depth (d_p) by the model used by Kendall *et al.* matched well with the experimentally obtained data (Tab. II.6) [10, 14]. Assuming a successful breaching of the SC, the velocity of the particles at the border to the viable epidermis ($v_{i,\mathrm{ve}}$) was calculated using eq. II.5. Based on the obtained particle velocity, the penetration depth into the viable epidermis (d_ve) and absolute penetration depth (d_t) was calculated (eq. II.6 and eq. II.7).

$$v_{i,\mathrm{ve}} = \sqrt{\left(v_i^2 + \frac{6\sigma_\mathrm{sc}}{\rho_\mathrm{sc}}\right) e^{\frac{-3\rho_\mathrm{sc} t_\mathrm{sc}}{4\rho_\mathrm{p} r_\mathrm{p}}} - \frac{6\sigma_\mathrm{sc}}{\rho_\mathrm{sc}}} \tag{II.5}$$

$$d_\mathrm{ve} = \frac{4\rho_\mathrm{p} r_\mathrm{p}}{3\rho_\mathrm{ve}} \left[\ln\left(\frac{\rho_\mathrm{ve} v_{i,\mathrm{ve}}^2}{6\sigma_\mathrm{ve}} + 1\right)\right] \tag{II.6}$$

$$d_\mathrm{t} = t_\mathrm{sc} + d_\mathrm{ve} \tag{II.7}$$

The calculations were performed assuming a ballistic yield stress of the SC (σ_{sc}) of 170 MPa as reported at ambient temperatures [14], a density (ρ_{sc}) of 1500 kg/m^3 [47] and a thickness (t_{sc}) of 10.9 µm [14, 48]. The properties of the viable epidermis were 2.2 MPa and 10 MPa as lower and upper limits of the yield stress of the viable epidermis (σ_{ve}) [14, 49, 50] and 1150 kg/m^3 for the tissue density (ρ_{ve}) [47]. The density (ρ_p) and radii (r_p) of the PS particles as well as the particle impact velocities (v_i) were from [15]. For the model vaccine powder, the density discussed in section 3.1.4 and the nominal particle size described in 2.2.1 were used for calculations.

The calculations show that the particle penetration depth increases with increasing particle density, radius, and velocity. Although it has been reported that the particle acceleration and velocity decrease with increasing density and radius for a different type of needle-free powder injector [51–53], no similar relationship was observed for the device used in this study (Tab. II.6) [15]. Nonetheless, the previously used theoretical prediction of the penetration depth [14], is expected to hold for this study.

During penetration of the SC, the particle velocity decreases. This effect is most pronounced with decreasing particle size and density. If the velocity is sufficiently high, the particle penetrates into the viable epidermis, which exhibits lower mechanical strength compared to the SC. For the PS particles, penetration depths between $50 - 120$ µm were observed, which is close to the theoretically predicted value of $47 - 81$ µm (Tab. II.6). The relatively high distribution of penetration depth may potentially originate from high particle payloads [50].

For the FITC-loaded vaccine powder with particle sizes in the range of $20-80$ µm, comparable penetration depths between $20 - 120$ µm were observed *in vivo* (Tab. II.6). Assuming full integrity upon particle impaction and penetration into the skin tissue, penetration depths between $33 - 223$ µm were predicted. Whereas lower penetration was expected for smaller particles, a larger diameter of 80 µm could potentially facilitate a penetration as deep as 223 µm. However, it remains unclear whether the sugar-based vaccine particles remain intact upon contact with the skin. More likely, the size of the particle decreases by breakage upon impaction and partial dissolution during tissue penetration, consequently lowering the effective particle velocity and leading to lower penetration depths.

As discussed in the previous paragraphs, the microscopic penetration of particles into the SC agrees well with theoretical predictions and is thus reasonably well understood. Considering potential medical applications, a macroscopic assessment of the administration side is also of major relevance and will be addressed in the following.

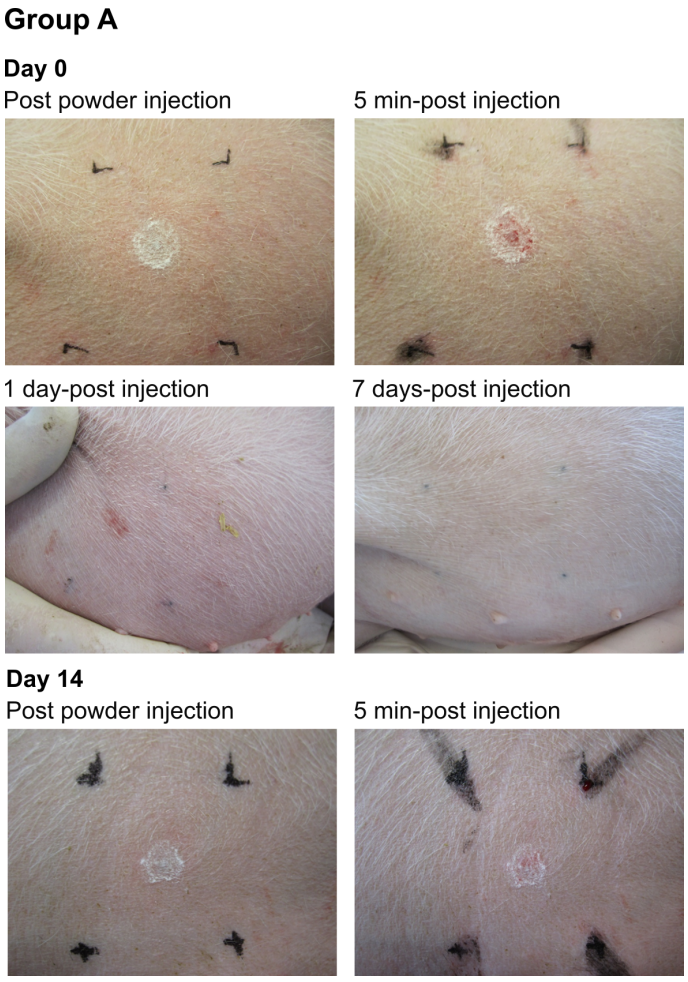

Figure II.15: Exemplary photographs of the powder injection site of study group A on day 0 directly after vaccine administration and 5 min, 1 d, and 7 d post administration. Furthermore, administration site of the booster powder injection on day 14 on the same study animal. Images used in [15]

Four different groups were studied in the the *in vivo* immunization study including three groups using needle-free powder injection for intradermal vaccine delivery (Tab. II.2, p. 54). For the needle-free powder injection, two main aspects were assessed: The impact of the adjuvant adhesive and the antigen loading. Placebo vaccine powder and paraffin without known adjuvant activity, administered by needle-free powder injection, served as negative control (A). Two verum groups used 200 µg/mg OVA vaccine powder coated onto the device using paraffin (B) or oily mixture F1 with the relative composition of the oily ingredients of AS03 (C). The outcome of the powder injection groups was compared to a positive control (D) using an i.m. injection of a OVA AS03-adjuvanted liquid vaccine.

Figure II.16: Exemplary photographs of the powder injection site of study group A on day 0 directly after vaccine administration and 5 min, 1 d, and 7 d post administration. Furthermore, administration site of the booster powder injection on day 14 on the same study animal. (Images used in [15])

The macroscopic evaluation of the application sites gave no signs of severe tissue damage after needle-free powder injection (Figs. II.15, II.16, II.17). The pig skin prior injection had a pink, healthy appearance. Directly after powder administration, a thin powder layer was observed on the skin surface, maintaining normal skin appearance. Within 5 min, the administration site developed diffuse purpura and a dot-shaped central lesion for some animals. These minor bleedings were mainly observed in the superficial skin below the skin surface. The intensity of purpura was not related to specific groups but occurred to variable degree. Notably, powder injection on day 14 affected the skin to a lesser extent. Histological evaluation showed no signs of severe or permanent tissue damage at the end

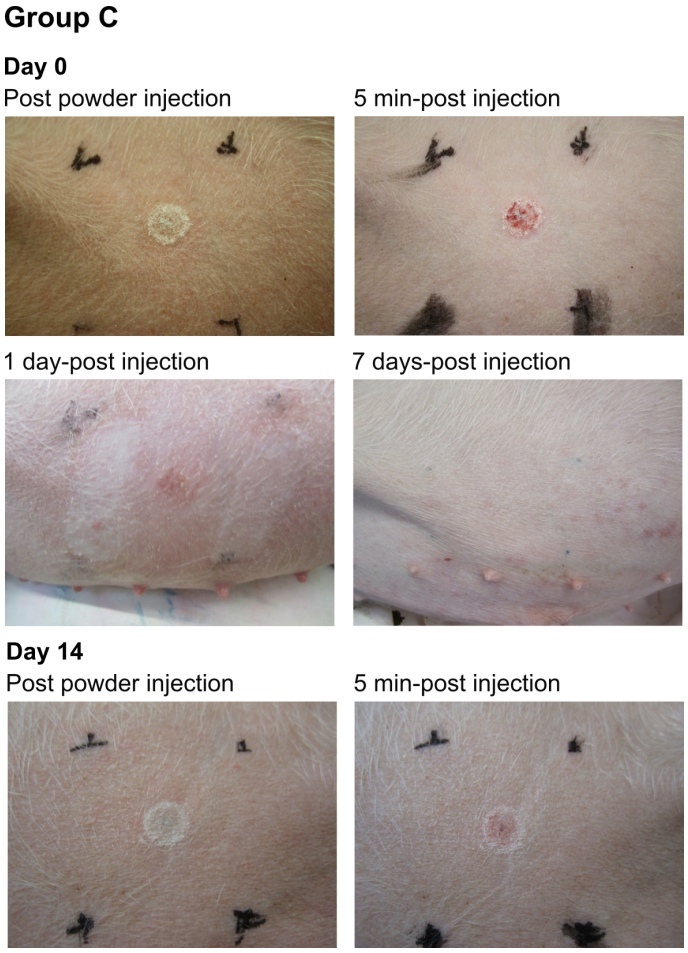

Figure II.17: Exemplary photographs of the powder injection site of study group B on day 0 directly after vaccine administration and 5 min, 1 d, and 7 d post administration. Furthermore, administration site of the booster powder injection on day 14 on the same study animal. (Images used in [15])

of the 28 days study.

The observations suggest a successful intradermal delivery of the vaccine powder for all powder injection groups. However, it has to be mentioned that a distinct, unknown amount of vaccine was not deposited in the skin but remained on the surface. Notably, confirmatory studies revealed that only a limited number of particles was found to penetrate into the tissue whereas the larger amount of ~ 75 % remained on the excised pig skin surface [15]. To maximize the chances of intradermal uptake of residual vaccine formulation after skin surface disruption by powder injection, a patch was used to cover the administration sites for a couple of hours. In literature, alternative options to increase the intradermal delivery involve the mechanical weakening of the skin barrier by elevated temperatures and

humidities [14], or by skin microporation [54].
The intracutaneous bleedings, which were visible one day after powder injection, disappeared completely within 7 days. This indicates a fast healing of the tissue damage induced by powder injection. It has been discussed that certain tissue disruption can serve as physical adjuvant supporting the induction of immune responses [55]. Therefore, the initial tissue damage was considered preferential for this study.

3.5.4 Immune responses upon immunization

At specific time points upon immunization, the immune response was evaluated by quantification of the OVA-specific IgG antibody titer in pig serum using a direct ELISA. The evaluation of the antibody titer revealed the lack of immune responses in all powder injection groups (A, B, C) (Fig. II.18). Both powder injection verum groups (B, C) showed titers comparable to the negative control (A) over the entire study duration. On the other hand, the positive control (D) exhibited increasing OVA-specific antibody titer during the study. Slightly higher values were detected for the positive control after day 14. Following 21 and 28 days after the first i.m. injection of OVA-AS03 vaccine, significantly higher specific antibody titers compared to the powder injection groups were detected.
Besides the antigen-specific antibody titer, the total IgG content of the pig sera was quantified using a self-developed sandwich-ELISA. No differences were detected between all time points of testing or the study groups (Fig. II.19). Due to the lack of difference in total IgG despite the observed changes in OVA-specific titer, this assay was not considered further for the evaluation of the immune response upon intradermal powder or i.m. immunization.
The results of the OVA-specific antibody titer show that no immune response was elicited by intradermal, needle-free powder injection using the highly concentrated OVA vaccine. Despite the high antigen content of 200 µg/mg OVA, it can be assumed that the dose delivered into the tissue was not sufficient to initiate an immunologic cascade within 28 days. Considering a total delivery of 25 % as stated before [15], only 50 µg OVA reached the dermal tissue. For the relatively weak antigen OVA, this dose was insufficient to generate a humoral IgG-based immunity.
Besides the actual antigen dose delivered into the skin, the adjuvant dose likely played an important role to enhance the immune response. Compared to the conventional dose of AS03 discussed in section 3.5.2, only $0.4 - 1.8$ % of this dose was delivered together with the vaccine considering $0.1 - 0.5$ mg adjuvant oil loading and 100 % delivery efficiency. Most likely, the adjuvant dose applied by powder injection was not sufficient to enhance

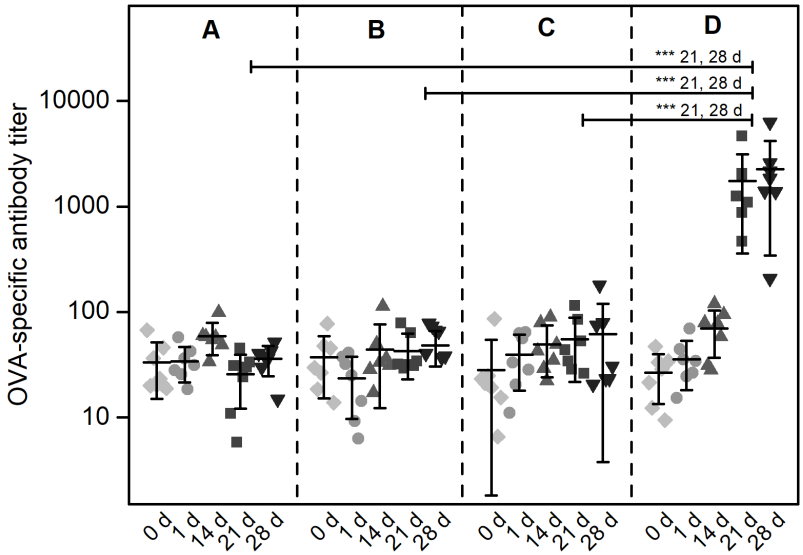

Figure II.18: OVA-specific antibody titer quantified by direct ELISA after 0, 1, 14, 21, and 28 days after immunization. Vaccine was administered on day 0 and day 14 by needle-free powder injection or i.m. injection for the different study groups as provided in table II.2. (One-way ANOVA on ranks, Kruskal-Wallis, $\alpha = 0.05$, n=7, *** $p < 0.001$).

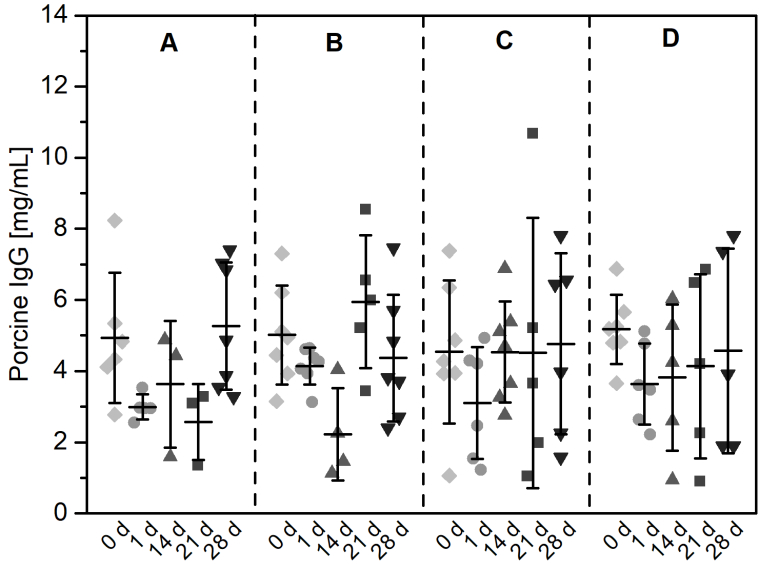

Figure II.19: Total amount of IgG in porcine serum quantified by Sandwich-ELISA 0, 1, 14, 21, and 28 days after immunization, administered on day 0 and 14 by needle-free powder injection or i.m. injection (Tab. II.2) (One-way ANOVA, $\alpha = 0.05$, n=7).

the immune response, which is supported by the results obtained using an influenza vaccine in the same study setup [15].
On the other hand, the full dose of both, 200 µg OVA plus AS03 adjuvant, was administered by i.m. injection and led to a significant immune response. Notably, even higher titers have been detected using stronger antigens, e.g. influenza [15, 56]. Retrospectively, with the current knowledge, an additional control group covering the i.m. injection of the full or 25 % of the dose OVA antigen in absence of adjuvant would have been beneficial to assess the potency of the cutaneous vaccination approach by needle-free powder injection. Moreover, a third vaccination by powder injection and the analysis of antibody titers at additional timepoints after 28 days should be considered in future studies.

4 Conclusion

This study shows that the combination of collapse lyophilization and cryogenic grinding allows for the manufacturing of a highly concentrated 200 µg/mg OVA-loaded, vaccine powder suitable for needle-free powder injection. The vaccine powder obtained by this approach provides an antigen dose per mg vaccine up to 13 times higher than a conventional dose of 15 µg antigen used for influenza vaccination [57–59]. Compared to the pandemic vaccine Pandemrix® the dose is even 53 times higher [21].
Despite the lack of antigen-specific immune responses upon intradermal delivery of the highly concentrated OVA vaccine, protective immune responses can be expected upon intradermal powder injection using antigens with higher potency. Considering a cutaneous delivery efficiency of 25 %, an influenza vaccine powder with a loading of 60 µg/mg would be required to achieve an intradermal deposition of a conventional influenza antigen dose. Furthermore, a loading of only 15 µg/mg would be required when the vaccine is administered in combination with a potent adjuvant system.
With the current device design, the AS03 adjuvant dose delivered was too low to potentiate the immune response. The particle fixation through the adjuvant is an attractive approach, however the common dose of 27.41 mg oily AS03 components [21] exceeds the existing device capacity by far. The use of alternative adjuvants suitable for cutaneous vaccination as discussed in section 2.3, incorporated into the vaccine powder, could be beneficial for the approach of intradermal needle-free powder immunization.
The highly concentrated vaccine provided good stability without loss of antigenicity or pronounced changes in vaccine quality within 12 months of storage at up to 40 °C. However,

other studies using influenza antigens have shown reduced stability of low-dose vaccine at elevated storage temperatures [15]. Therefore, the stability of the vaccine powder needs separate assessment for each type and concentration of vaccine antigen used.

The loading of the vaccine powder onto the device membrane is feasible using a mixture of the oily components of the AS03 adjuvant system. The oily mixture provides suitable spreading on the Ti membrane, good powder adhesion for storage and transportation, and also allowed for a full release of the vaccine powder upon device actuation. Notably, other oils and oily mixtures can be used for vaccine powder fixation. Liquids with good spreading behavior and high viscosity are expected to optimize the particle adhesion while maintaining a good release from the device. Notably, the liquids used for this purpose are required to maintain the sugar-based vaccine integrity, rendering hydrophobic oils and liquids the preferred choice for particle adhesion.

The vaccine powder-oil compatibility is a critical factor for the loading and storage of the device before use. In this study, the stability of the oil was investigated and revealed a tendency of increased oil stability when stored in direct contact with the vaccine powder. The vaccine stability in direct oil contact was not focus of this study and should be address ed in a different work.

All in all, the results of this study show that the immunization using needle-free powder injection is feasible, but requires precise optimizations. The manufacturing process allows for the preparation of vaccines at variable concentrations up to 200 µg/mg and the loading, storage, and transport of the device with oil-fixed vaccine powder provides notable stability. Cutaneous vaccination by needle-free powder injection is an attractive approach since it allows for an easy, quick, and pain-free administration of vaccine. The deposition of antigen in the skin tissue, rich of APCs, has been shown to successfully elicit protective immunity [60–62]. Compared to conventional i.m. injection, cutaneous vaccination can facilitate a dose reduction of up to 60 % [62]. The high flexibility of needle-free powder injection with regard to the loaded vaccine is a major advantage. The applied powder may be readily loaded with other potent vaccine and antigens, e.g. DNA or RNA, virus-like particles, inactivated or attenuated vaccine candidates. After solving the main disadvantages of high production costs and overcoming safety-related licensing hurdles, the powder injection device has a promising potential to become an alternative to conventional vaccination.

5 Acknowledgements

This work was financially supported by the Federal Ministry of Education and Research (BMBF), Germany, grant no. 13N11318.
I would like to thank Cihad Anamur, Julia Engert, Gerhard Winter (Department of Pharmacy, Pharmaceutical Technology and Biopharmaceutics, Ludwig-Maximilians-University Munich, Germany), Christian Fellner, Peter Lell (PyroGlobe GmbH, Hettenshausen, Germany), and Wolfgang Rebel for their support during the *in vivo* study (section 3.5). Special thanks go to Cihad Anamur, Christian Fellner, and Peter Lell, who developed a powder injector suitable for needle-free intradermal injection.
Also, I would like to express my gratitude towards Julia Stadler, Susanne Zöls, and Mathias Ritzmann (Clinic for Swine, Ludwig-Maximilians-University Munich, Oberschleissheim, Germany) for the successful collaboration during the *in vivo* study (section 3.5).
I would also like to thank Lydia Beresuzkij and Christine Göttsberger for their support in characterizing the particle adhesion, presented in section 3.3, during their internship, which was designed and supervised by myself.
Furthermore, I thank Florian Vetter and Christoph Müller (Department of Pharmacy, Center for Drug Research, group of Prof. Dr. Franz Bracher, Ludwig-Maximilians-University Munich) for performing the GC-MS analysis presented in section 3.4.

Bibliography

[1] B. G. Weniger, M. J. Papania, Alternative vaccine delivery methods, in: S. A. Plotkin, W. A. Orenstein, P. A. Offit (Eds.), Vaccines, 6th ed., Elsevier/Saunders, Philadelphia, 2013, pp. 1200–1231. URL: http://bit.ly/Vaccines6thChap61a. doi:10.1016/B978-1-4557-0090-5.00063-X.

[2] J. Canter, An outbreak of hepatitis b associated with jet injections in a weight reduction clinic, Arch Intern Med 150 (1990) 1923.

[3] S. Mitragotri, Immunization without needles, Nat Rev Immunol 5 (2005) 905–916.

[4] A. D. Ravi, D. Sadhna, D. Nagpaal, L. Chawla, Needle free injection technology: a complete insight, Int J Pharm Investig 5 (2015) 192–199.

[5] J. L. Brandes, R. K. Cady, F. G. Freitag, T. R. Smith, P. Chandler, A. W. Fox, L. Linn, S. J. Farr, Needle-Free Subcutaneous Sumatriptan (Sumavel DosePro): Bioequivalence and Ease of Use, Headache 49 (2009) 1435–1444.

[6] PharmaJet Inc., FDA approves use of AFLURIA®, influenza vaccine with PharmaJet's needle-free injector. King of Prussia, PA/Golden, CO, USA, 2014. URL: http://pharmajet.com/fda-approves-afluria-influenza-vaccine-pharmajets-needle-free-injector/, [accessed 2014-10-05].

[7] R. Matheson, Startup's needle-free drug injector gets commercialization deal - Collaboration with pharmaceutical giant will bring smart jet-injection device to market, 2017. URL: http://news.mit.edu/2017/startup-needle-free-drug-injector-gets-commercialization-deal-1208, [accessed 2018-03-11].

[8] D.-c. Tang, M. DeVit, S. A. Johnston, Genetic immunization is a simple method for eliciting an immune response, Nature 356 (1992) 152–154.

[9] M. D. Macklin, D. McCabe, M. W. McGregor, V. Neumann, T. Meyer, R. Callan, V. S. Hinshaw, W. F. Swain, Immunization of pigs with a particle-mediated DNA vaccine to influenza A virus protects against challenge with homologous virus, J Virol 72 (1998) 1491–1496.

[10] M. A. F. Kendall, F. V. Carter, T. J. Mitchell, B. J. Bellhouse, Comparison of the transdermal ballistic delivery of micro-particles into human and porcine skin, Conf Proc IEEE Eng Med Biol Soc 3 (2001) 2991–2994.

[11] J. Liu, N. C. Hogan, I. W. Hunter, Intradermal needle-free powdered drug injection by a helium-powered device, Conf Proc IEEE Eng Med Biol Soc 2012 (2012) 2068–2071.

[12] D. Chen, R. L. Endres, C. A. Erickson, K. F. Weis, M. W. McGregor, Y. Kawaoka,

L. G. Payne, Epidermal immunization by a needle-free powder delivery technology: immunogenicity of influenza vaccine and protection in mice, Nat Med 6 (2000) 1187–1190.

[13] D. Chen, C. Zuleger, Q. Chu, Y.-F. Maa, J. Osorio, L. G. Payne, Epidermal powder immunization with a recombinant HIV gp120 targets Langerhans cells and induces enhanced immune responses, AIDS Res Hum Retroviruses 18 (2002) 715–722.

[14] M. Kendall, S. Rishworth, F. Carter, T. Mitchell, Effects of relative humidity and ambient temperature on the ballistic delivery of micro-particles to excised porcine skin, J Investig Dermatol 122 (2004) 739–746.

[15] C. Anamur, Novel formulation approaches for ballistic intradermal vaccination, phdthesis, Ludwig-Maximilians-University Munich, 2015. URL: https://edoc.ub.uni-muenchen.de/18820/1/Anamur_Cihad.pdf.

[16] D. L. Lodmell, N. B. Ray, L. C. Ewalt, Gene gun particle-mediated vaccination with plasmid DNA confers protective immunity against rabies virus infection, Vaccine 16 (1998) 115–118.

[17] N. J. Quinlan, M. A. F. Kendall, B. J. Bellhouse, R. W. Ainsworth, Investigations of gas and particle dynamics in first generation needle-free drug delivery devices, Shock Waves 10 (2001) 395–404.

[18] E. E. Etzl, Collapse dried protein powders for needle-free ballistic injection, phdthesis, Ludwig-Maximilians-University Munich, 2016. URL: https://edoc.ub.uni-muenchen.de/20129/1/Etzl_Enikoe_Elsa.pdf.

[19] E. E. Etzl, G. Winter, J. Engert, Toward intradermal vaccination: preparation of powder formulations by collapse freeze-drying, Pharm Dev Technol 19 (2014) 213–222.

[20] P. Lell, G. Winter, J. Engert, E. Etzl, Fixation of vaccine formulations on devices for epidermal immunisation by oily adjuvants, Pat. EP2851066A1, 2015.

[21] GlaxoSmithKline Biologicals s.a, Fachinformation Pandemrix, 2010.

[22] J. Freund, The effect of paraffin oil and mycobacteria on antibody formation and sensitization; a review, Am J Clin Pathol 21 (1951) 645–656.

[23] A. I. Kim, M. J. Akers, S. L. Nail, The physical state of mannitol after freeze-drying: effects of mannitol concentration, freezing rate, and a noncrystallizing cosolute, J Pharm Sci 87 (1998) 931–935.

[24] A. Burger, J.-O. Henck, S. Hetz, J. M. Rollinger, A. A. Weissnicht, H. Stöttner, Energy/temperature diagram and compression behavior of the polymorphs of D-

mannitol, J Pharm Sci 89 (2000) 457–468.

[25] A. Stabenau, Trocknung und Stabilisierung von Proteinen mittels Warmlufttrocknung und Applikation von Mikrotropfen, phdthesis, Ludwid-Maximilians-University Munich, 2003. URL: https://edoc.ub.uni-muenchen.de/2060/1/Stabenau_Anke.pdf.

[26] I. D. Smith, W. G. Hoekstra, R. H. Grummer, H. Phillips, Studies on serum proteins of normal and parakeratotic pigs, J Anim Sci 19 (1960) 580–589.

[27] G. Widera, J. Johnson, L. Kim, L. Libiran, K. Nyam, P. E. Daddona, M. Cormier, Effect of delivery parameters on immunization to ovalbumin following intracutaneous administration by a coated microneedle array patch system, Vaccine 24 (2006) 1653–1664.

[28] S. Naito, Y. Ito, T. Kiyohara, M. Kataoka, M. Ochiai, K. Takada, Antigen-loaded dissolving microneedle array as a novel tool for percutaneous vaccination, Vaccine 30 (2012) 1191–1197.

[29] Council of Europe, 2.9.19. Subvisible Particles, in: European Pharmacopoeia, 9th ed., Strasbourg, France, 2017.

[30] <787> Particulate Matter in Injections, in: U. S. Pharmacopoeia-National Formulary, usp 40 nf ed., Rockville, MD, USA, 2017.

[31] M. O. Oyewumi, A. Kumar, Z. Cui, Nano-microparticles as immune adjuvants: correlating particle sizes and the resultant immune responses, Exp Rev Vaccines 9 (2010) 1095–1107.

[32] M. J. Pikal, S. Shah, M. L. Roy, R. Putman, The secondary drying stage of freeze drying: drying kinetics as a function of temperature and chamber pressure, Int J Pharm 60 (1990) 203–207.

[33] I. Pitkänen, P. Perkkalainen, H. Rautiainen, Thermoanalytical studies on phases of D-mannitol, Thermochimica Acta 214 (1993) 157–162.

[34] D. H. Bangham, R. I. Razouk, Adsorption and the wettability of solid surfaces, Trans Faraday Soc 33 (1937) 1459–1463.

[35] M. E. Schrader, Young-Dupre Revisited, Langmuir 11 (1995) 3585–3589.

[36] D. K. Owens, R. C. Wendt, Estimation of the surface free energy of polymers, J Appl Polym Sci 13 (1969) 1741–1747.

[37] D. H. Kaelble, Dispersion-Polar Surface Tension Properties of Organic Solids, J Adhesion 2 (1970) 66–81.

[38] Krüss GmbH, Technical Note - Practical Contact Angle Measurements (5), 2008. URL: https://www.kruss-scientific.com/fileadmin/user_upload/website/

literature/kruss-tn315-en.pdf, [accessed 2018-01-10].

[39] A. H. Pelofsky, Surface tension-viscosity relation for liquids, J Chem Eng Data 11 (1966) 394–397.

[40] V. Ohm, Konzentrationsabhängige Interaktionen zwischen alpha-Tocopherol und weiteren Antioxidantien in lipidhaltigen Systemen, Ph.D. thesis, Christian-Albrechts-Universität, Kiel, 2007.

[41] S. Morel, A. Didierlaurent, P. Bourguignon, S. Delhaye, B. Baras, V. Jacob, C. Planty, A. Elouahabi, P. Harvengt, H. Carlsen, A. Kielland, P. Chomez, N. Garçon, M. Van Mechelen, Adjuvant System AS03 containing α-tocopherol modulates innate immune response and leads to improved adaptive immunity, Vaccine 29 (2011) 2461–2473.

[42] Council of Europe, 2.6.14. Bacterial Endotoxins, in: European Pharmacopoeia, 8th ed., Strasbourg, France, 2014.

[43] Council of Europe, Influenza vaccine (split virion, inactivated) [Monograph 0158], in: European Pharmacopoeia, 8th ed., Strasbourg, France, 2014.

[44] R. L. Bronaugh, R. F. Stewart, E. R. Congdon, Methods for in vitro percutaneous absorption studies. II. Animal models for human skin, Toxicol Appl Pharmacol 62 (1982) 481–488.

[45] D. Marro, R. H. Guy, M. Begoña Delgado-Charro, Characterization of the iontophoretic permselectivity properties of human and pig skin, J Control Release 70 (2001) 213–217.

[46] T. P. Sullivan, W. H. Eaglstein, S. C. Davis, P. Mertz, The pig as a model for human wound healing, Wound Repair Regen 9 (2001) 66–76.

[47] F. A. Duck, Chapter 5 - Mechanical Properties of Tissue BT - Physical Properties of Tissues, Academic Press, London, 1990, pp. 137–165. URL: https://www.sciencedirect.com/science/article/pii/B9780122228001500097. doi:10.1016/B978-0-12-222800-1.50009-7.

[48] I. H. Blank, J. Moloney, A. G. Emslie, I. Simon, C. Apt, The diffusion of water across the stratum corneum as a function of its water content, J Investig Dermatol 82 (1984) 188–194.

[49] A. Kishino, T. Yanagida, Force measurements by micromanipulation of a single actin filament by glass needles, Nature 334 (1988) 74–76.

[50] T. J. Mitchell, M. A. F. Kendall, B. J. Bellhouse, A ballistic study of micro-particle penetration to the oral mucosa, Int J Impact Eng 28 (2003) 581–599.

[51] M. Kendall, B. Bellhouse, G. Brown, Needle-free, dermal delivery of dry powdered

drugs using contoured shock tubes, Fluids 2000 Conference and Exhibit, AIAA (2000).

[52] M. Kendall, T. Mitchell, P. Wrighton-Smith, Intradermal ballistic delivery of microparticles into excised human skin for pharmaceutical applications, J Biomech 37 (2004) 1733–1741.

[53] M. A. Iftekhar Rasel, H. D. Kim, A computational study of drug particle delivery through a shock tube, J Drug Deliv Sci 24 (2014) 425–432.

[54] D. Zhang, D. B. Das, C. D. Rielly, An experimental study of microneedle-assisted microparticle delivery, J Pharm Sci 102 (2013) 3632–3644.

[55] A. Tezel, S. Paliwal, Z. Shen, S. Mitragotri, Low-frequency ultrasound as a transcutaneous immunization adjuvant, Vaccine 23 (2005) 3800–3807.

[56] J. Engert, C. Anamur, L. Engelke, C. Fellner, P. Lell, S. Henke, J. Stadler, S. Zoels, M. Ritzmann, G. Winter, A pilot study using a novel pyrotechnically driven prototype applicator for epidermal powder immunization in piglets, Int J Pharm (2018) In revision.

[57] M. Sequirus GmbH, Fachinformation AFLURIA, 2017.

[58] M. Sequirus GmbH, Fachinformation FLUAD, 2017.

[59] H. Mylan Healthcare GmbH, Fachinformation Influvac Saison 2016/2017, 2016.

[60] P. van Damme, F. Oosterhuis-Kafeja, M. van der Wielen, Y. Almagor, O. Sharon, Y. Levin, Safety and efficacy of a novel microneedle device for dose sparing intradermal influenza vaccination in healthy adults, Vaccine 27 (2009) 454–459.

[61] R. Arakane, R. Annaka, A. Takahama, K. Ishida, M. Yoshiike, T. Nakayama, F. Takeshita, Superior immunogenicity profile of the new intradermal influenza vaccine compared to the standard subcutaneous vaccine in subjects 65 years and older: A randomized controlled phase III study, Vaccine 33 (2015) 6650–6658.

[62] H. Okayasu, C. Sein, D. Chang Blanc, A. R. Gonzalez, D. Zehrung, C. Jarrahian, G. Macklin, R. W. Sutter, Intradermal administration of fractional doses of inactivated poliovirus vaccine: a dose-sparing option for polio immunization, J Infect Dis 216 (2017) S161–S167.

III

COMPARING INTRADERMAL MICRO- AND NANOPARTICLE DELIVERY BY DIFFERENT MICRONEEDLE TREATMENTS

1 Introduction

Since the mid 1990s MNs have been extensively studied for their potential to enhance the transdermal delivery of small molecules and macromolecular drugs [1, 2]. The elegant concept of breaching the SC, the main barrier of the skin, using small needles that are minimally invasive, pain-free, and easy to produce, made them a popular tool in transdermal delivery research [1]. The transport of a variety of different molecules into and through the skin could be improved by microneedling. Particularly macromolecules, e.g. proteins or oligonucleotides, but also certain particulate formulations benefit from the skin barrier disruption, which is a prerequisite to facilitate transdermal drug delivery for these molecules [3–5]. Although proven successful in principle, the use of conventional MN arrays is still mainly restricted to research due to low dosing or insufficient delivery efficiency [6, 7]. For this reason, the focus of MN research has shifted in recent years from a systemic delivery towards the delivery of highly potent, low dose molecules with local targets in the skin tissue, particularly vaccines [8].

Nowadays, the skin is recognized as highly immunologic organ with a high density of LCs and dDCs residing in the viable skin tissue [9]. When a critical amount of antigen reaches the tissue, the skin-resident APCs initiate an immunologic cascade that can result in protective immunity. Furthermore, skin keratinocytes have a key function in innate immunological processing and can promote antigen-specific immunity [10]. Targeting of the epidermal and dermal layer for cutaneous vaccination has been proven successful in many studies and is particularly interesting for potential dose reductions and development of new treatment options [11]. Besides other passive and active techniques targeting the skin for vaccine delivery, skin microporation and particularly MNs have proven their potential to challenge the state-of-the-art administration of vaccines by s.c. or i.m. injection [12, 13].

Various types of MNs have been used for the i.d. delivery of antigens into the skin, including solid, coated, hollow, and degradable MNs [6, 14]. While solid MNs are mainly

used to breach the mechanical barrier of the skin and provide access to the viable tissue, other types of MNs, namely coated, hollow, or biodegradable MNs, can facilitate a direct, one-step delivery of antigens in the skin. Each MN type provides certain advantages and disadvantages over others and has been tested to varying extent in clinical trials [6, 14–16]. Hollow MN devices with needle lengths of up to 1500 µm provide a high and reproducible dosing, however still require the use of liquid vaccine formulations with limited storage stability [6, 7, 14, 16]. Polymeric MNs are conveniently applied as dissolving, swelling, or biodegradable MN patch and exhibit good delivery efficiency but are commonly manufactured by micromolding based on centrifugation, which is difficult to scale-up [14, 17]. Moreover, reduced mechanical stability represents a major challenge for a broader application of polymeric MN arrays [1]. Coated MNs based on silica or metal exhibit good mechanical stability but the amount of drug or antigen that can be coated onto and released from the MN tips is limited [1, 8]. Solid MNs provide the advantage of an easy and cost-effective manufacturing, good mechanical stability, easy handling and compatibility with different semi-automated MN insertion devices [6]. The two-step 'poke with patch' approach, using microneedles to breach the skin barrier followed by the application of a drug-loaded solution or patch, allows to study the i.d. delivery of a variety of different molecules, vehicles, and formulations [18]. This flexibility makes them a convenient tool for the initial testing of new i.d. vaccines and adjuvants, e.g. particulate formulations.

Different materials, tip geometries, and application modes have been developed to breach the skin barrier with solid MNs followed by administration of the molecule or vehicle of interest [18]. Most common materials for the manufacturing of solid MNs include silicon, metals (e.g. stainless steel, titanium), ceramics, silica glass, and non-degradable polymers (e.g. photolithographic epoxy, polycarbonate, poly(methyl methacrylate) (PMMA)) [1, 6]. Silicon MNs prepared by etching allow to produce high-precision, specifically tailored MNs with various shapes [6]. On the other hand, MN arrays from metals can be produced by different techniques including etching and laser-cutting, each leading to a different type of MN. The manufacturing of ceramic and polymeric MNs usually involves the micromolding technique [1, 19]. Today, different types of solid MNs, mainly from stainless-steel, are commercially available and widely applied for cosmetic treatments. Particularly handheld roller or stamp devices can be easily purchased from various suppliers, e.g. the Dermaroller®, Dermapen™, 3Ms solid microneedle system (sMTS), and others [20]. Only recently, a draft guidance has been published by the FDA to regulate the increasing number of requests for the licensing of microneedling devices. However, specific quality standards related to

Good Manufacturing Practice (GMP) remain to be defined [20, 21].

Cutaneous vaccination using particulate vaccine formulations has attracted increasing attention in recent years due to the growing knowledge about skin immunology and the adjuvant potential of particles [5]. Particle delivery to intact skin via the transfollicular route has been studied and characterized in several studies. The phase of hair follicle growth and the structure of the infundibulum have been identified to influence the deposition of particles in the skin. It has been found that drugs and particles are exclusively delivered to open (active) follicles [22, 23]. About 74 % of all follicles are open under normal conditions, while the orifice of inactive follicles is closed by sebum and shed corneocytes [24]. By peeling and hair plucking, follicles can be opened and made accessible for drug delivery [24]. Different types of particles with sizes between 3.5 nm and up to 6 µm have been successfully delivered to intact skin via hair follices [25–30]. Thereby, the deposition of particles was found to be superior compared to free dye and could be significantly improved if massage was applied to mimick hair follicle movement [25, 26, 28, 31]. Particles with a size of approximately 650 nm reached maximum penetration depths upon massage into the skin [27].

Although particles can be delivered into deeper parts of the skin targeting the follicular infundibulum, the penetration past the follicle into the epidermal and dermal layer remains limited. Based on previous studies, it is generally assumed that particles larger than ∼10 nm do not pass superficial skin layers [32], which also surround the follicular infundibulum. This consequently limits the uptake and processing by skin-resident APCs required for vaccination. Furthermore, the area of the skin, which is accessible via hair follicles, is highly restricted with densities between 0.09 % on the volar forearm and up to 1.28 % on the forehead [23]. Both factors, particle size and follicular density, limit the delivery of active drugs and vehicles and highlight the need for active administration techniques that increase the efficiency and reproducibility of delivery.

One technique to circumvent the limited access to the viable skin tissue via hair follicles is the i.d. delivery of film fragments by punching using MNs. The aim of this approach, tested in the course of this thesis, is to deliver micron-sized fragments from $50 - 500$ µm thin polymer films into the epidermal and dermal layer of the skin using MN rollers with needle lengths of 500 µm and 1000 µm. These films can be loaded with vaccine antigens, adjuvants, micro-, or nanoparticles. In a preliminary proof-of-principle study, thin polymer films with varying excipient compositions were prepared using pure film forming polymers or blends of polyvinyl alcohol (PVA), chitosan, methacrylic acid derivatives, or cellulose

derivatives of varying type and size, e.g. carboxymethyl cellulose (CMC), hydroxyethyl cellulose (HEC), methyl hydroxyethyl cellulose (MHEC), hydroxypropyl methyl cellulose (HPMC) [33]. These films were prepared using an automated film casting technique and different post-drying treatments, e.g. cross-linking or freeze-thaw curing, and characterized covering a range of mechanical strengths, flexibility, and brittleness [33]. Although the piercing of the polymer films was successfully proven, further studies are needed to assess the feasibility of i.d. delivery of particle-like film fragments using MNs with defined shapes and geometries.

The study presented in this chapter aims to characterize the delivery of particles into MN-treated skin by massage comparable to transfollicular delivery. The penetration behavior of particles was studied dependent on the particle size and the MN type. Two commercially available MN devices with different MN tip geometries and application modes were compared for their efficiency to assist the delivery of particulate formulations into the skin. A conventional MN array with out-of-plane, flat stain-less steel MNs and a MN roller with cone-shaped MNs were used to deliver particles in the micro- and nanometer range into the viable skin tissue. The MN array was pressed flat onto the skin, whereas the MN roller was applied by rolling a handheld device with MNs on a rotating drum over the skin surface (Fig. III.1). Both application modes were used as a pretreatment to breach the SC and access the viable skin tissue. In addition, model particles were delivered to the skin by reversing the application sequence using the MN roller as massage tool in the second application step.

Due to skin elasticity, certain closure of pores after MN treatment can be expected, leaving narrow channels for the delivery of particles [34]. Therefore, model particles were applied by massage in order to maximize the deposition in the skin. Fluorescent silica particles were used to determine the maximum penetration depth into the skin by fluorescence microscopy depending on the particle size and MN treatment. Additionally, the i.d. deposition of fluorescent poly(lactic-co-glycolic acid) (PLGA) particles was quantified upon extraction from the skin. The i.d. deposition was evaluated in relation to the particle size as well as the MN shape and application mode. The findings of this study will broaden the knowledge about the administration of particles within a size range of $0.1 - 7$ µm into MN-treated skin and help interpreting existing research on the i.d. delivery of micro- and nanoparticles after MN treatment. Moreover, this study demonstrates the need to select optimum conditions for future studies using MN and particles for i.d. drug or vaccine delivery.

2 Materials and Methods

2.1 Chemicals

Silica particles with diameters of 7.0 µm, 1.3 µm, 0.6 µm, and 0.1 µm were purchased from Microparticles GmbH (Berlin, Germany). Green fluorescent PLGA particles with diameters of 1.2 µm, 0.5 µm, and 0.1 µm were obtained from Phosphorex (Degradex®, Hopkinton, Massachusetts, USA). Poly(allylamine) hydrochloride (PAH) (15 kDa), FITC (isomer I), and polystyrene sulfonate (PSS) (70 kDa) were purchased from Sigma Aldrich (Steinheim, Germany). Sodium chloride was obtained from Bernd Kraft (Duisburg, Germany). Dimethyl sulfoxide (DMSO) was from Fisher Scientific (Leicestershire, United Kingdom) and dichloromethane was from Merck (Darmstadt Germany).

2.2 Fluorescent coating of silica particles

The preparation of fluorescently labeled PAH was adapted from Schneider et al. [35]. In precise, 1 g PAH was dissolved in 20 mL 100 mM carbonate-bicarbonate buffer at a pH of 9.4. Under vigorous stirring and exclusion from light, 1.5 mL of ∼8 mg/mL solution of FITC in DMSO was added dropwise in 5 µL aliquots to the PAH solution over a period of eight hours. The solution was stirred overnight under exclusion of light and dialyzed for 48 h against highly purified water using a CelluSep T1 dialysis tubing (MWCO 3,500, Orange Scientific, Braine-l'Alleud, Belgium) to remove unbound FITC. After dialysis, the fluorescein isothiocyanate- labeled poly(allylamine) hydrochloride (FITC-PAH) was lyophilized and stored at 4 °C or directly utilized for layer-by-layer coating.
Fluorescent silica particles were prepared according to the layer-by-layer (LbL) principle as described before [36, 37]. Silica particle suspensions with particle sizes of 7.0 µm, 1.3 µm, 0.6 µm, and 0.1 µm were diluted to 2 % (w/v) using 0.5 M sodium chloride solution at pH 6.5. For the coating process, FITC-PAH and PSS (MW 70,000) were adsorbed to silica particles in four consecutive layers, starting with positively charged FITC-PAH followed by negatively charged PSS. The layers were obtained by mixing equal volumes of the particle suspension and 5 mg/mL polymer solution in 0.5 M sodium chloride, followed by incubation for 3 h under stirring and exclusion from light. Subsequently, the particles were washed three times by centrifugation at 13,000 rpm for 10 min and resuspension with 0.5 M sodium chloride solution to a concentration of 2 % (w/w). Sonication was used to improve resuspension. Four polymer layers were adsorbed to the silica particles

starting with positively charged FITC-PAH and ending with negatively charged PSS. After LbL-coating, the particle suspensions were stored at 4 °C until further utilization.

2.3 Scanning electron microscopy

Scanning electron microscopy of the silica particles prior and after coating was performed using a Joel JSM-6500F electron microscope (Ebersberg, Germany). The samples were prepared by air drying of each particle suspension on self-adhesive carbon tape (Bal-tec GmbH, Witten, Germany) and subsequent carbon sputtering under vacuum using a MED 020 coating system (Bal-tec GmbH, Witten, Germany). Images were taken at a magnification of 5,000 for the 7.0 µm and 1.3 µmicroparticles and at 25,000 for the 0.6 µm and 0.1 µm nanoparticles, respectively.

2.4 Zeta-potential measurements

The surface charge of the particles was assessed using a Malvern Zetasizer Nano ZS (Malvern Instruments, Worcestershire, United Kingdom). A volume of 500 µL of plain and coated silica particle suspensions with sizes of 1.3 µm, 0.6 µm, and 0.1 µm at a concentration of 2 % (w/v) was pipetted into a folded capillary zeta-cell (Malvern Instruments, Worcestershire, United Kingdom). Subsequently, highly purified water was carefully pipetted on top of the sample until the cell was completely filled. After resting for 1 h to ensure a stable equilibrium, the zeta-potential was analyzed at 25 °C. Silica microparticles with a diameter of 7.0 µm were prepared similarly using 50 µL at a concentration of 5 % (w/v) to achieve comparable measurement quality.
The mean zeta-potential was calculated from four different measurements at 25 °C, each composed of three serial runs with 20 subruns. Malvern software 6.12 (Malvern Instruments, Worcestershire, United Kingdom) was used for data acquisition and analysis.

2.5 Static light scattering measurements

The particle size and distribution of plain and coated silica particles were characterized by laser diffractometry using a Partica-LA 950 (Horiba, Kyoto, Japan). Optimum laser transmission intensities were obtained by spiking approximately $10 - 20$ µL particle suspension into 0.5 M sodium chloride solution at pH 6.5. Moreover, 0.2 M sodium hydroxide and 0.1 M hydrochloric acid were spiked as needed to evaluate changes in the size distribution pattern. Refractive indices of 1.42 for silica and 1.33 for water was used for evaluation by

Table III.1: Overview of microneedle treatments and particle sizes for the evaluation of particle penetration depths into excised pig skin.

Group	Microneedle treatment	Particle sizes Silica [µm]	Particle sizes PLGA [µm]
A	MN array	7.0	-
	250 µm length	1.3	1.2
	Before particle admininstration	0.6	0.5
		0.1	0.1
B	MN roller	7.0	-
	200 µm length	1.3	1.2
	Before particle administration	0.6	0.5
		0.1	0.1
C	MN roller	7.0	-
	200 µm length	1.3	1.2
	After particle administration	0.6	0.5
		0.1	0.1

the system software. The particle size was provided as median size within one fraction of the static light scattering (SLS) size distribution analysis.

2.6 Particle suspensions for intradermal administration

LbL-coated silica particles as described above were used for microscopic evaluation of the i.d. penetration behavior upon MN treatment. For this purpose, particle suspensions with a concentration of 2 % (w/v) in 0.5 M sodium chloride solution at a pH of 6.5 were prepared. The quantitative i.d. particle deposition was analyzed using green fluorescent PLGA particles (Degradex®, Phosphorex, Hopkinton, Massachusetts, USA). The PLGA particles with diameters of 1.2 µm, 0.5 µm, and 0.1 µm were reconstituted as received with half volume to obtain 2 % (w/v) suspensions.

2.7 Microneedle treatment and particle administration

The particle administration was studied using excised pig skin from the ventrolateral region of $5-7$ week old piglets, provided by the Clinic for Swine (Faculty of Veterinary Medicine, LMU Munich, Oberschleißheim, Germany). Full thickness pig skin samples were prepared using a scalpel and stored at -80 °C for a maximum of three months. For particle administration, skin samples of at least 3x3 cm^2 were prepared and hydrated for 5 min in 0.9 % sodium chloride solution. After removing excess moisture from the surface, the skin samples were placed on a polystyrene foam support in order to avoid breakage or bending of the MNs. Three different MN application modes were used to study the particle penetration behavior (Tab. III.1).

For the treatment groups A and B, a MN pretreatment of the skin samples was performed. The pretreatment procedure of group A involved a MN array (AdminPatch® 300, AdminMed, Sunnyvale, USA) with 752 flat, hollow 250 µm MNs, which was applied to the skin surface using a 2 kg weight for 3 min (Fig. III.1). Subsequently, the MN array was turned 90 degrees and the application procedure was repeated, resulting in a microporated area of 0.8 cm^2. For group B, a MN roller (Dermaroller™ HC902, Dermaroller GmbH, Wolfenbüttel, Germany) with 162 cone-shaped 200 µm MNs was used. The microneedling procedure was performed as per manufacturers description by rolling 'back and forth' four times, each time turning at an angle of 45 degrees (Tab. III.1). Subsequently, partially microporated skin in the corners was covered with Leukoflex tape (BSN Medical, Hamburg, Germany), leaving a 2x2 cm^2 area for subsequent particle administration. After skin pretreatment in group A and B, the liquid particle suspension was topically applied and manually massaged into the skin for 3 min in a circular movement.

The particle administration in treatment group C was performed by reversing the application sequence. After placing the skin samples on the polystyrene foam support, an area of 2x2 cm^2 was prepared by covering the residual tissue with Leukoflex tape. Within the free skin area, the particle suspension was topically applied and followed by performing the microneedling procedure as described above using the MN roller. The MN roller procedure was repeated ten times to mimic the massage effect as compared to the other treatment groups. For all groups, a suspension volume equivalent to 2 mg/cm^2 was applied. After administration, excess formulation was gently removed using a cotton wipe and tap water, avoiding further pressure on the skin surface. Subsequent analysis was peformed using a 1x1 cm^2 sample of the central region of the treated skin sample. Each test was performed in triplicates.

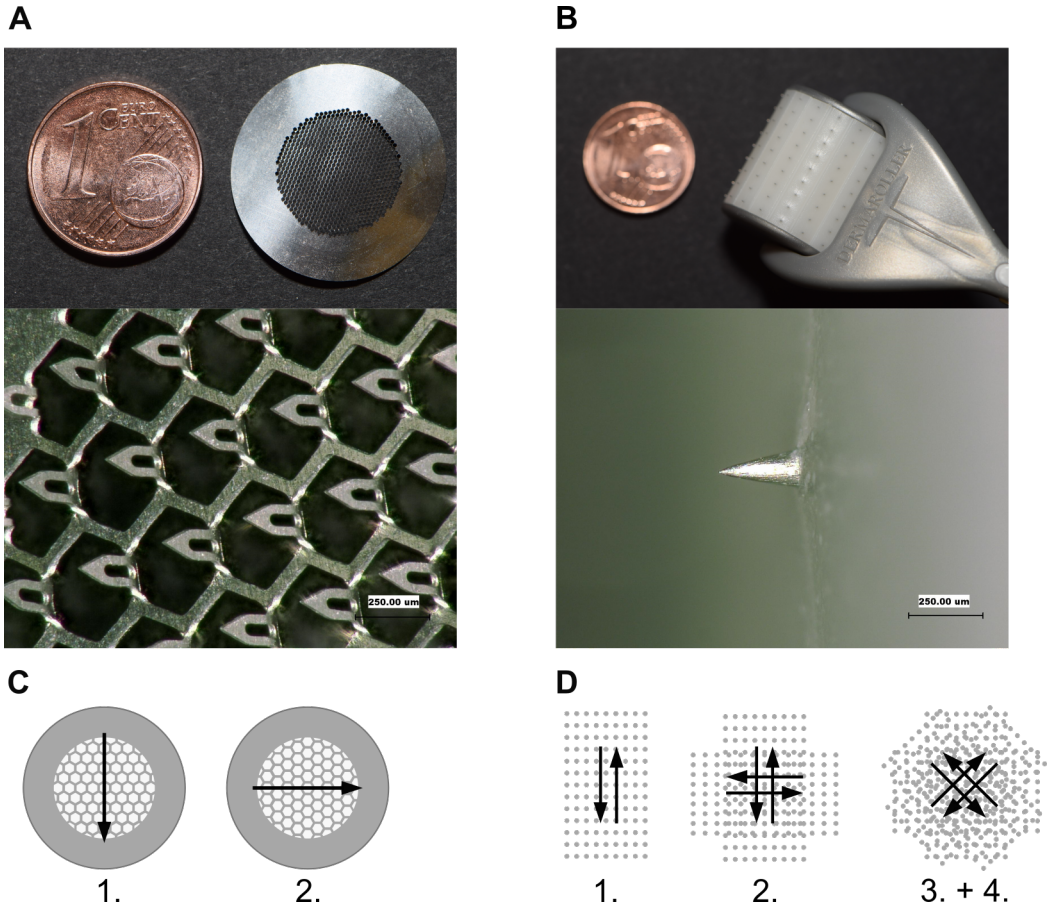

Figure III.1: Photographs and microscopic images of the commercially available MN array (A) and MN roller (B) used in this study. The MN array with 752 flat, 250 µm long, out-of-plane MN was applied twice in two different directions (C). The MN roller was applied by rolling a drum comprising 18 rows of nine 200 µm long MN over the skin surface at four different directions (D). For the MN roller, a central region of 2x2 cm^2 was used to study the particle penetration.

2.8 Laser scanning microscopy

Processed skin samples were embedded into tissue freezing medium (FSC 22® Clear, Leica Biosystems, Wetzlar, Germany) and stored overnight at −80 °C. Skin cross-sections of 10−20 µm were prepared at −18 °C using a Microm HM560 microtome (ThermoScientific™, Massachusetts, USA). The artifical introduction of particles into deeper skin layers was avoided by orienting the microtome blade parallel to the normal of the skin surface. Skin cross-sections from equally distributed locations of the entire skin sample area were prepared and collected for imaging. The cross-sections were mounted onto microscope slides

(SuperFrost® Plus, VWR, Leuven, Belgium) and analyzed without further staining.
The skin sections were mounted upside down on a Zeiss 510 LSM confocal laser scanning microscope (Carl-Zeiss AG, Oberkochen, Germany) and were imaged with identical settings for all groups using a EC Plan-Neofluar10x/0.3 air objective. At least 29 positions per particle size and MN treatment group were analyzed for the penetration depth. A position was defined as region of particle deposition and accumulation in the skin that was generated by one MN penetration. The penetration depth was measured as the maximum distance between the lowest visible particle deposition and the microporated skin surface using Fiji image analysis software [38]. The penetration depths were evaluated using one-way ANOVA statistical analysis by SigmaPlot 12.5 (Systat Software, San Jose, California, USA).

2.9 Extraction of PLGA particles from skin

The i.d. particle deposition was determined upon extraction from horizontal skin sections. The sections were prepared by placing the skin samples on a pre-cooled stainless steel plate with the SC facing the plate surface. After embedding into tissue freezing medium and overnight freezing at −80 °C, horizontal skin sections of 30 µm were prepared using a Microm HM560 microtome (ThermoScientific™, Massachusetts, USA). In total 25 sections were collected in 1.5 mL tubes reaching a maximum skin depth of 750 µm. Up to four skin sections were collected per sample tube. Green fluorescent PLGA particles were extracted by adding 200 µL dichloromethane into each sample tube followed by 20 min incubation at 60 °C during which PLGA and fluorescent dye was dissolved. The samples were centrifuged for 2 min at 13,000 rpm to remove skin residuals and the supernatant was transferred into black sample tubes. The content of green fluorescent PLGA particles was quantified by fluorescence spectroscopy.

2.10 Quantification of PLGA particles by fluorescence spectroscopy

The concentration of green fluorescent PLGA particles in the skin extract was quantified using a Cary Eclipse fluorescence spectrophotometer (Agilent, Santa Clara, CA, USA) at excitation and emission wavelengths of 460 nm and 500 nm, respectively. A standard curve was generated for each separate particle size by drying 100 µL of 2 % (m/v) particle suspension under vacuum and exclusion from light. Upon reconstitution in 200 µL dichloromethane, diluted standard solutions were analyzed by fluorescence spectroscopy

and correlated to the equivalent particle concentration. The experiment was performed in triplicates for each particle size. The curves showed linear ranges of $25 - 500$ ng/mL for 1.2 µm particles, $25 - 750$ ng/mL for 0.5 µm particles, and $100 - 3000$ ng/mL for 0.1 µm PLGA particles with regression factors of above 0.99 for each analysis.

3 Results and Discussion

3.1 Characterization of LbL-coated particles

The LbL technique is a well-known method for the preparation of coated particles or capsules and has been exploited for numerous applications in research [35, 37, 39–43]. The approach benefits from a high universality and the compatibility with various particle materials, e.g. melamine-formaldehyde, polystyrene, silica, as well as different coating polymers, e.g. PSS, PAH, or poly acrylic acid (PAA). Initially performed by charge-derived adsorption, the LbL technique has been further developed exploiting other molecular interactions [39].

In this study, charge-based LbL-assembly of silica micro- and nanoparticles was performed to successively coat four layers of positively charged FITC-PAH and negatively charged PSS, facilitating the imaging by fluorescence laser scanning microscopy (LSM). To ensure a good stability of the particles after LbL-coating, the microscopic appearance, zeta-potential, and static light scattering of the particles prior and after coating was studied.

Figure III.2 shows scanning electron microscopy (SEM) images of plain and LbL-coated silica micro- and nanoparticles with a diameter of 7.0 µm, 1.3 µm, 0.6 µm, and 0.1 µm. Generally, the surface morphology of the particles was smooth and homogeneous for all particle sizes before and after LbL-coating. At higher magnification, an uneven surface became visible on 0.6 µm nanoparticles before and after coating. Plain silica particles arranged in hexagonal superstructure, which has been reported for mesoporous silica structures before and appeared to be most pronounced for nanoparticles (Fig. III.2 C.1, D.1). After LbL-coating, the ordered superstructure disappeared (Fig. III.2 C.2, D.2), indicating a change of surface charge and particle interaction due to FITC-PAH and PSS coating. The comparison of surface morphology and particle appearance by SEM showed not signs of irreversible particle aggregation due to the coating process.

The particle size and size distribution of the silica particles prior and after LbL-coating was studied by SLS. Plain and LbL-coated microparticles of 7.0 µm and 1.3 µm showed

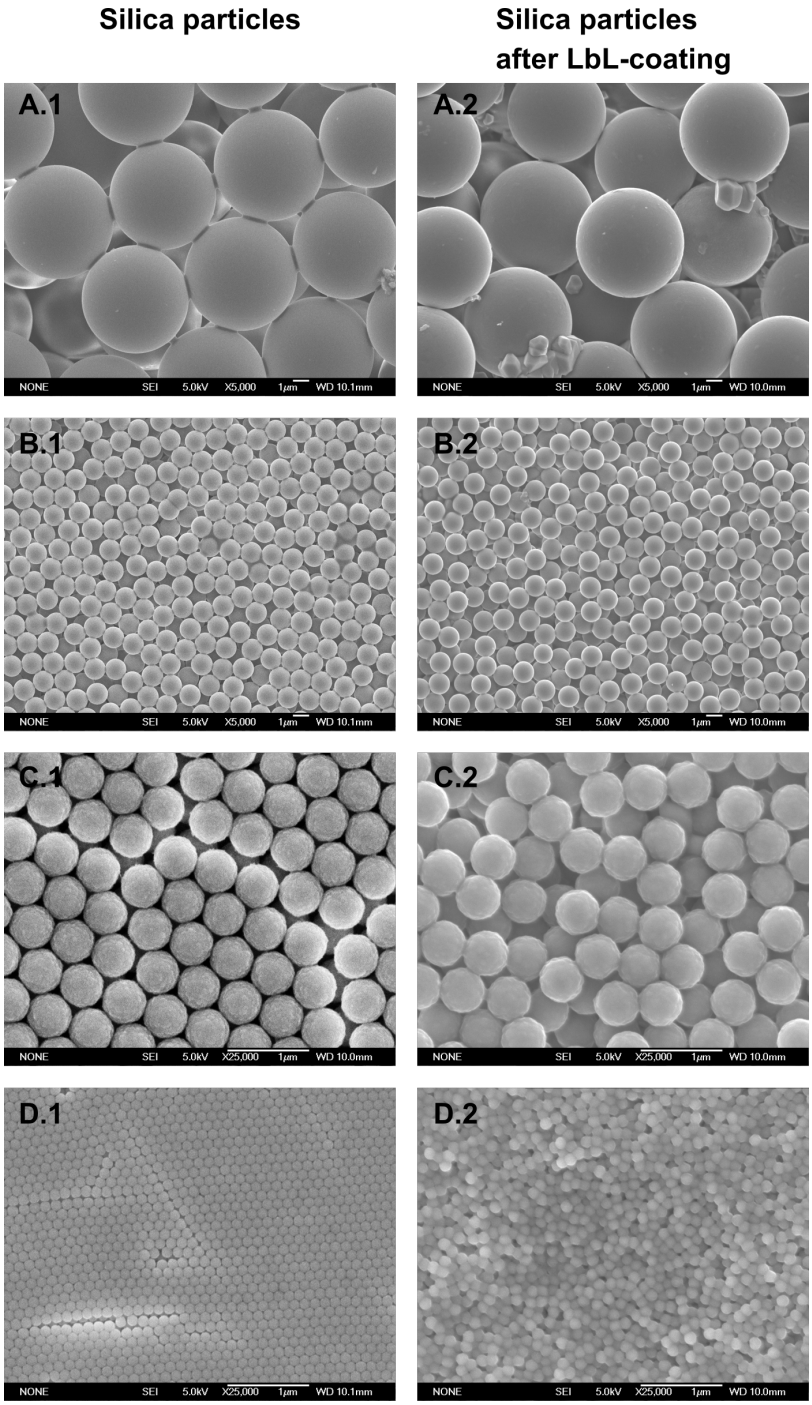

Figure III.2: Scanning electron microscopy images of silica particles prior (left column, index 1) and after (right column, index 2) coating with positively charged FITC-PAH and negatively charged PSS. Silica particle with sizes of 7.0 µm (A), 1.3 µm (B), 0.6 µm (C), and 0.1 µm (D) were used in this study. Scale bar 1 µm, Magnification 5,000x (A, B) and 25,000x (C, D).

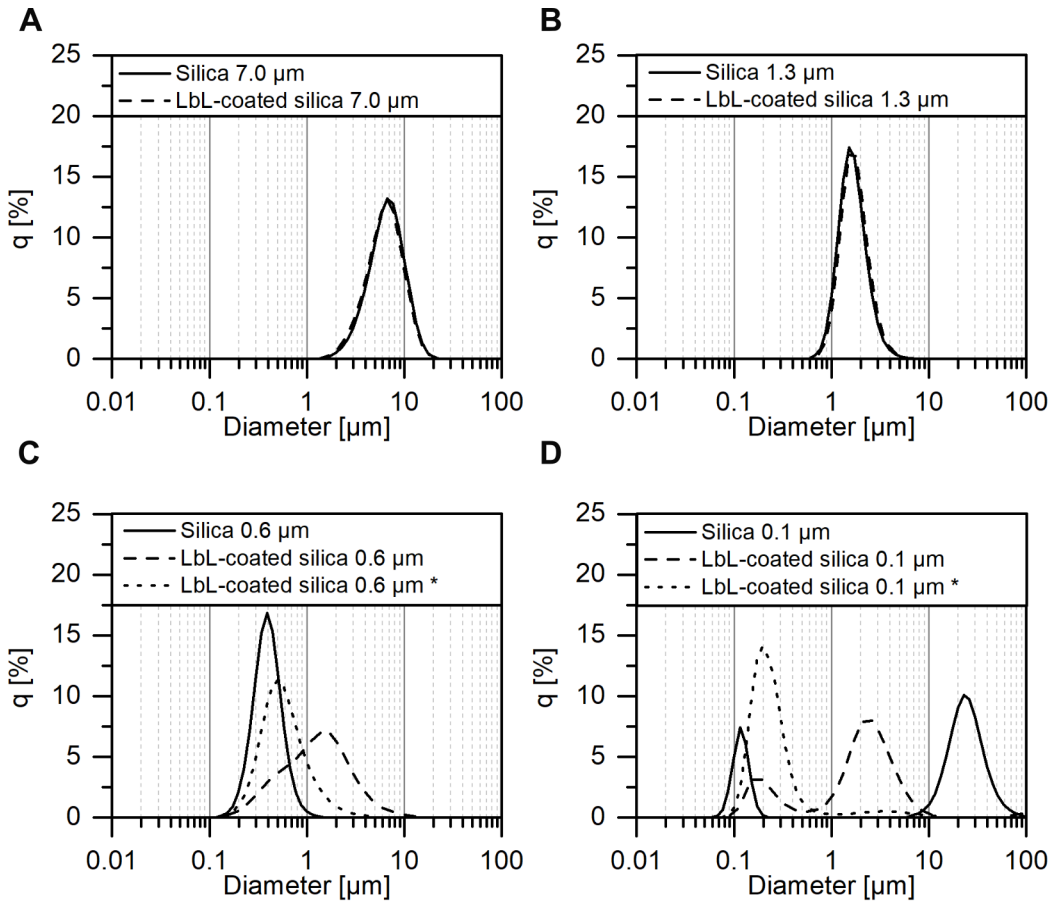

Figure III.3: Particle size distribution determined by static light scattering prior (solid line) and after LbL-coating (dashed line). LbL-coated silica nanoparticles showed reversible aggregation, which was improved at pH ∼11 (*, dotted line).

monomodal size distributions (Fig. III.3 A, B). Equivalent sizes before and after LbL-coating were measured, indicating that the LbL-coating did not affect the mean size of the microparticles (Tab. III.2). Plain silica nanoparticles with a diameter of 0.6 µm exhibited a single peak, which broadened and shifted towards larger sizes after LbL-coating (Fig. III.3 C). At higher pH around 11, by addition of sodium hydroxide, the shifting could be reversed towards smaller particle sizes. Plain and LbL-coated 0.1 µm nanoparticles exhibited a bimodal distribution during SLS analysis. The two particle size fractions detected for plain silica particles showed a mean diameter around 0.1 µm, indicative for single particles, and 22 µm, suggesting aggregate formation, respectively. In the same dispersion medium, the LbL-coated 0.1 µm nanoparticles exhibited a bimodal distribution with fractions around 0.2 µm and 3.1 µm. The increase of the pH to ∼11 induced a shifting of the larger size fraction of LbL-coated nanoparticles towards the peak

Table III.2: Particle size determined by static light scattering (SLS) and zeta-potential of plain and LbL-coated silica particles with nominal sizes of 7.0 µm, 1.3 µm, 0.6 µm, and 0.1 µm. The nanoparticle size with nominal diameters of 0.6 µm and 0.1 µm was derived from the particle fraction detected by SLS with lowest particle size (*). The size of the LbL-coated nanoparticles was derived from measurements at pH ∼11 (Fig. III.3).

	Mean particle size			Zeta- potential	
Nominal	Plain silica [µm]	LbL-coated [µm]	Size ratio (LbL/Plain)	Plain silica [mV]	LbL-coated [mV]
7.0 µm	6.17 ± 0.003	5.93 ± 0.011	0.96	-27.3 ± 2.3	3.2 ± 0.4
1.3 µm	1.51 ± 0.020	1.59 ± 0.008	1.06	-64.6 ± 0.5	-30.5 ± 0.3
0.6 µm	0.36 ± 0.004	0.47 ± 0.009 *	1.29	-29.0 ± 0.5	-26.3 ± 0.3
0.1 µm	0.12 ± 0.000 *	0.22 ± 0.001 *	1.79	-18.7 ± 0.6	-22.6 ± 0.3

at 0.2 µm diameter (Fig. III.3 D). The pH-induced shifting of larger size fractions towards smaller particle sizes indicates a reversible association of the LbL-coated nanoparticles of 0.6 µm and 0.1 µm. Notably, a comparable pH-dependent shifting of size fractions was also observed for plain silica nanoparticles of 0.1 µm (data not shown).

Measurements of the single nanoparticle diameter by SLS deviated slightly from the nominal diameter provided by the manufacturer (Tab. III.2). Moreover, after LbL-coating the diameter increased by approximately 0.1 µm. Notably, particle size measurements of plain silica nanoparticles by dynamic light scattering (DLS) provided results in agreement with the nominal value of 0.6 µm and 0.1 µm (data not shown). However, poor measurement quality was observed for larger particle sizes as well as LbL-coated nanoparticles. It can be assumed that SLS-related limitations in measuring particle sizes below 0.5 µm caused a deviation of SLS-measurement results from the actual particle diameter. Moreover, LbL-coating could induce a change of refractive indices of the particles, thus affecting SLS-measurement accuracy. On the other hand, the larger particle size fraction of the LbL-coated 0.1 µm nanoparticles showed a diameter almost ten times smaller than the larger size fraction of the plain silica particles. With a diameter around 3.1 µm, the LbL-coated particle aggregates might have interfered with size measurements by DLS. Therefore, despite its analytical limitations in submicron size measurements, SLS was selected as main technique to assess the particle size and the reversibility of particle aggregate formation.

The zeta-potential prior and after coating was measured to further characterize the particle interaction in suspension. Plain silica particles exhibited a size-independent negative zeta-potential between −20 mV for 1.3 µm particles and −65 mV for 0.1 µm nanoparticles (Fig. III.2). After LbL-coating, the zeta-potential leveled around −25 mV for all particles except the 7.0 µm microparticles. The largest silica particles exhibited a neutral to slightly positive zeta-potential. Although the neutral surface charge could be indicative for aggregation, this was not observed by SEM or SLS analysis. It can be speculated that the low surface to volume ratio of the larger microparticles prevented notable particle aggregation. Generally, a comparable zeta-potential was achieved by LbL-coating of particles within a size range of 1.3 µm to 0.1 µm. A good peak homogeneity was observed during measurements of the coated particles, indicating a homogeneous charge distribution generated by LbL-coating, which was superior to plain silica particles.
The LbL-coating procedure allowed for a preparation of fluorescent particles of 7.0 µm, 1.3 µm, 0.6 µm, and 0.1 µm with suitable properties to study the i.d. delivery upon MN treatment. The particles were easily detectable by fluorescence LSM using imaging parameters with low background fluorescence of the skin tissue. Analysis by SEM and SLS showed no signs of aggregation of microparticles $\geq$ 1.3 µm. Moreover, aggregation of LbL-coated nanoparticles $\leq$ 0.6 µm was shown to be reversible. It can be assumed that the application by massage provides sufficient energy to disrupt reversibly associated particles. Size measurements showed an increase in particle diameter, which was most pronounced at lower particle sizes (Tab. III.2). However, as the SLS measurements come with analytical limitations, it can be assumed that the single particle diameter prior and after LbL-coating was comparable for all particle sizes as seen by SEM imaging. We conclude that the particle size increase by LbL-coating was negligible and a direct comparison of the i.d. deposition can be done using the nominal particle diameter between 7.0 µm and 0.1 µm. Moreover, a similar approach has been used before to study the selective i.d. transfollicular delivery [27].

3.2 Particle penetration depths

The penetration depths of green fluorescent LbL-coated silica particles into excised MN-treated pig skin were determined by LSM. The particles were administered into the skin using different types of MNs and application modes. A conventional array of flat MNs (group A) or a handheld roller with cone-shaped MNs (group B) was applied as skin pretreatment followed by i.d. particle administration by massage for 3 min. Alternatively, the MN roller was used in reverse order after topical particle application (group C). Typically,

MNs have been used to disrupt the skin barrier, creating microchannels and facilitating the subsequent delivery of particulate formulations to the viable skin tissue [44, 45]. However, here, a reverse order of application was additionally studied to assess the possibility to reach deeper skin layers and to evaluate the delivery efficiency compared to conventional skin pretreatment.

The particle penetration depth was determined based on LSM images of skin cross-sections from different locations distributed over a total area of 1x1 cm^2 after i.d. particle administration. Figure III.4 shows four representative images of skin cross-sections prepared from treatment group C. MN-generated micropores and the deposition of particles with sizes of 7.0 µm, 1.3 µm, 0.6 µm, and 0.1 µm were visible upon topical administration of the particle suspension on intact skin followed by MN roller treatment. For the determination of penetration depths, each position of particle deposition was marked and the penetration depth was evaluated as maximum distance between skin surface and the deepest visible particle per MN-generated micropore. At least 29 positions of different microchannels in the skin were measured for each particle and MN treatment group.

Figure III.5 provides an overview of measured deposition depths in relation to the applied particle size and MN treatment. The mean particle penetration depth as well as depth distributions were comparable for all particle sizes when MNs were applied as skin pretreatment (group A+B). Compared to the MN pretreatment, broader depth distributions were obtained for the i.d. particle delivery by microneedling (group C). The reverse order application resulted in comparable mean deposition depths for particles of 7.0 µm, 1.3 µm, and 0.6 µm. However, significantly deeper penetration and wider depth distribution in the skin tissue was achieved for the smallest particle size of 0.1 µm. In general, maximum penetration depths per microchannel ranged from about 50 µm to 450 µm for all particle sizes and treatment groups.

The statistical evaluation of the particle penetration depth in relation to the applied MN treatment revealed a tendency of superior deposition depths for the MN roller compared to the MN array (Fig. III.5). No difference was detected between the application of the MN roller prior or after particle administration. The MN roller reached an average penetration depth of 166 µm compared to 131 µm for the MN array. The maximum depths that could be reached were up to 450 µm and 300 µm using the MN roller and array, respectively. Considering the skin structure, the results suggest that all treatment conditions can provide a deposition of particles in the epidermal layer and upper dermis (Fig. III.6). Thus, a particle delivery in the viable tissue, in close vicinity to skin-resident APC for immunologi-

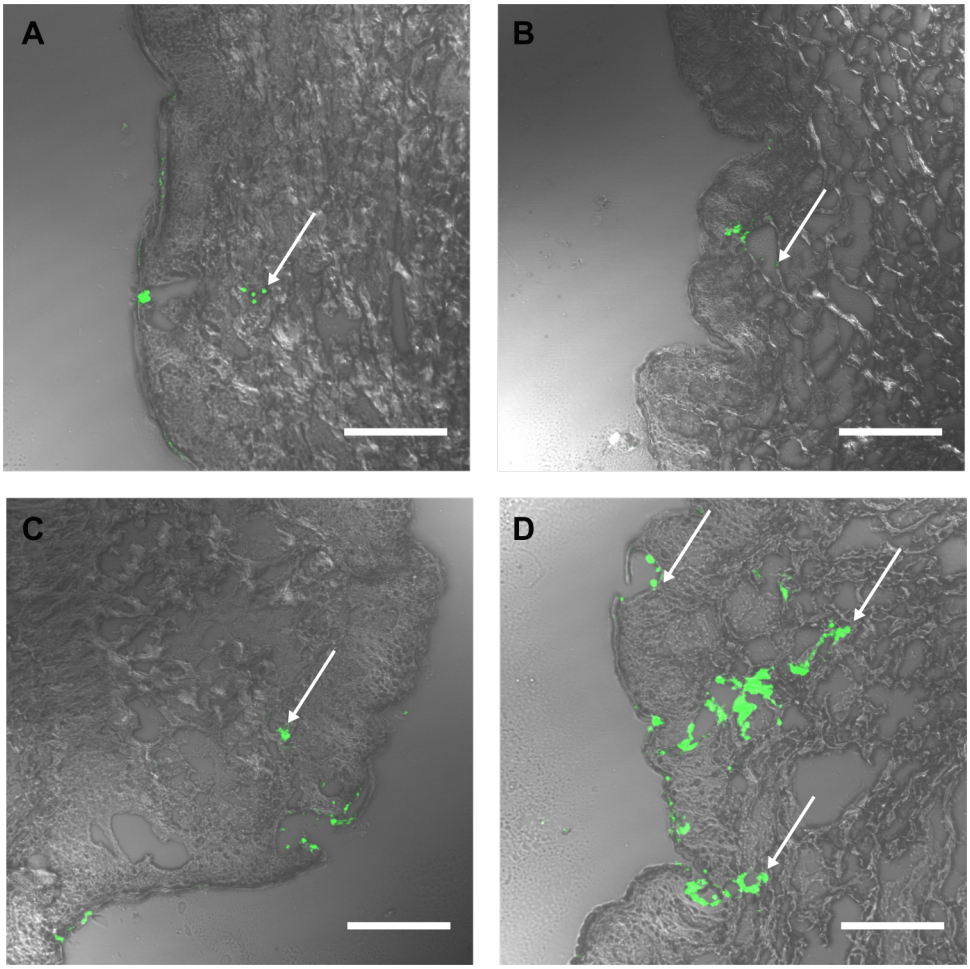

Figure III.4: Laser scanning images of vertical skin sections of treatment group C. Four different particle sizes (green) were used: 7.0 µm (A), 1.3 µm (B), 0.6 µm (C), and 0.1 µm (D). The images are representative for other treatment groups. Scale bar 200 µm, Magnification 10x.

cal processing could be achieved. While the median penetration depth was around 120 µm for the MN array pretreatment (group A), both application modes using the MN roller resulted in higher median values around 150 µm (group B+C).

Considering the differences in particle penetration by different MN treatments, the measured depths did not correlate with the needle length, which was 200 µm for the MN roller compared to a needle length of 250 µm for the array. This indicates that the tip geometry had a stronger influence on the penetration of particles into the skin than the needle length itself. Furthermore, the application modes of the MN array and roller differ significantly. The MN array is pressed onto the skin surface, whereas the MN insertion and retraction

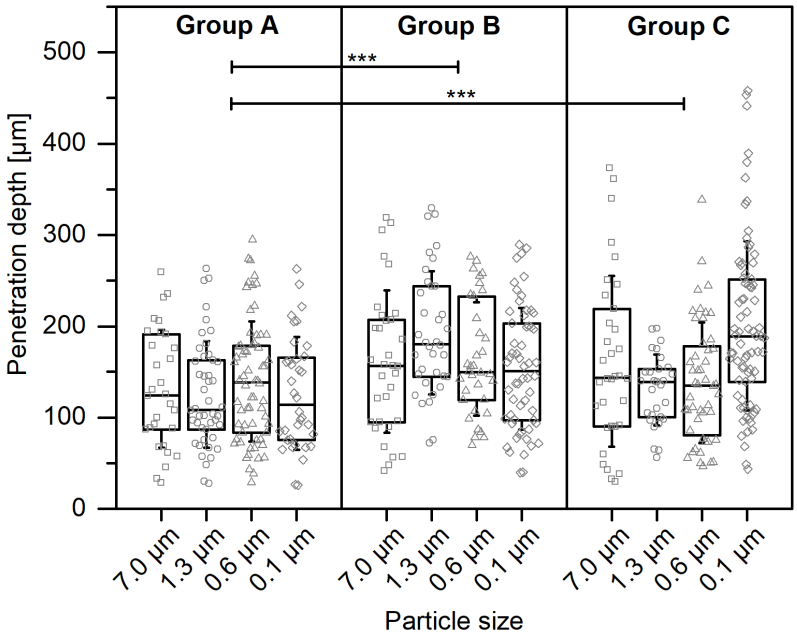

Figure III.5: Penetration depths of LbL-coated silica particles into excised pig skin after different microneedle treatments. Lbl-coated silica micro- and nanoparticles with a diameter of 7.0 µm, 1.3 µm, 0.6 µm, and 0.1 µm were massaged for 3 min into the skin upon MN array (group A) or MN roller (group B) pretreatment or reverse order of application using the MN roller (group C). Box plots represent the 25th and 75th quartiles, median and standard deviation (whiskers) derived from penetration depth measurements of separate microchannels (symbols). First statistical analysis was performed comparing the penetration depths of different particle sizes within one treatment group. Second statistical analysis was performed upon pooling the penetration depths within each treatment group using a one-way ANOVA (Tukey multiple comparisons, $\alpha = 0.05$, *** $p < 0.001$), revealing significant differences in the penetration depth between skin treatment using the MN array (group A) and the MN roller (group B+C).

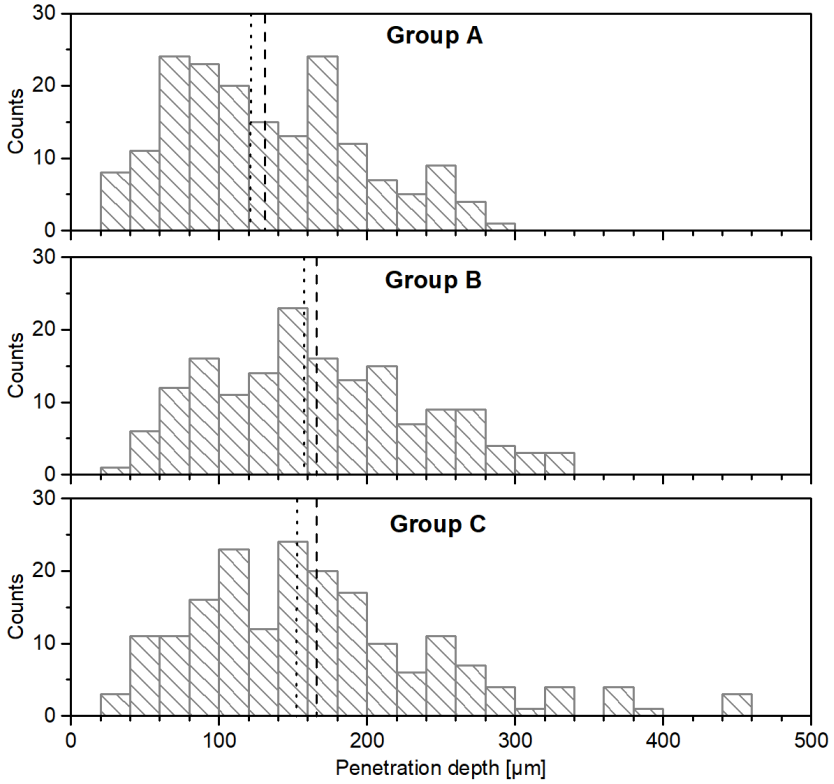

Figure III.6: Histogram of measured particle penetration depths upon MN skin pretreatment using a MN array (group A) or roller (group B), or in reverse order of application using the MN roller (group C). The median (dotted line) and mean (dashed line) penetration depth of particles is shown for each respective treatment group. All measured particle penetration depths were considered for this graph, independent of the particle size applied.

using the MN roller occurs at different angles. Due to the rolling process and cone-type shape of the MNs, the MN roller likely induced a more efficient disruption of the skin barrier compared to the small, well-defined microchannels created by the MN array. The results suggest that for such small differences in needle length, the needle tip geometry and the application mode govern the performance of the microneedling process and the related particle penetration.

3.3 Quantitative intradermal particle delivery

The quantitative deposition of PLGA micro- and nanoparticles with sizes of 1.2 µm, 0.5 µm, and 0.1 µm in the skin tissue was determined by extraction and quantification by fluores-

cence spectroscopy. Horizontal skin sections were prepared and collected after particle administration on intact skin (control) or after application by MN treatment as described above (group A, B, C). Green fluorescent PLGA particles, that penetrated into the skin tissue, were dissolved and the total particle content was determined in the extract.

Figure III.7 provides the total and relative amount of PLGA particles deposited per cm^2 skin tissue. In all treatment groups, a superior deposition of nanoparticles with a size of 0.5 µm was observed compared to the smaller nano- and larger microparticles. Up to 14 µg/cm^2 of 0.5 µm nanoparticles were delivered into the skin, whereas a maximum deposition of 5 µg/cm^2 and 3.5 µg/cm^2 was achieved applying 0.1 µm and 1.2 µm particles, respectively.

This finding is in agreement with previous studies that identified a particle diameter of ∼650 nm as optimum particle size to penetrate into intact skin via the transfollicular route [27, 46]. However, compared to the delivery to intact skin via hair follicles, in the present study, breaching of the skin barrier by microneedling improved the absolute i.d. deposition by factor ten. Although no clear effect of the particle size on the penetration depth was detected (Section 3.2), the deposited amount of particles revealed a clear dependency of the applied particle size on the quantitative i.d. deposition.

Interestingly, a slightly higher deposition of 0.1 µm nanoparticles was detected using the MN roller in reverse order compared to the MN array pretreatment. On the other hand, the particle deposition was marginally increased for 1.2 µm microparticles in combination with the MN array pretreatment in comparison to reverse order microneedling. Although the observed effect is minor, it could indicate that manual massage affects the i.d. delivery of larger particles to higher extent compared to nanoparticles around 0.1 µm. On the other hand, increasing particle sizes $\geq$ 1.2 µm appeared to hinder the simultaneous barrier disruption and particle transport into the skin by reverse order microneedling as performed in treatment group C. The reverse application of the MN roller might be particularly beneficial for suspensions of nanoparticles smaller than 0.1 µm and for solutions. However, it has to be noted that nanocarriers have been previously found to provide superior delivery compared to free molecules [31, 44, 47]. This suggests the existence of an optimum size for the efficient delivery of particles and macromolecules into the skin tissue.

A compromise between efficient i.d. delivery and uptake by skin-resident APCs has to be established to successfully facilitate cutaneous vaccination. Mechanical stimuli allow for the delivery of particles of up to 6 µm into deeper parts of follicles [25–30], however, no particle uptake from the follicles into deeper skin tissue has been detected [48]. Moreover,

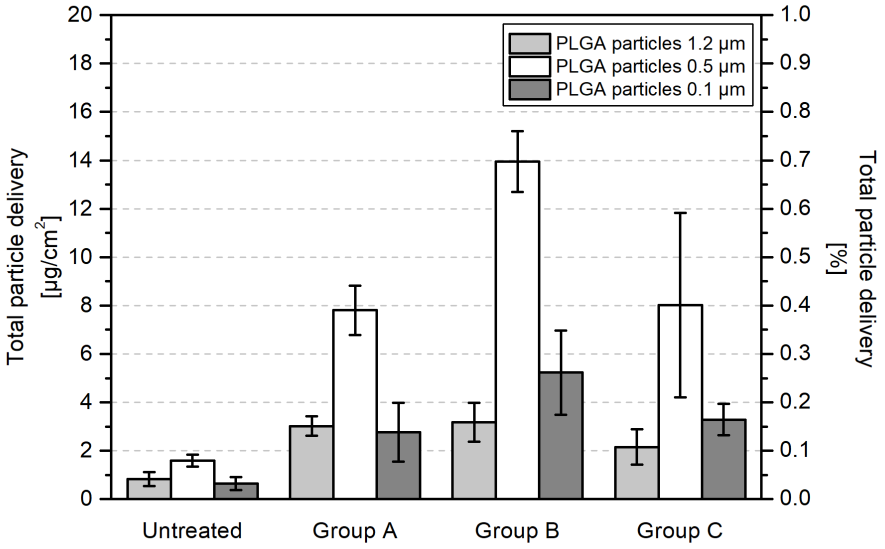

Figure III.7: Total intradermal delivery of PLGA particles with diameters of 1.2 µm (light gray), 0.5 µm (white), and 0.1 µm (dark gray). The particles were administered by massage on intact skin or after pretreatment using a MN array (group A) or MN roller (group B). Furthermore, particles were delivered by reversed sequence of application using the MN roller to massage particles into the skin (group C). (*Data of 1.2 µm and 0.5 µm (groups A-C) were acquired by Lisa M. Völk during her Bachelor's thesis [50].*)

after reaching the viable tissue, particles in the submicron range are preferably taken up by DCs, inducing a size-dependent type of immunity [49].

The comparison of the different treatment groups revealed that the lowest deposition of PLGA particles was detected in intact skin. The highest i.d. delivery for all particle sizes was achieved applying the MN roller pretreatment followed by particle administration by massage (group B). Skin pretreatment using the MN roller facilitated a deposition up to three times higher compared to the MN array pretreatment (group A) and reverse order application of the roller (group C). The MN array and the reverse order application of the MN roller provided particle deposition in comparable range for each respective particle size (Fig. III.7).

Similar to the penetration depth (discussed in section 3.2), the quantitative i.d. particle deposition was largely influenced by the MN tip geometry, application mode, and treatment sequence. Besides the efficient barrier disruption using the MN roller in treatment groups B+C, the particle administration was mainly dependent on the massage effect, whereas

the number of pores only played an inferior role. Previous studies have shown that about 125 micropores are generated by ten passes of a MN roller with 192 needles [51]. Notably, the MN roller used in this study provided only 162 MNs and was applied in eight passes for the MN pretreatment, likely resulting in less than 125 micropores. Neither ten repetitions of this microneedling sequence as performed in group C, nor the 752 MNs of the MN array resulted in a particle deposition comparable to the roller pretreatment. Interestingly, the reverse order treatment using the MN roller induced a particle deposition comparable to the MN array pretreatment (group A). This suggests that the relatively low skin barrier disruption induced by the flat MN array was compensated by efficient manual massage compared to the high disruption using the repeated application of the MN roller with an inferior massage effect.

Results suggest that the MN type is the key factor influencing the skin tissue disruption, whereas massage and the applied particle size additionally determine the associated i.d. particle delivery. Furthermore, a strong interplay between the application of MNs and the skin has been observed. When comparing the efficiency of different MN types to breach the skin surface, the mechanical properties of the skin tissue have to be considered. Several studies have reported the contraction of MN-generated micropores after their formation due to skin elasticity [14, 34, 51]. Besides micropore orifices, which turned out to be significantly smaller than the applied MN width [51, 52], studies have also concluded that only $10 - 30$ % of the nominal needle length enters the tissue [53]. It can be assumed that the efficiency of MN insertion strongly depends on the applied MN length, usually being more efficient with decreasing needle lengths. These observations are further supported by research that successfully applied densely packed MN arrays with even smaller needle lengths of $65 - 110$ µm for cutaneous vaccination [54].

Furthermore, the MN device itself as well as the skin treatment site determine the extent of MN penetration into the tissue [52, 55]. Dependent on the skin condition, application force and time, MN density, and repetitions, the skin tissue disruption occurs to variable extent [53]. Reportedly, higher insertion forces are required with increasing needle lengths [53]. The needle length of the MN array and the roller used in this study were in comparable range, therefore comparable insertion forces could be expected for both MN types. The force applied for insertion of the MN array was about 20 N. Similar forces are reportedly achieved by manual pressing by human volunteers [56]. Additionally, forces of ∼20 N were found to be sufficient for the insertion of MN arrays with needle lengths of up to 900 µm [56]. The relatively long application time of the MN array for 3 min in this

study allowed for a full penetration of the MN array into the skin tissue. Although no application force was measured during the microneedling using the MN roller, successful breaching of the skin barrier was proven by i.d. particle delivery. The results suggest that full insertion of the MN types used in this study were achieved and major differences in i.d. particle delivery were derived from variations in tip geometry, application mode and sequence.

The study shows that a notable i.d. delivery of particles between 1.2 µm and 0.1 µm can be achieved by only 3 min massage. The particles reached into the epidermal and dermal layer of MN-treated skin, increasing the delivery efficiency compared to (transfollicular) delivery to intact skin by factor ten. Moreover, this is the first time showing the possibility to deliver a formulation into the skin by applying simultaneous skin barrier disruption and particle delivery using a conventional solid MN roller. Compared to previous studies, the time required for i.d. particle delivery could be reduced by active massage compared to up to 48 h incubation [45, 57]. However, notably higher delivery efficiencies can be achieved by longer incubation. Considering the effects of particle size, MN tip geometry, length, and application mode, the development of MN devices requires the consideration of treatment site-specific conditions to achieve an optimum i.d. delivery to specific layers of the skin. The combination of repeated microneedling using a MN roller and manual massage at optimum duration represents an option to further maximize the i.d. particle delivery in future studies.

4 Conclusion

Cutaneous vaccine delivery is a promising alternative to conventional i.m. or s.c. injection for vaccination. Cutaneous vaccination provides the option for dose reduction and may potentially offer new treatments against cancer, Alzheimer's disease, or infectious diseases that are not yet preventable, e.g. malaria, ebola, or HIV. Although today i.d. liquid injections are the most widely used approach for cutaneous vaccination and studied in several clinical trials, the requirement of a stable cold-chain represents a major challenge. Therefore, the development of vaccine formulations with increased storage stability, suitable for i.d. delivery needs to be further intensified.

This study provides insights into the qualitative and quantitative deposition of micro- and nanoparticles in the context of different commercially available types of MNs. It was shown that the penetration depth of particles with diameters below 7 µm is independent

of the particle size. However, the quantitative amount deposited in the tissue was highly dependent on the particle diameter with an optimum around 0.5 µm.
Besides the particle size, the MN tip geometry and application mode strongly influenced the penetration behavior of the particles as well as the quantitative i.d. delivery. No clear impact of the MN length and the number of micropores was identified. Cone-shaped MNs applied using a roller device were superior in providing a high penetration depth and also induced the highest particle deposition compared to a dense array of flat MNs. Independent of the MN tip geometry, needle lengths between $200 - 250$ µm were suitable to facilitate a deposition of particles in the epidermal and dermal skin layer, which is the preferred delivery depth for cutaneous vaccination. The deposition of nanoparticles in close vicinity to epidermal and dermal APCs allows for the uptake and processing of antigen-loaded particles. Nanoparticles delivered intradermally by this approach can serve as suitable adjuvants for cutaneous vaccination. Microparticles, on the other hand, could serve as antigen-releasing depot in the skin tissue.
To date, an easy to develop and cost-effective approach for cutaneous vaccination that can truly compete with conventional vaccination is still missing. MNs are a promising tool to fill this gap. This study provides valuable insights regarding the key factors that affect the i.d. particle delivery upon microneedling, namely MN tip geometry, application mode, particle size, and massage. These findings help interpreting existing research and serve as starting point to select optimum MN treatment conditions. Although model particle suspensions have been used in this study, other drug and vaccine delivery systems can be easily combined with efficient MN treatment, e.g. virus-like-particle vaccines or dry powder patches. Additionally, microneedling is an attractive tool to enhance active delivery approaches, such as gene gun delivery [58].
The commercial availability of solid MNs makes them a useful and cost-efficient tool in research, especially for early screens of new vaccines and formulations. Particularly particles are a promising component in cutaneous vaccination due to their high potential to serve as sustained release depot or vaccine adjuvant. This study contributes to the thorough characterization of the mechanistics of particle application and MN treatment, which is of key relevance for the design of future studies.

Bibliography

[1] E. Larrañeta, R. E. M. Lutton, A. D. Woolfson, R. F. Donnelly, Microneedle arrays as transdermal and intradermal drug delivery systems: Materials science, manufacture and commercial development, Mater Sci Eng R Rep 104 (2016) 1–32.

[2] S. Henry, D. V. McAllister, M. G. Allen, M. R. Prausnitz, Microfabricated Microneedles: A Novel Approach to Transdermal Drug Delivery, J Pharm Sci 87 (1998) 922–925.

[3] M. R. Prausnitz, S. Mitragotri, R. Langer, Current status and future potential of transdermal drug delivery, Nat Rev Drug Discov 3 (2004) 115–124.

[4] R. F. Donnelly, T. R. Raj Singh, A. D. Woolfson, Microneedle-based drug delivery systems: microfabrication, drug delivery, and safety, Drug Deliv 17 (2010) 187–207.

[5] E. Larrañeta, M. T. C. McCrudden, A. J. Courtenay, R. F. Donnelly, Microneedles: a new frontier in nanomedicine delivery, Pharm Res 33 (2016) 1055–1073.

[6] Y.-C. Kim, J.-H. Park, M. R. Prausnitz, Microneedles for drug and vaccine delivery, Adv Drug Deliv Rev 64 (2012) 1547–1568.

[7] R. J. Pettis, A. J. Harvey, Microneedle delivery: clinical studies and emerging medical applications., Ther Deliv 3 (2012) 357–371.

[8] S. Marshall, L. J. Sahm, A. C. Moore, The success of microneedle-mediated vaccine delivery into skin, Hum Vaccin Immunother 12 (2016) 2975–2983.

[9] M. B. Teunissen, M. Haniffa, M. P. Collin, Insight into the immunobiology of human skin and functional specialization of skin dendritic cell subsets to innovate intradermal vaccination design, Curr Top Microbiol Immunol 351 (2012) 25–76.

[10] D. Gutowska-Owsiak, G. S. Ogg, The epidermis as an adjuvant, J Invest Dermatol 132 (2012) 940–948.

[11] L. Engelke, G. Winter, S. Hook, J. Engert, Recent insights into cutaneous immunization: how to vaccinate via the skin, Vaccine 33 (2015) 4663–4674.

[12] A. K. Banga, Microporation applications for enhancing drug delivery, Expert Opin Drug Deliv 6 (2009) 343–354.

[13] J. Arya, M. R. Prausnitz, Microneedle patches for vaccination in developing countries, J Control Release 240 (2016) 135–141.

[14] E. Caffarel-Salvador, R. F. Donnelly, Transdermal drug delivery mediated by microneedle arrays: innovations and barriers to success, Curr Pharm Des 22 (2016) 1105–1117.

[15] Intradermal delivery of vaccines: a review of the literature and the potential for development for use in low- and middle-income countries, PATH (2009).

[16] K. Ita, Transdermal delivery of drugs with microneedles-potential and challenges, Pharmaceutics 7 (2015) 90–105.

[17] M. Wang, L. Hu, C. Xu, Recent advances in the design of polymeric microneedles for transdermal drug delivery and biosensing, Lab Chip 17 (2017) 1373–1387.

[18] M. R. Prausnitz, Microneedles for transdermal drug delivery, Adv Drug Deliv Rev 56 (2004) 581–587.

[19] R. B. Groves, Quantifying the mechanical properties of skin in vivo and ex vivo to optimise microneedle device design, phdthesis, Cardiff University, 2011. URL: http://orca.cf.ac.uk/14980/. doi:10.1080/10255842.2011.596481.

[20] R. E. M. Lutton, J. Moore, E. Larraneta, S. Ligett, A. D. Woolfson, R. F. Donnelly, Microneedle characterisation: the need for universal acceptance criteria and GMP specifications when moving towards commercialisation, Drug Deliv Transl Res 5 (2015) 313–331.

[21] Food and Drug Administration, Regulatory considerations for microneedling devices draft guidance for industry and, 2017. URL: https://www.fda.gov/ucm/groups/fdagov-public/@fdagov-meddev-gen/documents/document/ucm575923.pdf[accessed15.04.18], [accessed 2018-04-15].

[22] J. Lademann, N. Otberg, H. Richter, H. J. Weigmann, U. Lindemann, H. Schaefer, W. Sterry, Investigation of follicular penetration of topically applied substances., Skin Pharmacol Appl Skin Physiol 14 Suppl 1 (2001) 17–22.

[23] N. Otberg, H. Richter, H. Schaefer, U. Blume-Peytavi, W. Sterry, J. Lademann, Variations of hair follicle size and distribution in different body sites, J Invest Dermatol 122 (2004) 14–19.

[24] N. Otberg, H. Richter, A. Knuttel, H. Schaefer, W. Sterry, J. Lademann, Laser spectroscopic methods for the characterization of open and closed follicles, Laser Phys Lett 1 (2004) 46–49.

[25] J. G. Rouse, J. Yang, J. P. Ryman-Rasmussen, A. R. Barron, N. A. Monteiro-Riviere, Effects of mechanical flexion on the penetration of fullerene amino acid-derivatized peptide nanoparticles through skin, Nano Lett 7 (2007) 155–160.

[26] J. Lademann, F. Knorr, H. Richter, U. Blume-Peytavi, A. Vogt, C. Antoniou, W. Sterry, A. Patzelt, Hair follicles-an efficient storage and penetration pathway for topically applied substances. Summary of recent results obtained at the Center of Ex-

perimental and Applied Cutaneous Physiology, Charité -Universitätsmedizin Berlin, Germany., Skin Pharmacol Physiol 21 (2008) 150–155.

[27] A. Patzelt, H. Richter, F. Knorr, U. Schäfer, C.-M. Lehr, L. Dähne, W. Sterry, J. Lademann, Selective follicular targeting by modification of the particle sizes, J Control Release 150 (2011) 45–48.

[28] S. S. Tinkle, J. M. Antonini, B. A. Rich, J. R. Roberts, R. Salmen, K. DePree, E. J. Adkins, Skin as a route of exposure and sensitization in chronic beryllium disease, Environ Health Perspect 111 (2003) 1202–8.

[29] M. Schneider, F. Stracke, S. Hansen, U. F. Schaefer, Nanoparticles and their interactions with the dermal barrier, Dermatoendocrinol 1 (2009) 197–206.

[30] R. Toll, U. Jacobi, H. Richter, J. Lademann, H. Schaefer, U. Blume-Peytavi, Penetration profile of microspheres in follicular targeting of terminal hair follicles, J Invest Dermatol 123 (2004) 168–176.

[31] J. Lademann, H. Richter, A. Teichmann, N. Otberg, U. Blume-Peytavi, J. Luengo, B. Weiss, U. F. Schaefer, C. M. Lehr, R. Wepf, W. Sterry, Nanoparticles - an efficient carrier for drug delivery into the hair follicles, Eur J Pharm Biopharm 66 (2007) 159–164.

[32] T. W. Prow, J. E. Grice, L. L. Lin, R. Faye, M. Butler, W. Becker, E. M. T. Wurm, C. Yoong, T. A. Robertson, H. P. Soyer, M. S. Roberts, Nanoparticles and microparticles for skin drug delivery, Adv Drug Deliv Rev 63 (2011) 470–491.

[33] D. Hüwel, Characterization of polymer films for intradermal vaccine delivery, bthesis, Ludwig-Maximilians-University Munich, 2015.

[34] Y. A. Gomaa, D. I. J. Morrow, M. J. Garland, R. F. Donnelly, L. K. El-Khordagui, V. M. Meidan, Effects of microneedle length, density, insertion time and multiple applications on human skin barrier function: Assessments by transepidermal water loss, Toxicol In Vitro 24 (2010) 1971–1978.

[35] G. Schneider, G. Decher, N. Nerambourg, R. Praho, M. H. V. Werts, M. Blanchard-Desce, Distance-dependent fluorescence quenching on gold nanoparticles ensheathed with layer-by-layer assembled polyelectrolytes, Nano Lett 6 (2006) 530–536.

[36] C. S. Peyratout, L. Dahne, L. Dähne, Tailor-made polyelectrolyte microcapsules: from multilayers to smart containers, Angew Chem Int Ed Engl 43 (2004) 3762–3783.

[37] W. Feng, X. Zhou, C. He, K. Qiu, W. Nie, L. Chen, H. Wang, X. Mo, Y. Zhang, Polyelectrolyte multilayer functionalized mesoporous silica nanoparticles for pH-responsive drug delivery: layer thickness-dependent release profiles and biocompatibility, J Mater

Chem B 1 (2013) 5886–5898.

[38] J. Schindelin, I. Arganda-Carreras, E. Frise, V. Kaynig, M. Longair, T. Pietzsch, S. Preibisch, C. Rueden, S. Saalfeld, B. Schmid, J.-Y. Tinevez, D. J. White, V. Hartenstein, K. Eliceiri, P. Tomancak, A. Cardona, Fiji: an open-source platform for biological-image analysis, Nat Meth 9 (2012) 676–682.

[39] J. J. Richardson, J. Cui, M. Bjornmalm, J. A. Braunger, H. Ejima, F. Caruso, Innovation in layer-by-layer assembly, Chem Rev 116 (2016) 14828–14867.

[40] D. V. Volodkin, A. I. Petrov, M. Prevot, G. B. Sukhorukov, Matrix polyelectrolyte microcapsules: new system for macromolecule encapsulation, Langmuir 20 (2004) 3398–3406.

[41] A. Schnäckel, S. Hiller, U. Reibetanz, E. Donath, A. Schnackel, S. Hiller, U. Reibetanz, E. Donath, Fluorescent bead arrays by means of layer-by-layer polyelectrolyte adsorption, Soft Matter 3 (2007) 200–206.

[42] B. G. De Geest, S. De Koker, K. Immesoete, J. Demeester, S. C. De Smedt, W. E. Hennink, Self-exploding beads releasing microcarriers, Adv Mat 20 (2008) 3687–3691.

[43] T. J. Powell, M. Mistillis, N. Palath, J. Tang, A. Jacobs, E. Cardenas, J. G. Boyd, M. Prausnitz, Immunization with synthetic LbL microparticle vaccine administered using a microneedle patch elicits humoral and cellular immune responses and protects mice from challenge with respiratory syncytial virus, J Immunol 196 (2016) 76.8.

[44] R. Paleco, S. R. Vučen, A. M. Crean, A. Moore, S. Scalia, Enhancement of the in vitro penetration of quercetin through pig skin by combined microneedles and lipid microparticles, Int J Pharm 472 (2014) 206–213.

[45] W. Zhang, J. Gao, Q. Zhu, M. Zhang, X. Ding, X. Wang, X. Hou, W. Fan, B. Ding, X. Wu, X. Wang, S. Gao, Penetration and distribution of PLGA nanoparticles in the human skin treated with microneedles, Int J Pharm 402 (2010) 205–212.

[46] M. Radtke, A. Patzelt, F. Knorr, J. Lademann, R. R. Netz, Ratchet effect for nanoparticle transport in hair follicles, Eur J Pharm Biopharm 116 (2017) 125–130.

[47] Y. A. Gomaa, L. K. El-Khordagui, M. J. Garland, R. F. Donnelly, F. McInnes, V. M. Meidan, Effect of microneedle treatment on the skin permeation of a nanoencapsulated dye, J Pharm Pharmacol 64 (2012) 1592–1602.

[48] R. Alvarez-Roman, A. Naik, Y. N. Kalia, R. H. Guy, H. Fessi, Skin penetration and distribution of polymeric nanoparticles, J Control Release 99 (2004) 53–62.

[49] M. O. Oyewumi, A. Kumar, Z. Cui, Nano-microparticles as immune adjuvants: correlating particle sizes and the resultant immune responses, Exp Rev Vaccines 9 (2010)

1095–1107.

[50] L. Völk, Characterization of the penetration behavior of micro- and nanoparticles into ex vivo pig skin after application of different microneedle treatments, bthesis, Ludwig-Maximilians-University Munich, 2016.

[51] H. Kalluri, C. S. Kolli, A. K. Banga, Characterization of microchannels created by metal microneedles: formation and closure, AAPS J 13 (2011) 473–481.

[52] S. A. Coulman, J. C. Birchall, A. Alex, M. Pearton, B. Hofer, C. O'Mahony, W. Drexler, B. Povazay, In vivo, in situ imaging of microneedle insertion into the skin of human volunteers using optical coherence tomography, Pharm Res 28 (2011) 66–81.

[53] W. Martanto, J. S. Moore, T. Couse, M. R. Prausnitz, Mechanism of fluid infusion during microneedle insertion and retraction, J Control Release 112 (2006) 357–361.

[54] T. W. Prow, X. Chen, N. A. Prow, G. J. P. Fernando, C. S. E. Tan, A. P. Raphael, D. Chang, M. P. Ruutu, D. W. K. Jenkins, A. Pyke, M. L. Crichton, K. Raphaelli, L. Y. H. Goh, I. H. Frazer, M. S. Roberts, J. Gardner, A. A. Khromykh, A. Suhrbier, R. A. Hall, M. A. F. Kendall, Nanopatch-targeted skin vaccination against West Nile Virus and Chikungunya virus in mice, Small 6 (2010) 1776–1784.

[55] J. Enfield, M.-L. O'Connell, K. Lawlor, E. Jonathan, C. O'Mahony, M. Leahy, In-vivo dynamic characterization of microneedle skin penetration using optical coherence tomography, J Biomed Opt 15 (2010) 46001.

[56] E. Larrañeta, J. Moore, E. M. Vicente-Pérez, P. González-Vázquez, R. Lutton, A. D. Woolfson, R. F. Donnelly, A proposed model membrane and test method for microneedle insertion studies, Int J Pharm 472 (2014) 65–73.

[57] S. A. Coulman, A. Anstey, C. Gateley, A. Morrissey, P. McLoughlin, C. Allender, J. C. Birchall, Microneedle mediated delivery of nanoparticles into human skin, Int J Pharm 366 (2009) 190–200.

[58] D. Zhang, D. B. Das, C. D. Rielly, An experimental study of microneedle-assisted microparticle delivery, J Pharm Sci 102 (2013) 3632–3644.

IV

APPLICATION OF WATER-SOLUBLE POLYVINYL ALCOHOL-BASED FILM PATCHES ON LASER MICROPORATED SKIN FACILITATES INTRADERMAL MACROMOLECULE AND NANOPARTICLE DELIVERY

This chapter has been published as L. Engelke, G. Winter, and J. Engert, Application of water-soluble polyvinyl alcohol-based film patches on laser microporated skin facilitates intradermal macromolecule and nanoparticle delivery, Eur J Pharm Biopharm 128 (2018) 119-130. I designed and conducted this study and wrote the manuscript by myself.

1 Introduction

During the past decades, the research and knowledge regarding the intradermal delivery of biologics and particularly vaccines has significantly increased [1, 2]. Proteins, peptides, and nucleic acids have been topically applied, including antigens for active vaccination, allergens for the treatment of type I allergies, and antibodies for local or systemic delivery [3–5]. However, the transdermal delivery of proteins into intact skin is known to be highly restricted due to their size, instability, and mostly hydrophilic properties [6]. The efficient and reproducible delivery of rather high-priced macromolecules into the skin therefore represents a major challenge with regards to their broad application in topical delivery.
To investigate and exploit the benefits of topically applied proteins, today, various techniques can be used which actively deliver drug formulations into the skin [7]. Fractional ablative laser microporation is a particularly attractive approach for the active intradermal delivery of molecules and provides the possibility to access specific layers of the skin [8]. Pulsed infrared lasers are used to induce a thermal ablation of tissue in micron sized columns with a diameter of $30 - 200$ µm [9], mainly referred to as microthermal zones (MTZs) [10] or microscopic ablation zones (MAZs) [11]. Carbon dioxide (CO_2) and Er:YAG lasers operating at wavelengths of 10.60 µm and 2.94 µm, respectively, are the two most common types of lasers used for ablative skin laser treatment [12]. At these wave-

lengths, water molecules show strong light absorption that induces vibrational excitation and heating in very short time, leading to vaporization and the ablation of surrounding tissue [13–15]. The thermal impact on the remaining tissue thereby depends on the system and parameters applied, e.g. laser fluence, local beam power density, pulse duration, and pore density [16]. Due to a higher absorption coefficient at ambient temperatures, Er:YAG devices are associated with a more precise microablation and reduced residual thermal damage (RTD), showing coagulation zones of $10-40$ µm compared to a thickness of $100-150$ µm for CO_2 lasers [12, 16]. Severe side effects, including erythema, edema, and postinflammatory hyperpigmentation, as well as overall healing times could be significantly reduced using fractional lasers and particularly Er:YAG devices emitting very short pulses of laser light [17]. 'Cold ablation' is characterized by minimal RTD on the tissue and provides a micropore closure within two days, driven by natural re-epithelialization [8, 18, 19]. The reduced thermal damage goes along with inferior skin contraction, collagen shrinkage, and tissue remodelling [20, 21], which are beneficial effects for the treatment of rhytides, photodamaged skin, scars, and other skin conditions [22].

Today, fractional laser microporation is an inherent part in the portfolio of skin resurfacing treatments and by that is well established as a safe dermatological method. Besides this, recent studies have reported on the delivery of drug substances into laser microporated skin, including small molecules [23–29], peptides [30, 31], macromolecules [32–36], nucleic acids [37, 38], particles [39, 40], and cells [41]. Of special interest is the precise targeting of specific skin layers for the intradermal delivery of immunogenic molecules. The skin has long been recognized as an immunologic organ comprising a high density of APCs, namely LCs in the epidermal and different subsets of dDCs in the dermal layer [42–44]. Moreover, epidermal keratinocytes are involved in early inflammation processes and play a key role in promoting adaptive immune responses when targeted by cutaneous vaccination [45, 46]. The high abundance of immunocompetent cells in the epidermis and dermis makes the skin a particularly attractive site for vaccine delivery. By directly addressing LCs and dDCs, it is possible to regulate the differentiation of CD4+ T helper cells (Ths) and CD8+ cytotoxic T lymphocytes (CTLs) [43]. Moreover, such specific targeting has a direct impact on the Th cell polarization [47, 48]. Without further adjuvantation, T cells tend to differentiate along the Th2 pathway upon intradermal delivery of antigens. However, a re-modelling towards Th1/Th2-balanced immune responses is possible using suitable adjuvants [8, 49, 50]. The advantage of a precise targeting of different skin layers and immune cells by fractional laser microporation has been exploited for cutaneous vaccination

Table IV.1: Drug formulations and molecule types that have been tested for skin delivery in connection with ablative fractional laser poration using CO_2 ($\lambda = 10.60$ µm), Er:YAG ($\lambda = 2.94$ µm), or erbium:yttrium scandium gallium garnet (Er:YSGG) lasers ($\lambda = 2.80$ µm).

	Type of molecule	Reference
Solution		
CO_2 lasers	Small molecules	5-Fluorouracil [23]; Vitamin C, magnesium ascorbyl phosphate [24]; Hydroquinone, Imiquimod, FITC [35]; Sulphorhodamine B, methylene blue [64]
	Macromolecules	FITC-dextranes 4, 20, 40 kDa [35]; Texas red-OVA [64]
Er:YAG lasers	Small molecules	Methotrexate [11]; 5-Fluorouracil [23]; Vitamin C, magnesium ascorbyl phosphate [24]; 5-Aminolevulinic acid [25,27]; Lidocaine [26]; Prednisone [28]; Diclofenac [29]; Imiquimod [31]; FITC [33]; Sulphorhodamine B [37]; Indomethacin, Nalbumphine [72]
	Peptides	Peptides (716 Da, 1429 Da, 2190 Da, 2354 Da) [30,31]
	Macromolecules	Lyzozyme [30]; FITC-dextranes 4, 20, 40, 70, 150 kDa [31] FITC-dextranes 4, 19, 38, 77 kDa, FITC-insuline hexamer [33]; ATG (Thymoglobulin®), Basiliximab (Simulect®) [34]; hGH [36, 55]; Phl p 5 [49, 51]; OVA [51]; OVA, XCL1-OVA Vaccibody [53]; HBsAg, conjugate vaccines (Menveo®, ActHIB®) [54]; Cyt c, FSH, FITC-BSA [55]; FITC-dextranes 4, 10, 20 kDa [71]
	Nucleic acids	Fluorescein-labeled oligonucleotides (15-mer, 25 mer), plasmid DNA [37]; siRNA [38]
Er:YSGG lasers	Small molecules	Hydrocortisone [32]
	Macromolecules	γ-IFN [32]
Suspension		
CO_2 lasers	Small molecules	Triamcinolon acetonide [56]
	Particles	Quantum dots [35]
Er:YAG lasers	Particles	Ti_2O nanoparticles, Al_2O_3 microparticles [39]; $CaCO_3$ microcontainers containing Fe_3O_4 nanoparticles [40]; Triamcinolone acetonide-, nile red-, fluorescein-loaded microparticles [57]
	Cells	Adipose-derived stem cells (ADSC) [41]
Liposomes		
CO_2 lasers	Small molecules	Carboxyfluorescein [58]
	Macromolecules	FITC-OVA [58]
Semi-solid preparation		
CO_2 lasers	Small molecules	Diclofenac [29]; Methylaminolevulinic acid [59]; 5-Fluorouracil [60]
Er:YAG lasers	Small molecules	Diclofenac [29]; Lidocaine [61]
Dry powder patch		
CO_2 lasers	Small molecules	Sulphorhodamine B [62,65]
	Macromolecules	OVA [62]; OVA, insuline, antibody [65]
	Nucleic acids	Vaccinia virus encoding OVA cDNA [62]
	Cells	BCG vaccine [62]
Er:YAG lasers	Macromolecules	OVA [52]

and transcutaneous/epicutaneous allergen-specific immunotherapy (TCIT/EPIT) [51–54].

Table IV.1 highlights that a wide range of different molecules have been successfully delivered into laser-generated micropores using liquid formulations, e.g. solutions [23, 55], suspensions [56, 57], or liposomes [58]. However, only few studies have been using formulations easier to apply under real-life conditions, e.g. semi-solid or dry patch formulations [59–62]. Many proteins and especially vaccines have limited stability in the solubilized state, which requires a cold chain and limits the shelf-life at ambient temperatures. On the other hand, superior micropore filling has been observed for liquid formulations compared to semi-solid preparations [63]. For these reasons, novel drug delivery systems should provide improved storage stability and liquid-like micropore filling properties. Based on these demands, powder-loaded patches, which are based on an array of laser-generated and drug powder-loaded microchannels, have been developed and tested for immunotherapy [52, 64, 65]. The present study introduces an alternative formulation strategy exploiting water-soluble dry film patches as a drug delivery system. We aimed to solubilize hydrophilic polymer films directly on laser microporated skin, taking advantage of an enhanced water transport from the tissue through the porated skin into the film under occlusion. Occlusive backings, used for fixation on the skin, prevent water loss and accelerated a dissolution of the polymer films. The drug is then released upon dissolution of the film matrix, which allows the molecule to diffuse through the micropores into the viable skin tissue.

Different polymer film formulations based on water-soluble PVA or blends of PVA with carboxmethyl cellulose (CMC) or cross-linked carbomer as gelling agents were prepared using the film casting technique. This easily scalable fabrication approach resulted in thin, fast-releasing polymer films that could be loaded with a broad variety of molecules and concentrations. To validate the feasibility of our approach, the release from the film patches and the delivery of FITC, rhodamine B-labeled dextrane 70 kDa (RD70), and PS-particles into laser microporated pig skin was tested using the P.L.E.A.S.E.® fractional laser poration technology (Pantec Biosolutions, Ruggell, Liechtenstein). The P.L.E.A.S.E.® laser system enables a safe and pain-free ablation of superficial skin layers and has been successfully tested for immunotherapy in research [49, 51–54].

This study presents a novel drug delivery platform based on PVA polymer films suitable for the intradermal administration of macromolecules and nanoparticles upon fractional skin laser microporation. The water-soluble polymer films provide the potential to enhance the drug storage stability while preserving liquid-like diffusion properties upon administration. Furthermore, the polymer film patch reduces the risk of infection by covering the impaired

skin barrier during micropore closure.

2 Materials and Methods

2.1 Chemicals

FITC, OVA, polysorbate 20, polyvinyl alcohol (PVA, Mowiol® 4-88, MW ∼31 kDa), rhodamine B-labeled dextrane 70 kDa (RD70, MW 70 kDa), sucrose, and trichloroacetic acid (TCA) were purchased from Sigma-Aldrich (Taufkirchen, Germany). Red-fluorescent PS-particles (ex 530 nm/em 607 nm) were purchased from microparticles GmbH (Berlin, Germany). CMC (Tylopur® C30 G1) was obtained from Clariant (Wiesbaden, Germany). Cross-linked carbomer (Carbopol® 974P) was obtained from BF Goodrich Chemical (Brussels, Belgium). Trehalose and sodium dihydrogen phosphate were purchased from VWR International (Leuven, Netherlands). Potassium carbonate and Tris were obtained from Merck (Darmstadt, Germany). Propylene glycol was from BASF (Ludwigshafen, Germany). Di-sodium hydrogen phosphate was purchased from Applichem (Darmstadt, Germany). Sodium chloride was obtained from Bernd Kraft (Duisburg, Germany).

2.2 Liquid polymer film formulations

PVA was dissolved alone or together with CMC in 10 mM PBS (pH 7.0, 50 mM ionic strength) at 80 °C in a water bath. Propylene glycol and polysorbate 20 were added to the polymer solutions and mixed thoroughly. The PVA-carbomer blend formulation was prepared as described above using water for dissolution and Tris for subsequent pH adjustment. After cooling down to RT, solutions of different model substances were added to the polymer mixtures, using OVA, FITC, RD70, or red-fluorescent 5 µm or 0.5 µm PS-particles as model substances and vehicles. The model substance was dissolved in 10 mM PBS or water containing sucrose and trehalose as protein stabilizers in a molar ratio of 1/500 for each stabilizer. Different OVA loadings were obtained by adjusting the amount of model substance and PVA (Tab. IV.2). Film formulations containing FITC or RD70 were prepared similarly, providing molar concentrations equal to *sim*25 µg/mg and *sim*100 µg/mg OVA-loaded films, respectively. Particle-loaded films were obtained by adding an appropriate volume of 2.5% (w/v) particle suspension (as provided by the manufacturer) to the polymer mixture with a target concentration of 100 µg particles/mg dry film.

Table IV.2: Composition of ovalbumin (OVA)-loaded polymer film formulations with target concentrations from 25 µg to 100 µg OVA per mg dry film.

	Polymer film formulation		
Component [% (w/w)]	PVA	PVA-CMC	PVA-Carbomer
Ovalbumin (OVA)	0.6 - 2.4	0.3 - 1.2	0.3 - 1.2
Trehalose/Sucrose (1:1)	3.4 - 13.4	2.4 - 9.7	2.3 - 9.2
Propylene glycol	5.0	8.7	8.7
Polysorbate 20	0.07	0.04	0.04
Carboxymethyl cellulose (CMC)	-	4.4	-
Cross-linked carbomer	-	-	4.4
Polyvinyl alcohol (PVA)	ad 100	ad 100	ad 100
Solid content	15.1 % (w/v)	23.6 % (w/v)	23.6 % (w/v)
Knife height	1000 µm	500 µm	500 µm
Casting speed	1.0 mm/s	1.0 mm/s	0.5 mm/s

2.3 Casting of the polymer films

The liquid film formulations were cast onto polytetrafluoroethylene (PTFE)-coated cards (mtv messtechnik, Erftstadt, Germany) using an Erichsen Coatmaster 510 (Erichsen GmbH, Hemer, Germany). The automated film applicator operated at a working speed of 1mm/s for the PVA and PVA-CMC blend films or at 0.5 mm/s for the PVA-carbomer blend films. PVA films were prepared using a 1000 µm casting knife whereas a 500 µm casting knife was used for the PVA-CMC and PVA-carbomer blend films. The polymer films were dried overnight at RT and cut into 15x15 mm^2 samples. The film sample dimensions and weight were determined prior to each experiment. The OVA loading was quantified upon reconstitution of the dry polymer films using a bicinchoninic acid (BCA) assay (Micro BCA™ Protein Assay Kit, Thermo Scientific, Waltham, MA, USA). The FITC and RD70 contents were determined by fluorescence spectroscopy upon dissolution in 100 mM Tris buffer (pH 9.0, 150 mM ionic strength).

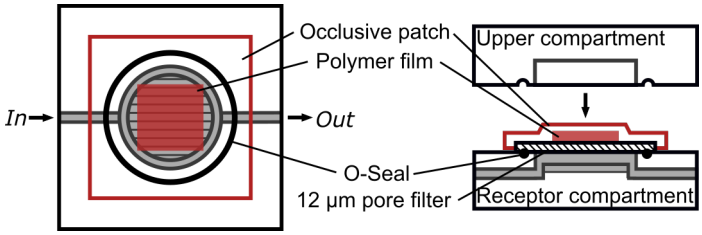

Figure IV.1: Schematic illustration of the customized flow-through diffusion chamber to assess the release from polymer films.

2.4 Fluorescence spectroscopy

The model substances FITC and RD70 were quantified using a Cary Eclipse fluorescence spectrophotometer (Agilent, Santa Clara, CA, USA) at excitation and emission wavelengths of 492 nm/ 518 nm and 555 nm/ 576 nm, respectively. Calibration resulted in linear detection ranges between 1-400 ng/mL for FITC and 50-3,000 ng/mL for RD70 solutions (both $R^2 = 0.999$). The limit of detection was 1 ng/mL for FITC and 50 ng/mL for RD70, respectively. Each value was determined as the average out of 5 consecutive measurements. The fluorescence intensity of each sample was analyzed in triplicates.

2.5 Release from polymer films

The release of FITC as model substance from dry polymer films was tested in a customized flow-through diffusion chamber (Fig. IV.1). In precise, the dry film patches were mounted in the donor compartment with the polymer film facing the circular opening of a low-volume receptor chamber. The receptor chamber provided a medium in- and outlet on opposite sides, generating a laminar flow of the receptor medium. Nucleopore™ membrane filters with a pore size of 12 µm (25 mm diameter, Whatman™, GE Healthcare, Freiburg, Germany) were used to separate donor and receptor compartments and Leukoflex® occlusive tape (BSN Medical, Hamburg, Germany) was used for fixation of the polymer films. At a flow-rate of 400 µL/h, Tris buffer (100 mM, pH 9.0, 150 mM ionic strength) was pumped through the receptor chamber using a LA-160 syringe pump (Landgraf Laborsysteme, Langenhagen, Germany). At the chamber outlet, receptor medium was collected in fractions after 30 min, every hour until 8 h, and after 10 h. The amount of FITC in each fraction was quantified and compared to the total FITC content of each film sample. The total FITC content was calculated from the theoretical loading determined by dissolution of film samples in a defined volume. All experiments were performed in triplicates.

2.6 Laser microporation treatment

Excised skin from both sides of the ventrolateral region between mammary ridge and the lateral side of the body of $5 - 7$ week old piglets was supplied by the Clinic for Swine (Faculty of Veterinary Medicine, LMU Munich, Oberschleißheim, Germany). Skin samples were cleaned with water and bristles were removed using a hair clipper. Full thickness pig skin was prepared by removing excess subcutaneous tissue with a scalpel. The skin samples were stored at −80 °C for no longer than one month. Before use, the pig skin was thawed and approximately 3x3 cm^2 skin samples were prepared. After equilibration in 0.9 % saline for 10 min, the skin surface was dried using a cotton wipe and positioned on a flat surface. For laser microporation using the P.L.E.A.S.E.® fractional laser poration system (Pantec Biosolutions, Ruggell, Liechtenstein), two pulses of 125 µs per pore with a fluence of 17.8 J/cm^2 were applied, creating a nominal pore depth of 71 µm on a total treatment area of 14x14 mm^2 and a pore density of 15 %. For cosmetic applications typically 100 µm pore depth and 5 % pore density are targeted. The pore density in pores per cm^2 was determined by counting and the pore diameter was assessed by histological imaging.

2.7 Transepidermal water loss measurement

The transepidermal water loss (TEWL) before and after laser microporation was quantified using a Tewameter® TM 300 (Courage + Khazaka electronic, Cologne, Germany). The TEWL was determined in triplicates, each value being calculated as the mean of 5 consecutive stable measurements within equilibration for ∼5 min. Freshly excised pig skin and pig skin stored at −80 °C for 1, 14, or 28 days were compared in this experiment. The skin samples were hydrated for 10 min in 0.9 % saline and subsequently adjusted onto a flat surface. Skin surface moisture was removed using a cotton wipe and the TEWL was measured after 10 min resting at ambient conditions. Laser microporation was performed as described above. After mounting onto Franz diffusion cells and equilibration for 30 min, the TEWL of intact and laser microporated skin was measured as described above.

2.8 Skin penetration and permeation

RD70 or PS-particle loaded polymer film samples were attached to laser microporated or intact skin using Leukoflex occlusive tape (BSN Medical, Hamburg, Germany). Subsequently, the skin samples were mounted in jacketed Franz diffusion cells with an orifice

diameter of 15 mm (A = 1.77 cm^2). The conjunction of donor and receptor compartment was covered with parafilm to avoid leakage and fixated with a clamp. The receptor compartment (12 mL) was filled with 100 mM Tris buffer (pH 9.0, 150 mM ionic strength) and the samples were incubated for 24 h at 32 °C. After 2, 4, 6, 12, and 24 h, 1 mL of the receptor volume was withdrawn and replaced by fresh medium. The amount of RD70 in the receptor medium was quantified by fluorescence spectroscopy. After 24 h incubation, Franz cells were dismantled, excess formulation was removed from the skin surface and an area of 1x1 cm of the treatment region was prepared for further analysis. All experiments were performed in triplicates.

2.9 Histological analysis

Incubated skin samples were embedded in tissue freezing medium (Leica Biosystems, Wetzlar, Germany) and shock frozen in liquid nitrogen. Vertical skin sections with a thickness of 10 µm were prepared using a Microm HM560 cryostat (Thermo Scientific, Waltham, MA, USA). Histological samples were prepared using 4',6-diamidino-2-phenylindole (DAPI) mounting medium (Fluoroshield™, Sigma-Aldrich, Taufkirchen, Germany). The skin cross-sections were imaged upside down using a LSM 510 laser scanning microscope equipped with a LD-Achroplan 40x/0.6 corr objective (both from Carl-Zeiss, Jena, Germany). The settings were kept constant for each image. Image analysis was performed using Fiji image analysis software [66].

2.10 Quantification of RD70 in skin

The amount of RD70 that penetrated into the skin was quantified upon extraction from horizontal skin sections. In precise, incubated skin samples were fixed with the surface down onto a pre-cooled plate, embedded in tissue freezing medium (Leica Biosystems, Wetzlar, Germany), and frozen at −80 °C. Horizontal skin sections with a thickness of 20 µm were prepared by cryosectioning. Five slices were collected in a tube, adding up in a total thickness of 100 µm for each extracted skin layer. RD70 was extracted from the skin sections by incubation in 200 µL of 100 mM Tris buffer (pH 9.0, 150 mM ionic strength) for 20 min at 60 °C. After cooling down to RT, proteins were removed from the extract using TCA. For deproteinization, the extracted samples were centrifuged at 13,000 rpm for 2 min and 180 µL supernatant was transferred to a fresh tube. Subsequently, 30 µL of ice cold 100 % TCA was added to the solution and the mixture was incubated for 5 min on ice.

After centrifugation at 13,000 rpm for 2 min, 200 µL supernatant was quickly transferred to a fresh tube and mixed with 30 µL ice cold 5 M potassium carbonate solution. The basic pH of the extract was checked using pH paper. The RD70 content of the deproteinized extract was analyzed by fluorescence spectroscopy. The experimental flux was calculated based on the amount of RD70 detected in the skin tissue below 300 µm per cm^2 and the amount detected in the receptor compartment after 24 h.

3 Results

3.1 Film properties and release behavior

Transparent, water-soluble polymer films with an average thickness of 36 ± 14 µm for pure PVA, 71 ± 12 µm for PVA-CMC, and 58 ± 13 µm for the PVA-carbomer blend were prepared using the film casting technique followed by overnight drying at ambient temperatures. Different hydrophilic model substances could be incorporated into the polymer films by direct loading. The addition of varying amounts of model substance to the polymer solution while adapting the PVA content allowed to adjust the target concentration per area unit as preferred (Tab. IV.3).

Stable, homogeneous films were obtained with up to 389.4 ng/^{2} FITC or 268.6 µg/^{2} RD70 incorporated as model substances into the polymer films. Although polysaccharides can increase the brittleness of dry polymer films [67], films loaded with RD70 provided suitable properties for the patch application. RD70 is a branched polysaccharide composed of 1,6-alpha and 1,3-glycosidic linkages between glucose units, which is labeled with rhodamine B fluorescent dye molecules via thioester links to free glucose hydroxyl groups. The macromolecular model substance exhibited a molecular weight of 70 kDa and hydrophilic properties to simulate the behavior of protein antigens and other hydrophilic macromolecules.

Besides small and macromolecular model substances, films with suitable properties were obtained when PS-particles with a size of 5 µm or 0.5 µm were loaded as model vaccine vehicles into the formulations. The content of model substance or vehicle could be adjusted by varying film thickness and polymer content of the film formulation.

All films showed a high solubility and dissolved in large amounts of water within seconds. To simulate the restricted access of the films to tissue fluids through laser-generated micropores, FITC-loaded films were attached to a customized diffusion chamber, separated

Table IV.3: Film properties and maximum concentrations per mass or area unit that were achieved by direct loading of the model substances fluorescein isothiocyanate (FITC) and rhodamine B-labeled dextrane 70 kDa (RD70). (* used for skin penetration and permeation experiments)

Film formulation	Film thickness [µm]	Weight per 15x15 mm^2 * [mg]	FITC content [ng/cm^2]	RD70 content [$\mu g/cm^2$]
PVA	36 ± 14	6.0 ± 0.5	242.5 ± 36.5	92.4 ± 18.6
PVA-CMC	71 ± 12	20.2 ± 0.2	389.4 ± 51.1	268.6 ± 79.6
PVA-Carbomer	58 ± 13	17.2 ± 0.2	203.5 ± 16.8	207.5 ± 7.7

from the receptor medium by a filter with a nominal pore size of 12 µm. Upon contact with the receptor medium, which was passing below the filter at a low flow-rate, the hydrophilic film polymer dissolved and led to a fast release of the model substance. The occlusive tape that was used for fixation of the polymer films served as a tight, water-resistant seal within the diffusion chamber entrapping the solubilized film formulation. Within six hours, $75 - 100$ % of the incorporated FITC was released from the films regardless of the investigated polymer film formulation(Fig. IV.2). The comparison of low and high FITC loading in pure PVA, PVA-CMC, and PVA-carbomer films revealed a tendency of inferior release after 12 h for the high FITC content with a total release around 80 %. The incorporation of lower amounts of FITC into the films resulted in an improved release behavior close to 100 % total release. Considering the release kinetics of different film compositions, no obvious differences between PVA, PVA-CMC, and PVA-carbomer films with comparable FITC content were detected.

3.2 Transepidermal water transport and film dissolution

To evaluate the suitability of the utilized experimental setup to provide a good transferability to in vivo skin conditions, different aspects of the Franz diffusion cell experiment were examined. The pore formation process as well as the micropore dimensions are affected not only by laser parameters but also by skin condition and the level of hydration [68]. Furthermore, the extent of skin barrier disruption and the storage-induced damage of excised skin samples might affect the water transport through the tissue. To ensure a pore formation comparable to in vivo conditions, the release of water from freshly excised and stored pig

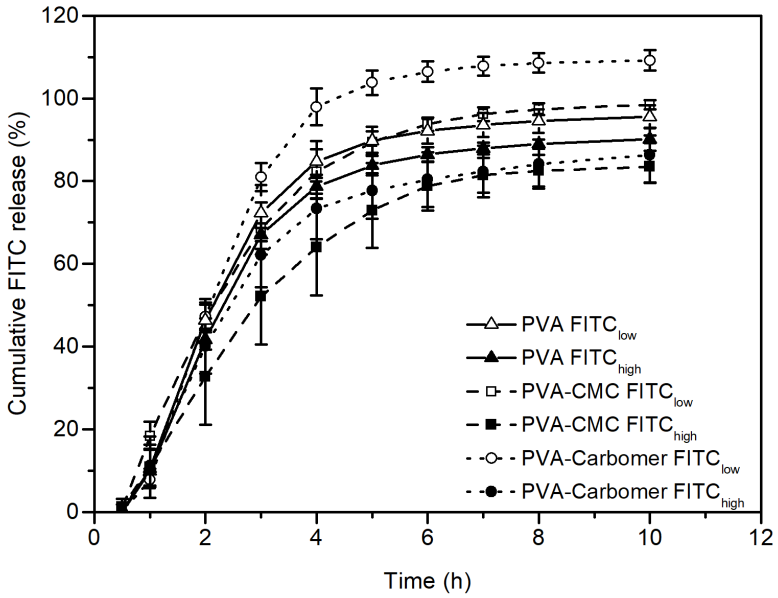

Figure IV.2: Cumulative release of the hydrophilic model substance FITC from PVA and PVA-CMC/ PVA-carbomer blend films loaded with 50-100 ng (low) and 200-400 ng (high) FITC per cm^2 film. All film formulations provide a fast drug release within 6 h with restricted water contact through 12 µm filter pores.

skin at the time of microporation was examined by TEWL measurements. Similarly, the water transport through intact and laser microporated pig skin was characterized in the Franz cell setup.

After hydration, the skin samples were prepared for laser treatment, which was performed $\sim$ 10 min after removal from saline solution. At this point in time, all skin samples showed TEWL values between $4-15$ g/m^2/h regardless of the storage duration (Fig. IV.3). Furthermore, comparable results were obtained for each sample when the untreated pig skin was assembled in the Franz diffusion cell setup. Fresh pig skin and skin samples that were stored for one day provided slightly higher TEWL values compared to skin samples with a storage duration of 14 or 28 days at -80 °C. The lowest values were detected using pig skin that was stored for 14 days. Fractional laser microporation using the previously specified parameters led to a 4- to 5-fold increase in the water transport trough the skin.

The dissolution of the polymer films was studied macroscopically over an incubation period of 24 h using untreated and laser microporated pig skin. It was observed that all polymer film formulations dissolved within less than 6 h when attached on top of laser-generated micropores. However, no or incomplete disintegration was detected when untreated skin was used in the Franz cell setup. Figure IV.4 gives a representative overview of the film

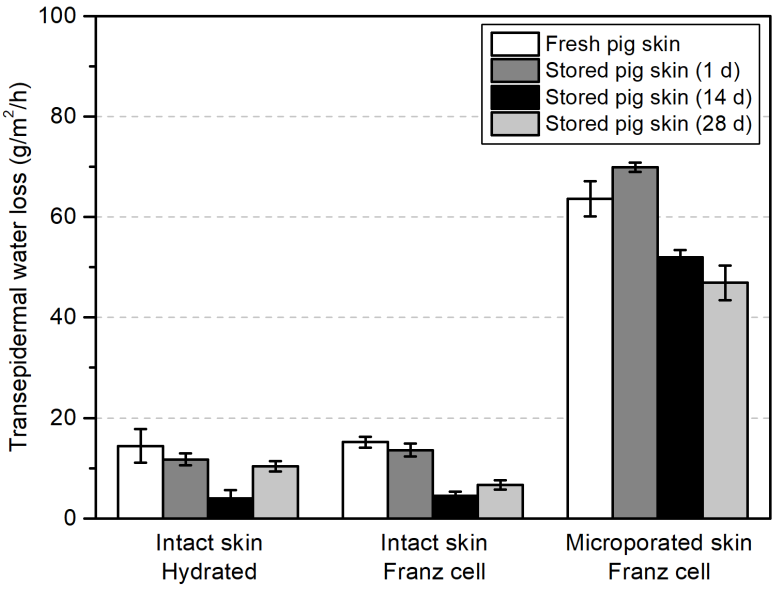

Figure IV.3: Water loss of excised pig skin after different treatments.

dissolution behavior in the Franz diffusion cell setup, showing PVA-CMC blend films directly after fixation to laser microporated skin and after 6 h incubation. The dissolution of the films was macroscopically visible. Upon solubilization, air bubbles were formed due to a small residual interspace between film patch and skin surface at the time of patch application. The occlusive tape used for film fixation, facilitated the generation of a liquid depot between skin surface and tape. After disintegration of the polymer matrix, the model substance or particles were free to diffuse into the underlying tissue. Using untreated skin, first signs of a beginning dissolution were detectable only after 24 h incubation. Upon dismantling, shape and surface of these polymer films was predominantly intact but sticky due to incomplete hydration.

3.3 Intradermal delivery of RD70 and PS-particles

The intradermal delivery of RD70 and PS-particles was evaluated qualitatively by laser scanning fluorescence microscopy. After 24 h, excess solubilized film was removed from the skin surface and vertical sections were prepared. Cell nuclei of the viable tissue were stained with DAPI to enable the distinction between epidermal and dermal skin layer. Microscopic imaging revealed an increasing deposition of RD70 in the epidermis and upper dermis of micropores over 6, 12 and 24 hours (images not shown). After 24 h incubation, the penetration of RD70 into the micropores was comparable for each polymer film formulation

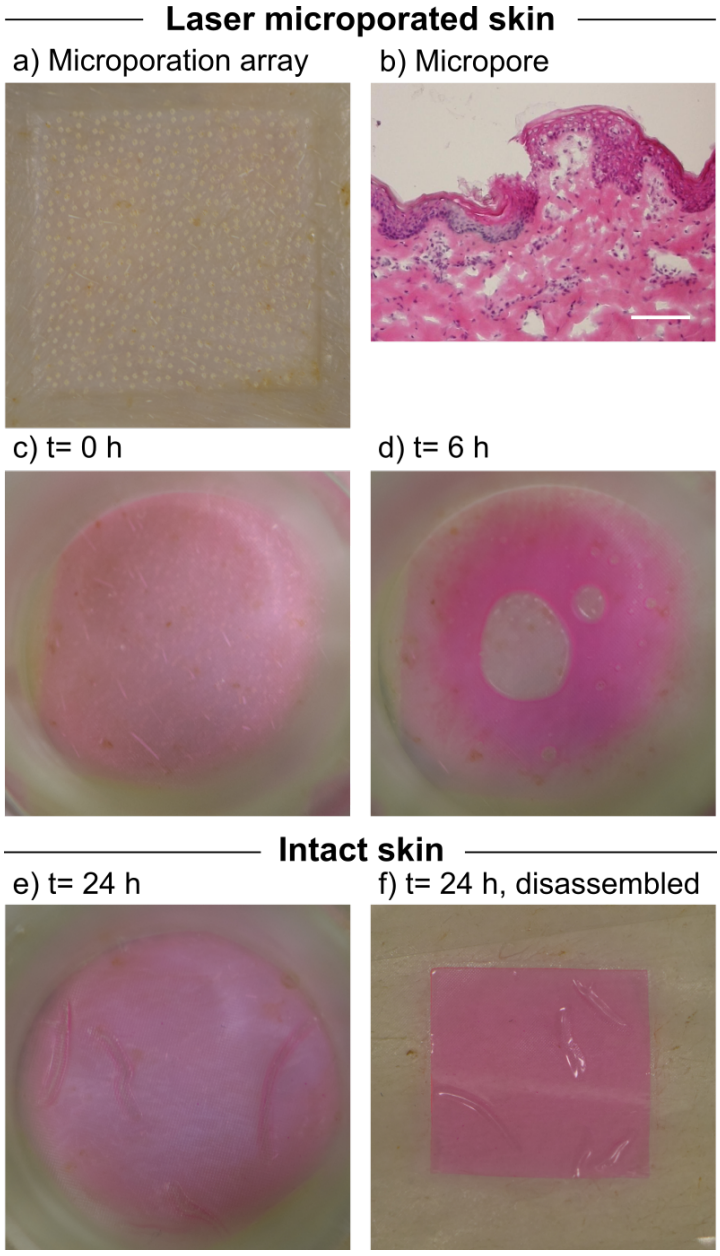

Figure IV.4: Dissolution behavior of representative polymer films observed during incubation in Franz diffusion cells using red-fluorescent RD70 as model substance. The images display an array of laser-generated micropores on excised pig skin (a), a single laser-generated micropore (b), as well as RD70-loaded PVA-CMC blend films directly after mounting onto Franz diffusion cells (c) and after 6 h incubation on laser microporated pig skin (d). Furthermore, polymer films are shown after incubation for 24 h (e) and after disassembly from Franz cells using untreated pig skin (f). (Magnification 200x, scale bar=100 µm)

(Fig. IV.5a – c). The delivery of the PS-particles however, was dependent on the particle size and the used polymer formulation. The application of nanoparticle-loaded films with a size of 0.5 µm led to a deposition over the entire micropore surface (Fig. IV.5d – f), whereas no particle delivery was observed for microparticles with a diameter of 5 µm (Fig. IV.5g – i). Moreover, the nanoparticle delivery using PVA polymer films was found superior over the deposition using PVA blend formulations. No substantial deposition of RD70 or PS-particles was detected on intact skin.

The penetration of RD70 was quantified by fluorescence spectroscopy after extraction from 100 µm horizontal skin sections and sample deproteinization. The incubation of laser microporated skin with RD70-loaded polymer films facilitated a penetration of the macromolecule into the epidermal and dermal layer of the skin. For all tested film formulations, an amount of 150 – 300 ng RD70 per cm^2 was extracted per 100 µm horizontal skin section up to a depth of 500 µm (Fig. IV.6). Furthermore, it was shown that RD70 permeated through the skin during incubation on laser microporated skin. Although the amount of RD70 in the Franz cell receptor compartment remained below the limit of detection within 12 h incubation, the macromolecule was quantifiable in the receptor medium after 24 h incubation. PVA films provided a slightly higher RD70 delivery into and through excised pig skin compared to the PVA-CMC and PVA-carbomer blend formulations, which both showed comparable RD70 penetration and permeation behavior. The calculated total amount of RD70 that was delivered into and through the skin over a microporated area of 14x14 mm^2 was highest for the pure PVA polymer film formulation with a total amount of 4.8 µg (Tab. IV.4). In comparison, 3.4 µg and 3.0 µg were delivered into the skin applying RD70 loaded PVA-CMC and PVA-carbomer films. Approximately 75 % of the total amount was detected in deeper skin layers or permeated into the Franz cell receptor compartment with values of 2.8 µg, 1.8 µg, and 1.7 µg for the pure PVA, PVA-CMC, and PVA-carbomer film patches.

The experimentally determined flux upon 24 h provided relatively low values between 0.07 – 0.12 µg/cm^2/h (Tab. IV.4). A slightly superior flux was detected for pure PVA films compared to the PVA blend formulations, which provided comparable values. Based on theoretical considerations the predicted flux was calculated based on the intuitive model (J_{int}) and the proposed model (J_{model}) by Rzhevskiy *et al.* (Tab. IV.4) [69]. A pore density of 273 pores/cm^2 determined by counting and a pore diameter of 200 µm was used for flux prediction. The molecular weight of 70 kDa of RD70 was used as provided by the manufacturer. Furthermore, the RD70 concentration was determined based on the

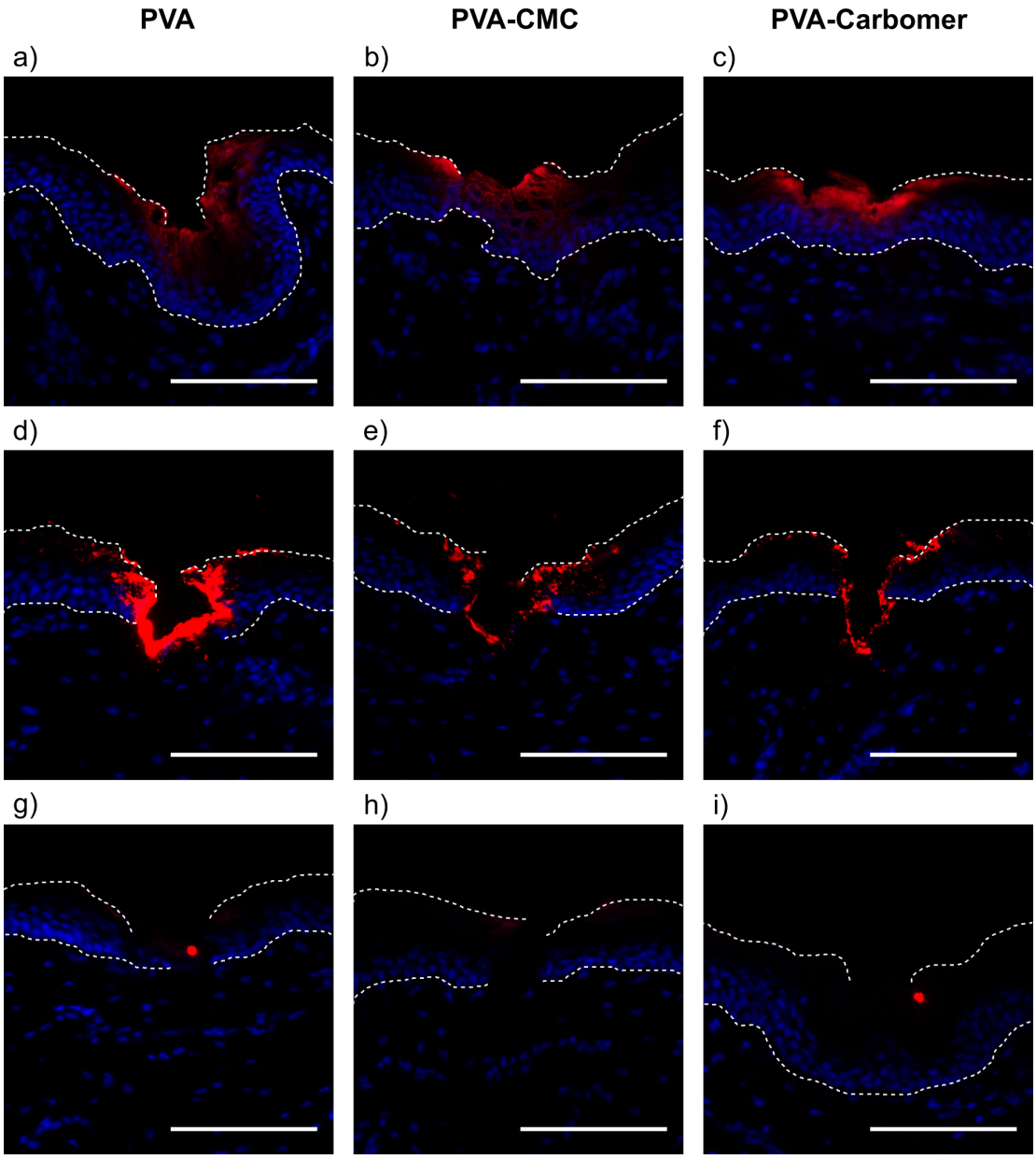

Figure IV.5: Fluorescence microscopy images of excised pig skin cross-sections after laser microporation and incubation with PVA, PVA-CMC or PVA-carbomer blend films for 24 h on Franz cells. Intradermal deposition of RD70 (a-c), 0.5 µm PS-nanoparticles (d-f), or 5 µm (g-i) PS-microparticles was shown by red fluoresce surrounding the micropore tissue. Dashed lines frame the skin surface (upper, determined in transmission mode) and the border between epidermal and dermal layer (lower). (Magnification 40x, scale bar= 100 µm)

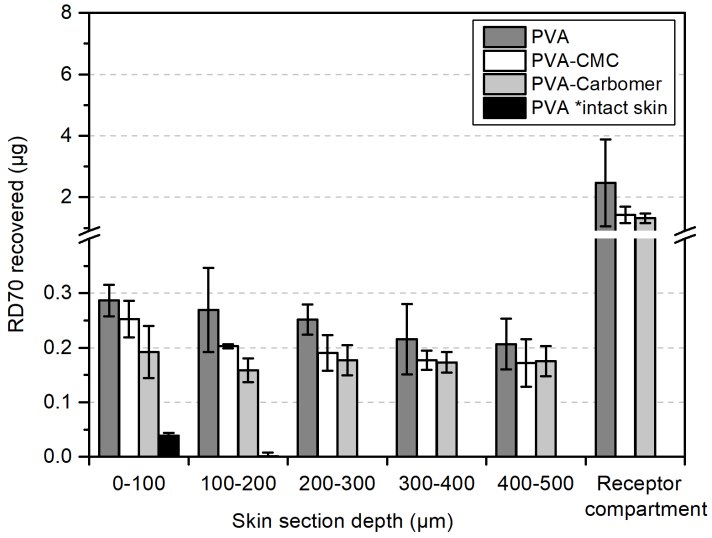

Figure IV.6: Quantitative amount of RD70 per square centimeter extracted from 100 µm horizontal skin sections and recovery of RD70 from the receptor compartment after 24 h incubation of polymer films on laser microporated pig skin.

RD70 content per cm^2 of each sample and the mean TEWL of 58.1 $g/m^2/h$ upon laser microporation per cm^2 within 24 h.

For the flux prediction using the intuitive model, a thickness of 1500 µm of the skin tissue below the SC h_s was used to represent full thickness skin. Moreover, a thickness equivalent to the average film sample thickness (Tab. IV.3) was used as height h_v above the SC. The theoretical model by Rzhevskiy *et al.* predicted 4- to 10-times higher flux values compared to the experimental flux. Higher deviations were observed for the CMC and carbomer blend formulations. On the other hand, the intuitive model provided good estimates for PVA-CMC and PVA-carbomer films but estimated a lower value for the pure PVA film.

The incubation of untreated pig skin with RD70-loaded PVA films did not result in a substantial delivery into the skin. A total amount of 0.08 µg was recovered from intact skin after 24 h incubation. This represents a delivery of approximately 0.08 % of the total RD70 applied in a PVA film patch on intact skin. The model substance was mainly detected in the first 100 µm horizontal layer of the skin, providing a deposition below 50 ng/cm^2 (Fig. IV.6). Moreover, no RD70 could be quantified in the Franz cell receptor compartment after 24 h incubation with a level below the limit of detection.

Table IV.4: Total amount of RD70 delivered into the skin after 24 h, calculated as the sum of substance that penetrated into and permeated through the skin and the experimental and theoretically predicted RD70 flux per cm^2 and hour. The predicted flux was calculated based on the intuitive model (J_{int}) and the proposed model by Rzhevskiy et al. (J_{model}) [69].

Film formulation	Total RD70 delivery			J_{exp}	J_{int}	J_{model}
	[µg/cm^2]	[µg]	[%]	[µg/cm^2/h]	[µg/cm^2/h]	[µg/cm^2/h]
PVA	3.6 ± 1.5	4.8 ± 1.7	2.3 ± 1.0	0.12	0.03	0.47
PVA-CMC	2.5 ± 0.4	3.4 ± 0.4	0.7 ± 0.1	0.08	0.08	1.06
PVA-Carbomer	2.2 ± 0.2	3.0 ± 0.4	0.7 ± 0.1	0.07	0.07	0.92

4 Discussion

4.1 Transepidermal water loss and film dissolution behavior

The TEWL of excised pig skin was determined under varying conditions to evaluate its comparability to in vivo human skin. Furthermore, the influence of a short-term storage of skin samples was assessed using freshly excised pig skin and skin samples that were stored at −80 °C for up to 28 days.

Intact skin samples showed a water release between $4 - 15$ g/m^2/h, which lies within the range of TEWL values observed on humans. Besides skin hydration and environmental conditions, the water release measured on human skin was shown to be mainly dependent on the site of the body and the circadian rhythm [70, 71]. Lower values between $3 - 14$ g/m^2/h have been measured on the forearm, whereas palms, soles, or the forehead release higher amounts of water with TEWL values of up to 48 g/m^2/h [70, 71]. The TEWL of excised, intact pig skin samples was comparable to the TEWL measured on human forearms, indicating that a comparable micropore formation with similar depths and RTD should be possible at this site of the body. Moreover, intact skin samples, freshly excised or stored, showed consistent TEWL values at the time of laser microporation and in the Franz cell setup, indicating that optimum conditions were reached for the laser microporation treatment. Certain variations of the TEWL between fresh and stored skin samples were recognized but could not be linked to the storage duration. The differences detected were in the range of variation observed on human skin with TEWL fluctuations

of up to 14 g/m^2/h [70, 71]. Based on these results, we assume that a storage of pig skin samples for up to 28 days at −80 °C is suitable to maintain a water release behavior comparable to in vivo human skin. To ensure comparability in the following delivery studies, only pig skin from the dorsal region of $5 - 7$ week old pigs was used.
Laser microporation using the P.L.E.A.S.E.® laser device induced a 4- to 5-fold increase of the TEWL in vitro. A comparable impact by laser microporation has been reported on human skin with an increase of the TEWL by factor 4.5 to 6.3 [29]. The enhanced TEWL through the skin facilitated a fast dissolution of the polymer films for all tested compositions. All film formulations disintegrated within a similar time period, thereby providing at least 18 h during which the model substance could diffuse into the micropore tissue before the pores would close. On the other hand, the low water transport through intact skin was insufficient to dissolve the polymer films within a total incubation time of 24 h. We therefore conclude that a fast dissolution of the polymer films is ensured with a TEWL above 40 g/m^2/h and should further improve with elevating TEWL values. Besides that, it should be considered that an efficient film dissolution requires the use of occlusive backings that entrap the transpired water and maximize the water contact with the polymer films.

4.2 Influence of the polymer film formulation on the RD70 delivery

Histological images and the quantification of RD70 in horizontal skin sections revealed that macromolecules were successfully delivered into laser microporated skin. Although most significant deposition of RD70 was visible in the epidermis, extracts from deeper skin sections showed that RD70 also penetrated into the dermal skin layer. Due to the high density of LCs and dDCs in the epidermis and dermis, an antigen-specific immune response is supposedly enhanced when the antigen deposition in these layers is maximized. It has been reported that both, the vehicle formulation and the molecular structure of the applied substance, influence the drug delivery and hence also the APC targeting [63, 72]. The amount of RD70 delivered into the skin was comparable to results of previous *in vitro* studies using macromolecules [34]. *In vivo* a delivery efficiency of up to 80 % has been reported for OVA-loaded dry patches [62].
We have shown that RD70 did not penetrate into intact skin, but was exclusively delivered into laser microporated skin. The intradermal deposition of RD70 was slightly higher using PVA polymer films compared to PVA-CMC and PVA-carbomer blends. Although

this trend was not supported by microscopic imaging, the absolute quantification of RD70 by fluorescence spectroscopy suggested superior delivery properties using pure PVA films. This effect could be attributed to the increased film thicknesses of the PVA blend formulations, which led to slightly slower dissolution during incubation. Although a smaller casting knife was used for the manufacturing of the PVA blend films, the final film thickness of PVA-CMC and PVA-carbomer films was up to two times higher compared to the pure PVA formulation. The addition of the gelling agents CMC and carbomer improved the film casting properties of the polymer solutions by increasing the viscosity but reduced the diffusion of RD70 into the skin.

The in vitro release study could simulate the restricted liquid contact through the micropores. The drug release in the diffusion chamber was comparable for all film formulations due to a simultaneous solubilization and release of model substance and film forming polymer. Slightly inferior release was observed for polymer films with a higher content of model drug. However, these differences were negligible with a generally high total release after 12 h incubation despite limited contact to the release medium. Generally, no differences in the dissolution and release behavior were detected for pure PVA, PVA-CMC, and PVA-carbomer films. Also, no difference in complete film dissolution in different aqueous media with direct liquid contact at pH $6-9$ was observed in preliminary studies (data nor shown). The pore diameter of 12 µm used in the experimental setup was suitable to simulate the limited access to the tissue fluid. Although this pore size is smaller compared to the diameter of laser-generated micropores of $100-200$ µm, both diameters are significantly larger than the molecules that pass through the pores into the release medium or skin tissue upon dissolution.

The diffusion into the skin tissue was assessed using the Franz cell setup and showed a formulation-dependent penetration and permeation behavior. Although a non-physiological pH of 9 was used as Franz cell receptor medium, the short exposure $\leq$ 24 h of the skin tissue to the elevated pH was not expected to induce major changes to the tissue during incubation time. Moreover, dextrane molecules are expected to exhibit a neutral surface charge. The low pKa of the attached rhodamine dye of $\sim$3 would induce a deprotonation of carboxylic functional groups at slightly elevated as well as physiological pH. We therefore expect comparable diffusion behavior of the model substance RD70 in the present study setup using aqueous receptor media at pH 9 as well as physiological pH.

The total RD70 delivery results suggest that the film composition and film thickness were the main factors to influence the RD70 penetration and permeation. Upon hydration

and dissolution of the films on the skin surface, the model substance could diffuse into the accessible micropore tissue. Compared to pure PVA films, the addition of CMC and carbomer increased the formulation viscosity upon dissolution on the skin. The viscous gel matrix could not diffuse into the micropores but remained on the skin surface, lowering the diffusivity of the model substance. Lower values for the total delivery of RD70 into and through the skin for PVA-CMC and PVA-carbomer films indicate that the release from the gel matrix upon dissolution was reduced due to increased viscosity. Moreover, the higher polymer content for PVA blend films further reduced the diffusion of RD70 into the tissue.

Besides film thickness, the relative composition of pure PVA and PVA blend formulations could influence the RD70 penetration behavior. In comparison to the blend formulations, pure PVA films provided a higher relative sucrose and trehalose content, enhancing the initial film dissolution due to osmotic effects. With respect to the total amount of sucrose and trehalose, PVA-CMC and PVA-carbomer films had higher contents per cm^2 related to loading of the model substance. Upon film dissolution, the resulting osmotic gel could have induced a draining of water from the tissue, thereby reducing the penetration of RD70 into the skin in opposite direction. Furthermore, the addition of plasticizers, e.g. propylene glycol, can affect the release behavior from films. Higher contents of propylene glycol were used for PVA blend formulations in order to reduce the film brittleness, which was increased by CMC and carbomer polymers. Due to its hygroscopic properties, propylene glycol can improve the wetting and dissolution behavior of the polymer films. Although the relative propylene glycol content was higher in the PVA blend formulations, the dissolution behavior of PVA-CMC and PVA-carbomer films was comparable to pure PVA films with lower amounts of the plasticizer. Our findings indicate that the major rate limiting step in this study was the diffusion of model substance into the skin. The film dissolution played a minor role and was comparably fast for all tested formulations. The experimentally determined flux indicated a relatively slow diffusion of the macromolecule through the tissue which was further decreased by addition of the gelling agents CMC and carbomer to the film composition (Tab. IV.4). The intuitive model resulted in well-matching fluxes for the PVA-CMC and PVA-carbomer films whereas the proposed new model [69] generally overestimated the flux for all formulations. It has to be noted that generally higher fluxes were predicted for the CMC and carbomer blend formulation, although experimental data revealed a reduced diffusion for these formulations. This observation, likely due to increased viscosity compared to the pure PVA films, highlights the need to include the formulation viscosity into predictive models of flux predictions. Furthermore, we conclude that the

formulation viscosity and the polymer content per cm^2 are important parameters affecting dissolution time and, more importantly, the RD70 penetration into the skin. Moreover, films with increasing thickness with even slower dissolution may potentially provide limited capability to deliver macromolecules and other drug substances into laser microporated skin.

Considering the micropore filling in vitro, we expected a filling behavior of the solubilized polymer films comparable to liquid solutions or gels, for which good filling properties have been demonstrated before [63]. Under in vivo conditions, topically applied liquid is absorbed by laser microporated skin tissue within approximately 10 min [51, 53, 54]. These findings suggest similar behavior for the present patch delivery system when tested under *in vivo* conditions. Upon dissolution on laser microporated skin, the solubilized film formulation could be absorbed by the viable tissue, thereby delivering the drug substance as well as film forming polymers with lower molecular weight. Although the ratio of delivered to applied RD70 remained relatively low in the present Franz diffusion cell study, we assume that the delivery efficiency might be improved under in vivo conditions. Particularly the application of unblended PVA polymer film patches on laser microporated skin provides the chance of low viscosity PVA formulation to be absorbed by the viable tissue.

4.3 RD70 delivery using soft laser microporation parameters

The efficient delivery into laser microporated skin depends not only on the vehicle formulation, but also on drug substance properties like molecular weight, hydrophilicity and lipophilicity, and their interplay with micropore characteristics. It has been shown that small hydrophilic molecules diffuse easier through the tissue upon laser microporation compared to larger molecules [31, 72]. Furthermore, the drug transport of small, hydrophilic molecules can be enhanced by increasing not only the number of pores per cm^2 (pore density) but also the micropore depth [11, 31, 55, 72, 73]. Notably, increasing laser pulse durations from 50 µs (super short pulse) up to 1000 µs (very long pulse) do not substantially increase the micropore dimensions but mainly influence the extent of RTD, which compromises the molecule permeation at the tissue interface [72]. The transdermal delivery of small molecules could be significantly increased by optimizing the laser microporation treatment, in some cases leading to systemic side effects [74, 75]. Considering other molecule types, the influence of laser settings on the delivery efficiency is less pronounced. Small, lipophilic substances mainly penetrate into the skin via passive diffusion, whereas the diffusion capabilities of macromolecules are highly dependent on their molecular structure

and charge [31].
In the present study, we used RD70 as a stable, hydrophilic model macromolecule that cannot diffuse through intact skin [31]. Our results prove that a substantial amount of the macromolecule with a size of 70 kDa was delivered into laser microporated skin using 'cold ablation' laser parameters. The P.L.E.A.S.E.® fractional laser poration device was used to create shallow micropores that reached the epidermal and superficial dermal layer, employing two pulses per pore with a low laser fluence of 17.8 J/cm^2 and a pore density of 15 %. In previous studies, laser fluences of up to 13.59 J/cm^2 and about 22.65 J/cm^2 have resulted in micropores with a diameter between $150 - 200$ µm, reaching depths of up to 30 µm and 100 µm, respectively [26]. With the parameters used in this study, we were able to generate micropores with equal diameter and a pore depth well comparable to the expected nominal value provided by the laser poration device (Fig. IV.4). The application of two pulses with a laser fluence of 17.8 J/cm^2 facilitated the creation of micropores with relatively small diameter but reaching deeper into the tissue compared to a one pulse application. We assume that similar depths could be achieved at higher laser fluences, however this would likely result in larger pore diameters and increased RTD, which would affect penetration negatively. The laser poration treatment in the presented study resulted in a distinct coagulation zone (RTD), which was observed around the micropore and most likely attributed to a medium short pulse duration of 125 µs. Considering previous studies, we expect that the delivery efficiency of RD70 could be further improved by optimizing the micropore dimensions (laser fluence, number of pulses per pore), increasing the number of pores per cm^2 (pore density), and reducing the RTD-related tissue barrier (laser fluence, pulse duration) [55, 72].

4.4 Nanoparticle delivery facilitated by fractional laser microporation

To evaluate the intradermal delivery of particles as model vaccine vehicles, PS-nano- and microparticles with a diameter of 0.5 µm and 5 µm were incorporated into the polymer films. Fluorescence microscopy revealed that a substantial deposition of PS-nanoparticles over the entire micropore surface was achieved. On the other hand, PS-microparticles did not attach to the micropore surface or penetrate into the tissue. Unlike the PS-microparticles, the smaller nanoparticles of 0.5 µm exhibited suitable properties to diffuse into the skin upon tissue ablation. The differences in the deposition behavior can be attributed to a smaller diffusivity for larger particles. We assume that an intermediate deposition of PS-

microparticles was most likely mediated by sedimentation in the solubilized polymer films. In contrast to PS-nanoparticles, larger microparticles could not enter the skin tissue and were easily removed together with residual film in a post application cleaning treatment.

Just as described for RD70, the polymer formulation influenced the particle delivery significantly. Histological images show that PVA films provided a superior deposition of PS-nanoparticles compared to PVA films blended with CMC or cross-linked carbomer. This effect was even more pronounced for the PS-nanoparticles which suggests a particularly strong sustaining effect on the particulate vehicles induced by the gelling agents. Moreover, the gelling polymers might have interacted with the PS-nanoparticle surface as observed with other polymers [76], thereby increasing the hydrodynamic radius and compromising the diffusion into the tissue. Therefore, a minimized content of film forming polymer that maintains sufficient mechanical stability might be beneficial for the delivery of nanoparticles from film patches into laser microporated skin.

Due to their immunostimulatory properties, nanoparticles are considered as a particularly attractive adjuvant for vaccination [77]. Regarding the intradermal delivery of nanoparticles, recent advances have shed more light on the delivery characteristics via the transfollicular route [78, 79]. Although a diameter between $0.4 - 0.7$ µm has been identified as the optimum particle size [80], transfollicular delivery fails to provide an efficient deposition of substantial particle amounts in close vicinity to cutaneous APCs. Moreover, a penetration of nanoparticles larger than 10 nm into the viable skin is unlikely without further disruption of the skin barrier [81]. Furthermore, it has been reported that the particle uptake by dendritic cells increases with decreasing particle diameters below 0.5µm [82].

5 Conclusion

We successfully demonstrated that PVA-based polymer films are easily water-soluble and facilitate the delivery of macromolecules and nanoparticles into laser microporated skin. The utilized film casting technique is easily scalable and would allow for a cost-effective mass production of the film patches. Moreover, the good mechanical stability after direct loading of different hydrophilic model substances into the formulations at varying concentrations suggests a good formulation compatibility with a wide range of molecules and vehicles, e.g. vaccine antigens, allergens, nanoparticles, and adjuvants. However, the influence of different molecule types on the mechanical properties and storage stability of the polymer films still requires an all-embracing investigation and shall be subject to future

studies.
The patch delivery system, which is composed of a water-soluble polymer film and occlusive backing, facilitates effective skin hydration, thereby promoting the antigen processing by skin-resident APCs. Although immune responses have been observed upon prolonged antigen contact with intact skin [83–85], the active delivery of vaccines into the viable tissue is necessary to substantially boost the delivery efficiency and thus the immune response [4]. Reduced film thicknesses combined with higher loadings or the manufacturing of drug-loaded droplet arrays are two further approaches to improve the delivery efficiency. Besides that, the patch system allows to cover the impaired skin barrier during re-epithelialization, thus rendering the application of plasters after microporation unnecessary.
In connection with fractional laser microporation, the presented PVA-based polymer film patches offer a safe, minimally invasive route for cutaneous immunization and reduce sharp waste and biohazard disposal, which are major disadvantages of intramuscular (i.m.) or subcutaneous (s.c.) injections. The utilized P.L.E.A.S.E.® fractional laser poration system provides the possibility to ablate the skin tissue with minimal RTD, offers a favorable side effect profile, and provides the opportunity to safely and reproducibly increase the TEWL through the skin. The development of a hand-held device might further increase the patient compliance and particularly the commercial appeal.
The presented concept combines the advantages of both systems providing a minimally-invasive access to viable layers of the skin and exploiting dry polymer films as vaccine delivery formulations. The combination of the physical stimulus with the potency of nanoparticle carriers as vaccines is consequently another appealing idea to maximize immune responses upon cutaneous immunization. Good functionality, easy applicability, and the readily available manufacturing technology makes the microporation-patch combination an attractive concept which is worth further investigation.

6 Acknowledgements

We would like to thank our cooperation partners Pantec Biosolutions (Liechtenstein) for kindly providing the laser poration system and the Clinic for Swine, Faculty of Veterinary Medicine, Ludwig-Maximilians-University Munich, Oberschleissheim (Germany) for providing pig skin. Furthermore, the authors would like to thank Michael K. Schmidt (Center for Neuropathology and Prion Research, ZNP, Ludwig-Maximilians-University Munich) for his support with the cryostat sectioning.

Bibliography

[1] H. Kalluri, A. K. Banga, Transdermal delivery of proteins, AAPS PharmSciTech 12 (2011) 431–441.

[2] M. B. M. Teunissen, D. Zehrung, Cutaneous vaccination Protective immunization is just a skin-deep step away, Vaccine 33 (2015) 4659–4662.

[3] K. Schulze, T. Ebensen, P. Riese, B. Prochnow, C.-M. Lehr, C. A. Guzmán, New Horizons in the Development of Novel Needle-Free Immunization Strategies to Increase Vaccination Efficacy, in: M. Stadler, P. Dersch (Eds.), How to Overcome the Antibiotic Crisis, volume 398, Springer, Cham, 2016, pp. 207–234. URL: http://link.springer.com/10.1007/82_2016_495. doi:10.1007/82_2016_495.

[4] G. Senti, S. Von Moos, T. M. Kündig, Epicutaneous allergen administration: is this the future of allergen-specific immunotherapy?, Allergy 66 (2011) 798–809.

[5] J. O. Morales, K. R. Fathe, A. Brunaugh, S. Ferrati, S. Li, M. Montenegro-Nicolini, Z. Mousavikhamene, J. T. McConville, M. R. Prausnitz, H. D. C. Smyth, Challenges and future prospects for the delivery of biologics: oral mucosal, pulmonary, and transdermal routes, AAPS J 19 (2017) 652–668.

[6] B. G. Amsden, M. F. A. Goosen, Transdermal delivery of peptide and protein drugs: an overview, AIChE J 41 (1995) 1972–1997.

[7] S. Mitragotri, Immunization without needles, Nat Rev Immunol 5 (2005) 905–916.

[8] R. Weiss, M. Hessenberger, S. Kitzmueller, D. Bach, E. E. Weinberger, W. D. Krautgartner, C. Hauser-Kronberger, B. Malissen, C. Boehler, Y. N. Kalia, J. Thalhamer, S. Scheiblhofer, Transcutaneous vaccination via laser microporation, J Control Release 162 (2012) 391–399.

[9] L. Engelke, G. Winter, S. Hook, J. Engert, Recent insights into cutaneous immunization: how to vaccinate via the skin, Vaccine 33 (2015) 4663–4674.

[10] M. H. Gold, Update on Fractional Laser Technology, J Clin Aesthet Dermatol 3 (2010) 42–50.

[11] E. H. Taudorf, C. M. Lerche, A. M. Erlendsson, P. A. Philipsen, S. H. Hansen, C. Janfelt, U. Paasch, R. R. Anderson, M. Hædersdal, Fractional laser-assisted drug delivery: laser channel depth influences biodistribution and skin deposition of methotrexate, Lasers Surg Med 48 (2016) 519–529.

[12] M. R. Alexiades-Armenakas, J. S. Dover, K. A. Arndt, The spectrum of laser skin resurfacing: nonablative, fractional, and ablative laser resurfacing, J Am Acad Der-

matol 58 (2008) 719–740.

[13] N. A. Marley, J. S. Gaffney, M. M. Cunningham, Lambert absorption coefficients of water in the frequency range of 3000-934 cm-1, Appl Opt 33 (1994) 8041–8054.

[14] S. Y. Venyaminov, F. G. Prendergast, Water (H2O and D2O) molar absorptivity in the 1000-4000 cm-1 range and quantitative infrared spectroscopy of aqueous solutions, Anal Biochem 248 (1997) 234–245.

[15] J. T. Walsh, T. F. Deutsch, Er:YAG laser ablation of tissue: measurement of ablation rates, Lasers Surg Med 9 (1989) 327–337.

[16] C. C. Dierickx, K. A. Khatri, Z. S. Tannous, J. J. Childs, R. H. Cohen, A. Erofeev, D. Tabatadze, I. V. Yaroslavsky, G. B. Altshuler, Micro-fractional ablative skin resurfacing with two novel erbium laser systems, Lasers Surg Med 40 (2008) 113–123.

[17] A. I. Metelitsa, T. S. Alster, Fractionated laser skin resurfacing treatment complications: a review, Dermatol Surg 36 (2010) 299–306.

[18] S. Scheiblhofer, J. Thalhamer, R. Weiss, Laser microporation of the skin: prospects for painless application of protective and therapeutic vaccines, Expert Opin Drug Deliv 10 (2013) 761–773.

[19] S. A. Braun, H. Schrumpf, B. A. Buhren, B. Homey, P. A. Gerber, Laser assisted drug delivery: grundlagen und praxis, J Dtsch Dermatol Ges 14 (2016) 480–489.

[20] R. M. Adrian, Pulsed carbon dioxide and long pulse 10-ms erbium-YAG laser resurfacing: a comparative clinical and histologic study, J Cutan Laser Ther 1 (1999) 197–202.

[21] J. B. Newman, J. L. Lord, K. Ash, D. H. McDaniel, Variable pulse erbium:YAG laser skin resurfacing of perioral rhytides and side-by-side comparison with carbon dioxide laser, Lasers Surg Med 26 (2000) 208–214.

[22] G. J. Goodman, Lasers and Lights, in: D. J. Goldberg (Ed.), Facial Rejuvenation, Springer, Berlin, 2007, pp. 1–48. doi:10.1007/978-3-540-69518-9_1.

[23] W.-R. Lee, S.-C. Shen, K.-H. Wang, C.-H. Hu, J.-Y. Fang, The effect of laser treatment on skin to enhance and control transdermal delivery of 5-fluorouracil, J Pharm Sci 91 (2002) 1613–1626.

[24] W.-R. Lee, S.-C. Shen, W. Kuo-Hsien, C.-H. Hu, J.-Y. Fang, Lasers and microdermabrasion enhance and control topical delivery of vitamin C, J Invest Dermatol 121 (2003) 1118–1125.

[25] S.-C. Shen, W.-R. Lee, Y.-P. Fang, C.-H. Hu, J.-Y. Fang, In vitro percutaneous absorption and in vivo protoporphyrin IX accumulation in skin and tumors after

topical 5-aminolevulinic acid application with enhancement using an erbium:YAG laser, J Pharm Sci 95 (2006) 929–938.

[26] Y. G. Bachhav, S. Summer, A. Heinrich, T. Bragagna, C. Böhler, Y. N. Kalia, Effect of controlled laser microporation on drug transport kinetics into and across the skin, J Control Release 146 (2010) 31–36.

[27] W.-R. Lee, S.-C. Shen, M.-H. Pai, H.-H. Yang, C.-Y. Yuan, J.-Y. Fang, Fractional laser as a tool to enhance the skin permeation of 5-aminolevulinic acid with minimal skin disruption: A comparison with conventional erbium:YAG laser, J Control Release 145 (2010) 124–133.

[28] J. Yu, Y. G. Bachhav, S. Summer, A. Heinrich, T. Bragagna, C. Böhler, Y. N. Kalia, Using controlled laser-microporation to increase transdermal delivery of prednisone, J Control Release 148 (2010) e71–e73.

[29] Y. G. Bachhav, A. Heinrich, Y. N. Kalia, Using laser microporation to improve transdermal delivery of diclofenac: Increasing bioavailability and the range of therapeutic applications, Eur J Pharm Biopharm 78 (2011) 408–414.

[30] W.-R. Lee, T.-L. Pan, P.-W. Wang, R.-Z. Zhuo, C.-M. Huang, J.-Y. Fang, Erbium:YAG laser enhances transdermal peptide delivery and skin vaccination, J Control Release 128 (2008) 200–208.

[31] W.-R. Lee, S.-C. Shen, S. A. Al-Suwayeh, H.-H. Yang, C.-Y. Yuan, J.-Y. Fang, Laser-assisted topical drug delivery by using a low-fluence fractional laser: Imiquimod and macromolecules, J Control Release 153 (2011) 240–248.

[32] J. S. Nelson, J. L. McCullough, T. C. Glenn, W. H. Wright, L.-H. L. Liaw, S. L. Jacques, Mid-infrared laser ablation of stratum corneum enhances in vitro percutaneous transport of drugs, J Invest Dermatol 97 (1991) 874–879.

[33] J.-Y. Fang, W.-R. Lee, S.-C. Shen, H.-Y. Wang, C.-L. Fang, C.-H. Hu, Transdermal delivery of macromolecules by erbium:YAG laser, J Control Release 100 (2004) 75–85.

[34] J. Yu, D. R. Kalaria, Y. N. Kalia, Erbium:YAG fractional laser ablation for the percutaneous delivery of intact functional therapeutic antibodies, J Control Release 156 (2011) 53–59.

[35] W.-R. Lee, S.-C. Shen, S. A. Al-Suwayeh, H.-H. Yang, Y.-C. Li, J.-Y. Fang, Skin permeation of small-molecule drugs, macromolecules, and nanoparticles mediated by a fractional carbon dioxide laser: the role of hair follicles, Pharm Res 30 (2013) 792–802.

[36] Y. Song, K. Hemmady, A. Puri, A. K. Banga, Transdermal delivery of human growth

hormone via laser-generated micropores, Drug Deliv Transl Res (2017).

[37] W.-R. Lee, S.-C. Shen, C.-R. Liu, C.-L. Fang, C.-H. Hu, J.-Y. Fang, Erbium:YAG laser-mediated oligonucleotide and DNA delivery via the skin: an animal study, J Control Release 115 (2006) 344–353.

[38] W.-R. Lee, S.-C. Shen, R.-Z. Zhuo, K.-C. Wang, J.-Y. Fang, Enhancement of topical small interfering RNA delivery and expression by low-fluence erbium:YAG laser pretreatment of skin, Hum Gene Ther 20 (2009) 580–588.

[39] E. A. Genina, A. N. Bashkatov, L. E. Dolotov, G. N. Maslyakova, V. I. Kochubey, I. V. Yaroslavsky, G. B. Altshuler, V. V. Tuchin, Transcutaneous delivery of micro- and nanoparticles with laser microporation, J Biomed Opt 18 (2013) 111406.

[40] E. A. Genina, Y. I. Svenskaya, I. Y. Yanina, L. E. Dolotov, N. A. Navolokin, A. N. Bashkatov, G. S. Terentyuk, A. B. Bucharskaya, G. N. Maslyakova, D. A. Gorin, V. V. Tuchin, G. B. Sukhorukov, In vivo optical monitoring of transcutaneous delivery of calcium carbonate microcontainers, Biomed Opt Express 7 (2016) 2082–2087.

[41] G. Oni, C. Lequeux, M.-J. Cho, D. Zhang, E. Lazcano, S. A. Brown, J. M. Kenkel, Transdermal delivery of adipocyte-derived stem cells using a fractional ablative laser, Aesthet Surg J 33 (2013) 109–116.

[42] J. D. Bos, M. L. Kapsenberg, The skin immune system: progress in cutaneous biology, Immunol Today 14 (1993) 75–78.

[43] M. B. Teunissen, M. Haniffa, M. P. Collin, Insight into the immunobiology of human skin and functional specialization of skin dendritic cell subsets to innovate intradermal vaccination design, Curr Top Microbiol Immunol 351 (2012) 25–76.

[44] F. Ginhoux, L. G. Ng, M. Merad, Understanding the murine cutaneous dendritic cell network to improve intradermal vaccination strategies, in: M. Teunissen (Ed.), Intradermal Immunization. Curr Top Microbiol Immunol, volume 351, 2010/11/09 ed., Springer, Berlin, Heidelberg, 2010, pp. 1–24. URL: http://link.springer.com/10.1007/82_2010_115. doi:10.1007/82_2010_115.

[45] D. Gutowska-Owsiak, G. S. Ogg, The epidermis as an adjuvant, J Invest Dermatol 132 (2012) 940–948.

[46] K. Sugita, K. Kabashima, K. Atarashi, T. Shimauchi, M. Kobayashi, Y. Tokura, Innate immunity mediated by epidermal keratinocytes promotes acquired immunity involving Langerhans cells and T cells in the skin, Clin Exp Immunol 147 (2007) 176–183.

[47] B. Z. Igyártó, K. Haley, D. Ortner, A. Bobr, M. Gerami-Nejad, B. T. Edelson, S. M.

Zurawski, B. Malissen, G. Zurawski, J. Berman, D. H. Kaplan, Skin-resident murine dendritic cell subsets promote distinct and opposing antigen-specific T helper cell responses, Immunity 35 (2011) 260–272.

[48] K. Palucka, J. Banchereau, I. Mellman, Designing vaccines based on biology of human dendritic cell subsets, Immunity 33 (2010) 464–478.

[49] M. Hessenberger, R. Weiss, E. E. Weinberger, C. Boehler, J. Thalhamer, S. Scheiblhofer, Transcutaneous delivery of CpG-adjuvanted allergen via laser-generated micropores, Vaccine 31 (2013) 3427–3434.

[50] P. C. DeMuth, Y. Min, D. J. Irvine, P. T. Hammond, Implantable silk composite microneedles for programmable vaccine release kinetics and enhanced immunogenicity in transcutaneous immunization, Adv Healthc Mater 3 (2014) 47–58.

[51] D. Bach, R. Weiss, M. Hessenberger, S. Kitzmueller, E. E. Weinberger, W. D. Krautgartner, C. Hauser-Kronberger, C. Boehler, J. Thalhamer, S. Scheiblhofer, Transcutaneous immunotherapy via laser-generated micropores efficiently alleviates allergic asthma in Phl p 5-sensitized mice, Allergy 67 (2012) 1365–1374.

[52] M. N. K. Kumar, C. Zhou, M. X. Wu, Laser-facilitated epicutaneous immunotherapy to IgE-mediated allergy, J Control Release 235 (2016) 82–90.

[53] D. Terhorst, E. Fossum, A. Baranska, S. Tamoutounour, C. Malosse, M. Garbani, R. Braun, E. Lechat, R. Crameri, B. Bogen, S. Henri, B. Malissen, Laser-assisted intradermal delivery of adjuvant-free vaccines targeting XCR1+ dendritic cells induces potent antitumoral responses, J Immunol 194 (2015) 5895–5902.

[54] S. Scheiblhofer, A. Strobl, V. Hoepflinger, T. Thalhamer, M. Steiner, J. Thalhamer, R. Weiss, Skin vaccination via fractional infrared laser ablation - optimization of laser-parameters and adjuvantation, Vaccine 35 (2017) 1802–1809.

[55] Y. G. Bachhav, A. Heinrich, Y. N. Kalia, Controlled intra- and transdermal protein delivery using a minimally invasive Erbium:YAG fractional laser ablation technology, Eur J Pharm Biopharm 84 (2013) 355–364.

[56] J. S. Waibel, A. J. Wulkan, P. R. Shumaker, Treatment of hypertrophic scars using laser and laser assisted corticosteroid delivery, Lasers Surg Med 45 (2013) 135–140.

[57] M. Singhal, S. Del Rio-Sancho, K. Sonaje, Y. N. Kalia, S. Del Río-Sancho, K. Sonaje, Y. N. Kalia, Fractional laser ablation for the cutaneous delivery of triamcinolone acetonide from cryomilled polymeric microparticles: creating intraepidermal drug depots, Mol Pharm 13 (2016) 500–511.

[58] T. Fujimoto, J. Wang, K. Baba, Y. Oki, Y. Hiruta, M. Ito, S. Ito, H. Kanazawa,

Transcutaneous drug delivery by liposomes using fractional laser technology, Lasers Surg Med (2016).

[59] M. Hædersdal, F. H. Sakamoto, W. A. Farinelli, A. G. Doukas, J. Tam, R. R. Anderson, Fractional CO2 laser-assisted drug delivery, Lasers Surg Med 42 (2010) 113–122.

[60] B. T. Nguyen, S. D. Gan, N. Konnikov, C. A. Liang, Treatment of superficial basal cell carcinoma and squamous cell carcinoma in situ on the trunk and extremities with ablative fractional laser-assisted delivery of topical fluorouracil, J Am Acad Dermatol 72 (2015) 558–560.

[61] G. Oni, S. A. Brown, J. M. Kenkel, Can fractional lasers enhance transdermal absorption of topical lidocaine in an in vivo animal model?, Lasers Surg Med 44 (2012) 168–174.

[62] X. Chen, G. Kositratna, C. Zhou, D. Manstein, M. X. Wu, Micro-fractional epidermal powder delivery for improved skin vaccination, J Control Release 192 (2014) 310–316.

[63] U. H. Olesen, M. Mogensen, M. Hædersdal, Vehicle type affects filling of fractional laser-ablated channels imaged by optical coherence tomography, Lasers Med Sci 32 (2017) 679–684.

[64] X. Chen, D. Shah, G. Kositratna, D. Manstein, R. R. Anderson, M. X. Wu, Facilitation of transcutaneous drug delivery and vaccine immunization by a safe laser technology, J Control Release 159 (2012) 43–51.

[65] Y. Cao, P. Kakar, M. N. Hossen, M. X. Wu, X. Chen, Sustained epidermal powder drug delivery via skin microchannels, J Control Release 249 (2017) 94–102.

[66] J. Schindelin, I. Arganda-Carreras, E. Frise, V. Kaynig, M. Longair, T. Pietzsch, S. Preibisch, C. Rueden, S. Saalfeld, B. Schmid, J.-Y. Tinevez, D. J. White, V. Hartenstein, K. Eliceiri, P. Tomancak, A. Cardona, Fiji: an open-source platform for biological-image analysis, Nat Meth 9 (2012) 676–682.

[67] C. Remuñán-López, R. Bodmeier, Mechanical and water vapor transmission properties of polysaccharide films, Drug Dev Ind Pharm 22 (1996) 1201–1209.

[68] M. Lukac, T. Perhavec, K. Nemes, U. Ahcan, Ablation and thermal depths in VSP Er:YAG laser skin resurfacing, J Laser Health Acad 1 (2010) 56–71.

[69] A. S. Rzhevskiy, R. H. Guy, Y. G. Anissimov, Modelling drug flux through microporated skin, J Control Release 241 (2016) 194–199.

[70] G. Yosipovitch, G. L. Xiong, E. Haus, L. Sackett-Lundeen, I. Ashkenazi, H. I. Maibach, Time-dependent variations of the skin barrier function in humans: transepidermal water loss, stratum corneum hydration, skin surface pH, and skin temperature, J

Invest Dermatol 110 (1998) 20–23.

[71] J. Pinnagoda, R. A. Tupker, T. Agner, J. Serup, Guidelines for transepidermal water loss (TEWL) measurement. A report from the Standardization Group of the European Society of Contact Dermatitis, Contact Derm 22 (1990) 164–178.

[72] B. Zorec, D. Skrabelj, M. Marincek, D. Miklavcic, N. Pavselj, The effect of pulse duration, power and energy of fractional Er:YAG laser for transdermal delivery of differently sized FITC dextrans, Int J Pharm Investig 516 (2017) 204–213.

[73] W.-R. Lee, S.-C. Shen, H.-H. Lai, C.-H. Hu, J.-Y. Fang, Transdermal drug delivery enhanced and controlled by erbium:YAG laser: a comparative study of lipophilic and hydrophilic drugs, J Control Release 75 (2001) 155–166.

[74] D. E. Marra, D. Yip, E. F. Fincher, R. L. Moy, Systemic toxicity from topically applied lidocaine in conjunction with fractional photothermolysis, Arch Dermatol 142 (2006) 1024–1026.

[75] M. Hædersdal, A. M. Erlendsson, U. Paasch, R. R. Anderson, Translational medicine in the field of ablative fractional laser (AFXL)-assisted drug delivery: a critical review from basics to current clinical status, J Am Acad Derm 74 (2016) 981–1004.

[76] T. Hu, J. Gao, H. Auweter, R. Iden, E. Lueddecke, C. Wu, Adsorption of gelatins on surfactant-free PS nanoparticles, Polymer 43 (2002) 5545–5550.

[77] P. Sahdev, L. J. Ochyl, J. J. Moon, Biomaterials for nanoparticle vaccine delivery systems, Pharm Res 31 (2014) 2563–2582.

[78] S. Hansen, C.-M. M. Lehr, Nanoparticles for transcutaneous vaccination, Microb Biotechnol 5 (2012) 156–167.

[79] M. Radtke, A. Patzelt, F. Knorr, J. Lademann, R. R. Netz, Ratchet effect for nanoparticle transport in hair follicles, Eur J Pharm Biopharm 116 (2017) 125–130.

[80] A. Patzelt, H. Richter, F. Knorr, U. Schäfer, C.-M. Lehr, L. Dähne, W. Sterry, J. Lademann, Selective follicular targeting by modification of the particle sizes, J Control Release 150 (2011) 45–48.

[81] T. W. Prow, X. Chen, N. A. Prow, G. J. P. Fernando, C. S. E. Tan, A. P. Raphael, D. Chang, M. P. Ruutu, D. W. K. Jenkins, A. Pyke, M. L. Crichton, K. Raphaelli, L. Y. H. Goh, I. H. Frazer, M. S. Roberts, J. Gardner, A. A. Khromykh, A. Suhrbier, R. A. Hall, M. A. F. Kendall, Nanopatch-targeted skin vaccination against West Nile Virus and Chikungunya virus in mice, Small 6 (2010) 1776–1784.

[82] C. Foged, B. Brodin, S. Frokjaer, A. Sundblad, Particle size and surface charge affect particle uptake by human dendritic cells in an in vitro model, Int J Pharm 298 (2005)

315–322.

[83] S. Naito, J.-i. Maeyama, T. Mizukami, M. Takahashi, I. Hamaguchi, K. Yamaguchi, Transcutaneous immunization by merely prolonging the duration of antigen presence on the skin of mice induces a potent antigen-specific antibody response even in the absence of an adjuvant, Vaccine 25 (2007) 8762–8770.

[84] C. Dupont, N. Kalach, P. Soulaines, S. Legoue-Morillon, H. Piloquet, P.-H. Benhamou, Cow's milk epicutaneous immunotherapy in children: a pilot trial of safety, acceptability, and impact on allergic reactivity, J Allergy Clin Immunol 125 (2010) 1165–1167.

[85] R. H. Behrens, J. P. Cramer, T. Jelinek, H. Shaw, F. von Sonnenburg, D. Wilbraham, T. Weinke, D. J. Bell, E. Asturias, H. L. E. Pauwells, R. Maxwell, M. Paredes-Paredes, G. M. Glenn, S. Dewasthaly, D. M. Stablein, Z.-D. Jiang, H. L. DuPont, Efficacy and safety of a patch vaccine containing heat-labile toxin from Escherichia coli against travellers' diarrhoea: a phase 3, randomised, double-blind, placebo-controlled field trial in travellers from Europe to Mexico and Guatemala, Lancet Infect Dis 14 (2014) 197–204.

V

SUMMARY OF THIS THESIS

1 Summary

The aim of this thesis was to evaluate the i.d. delivery of model vaccines using selected needle-free, minimally invasive delivery techniques and to assess their potential application for cutaneous vaccination.

Chapter II is focused on the i.d. delivery of vaccine microparticles using a hand-held powder injector. A highly concentrated sugar-based vaccine using ovalbumin (OVA) as model antigen was manufactured using a two-step process combining collapse lyophilization and cryogenic milling. The resulting vaccine with a loading of 200 µg/mg OVA showed good stability for up to 12 months at ambient conditions. The vaccine powder, which was loaded into the powder injector using an oily mixture of the components of the adjuvant system 03 (AS03), namely squalene, D/L-α-tocopherol, and polysorbate 80, exhibited good adhesion on the device membrane. The powder adhesion increased with the viscosity for a range of different oily liquids tested. The stability of the oily adhesive composed of AS03 adjuvant components was shown to provide a superior persistence against UV/Vis light and improved long-term stability when stored in direct contact with the highly concentrated OVA vaccine powder. Qualitatively, the successful i.d. delivery of vaccine microparticles into the epidermal and upper dermal skin layers by needle-free powder injection was demonstrated. However, the *in vivo* immunization study in piglets showed no detectable immune response within 28 days upon two applications of the highly concentrated OVA vaccine by powder injection on day 0 and 14.

In chapter III, micro- and nanoparticles were delivered into the skin using different types of solid microneedles (MN). In this study the maximum penetration depths and quantitative i.d. deposition depending on the particle size ranging from $0.1 - 7.0$ µm and the type of MN was evaluated, comparing a flat MN array and a MN roller. It was shown that the MN tip geometry and application mode influence the maximum penetration depth as well as the quantitative deposition. On the other hand, the particle size affects the quantitative deposition only. Moreover, manual massage can improve the i.d. delivery significantly. In summary, MN roller pretreatment and a particle size of 0.5 µm were identified to provide maximum delivery depth and i.d. particle deposition.

Another concept for the delivery of macromolecules and nanoparticles using water-soluble polyvinyl alcohol (PVA)-based polymer films was presented in chapter IV. Pure PVA films and blends with carboxymethyl cellulose (CMC) or cross-linked carbomer were prepared using an easily scalable film casting technique. Fluorescein isothiocyanate (FITC) and rhodamine B-labeled dextrane 70 kDa (RD70), used as small and macromolecular model substances, or nano- and microparticles with diameters of 0.5 µm and 5 µm were directly incorporated into the polymer formulations at varying concentrations. Fractional laser microporation using a pulsed Er:YAG laser (λ = 2.94 µm) was applied to provide access to the viable skin inducing a 4- to 5-fold increase of water transport (TEWL) through the porated skin compared to intact skin. Within 6 h, the polymer films dissolved on laser microporated skin only and facilitated a considerable intradermal delivery of RD70 and nanoparticles over 24 h. The quantitative RD70 deposition was superior for pure PVA films compared to PVA-CMC or PVA-carbomer blend formulations.

2 Conclusion and outlook

Cutaneous vaccination is a promising alternative to conventional i.m. immunization and has been extensively studied during the past decade. The potential for dose sparing due to the high abundance of professional antigen presenting cells (APCs) in the skin tissue and the effective initiation of adaptive and innate immune responses have put i.d. vaccine delivery into the focus of research. Despite the advantages of i.d. vaccination, its practical realization still poses many challenges, some of which are addressed in this thesis. Although several studies have shown increased cost-efficiency of fractional dose vaccination by i.d. injection [1–4], many needle-free i.d. delivery techniques are lacking sufficient delivery efficiency and reproducibility of delivery. The inefficient use of the vaccine by many needle-free approaches attenuates the key benefit of i.d. vaccine delivery and thus increases the overall costs per vaccination. Nevertheless, to date, an impressive variety of different i.d. delivery approaches have been developed and tested in preclinical and clinical trails aiming to tackle poor vaccine delivery and to challenge conventional i.m. immunization.

In this thesis, three different active i.d. delivery techniques were presented: Needle-free powder injection, microneedling using solid MNs, and fractional laser microporation. Considering the key attributes of these techniques, each approach provides different advantages and disadvantages. Figure V.1 highlights the characteristics of the delivery techniques presented in this thesis and allows for a direct comparison. Each technique was subjectively

rated (0=poor, 4=good) with respect to a set of key attributes previously discussed elsewhere [5], and additional aspects related to efficiency and reproducibility of delivery and vaccine stability.

Needle-free powder injection using a single-use, hand-held injector is a highly attractive approach for cutaneous vaccination. It facilitates the administration of a vaccine in one step, is pain-free and minimally invasive, avoids sharps and is expected to yield a high patient acceptability. The device design potentially allows for self-administration and the dry formulation provides a superior storage stability over liquid vaccines. However, another study and the results presented in this thesis show that the reproducibility of i.d. delivery by powder injection depends on the skin condition [6]. The limited reproducibility of delivery is a major concern for the efficacy of vaccination. Furthermore, needle-free powder injection requires advanced technological devices, which further increases the costs per vaccination. In the context of this work, the pyrotechnical accelerator requires elaborated engineering to ensure effectiveness and safety, in particular, to receive regulatory approval. Different approaches can be taken to further improve the performance of powder immunization in future studies. Regarding the powder injector, further optimization can include the design of a customized nozzle, which could create a directional particle flow at high speed towards the skin surface compared to the relatively large area of particle administration in the presented design. Considering the vaccine formulation, vaccine powders with increased density, achieved for example by incorporation of crystalline nanoparticles, can be used to enhance the i.d. particle deposition. Moreover, the potency of the vaccine can be improved using chemical adjuvants, which are either directly incorporated into the vaccine formulation or obtained by mixing of vaccine and adjuvant powder. Further results associated to chapter II indicate that potent vaccines, e.g. influenza antigens, can increase the immune response upon powder immunization [7].

Compared to the powder injector, solid MNs are an established tool for intra- and transdermal drug delivery for cosmetic or research applications. Various designs of MNs are commercially available and cost-efficient to produce in large scale. In this thesis, solid MNs were used for the i.d. delivery of micro- and nanoparticles. Considering this approach for cutaneous vaccination, the complex particle administration procedure represents a significant drawback. Although microneedling is pain-free, widely accepted, and generally improves the i.d. delivery compared to intact skin, the efficiency and reproducibility of particle delivery by manual massage requires further improvement. Nevertheless, the high flexibility of MN skin pretreatment makes it an attractive technique for the screening of

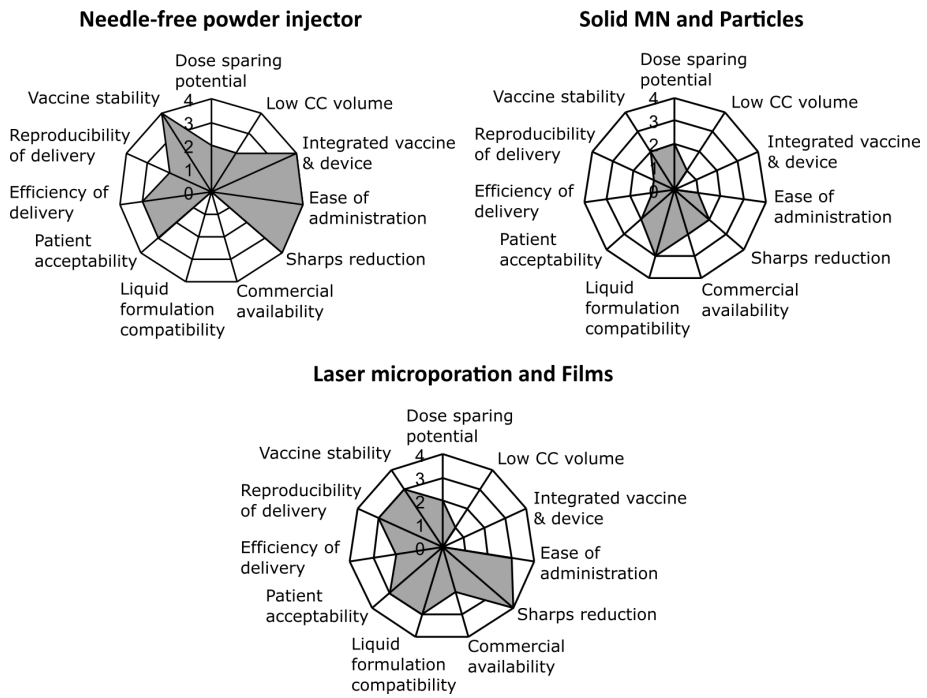

Figure V.1: Key attributes considering the development and commercial use of the intradermal delivery techniques discussed in this thesis. Approach was inspired by [5]. (0=poor, 4=good)

new types of antigens, adjuvants, and vaccine formulations. Considering this flexibility, solid MNs are an ideal tool for a thorough screening of potential chemical and particulate adjuvants to evaluate their potency and safety for cutaneous vaccination. Moreover, different types of particles providing immediate or extended release of antigens and adjuvants should be subject to future studies. A device facilitating reproducible MN insertion and application of the formulation in one step would further increase the attractivity of this rather easy i.d. delivery approach.

On the other hand, the combination of skin laser microporation with a model vaccine-loaded film patch provides a more convenient approach for i.d. vaccine delivery. This work demonstrates that fractional laser microporation reproducibly breaches the skin barrier. Although the subsequent application of a vaccine-loaded water-soluble film patch for 24 h provided insufficient delivery efficiency *ex vivo*, higher deposition can be expected under *in vivo* conditions as discussed in chapter IV. The development of a hand-held device for skin laser treatment would further enhance the commercial potential of this cutaneous vaccination approach. Interestingly, tesa Labtec and Pantec Biosolutions are pursuing the combination of laser poration and vaccine patches [8]. Future studies should focus on the

in vivo testing using commercially available i.d. vaccines, e.g. influenza, and new types of vaccines. Additionally, the optimization of the vaccine patch manufacturing, e.g. by 3D-printing, and the up-scaling of conventional casting techniques should be subject to further development. In addition to the potential compatibility of vaccine films with protein antigens, attenuated or inactivated vaccines are further promising loads for cutaneous vaccination. Similarly, different types of nanoparticles can be loaded into the films serving as adjuvant or vaccine stabilizer and reservoir.

Despite the key attributes discussed, to date the most critical factor limiting the success of most i.d. delivery techniques are the associated costs. Recent prices per vaccine dose in low-income countries have been estimated below US$ 1 [9, 10]. On the other hand, vaccine costs in a range of US$ $53 - 271$ (1.0€ $\approx$ US$ 1.2) per pathogen are expected for a Western European citizen [11]. This dramatic difference in costs per vaccination underlines the current ambivalence in the development of cutaneous vaccination approaches. The administration of fractional doses of existing vaccines by i.d. injection by N&S allows for a clear cost reduction with only minimal change in administration routine compared to conventional i.m. injection. On the other hand, alternative needle-free i.d. delivery techniques, e.g. jet injection, increase the costs per vaccination significantly [4]. In many cases, this renders needle-free techniques unsuitable for low- to middle-income countries. However, the high costs associated with new i.d. delivery techniques also makes them rather unattractive for Western economies. In a recent example, the development a different hand-held powder injector, acquired by Novartis and Pfizer in 2006, was discontinued supposedly because of high development costs. Provided the cost of needle-free powder injectors can be further reduced, e.g. by large-scale production, powder injection is a promising alternative to conventional vaccination by N&S.

The success of low-dose i.d. vaccination and the fast progress in the design of large scale manufacturing processes for certain delivery techniques, such as i.d. injectors, dissolving MNs, and vaccine patches, provide a promising view on the implementation of cutaneous vaccination in future. The greatest potential is the exploitation of cutaneous vaccination for new therapeutic areas, e.g. cancer immunotherapy, prevention against infectious diseases, which are not yet preventable, or neurodegenerative diseases. The use of fractional vaccine doses by i.d. injection is most likely only the starting point for the growing success and establishment of cutaneous vaccination in healthcare.

Bibliography

[1] J. Hickling, K. Jones, M. Friede, D. Zehrung, D. Chen, D. Kristensen, Intradermal delivery of vaccines: potential benefits and current challenges, Bull World Health Organ 89 (2011) 221–226.

[2] P. Soentjens, A. Aerssens, S. Van Gucht, R. Ravinetto, A. Van Gompel, Low-cost intradermal rabies vaccination is indeed very promising, Clin Infect Dis 56 (2013) 1509–1510.

[3] M.-K. Leung, J. H. S. You, Cost-effectiveness of an influenza vaccination program offering intramuscular and intradermal vaccines versus intramuscular vaccine alone for elderly, Vaccine 34 (2016) 2469–2476.

[4] H. Okayasu, C. Sein, D. Chang Blanc, A. R. Gonzalez, D. Zehrung, C. Jarrahian, G. Macklin, R. W. Sutter, Intradermal administration of fractional doses of inactivated poliovirus vaccine: a dose-sparing option for polio immunization, J Infect Dis 216 (2017) S161–S167.

[5] Intradermal delivery of vaccines: a review of the literature and the potential for development for use in low- and middle-income countries, PATH (2009).

[6] M. Kendall, S. Rishworth, F. Carter, T. Mitchell, Effects of relative humidity and ambient temperature on the ballistic delivery of micro-particles to excised porcine skin, J Investig Dermatol 122 (2004) 739–746.

[7] J. Engert, C. Anamur, L. Engelke, C. Fellner, P. Lell, S. Henke, J. Stadler, S. Zoels, M. Ritzmann, G. Winter, A pilot study using a novel pyrotechnically driven prototype applicator for epidermal powder immunization in piglets, Int J Pharm (2018) In revision.

[8] A. Ghoniem, A patch and a laser = vaccination without a cold chain?, World Vaccine Congress Washington (2018).

[9] L. J. Wolfson, F. Gasse, S. P. Lee-Martin, P. Lydon, A. Magan, A. Tibouti, B. Johns, R. Hutubessy, P. Salama, J. M. Okwo-Bele, Estimating the costs of achieving the WHO-UNICEF global immunization vision and strategy, 2006-2015, 2008. URL: http://www.who.int/choice/publications/p_2007_Scaling-up_Immunisation.pdf. doi:10.2471/BLT.07.045096, [accessed 2018-03-31].

[10] Unicef, Supply of children's five-in-one vaccine secured at lowest-ever price, 2016. URL: https://www.unicef.org/supply/files/UNICEF_release_penta_pricing_19OCT16.pdf. doi:10.5235/204976114814222476,

[accessed 2018-03-31].

[11] O. Ethgen, M. Cornier, E. Chriv, F. Baron-Papillon, The cost of vaccination throughout life: A western European overview, Hum Vaccin Immunother 12 (2016) 2029–2037.

PUBLICATIONS, PRESENTATIONS, AND SUPERVISED THESES

Publications

L. Engelke, G. Winter, S. Hook, and J. Engert, Recent insights into cutaneous immunization: how to vaccinate via the skin, Vaccine 33 (2015) 4663-74. doi:10.1016/j.vaccine.2015.05.012

L. Engelke, G. Winter, and J. Engert, Application of water-soluble polyvinyl alcohol-based film patches on laser microporated skin facilitates intradermal macromolecule and nanoparticle delivery, Eur J Pharm Biopharm 128 (2018) 119-130. doi:10.1016/j.ejpb.2018.04.008

J. Engert, C. Anamur, **L. Engelke**, C. Fellner, P. Lell, S. Henke, J. Stadler, S. Zöls, M. Ritzmann, and G. Winter, A pilot study using a novel pyrotechnically driven prototype applicator for epidermal powder immunization in piglets, Int J Pharm 545(1-2) (2018) 215-228. doi:10.1016/j.ijpharm.2018.04.039

K. J. Geh, A. Stelz, K. Godl, **L. Engelke**, B. Förster, and G. Winter, Development of a sprayable hydrogel formulation as drug carrier for the skin application of therapeutic antibodies. (Manuscript in preparation)

Conference talks

L. Engelke, J. Engert, and G. Winter, Comparing the intradermal micro- and nanoparticle delivery depth after different microneedle treatments. 10th PBP World Meeting (2016) Glasgow, United Kingdom.

Poster presentations

L. Engelke, F. Vetter, C. Müller, F. Bracher, G. Winter, and J. Engert, Influence of a highly-concentrated dry vaccine powder on the stability of different oily mixtures containing squalene, -tocopherol and polysorbate 80, Skin Vaccination Summit (2015) Lausanne, Switzerland.

L. Engelke, G. Winter, and J. Engert, Preparation and long-term stability investigation of a highly concentrated vaccine powder for ballistic powder injection using ovalbumin as model antigen, AAPS Annual Meeting & Exposition (2015) Orlando, Florida.

L. Engelke, G. Winter, and J. Engert, Water-soluble polyvinyl alcohol (PVA)-based polymer films as cutaneous vaccine delivery platform for macromolecules and nanoparticles into laser-generated micropores, 5th Galenus Workshop (2016) Berlin, Germany.

Supervised theses

D. Hüwel, Formulation and analysis of polymer thin films for application in transcutaneous vaccination. Ludwig-Maximilians-University Munich, Germany, 2015. (Bachelor's thesis)

L. M. Völk, Characterization of the penetration behavior of micro- and nanoparticles into ex vivo pig skin after application of different microneedle treatments, Ludwig-Maximilians-University Munich, Germany, 2016. (Bachelor's thesis)